SIMULATION OF EARTHQUAKE GROUND MOTIONS FOR SAN ONOFRE NUCLEAR GENERATING STATION UNIT 1

SUPPLEMENT 1

Submitted to:

Southern California Edison Company
2244 Walnut Grove Avenue
Rosemead, California 91770

by:

DEL MAR TECHNICAL ASSOCIATES
A DIVISION OF TERA CORPORATION
1130 Camino Del Mar, Suite H
Del Mar, California 92014
714-481-9292

a division of:

TERA CORPORATION
Teknekron Energy Resource Analysts

2150 Shattuck Avenue
Berkeley, California 94704
415·845·5200

July 1979

Berkeley
Dallas
Bethesda
Washington
Del Mar
Baton Rouge

TABLE OF CONTENTS

TABLE OF CONTENTS

(CONT.)

1.0 INTRODUCTION

1.1 OBJECTIVE

Southern California Edison has submitted a technical report to the Nuclear Regulatory Commission as a basis for establishing conservative estimates of ground shaking at the San Onofre Nuclear Generating Station considering a hypothesized major earthquake 8 km offshore. The report, prepared by the consulting firm TERA/DELTA Corporation, is entitled "Simulation of Earthquake Ground Motions for San Onofre Nuclear Generating Station -- Unit 1," dated May 1978.[3] The purpose of this supplementary report is to answer questions and concerns expressed in meetings with the NRC staff and their consultants regarding methods used to extrapolate ground motion characteristics for the San Onofre site. This supplementary report also addresses many of the questions and comments brought to our attention since the last meeting with the NRC staff and their consultants in October, 1978.

The basic objective of this project is to obtain conservative predictions of site-specific response spectra considering a hypothesized major offshore earthquake. Because of the deficiency of actual earthquake recordings under conditions similar to those at San Onofre, considerable uncertainty in the conservative direction probably would result from direct extrapolation of past data. Using a computer model that simulates the physical processes of earthquakes provides a more rational means for extrapolating site-specific ground motions from past recorded earthquake data while still providing a conservative site specific design basis.

In order to achieve our objective, it has been necessary to develop and validate an earthquake model that possesses sufficient physics to reproduce smoothed response spectra obtained from key past earthquakes using only properties that can be reasonably extrapolated to site-specific conditions. By contrast, we have not attempted to search for rupture sequences that enable wiggle-for-wiggle matches with time recorded ground motions. While such an endeavor would be of considerable scientific interest, it is beyond the scope of this project, since such

rupture detail most certainly varies from one earthquake to the next and would not be relevant for an extrapolation for San Onofre conditions. Rather, our attempt has been to select generic earthquake parameters, as few in number as plausible, which can be extrapolated to site-specific conditions.

The earthquake model should thus be viewed as a highly sophisticated method for extrapolating site-specific ground motions from recorded past earthquakes. Because of the degree of sophistication (rupture physics and wave mechanics), fewer data are needed to make reliable extrapolations than for conventional methods.

1.2 SUMMARY

Three general categories of concern were established in the October 1978 meeting for further work. These include studies of the suitability of mesh treatment, consideration of an alternate slip function and additional parameter studies. These three categories form the basis of this supplementary report.

1.2.1 MESH STUDIES

(a) Suitability of Mesh Treatment

Concern was expressed regarding the suitability of DELTA's procedure for simulating coherent rupture using Green's functions spaced at approximately 1-km intervals over the surface of incipient rupture. The concern stems from the fact that wavelengths on the order of one-tenth of this spacing or 100 meters (20 Hz) are being modeled. This issue would be particularly pertinent if earthquake rupture could be reasonably approximated by coherent rupture. However, there is considerable evidence that actual earthquake ruptures are quite incoherent, as discussed in later sections. In fact, we have been unable to completely describe the rupture process in terms of basic principles of physics due to its complexity. Consequently, certain properties of the earthquake model must be calibrated using recorded strong motion data, particularly at high frequencies.

Due to the lack of coherence evidenced in physical rupture processes, the issue of being able to model an idealized coherent rupture is subordinate in importance to being able to achieve consistency. That is, the method must provide unbiased extrapolations from calibration earthquakes to predicted ground motions. Uniform spacings of Green's functions are used to provide such consistency. The ability to obtain mesh-independent results provides additional confidence in the suitability of the earthquake model for extrapolating results.

Studies were performed to establish the suitability of the mathematical treatment of these high frequencies under idealized conditions of coherent rupture. The first study performed dealt with a 1-km-square surface of rupture in the offshore geologic structure. Results from these studies were presented at the October 1978 meeting where the concensus was that these results demonstrated the suitability of the mesh treatment for that particular rupture surface. The staff and their consultants indicated that the problem of treating wavelengths shorter than the spacing of Green's functions would be acceptable if additional studies involving longer surfaces of rupture were equally mesh-size independent. Results presented in Section 2 of this report indicate that this is indeed the case. These results should serve to resolve the issue regarding the suitability of mesh treatment.

(b) Characterization of Incoherent Rupture

Mathematical idealization of coherent rupture has several drawbacks for modeling recorded earthquake ground motions. Coherent rupture excessively focuses energy in the direction of rupture, thereby producing a synthetic acceleration record made up principally of one large, isolated spike. Irregularities in actual earthquake ruptures represent a significant departure from such idealized focusing. To accommodate such phenomena, randomness has been introduced into the computer model.

Five types of incoherence have been introduced into DELTA's earthquake model. One to account for phenomena on length scales less than 1 km -- termed

"micro-incoherence," and four to account for phenomena on length scales of 1 km and greater -- termed "macro-randomness." The micro-incoherence has been introduced to prevent continuous rupture over a 1-km-square cell from focusing within one-tenth of a second at the receiver's station. Macro-randomness has been introduced into the earthquake model to: first, delay the time of rupture initiation; second, to alter the direction in which rupture progresses through the rupture segment; third, to alter the orientation of the rupture segment; and fourth to alter the orientation of particle motion at the receiver's position as generated by the rupture segment. Further explanation is given in Section 4 of this report, and several parameter studies are presented in Section 6.2 to illustrate the influence of each type of randomness. Basically, the randomness diminishes the extreme focusing that is produced by the coherent rupture, scatters the energy to produce a more realistic synthetic acceleration record, and diminishes the possibility of one horizontal component of synthetic ground motion being many times greater than the other component. Over all, the randomness provides a considerable improvement in modeling observed ground motions at the expense of obtaining results that vary somewhat for repetitious earthquake modeling.

1.2.2 SLIP FUNCTION STUDIES

There are two principal concerns expressed by the NRC and their consultants regarding the May 1978 slip function. First, there is a concern regarding the number of parameters it takes to define the slip function; that is, there may be more parameters than can be uniquely determined from earthquake data. The second concern pertains to the lack of variation in the maximum slip velocity from one earthquake to the next. The suggestion was made that the maximum slip velocity be adjusted as a function of earthquake magnitude (or, more preferably, static stress drop), and that results using this interpretation be extrapolated to obtain a demonstrational site-specific spectrum.

To satisfy these concerns, and to circumvent deficiencies resulting from a two-parameter slip function, a revised slip function has been developed which

involves three parameters: initial slip velocity, duration of slip, and final offset. As the duration of slip approaches the final offset divided by the maximum slip velocity, the new slip function reduces to the two-parameter slip function composed of a ramped step or a box function in slip velocity. Using this new slip function, an investigation has been conducted to determine how site-specific results depend on alternate interpretations of fault slip. In this study, each particular slip function is calibrated for the Parkfield and Imperial Valley Earthquakes. Results are then extrapolated to obtain site-specific spectra at San Onofre. This procedure is carried out for both the two-parameter slip function, and the more general three-parameter slip function, with and without randomness. The important conclusion from these studies is that the response spectrum for an earthquake offshore at San Onofre does not depend on the character of the particular slip function that is assumed for frequencies greater than 2 Hz, provided the particular slip function is calibrated to match high frequencies, as recorded for the Parkfield and Imperial Valley earthquakes. In other words, site-specific response spectra appear to be rather slip-function-independent when extrapolating from these two earthquakes. Furthermore, the three-parameter slip function, with a rise time of two to three seconds, provides a better match with observed data than the two-parameter function for frequencies of one Hz and below.

1.2.3 MODEL PARAMETER AND SENSITIVITY STUDIES

Some features of the current earthquake modeling procedure are different from those used in the May 1978 report. The principal differences include the spacing of Green's functions along rupture surfaces, particularly in the vertical direction; the method for simulating continuous rupture over intervals between the Green's functions; the particular details of the slip function; and the type of randomness included in the model. Because of these differences, the parameter studies presented in the May 1978 report have been repeated in this report. Additional parameter studies requested by the staff and their consultants have also been performed. First, we will summarize parameter studies presented in the May 1978 report.

Computed response spectra depend on the slip parameters (maximum slip velocity, duration of slip, and final offset) in essentially the same manner as demonstrated in the May 1978 report. The same is true for rupture velocity and fault length. Due to the significant increase in the amount of incoherence allowed in the rupture process, results are now less dependent upon hypocentral depth than in the earlier report. More significantly, the strong dependence of peak acceleration upon fault depth has nearly vanished, so that peak acceleration for a 13-km deep rupture is only about ten to twenty percent greater than the corresponding peak acceleration for a 10-km-deep rupture. This behavior is independent of randomness. As found in the earlier report, peak acceleration does not significantly depend upon the shallowness of the top of the rupture surface, provided the rupture extends to within two or three kilometers of the earth's surface.

Additional parameter studies were performed to illustrate how properties of the layered earth structure influence results as a function of frequency. Overall, these parameter studies indicate a very complex dependence of the results upon the layer properties. For example, changing layer thickness to arrive at a cruder geologic representation causes no discernible trend at high frequencies or low frequencies. The same is true for biases in the P-wave and S-wave velocities. On the other hand, biases in the earth's quality factor, Q, do show distinct trends which can be explained using simple geometric ray theory. The influence of Q is most pronounced for shallow source and distant receiver combinations. Such combinations do not produce maximum ground accelerations.

1.3 CONCLUSIONS

Three general categories of concern have been addressed in this supplementary report: mesh spacing, slip function, and model behavior (sensitivity). Mesh studies demonstrate the suitability of our method for obtaining mesh-independent results using the criterion established in the October 1978 meeting with the NRC staff and their consultants. The slip function used in the May 1978 report has been improved, and tests have been performed using this modified form as

well as a two-parameter slip function. Response spectra obtained using the two-parameter slip function are consistently above those obtained from recorded motions for periods longer than 0.5 sec. Results from shorter periods indicate that site-specific response spectra do not strongly depend upon the details of the slip functon or the rupture physics, provided each particular model is calibrated using strong motion recordings of the Parkfield and Imperial Valley Earthquakes. This conclusion is supported by Figures 1-1 through 1-3.

Earthquake models with a significant degree of rupture incoherence match recorded motions more closely than strictly coherent models. The vertical component of synthetic ground motion matches data more closely than that presented in the May 1978 report. Additionally, using the earthquake model with current improvements, we find the same maximum slip velocity for the Parkfield and Imperial Valley earthquakes. This result further supports our earlier hypothesis that maximum slip velocity is nearly constant from one earthquake to the next.

A conservative prediction of site-specific response spectra is obtained from a 40-km rupture located in a critical position with respect to the plant. Rupture parameters are set to the most extreme values extracted from calibration earthquakes. Stochastic properties of the earthquake model cause results to vary somewhat or the critical earthquake is simulated repetitiously. The mean and one standard deviation response spectra for these variations are compared with Housner's 2/3 g spectrum using two percent damping in Figures 1-4 through 1-6, and 10 percent damping in Figures 1-7 through 1-9.

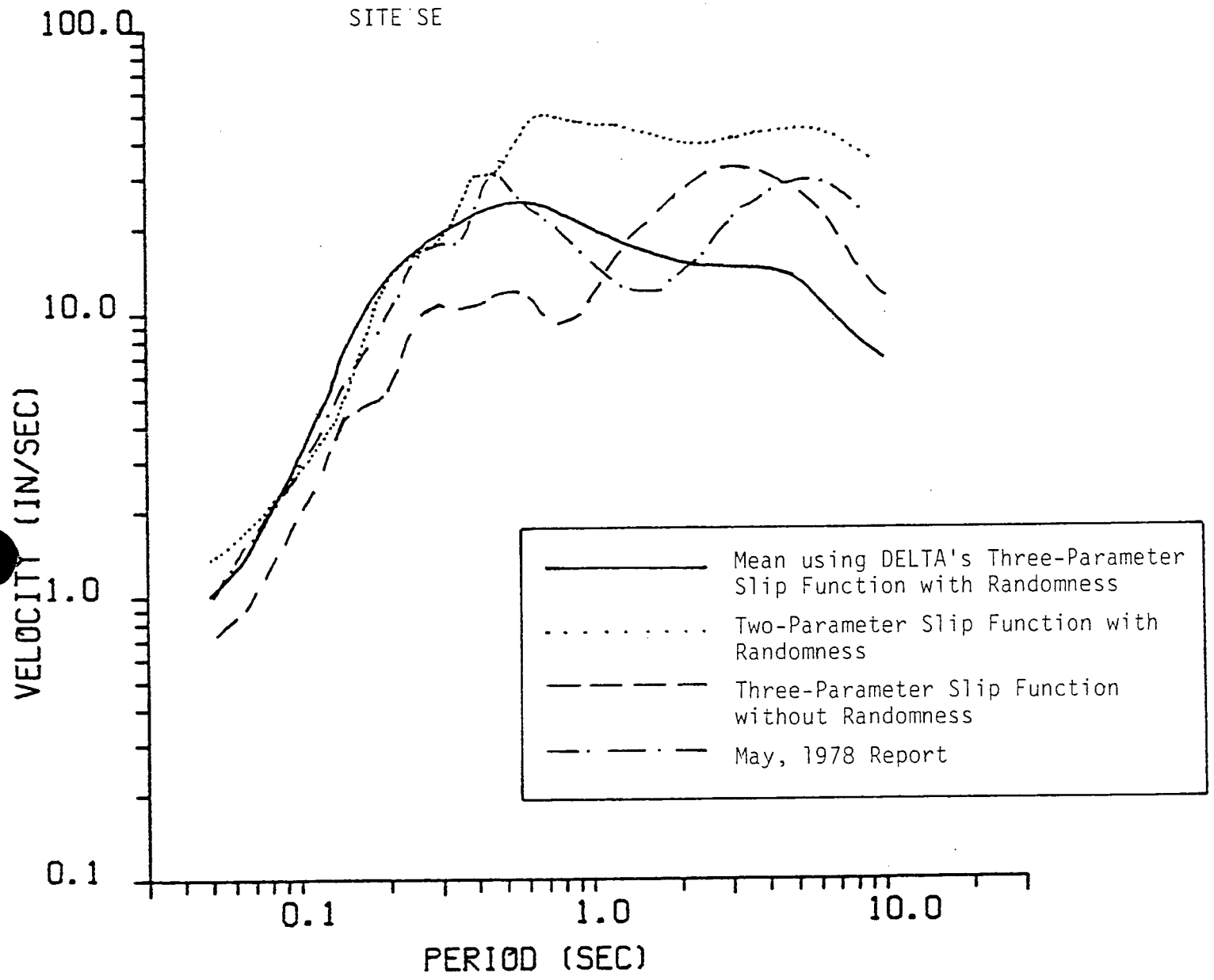

Figure 1-1. Site specific results using alternate rupture processes for southeast component.

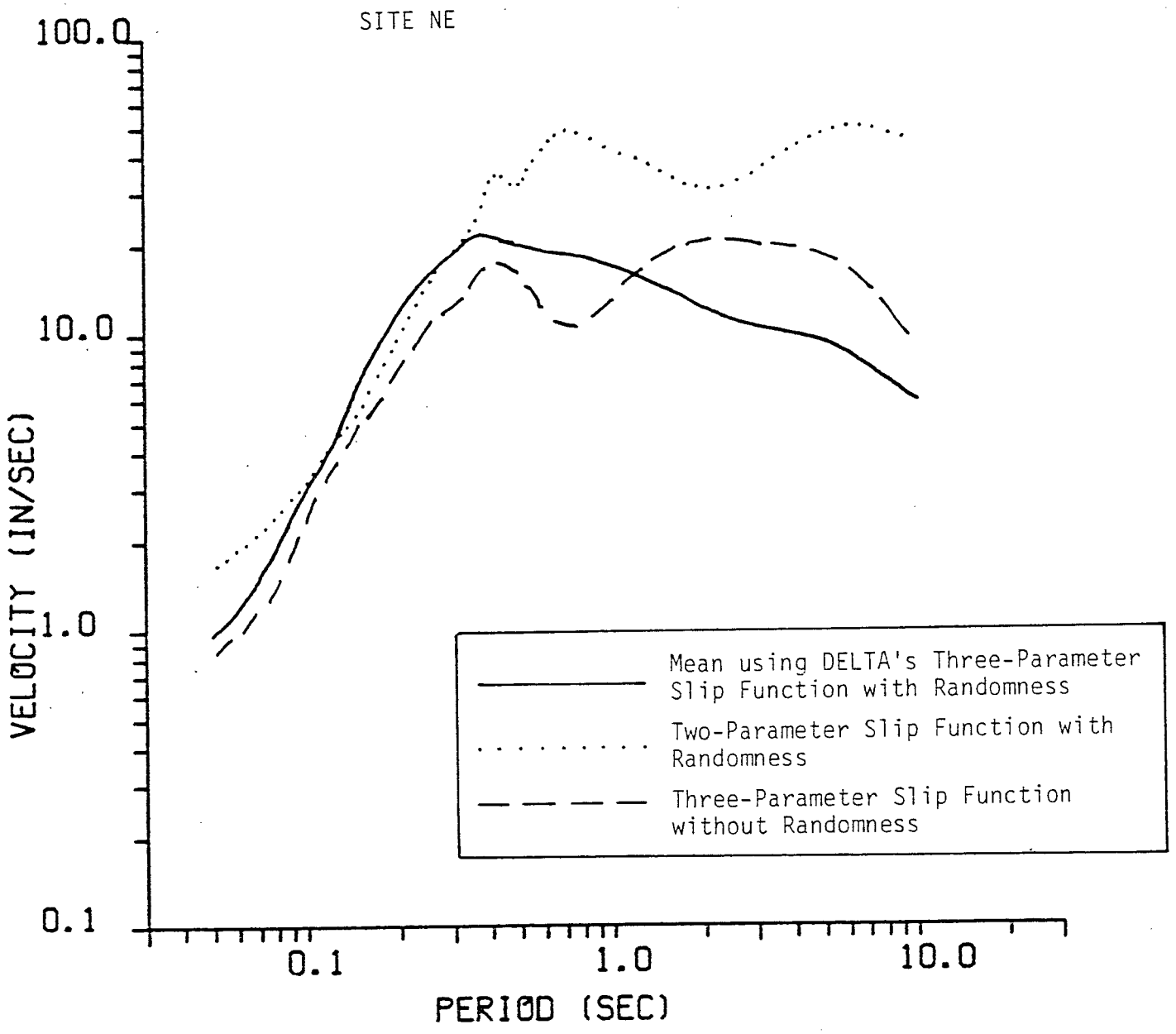

Figure 1-2. Site specific results using alternate rupture processes for northeast component.

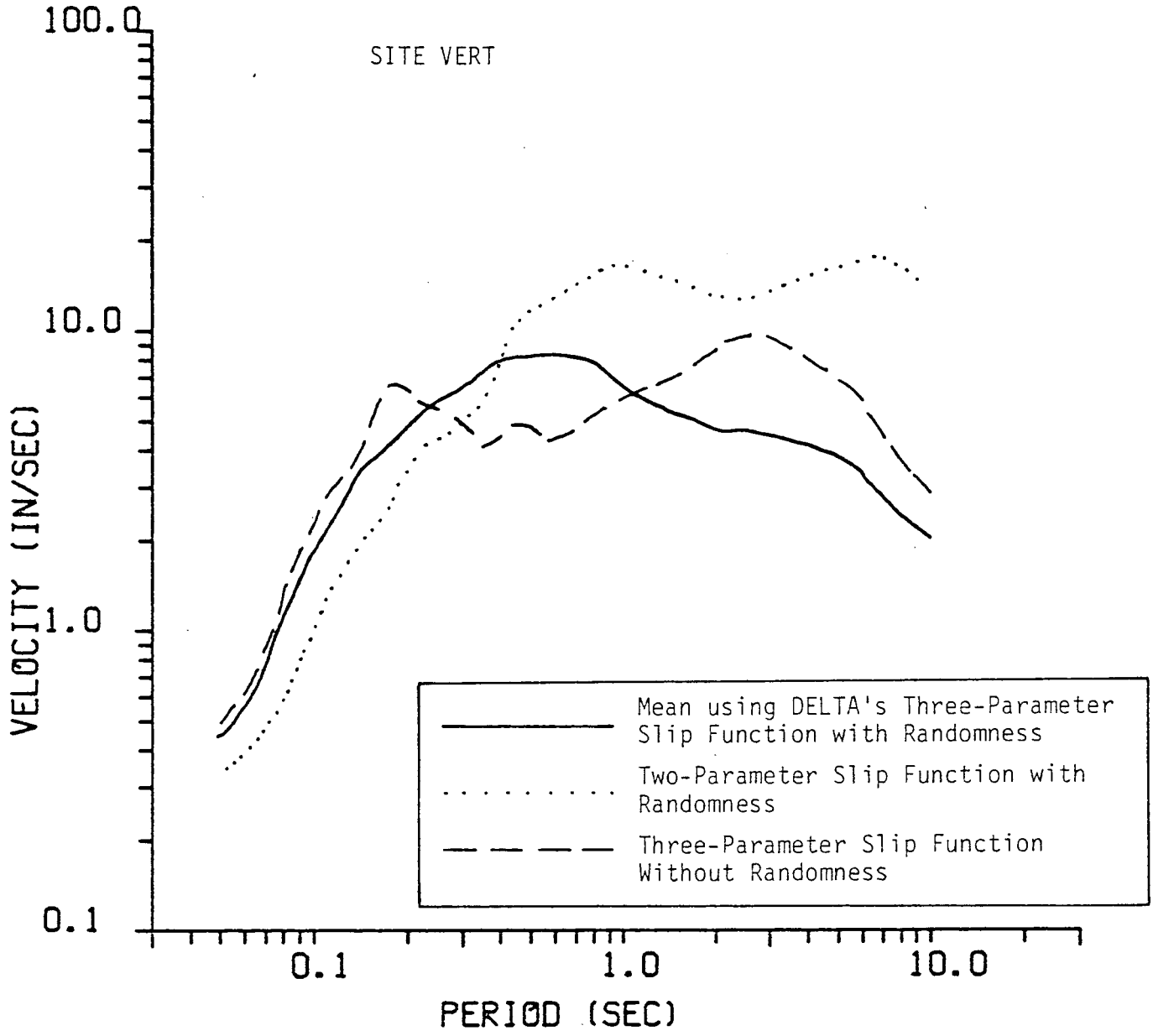

Figure 1-3. Site specific results using alternate rupture processes for vertical component.

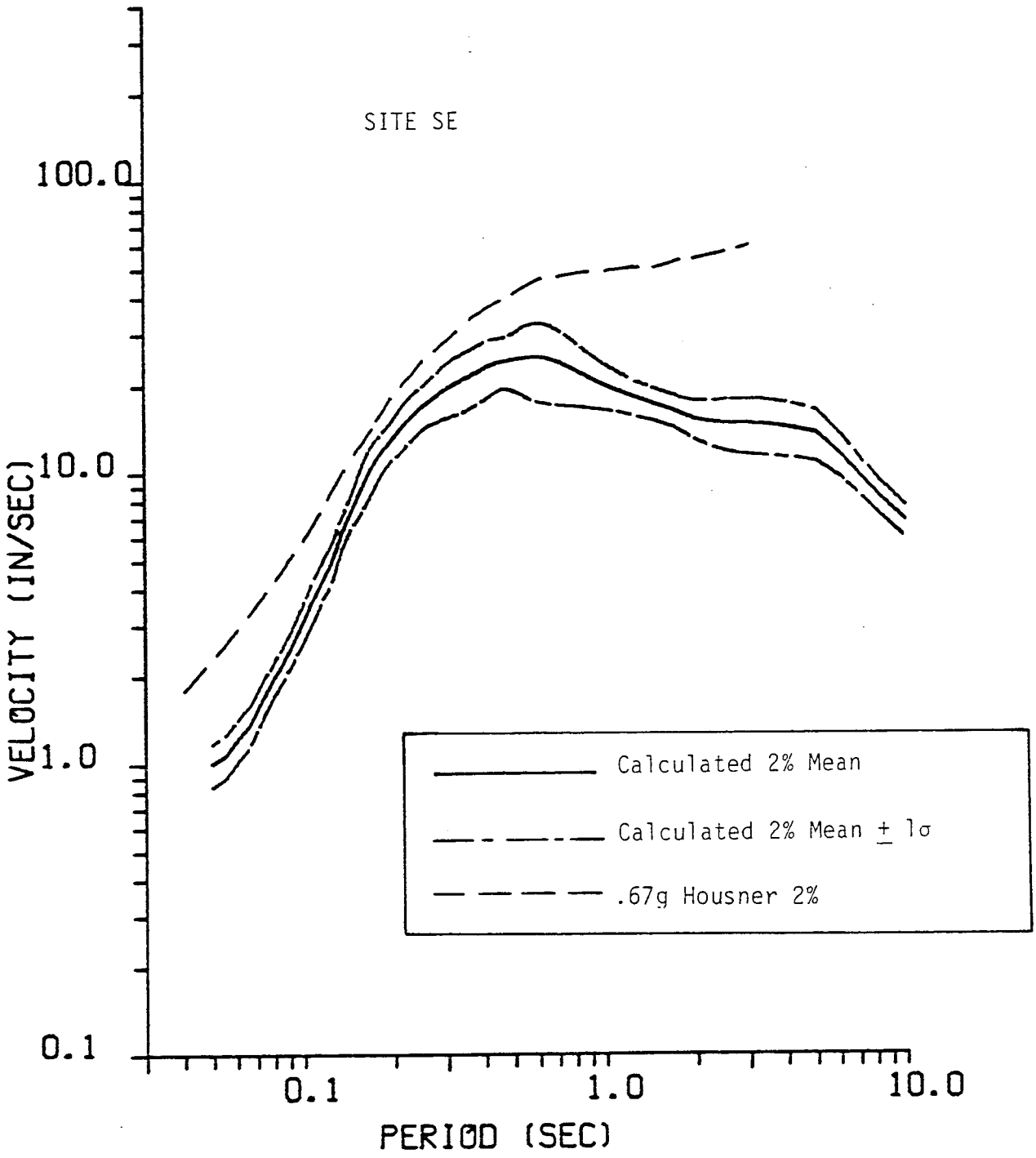

Figure 1-4. Calculated mean plus and minus one standard deviation for southeast component of response spectra (2% damping) for hypothesized earthquake "D", 8 km offshore from San Onofre Site.

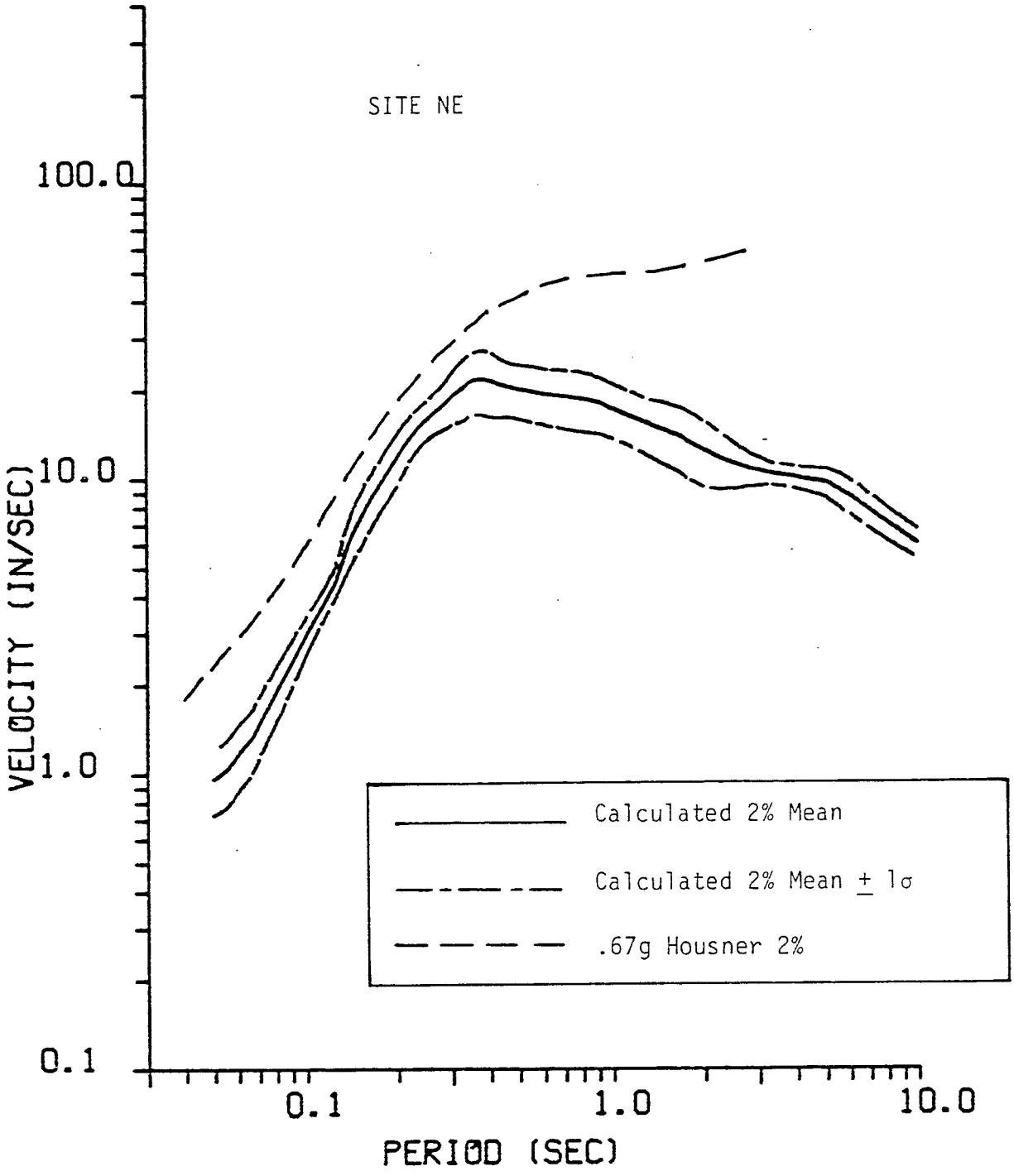

Figure 1-5. Calculated mean plus and minus one standard deviation for northeast component of response spectra (2% damping) for hypothesized earthquake "D", 8 km offshore from San Onofre Site.

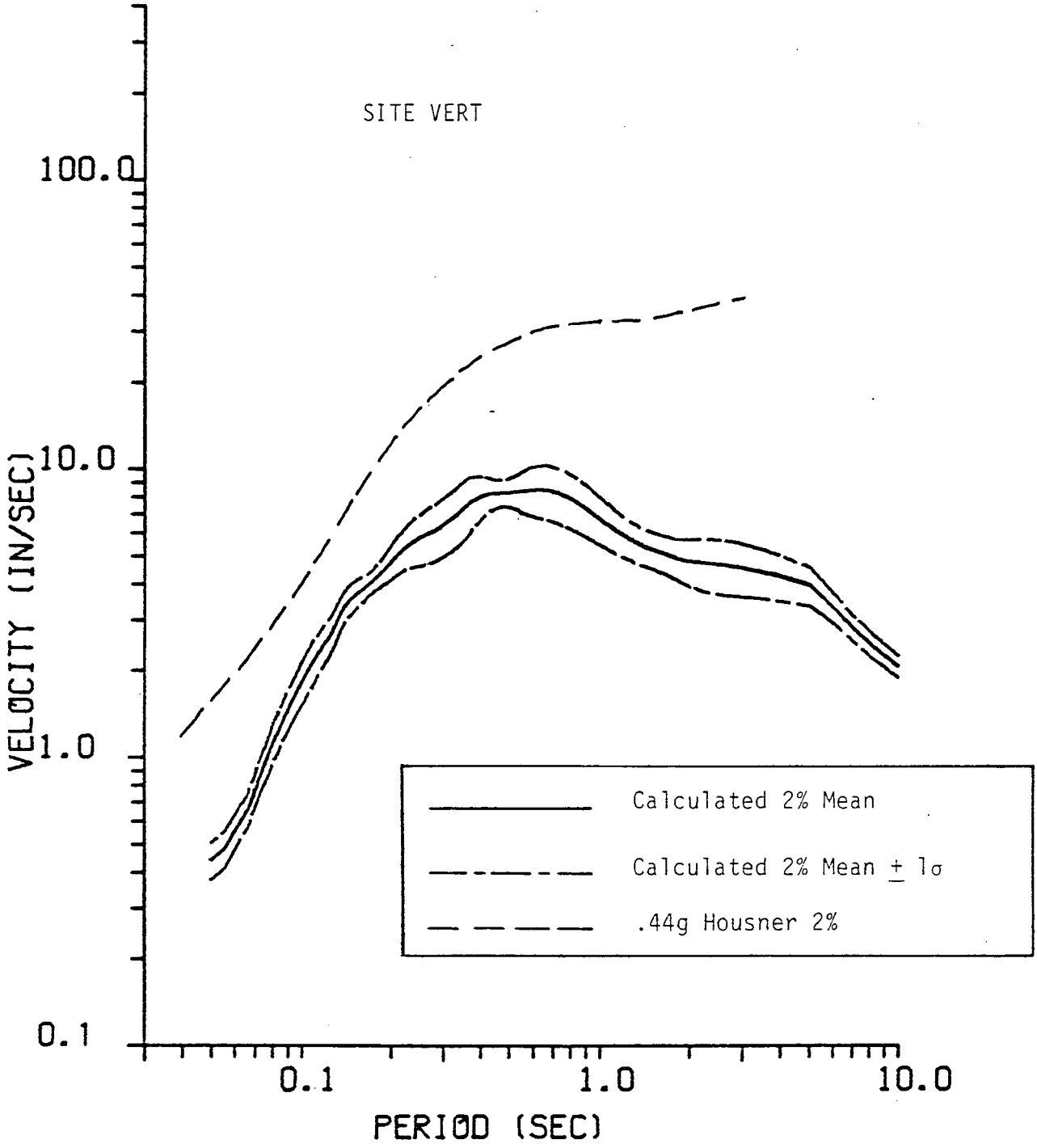

Figure 1-6. Calculated mean plus and minus one standard deviation for vertical component of response spectra (2% damping) for hypothesized earthquake "D", 8 km offshore from San Onofre Site.

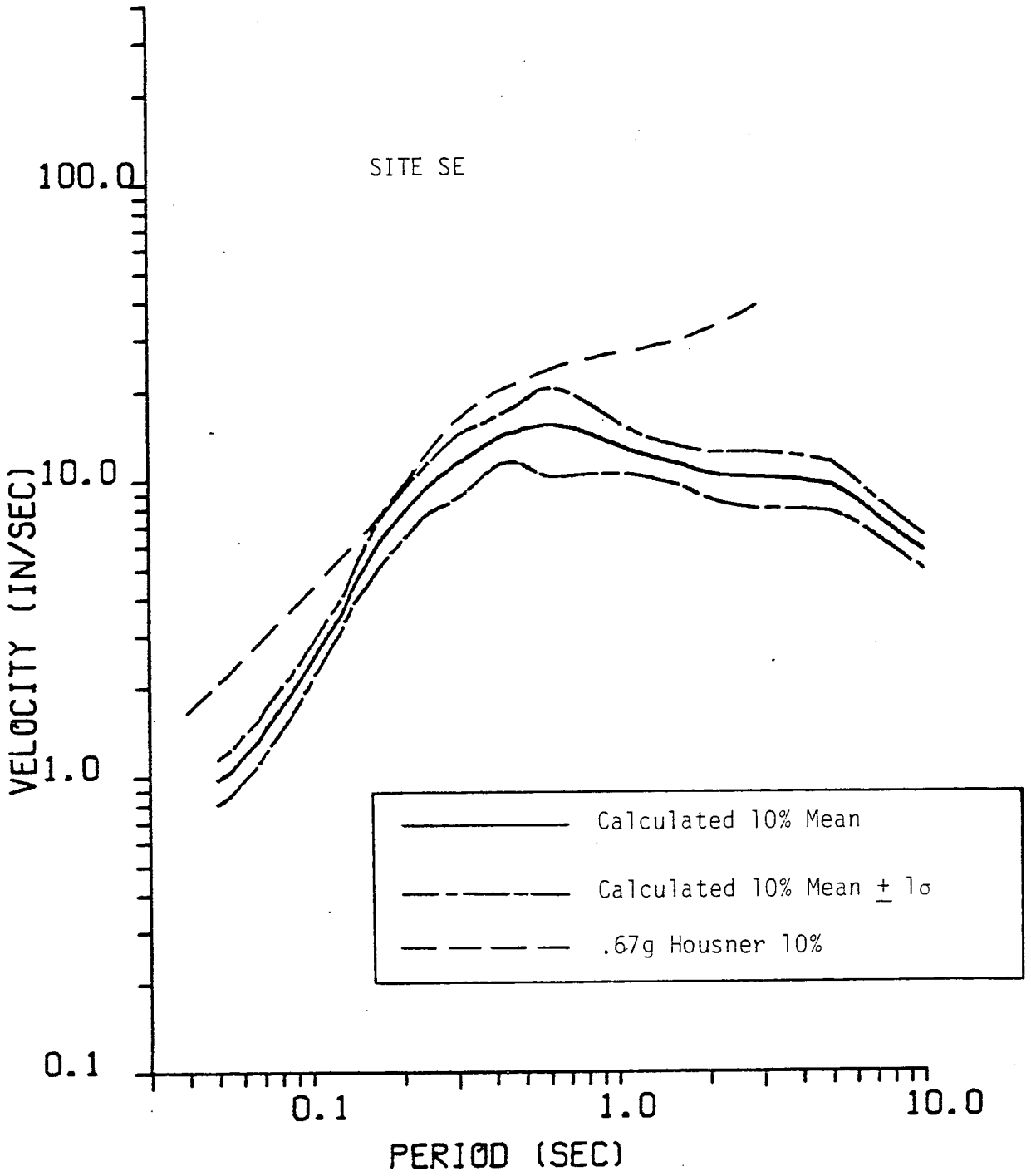

Figure 1-7. Calculated mean plus and minus one standard deviation for southeast component of response spectra (10% damping) for hypothesized earthquake "D", 8 km offshore from San Onofre Site.

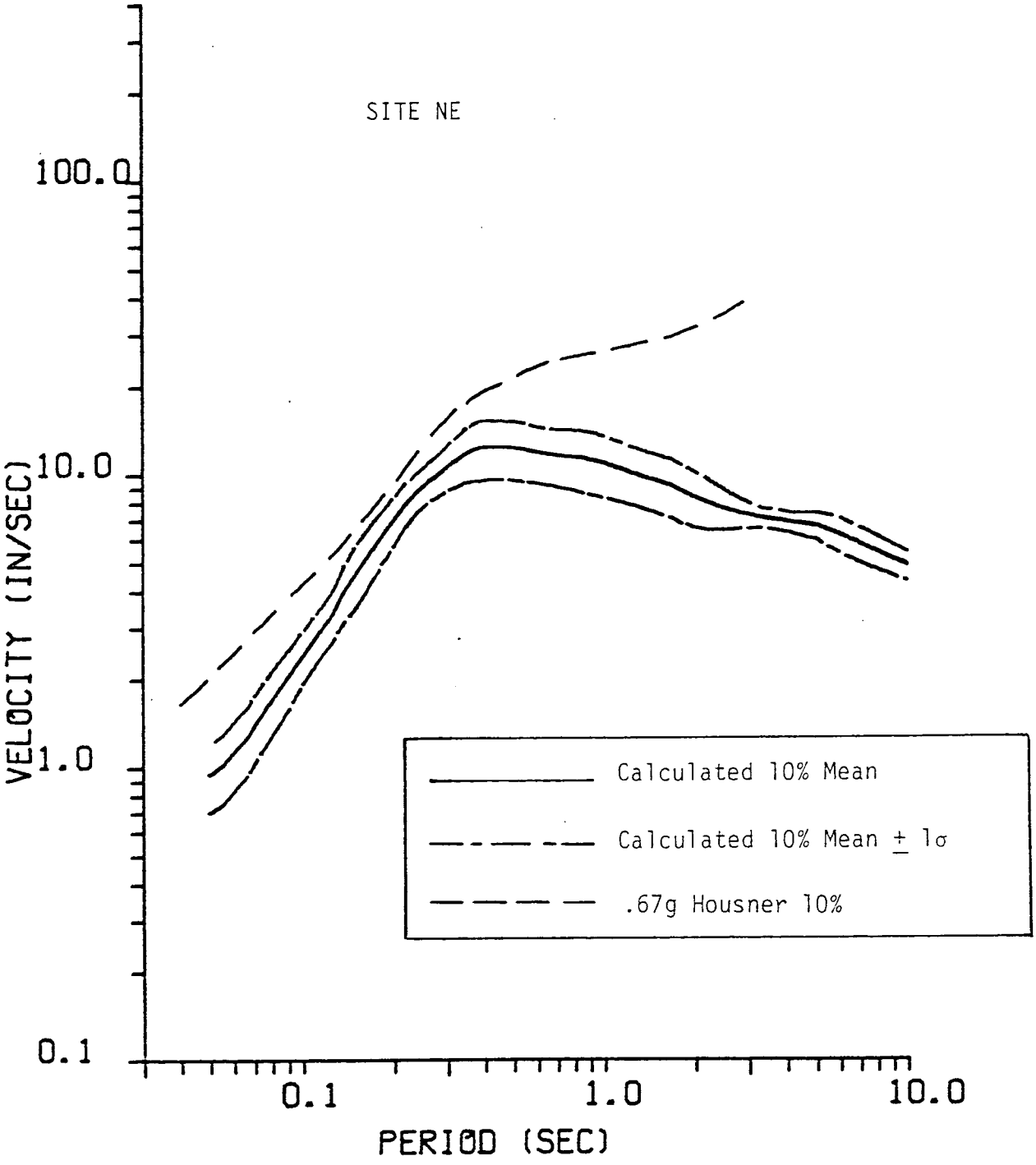

Figure 1-8. Calculated mean plus and minus one standard deviation for northeast component of response spectra (10% damping) for hypothesized earthquake "D", 8 km offshore from San Onofre Site.

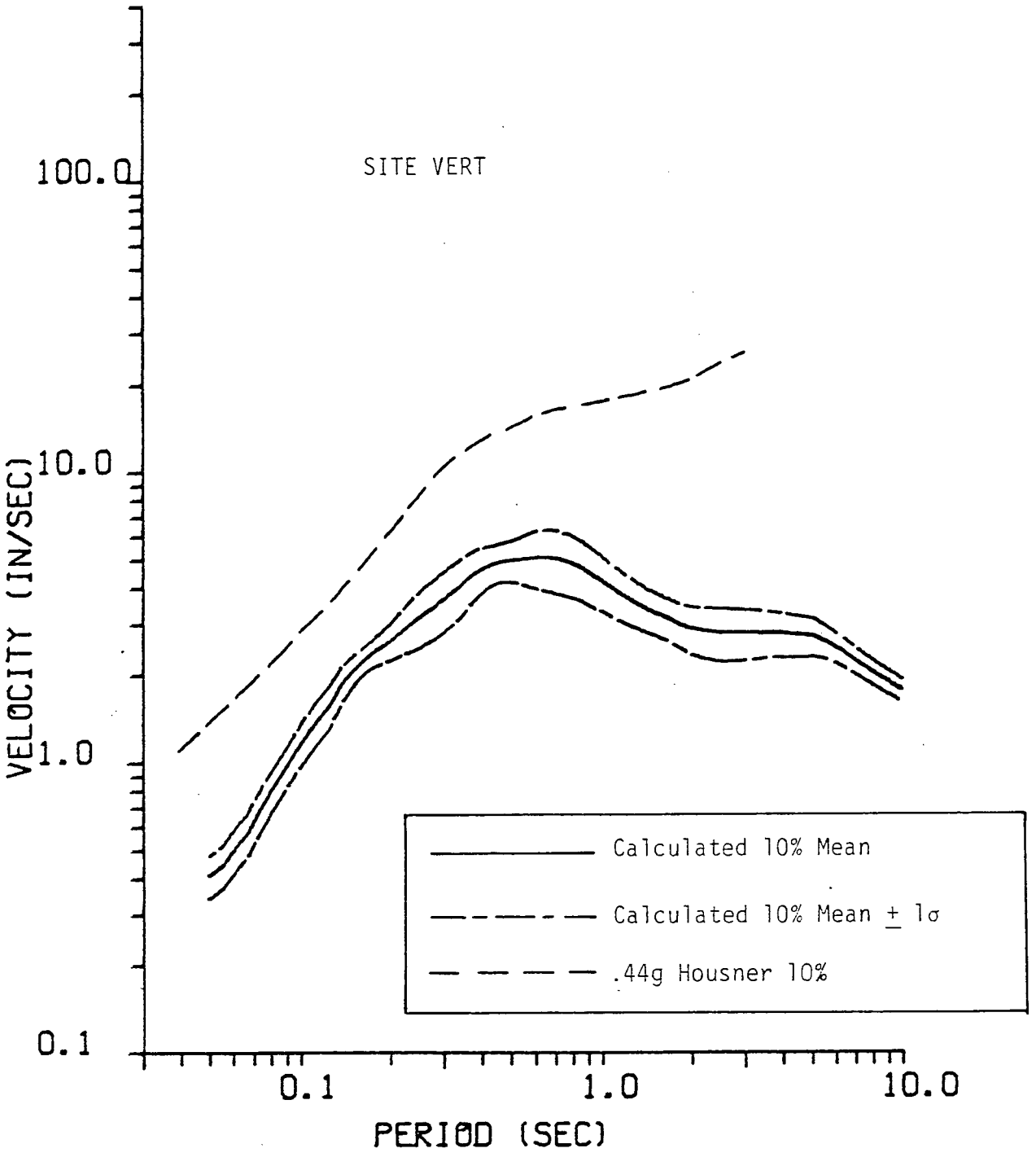

Figure 1-9. Calculated mean plus and minus one standard deviation for vertical component of response spectra (10% damping) for hypothesized earthquake "D", 8 km offshore from San Onofre Site.

2.0 MESH SIZE STUDIES

2.1 MESH SIZE -- INTRODUCTION

Synthetic earthquake ground motions are modeled using digital computers. A mathematical characterization of fault slip is convolved, spatially and temporally, with the Green's function of a somewhat idealized representation of the earth to produce synthetic records of ground motions. The response of the earth to fault slippage, as portrayed by the Green's functions, is calculated at several hundred positions along that portion of the fault surface that is to undergo rupture. Because of computing limitations, these Green's functions are typically spaced at one-km intervals over the surface of incipient rupture. The issue regarding mesh spacing is: To what degree are the computed ground motions influenced by the spacing of the Green's functions along the fault surface?

The objective in resolving this issue has been to determine whether or not calculated ground motions (response spectra) are significantly influenced by the mesh spacing along the fault surface. The ideal demonstration would be to simply perform a comparative calculation using a mesh spacing of 100 m. However, this direct approach is computationally intractible. For this reason, comparative calculations are performed using mesh spacing of 1, ½, and ¼ km along restricted portions of the entire rupture surface, namely:

(a) A one-km-square surface of rupture centered at a depth of 1.94 km;

(b) An approximately 10-km-long horizontal band of rupture with a width of 0.2 km and centered at a depth of 1.5 km; and

(c) An approximately 13-km-long vertical band rupture with a width of 0.25 km which extends to within 0.32 km of the earth's surface.

Response spectra are computed for focused and defocused receivers at epicentral distances of approximately 1 km to 20 km for the three fault configurations described above. Results using the three mesh spacings (1, ½, and ¼ km) are compared for the geometric configurations just described.

This calculational sequence is considered sufficient to reveal how sensitive ground motions are to mesh spacing. Results from these calculations, which are summarized below, indicate that computed response spectra are not significantly influenced by mesh spacing.

2.2 MESH SIZE -- FORMULATION

Figure 2-1 presents the mathematical principle for convolving fault slip, $s(\underset{\sim}{y}, \tau)$, with the Green's function of earth, $g(\underset{\sim}{x}, t; \underset{\sim}{y}, \tau)$, to obtain the synthetic ground motion record, $u(\underset{\sim}{x}, t)$, where $(\underset{\sim}{y}, \tau)$ denote receiver coordinates. Figure 2-2 presents the basic simplifications that are adopted to facilitate use of a discrete mesh of Green's functions. These simplifications first include the mathematical statement that fault slip is spatially invariant. This approximation is presented to facilitate the current discussion; the validity of the mesh treatment, established in this manner, does not limit the model to spatially invariant slip.

The second simplification presented in Figure 2-2 pertains to the way in which Green's functions are interpolated between mesh points along the fault surface. Basically, the Green's function at each point on the fault surface is approximated by the Green's function of the nearest mesh point, shifted in time to reflect the travel time delay of the direct shear wave from the source to the receiver. The amplitude of the neighboring Green's function is also scaled to reflect change in amplitude with change in distance. The time shift is of considerably greater consequence than the amplitude scaling which is only significant for distances less than about 5 to 10 km.

The third simplification presented in Figure 2-2, which involves a spatial integral over one area of mesh, has been eliminated in recent calculations, i.e.,

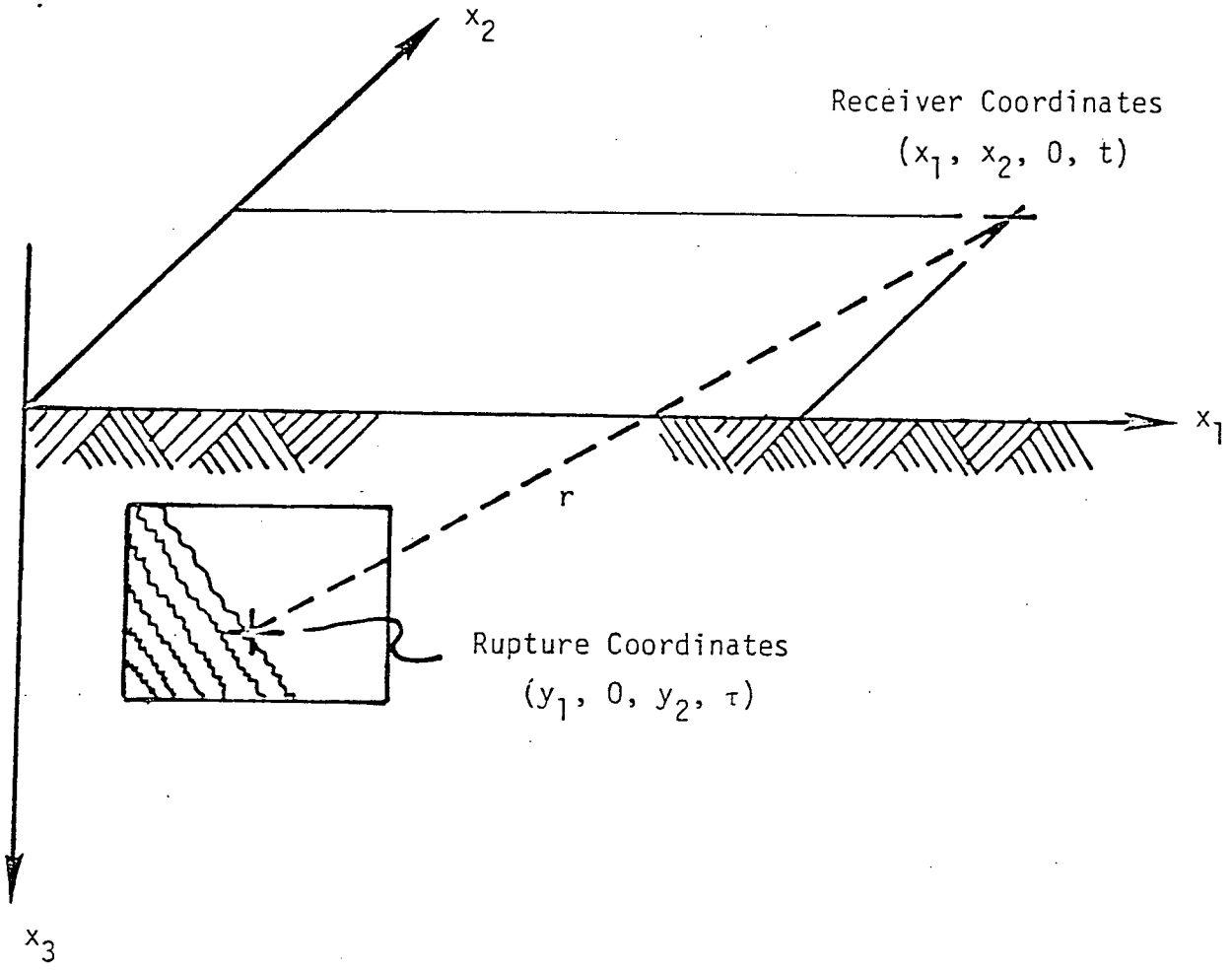

$$\begin{pmatrix}\text{Ground}\\ \text{Motion}\end{pmatrix} = \begin{pmatrix}\text{Slip}\\ \text{Function}\end{pmatrix} * * \begin{pmatrix}\text{Green's}\\ \text{Function}\end{pmatrix}$$

$$u(\underset{\sim}{x},\ t) = \int\int_{A} dS(\underset{\sim}{y}) \int_{\tau=0}^{t} d\tau\ s(\underset{\sim}{y},\ \tau)\ g(\underset{\sim}{x},\ t;\ \underset{\sim}{y},\ \tau)$$

Figure 2-1. Ground motion equation.

1. SPATIALLY INVARIANT SLIP

$$s(\underset{\sim}{y}, \tau) = s(\tau) * \delta(\tau - \tau_R)$$

where $\tau_R \sim \underset{\sim}{y} \cdot \underset{\sim}{n}/V_R$ is the time of rupture initiation.

2. LOCALLY SIMILAR GREEN'S FUNCTIONS

$$g(\underset{\sim}{x}, t; \underset{\sim}{y}, \tau) \approx g(\underset{\sim}{x}, t; \underset{\sim}{y}_n, \tau) * \delta(\tau - \Delta\tau_n)\left(\frac{r_n}{r}\right)^p$$

where $\Delta\tau_n \sim (r - r_n)/\beta$ is the travel time delay

3. LOCAL INTEGRAL APPROXIMATION

$$\iint_{A_n} dS(\underset{\sim}{y})\,\delta(\tau - \tau_R - \Delta\tau_n)\left(\frac{r_n}{r}\right)^p \approx$$

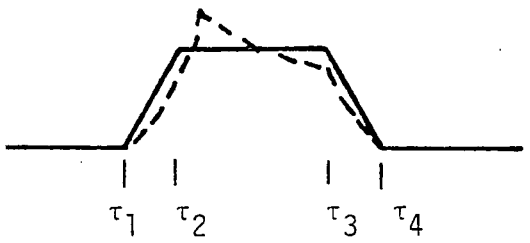

where $\tau_i = (\tau_R + \Delta\tau_n)_i$ is the time delay due to both rupture and travel time at the ith corner of the rupture segment.

Figure 2-2. Simplifications to be incorporated into the ground motion equation.

$$u(\underset{\sim}{x},\ t) = \iint_A dS(\underset{\sim}{y}) \int_{\tau=0}^{t} d\tau\ s(\underset{\sim}{y},\ \tau)\ g(\underset{\sim}{x},\ t;\ \underset{\sim}{y},\ \tau)$$

$$\approx \sum_n \iint_{A_n} dS(\underset{\sim}{y})\ s(\tau) * \delta(\tau - \tau_R) * g(\underset{\sim}{x},\ t;\ \underset{\sim}{y}_n,\ \tau) * \delta(\tau - \Delta\tau_n) \left(\frac{r_n}{r}\right)^p$$

$$\approx \sum_n s_n(\tau) * g(\underset{\sim}{x},\ t;\ \underset{\sim}{y}_n,\ \tau) * \iint_{A_n} dS(y)\ \delta(\tau - \tau_R - \Delta\tau_n) \left(\frac{r_n}{r}\right)^p$$

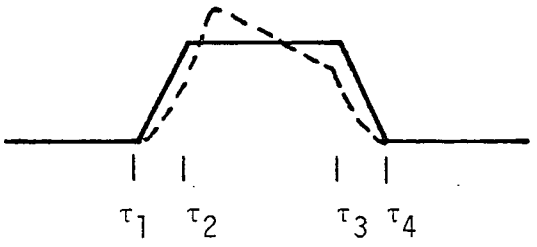

Figure 2-3. Reduction of the general ground motion equation to obtain DELTA's computational scheme.

essentially exact integrals are now being used. In work prior to July 1978, the integral of delay times over each mesh area was approximated by a trapezoidal shaped time function portraying the rupture front passing through the mesh area as described in TERA/DELTA's report on modeling earthquake ground motions.[3] Approximations arise in the use of the trapezoidal filter for fault zones in which the radius of curvature of the rupture front approaches the mesh spacing.

Simplifications one and two, presented in Figure 2-2, are used in Figure 2-3 to reduce the general ground motion equation to the current computational scheme for treating a discrete mesh of Green's functions. The summation over n represents a summation of the contributions of rupture over individual mesh areas, typically spaced at 1 km. Thus, the modified ground motion equation involves three terms which are convolved in time and summed over the surface of rupture. The three terms consist of the slip function, the Green's function, and a filter which characterizes the spatially distributed nature of the rupture process over each mesh area.

2.3 MESH SIZE -- RESULTS

Calculated ground motions (response spectra) are compared for the three fault configurations described in Section 2.1 using mesh spacings of 1, ½, and ¼ km. The comparative calculations are displayed in Figures 2-4 through 2-13 for unsmoothed response spectra and in Figures 2-14 through 2-23 for the corresponding smoothed response spectra. In all of the response spectral calculations, two percent damping is used.

The particular fault/receiver geometry, as well as the rupture orientation, is shown graphically above each comparative study. The rupture and receiver coordinates are consistent with the definition of Figure 2-1. For example, in Figure 2-4, the hypocenter is located at a depth of 2.44 km. The rupture is focused toward the receiver at an epicentral distance of 2 km from the hypocenter with the receiver located a surface distance of 1 km from the nearest point on the one-km-square rupture surface. The geological structure

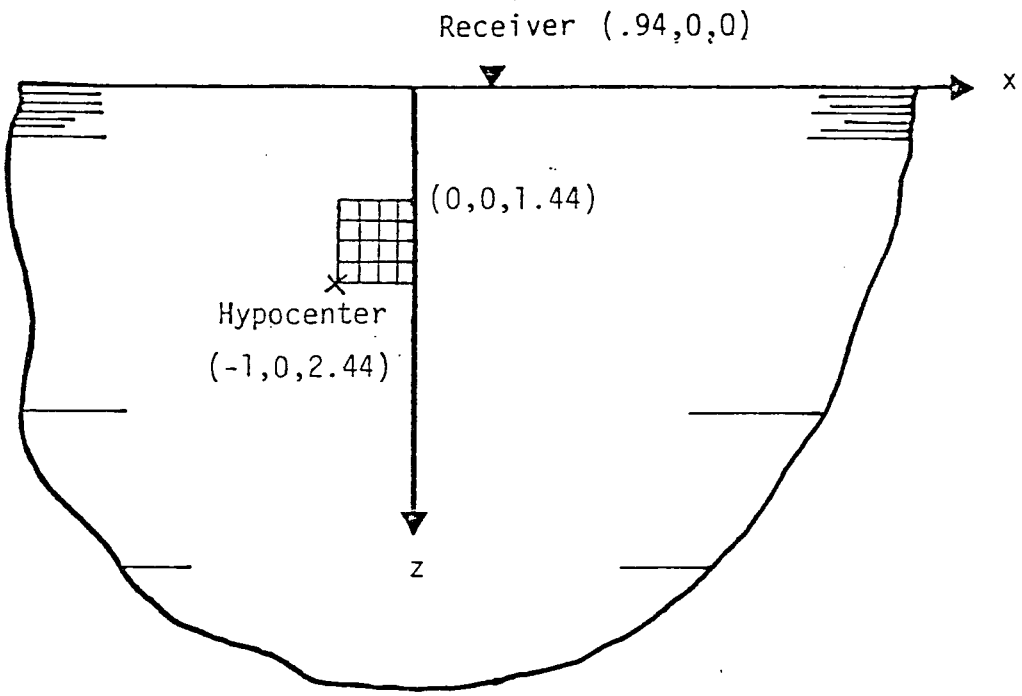

Figure 2-4. Close in mesh size study (focussed).

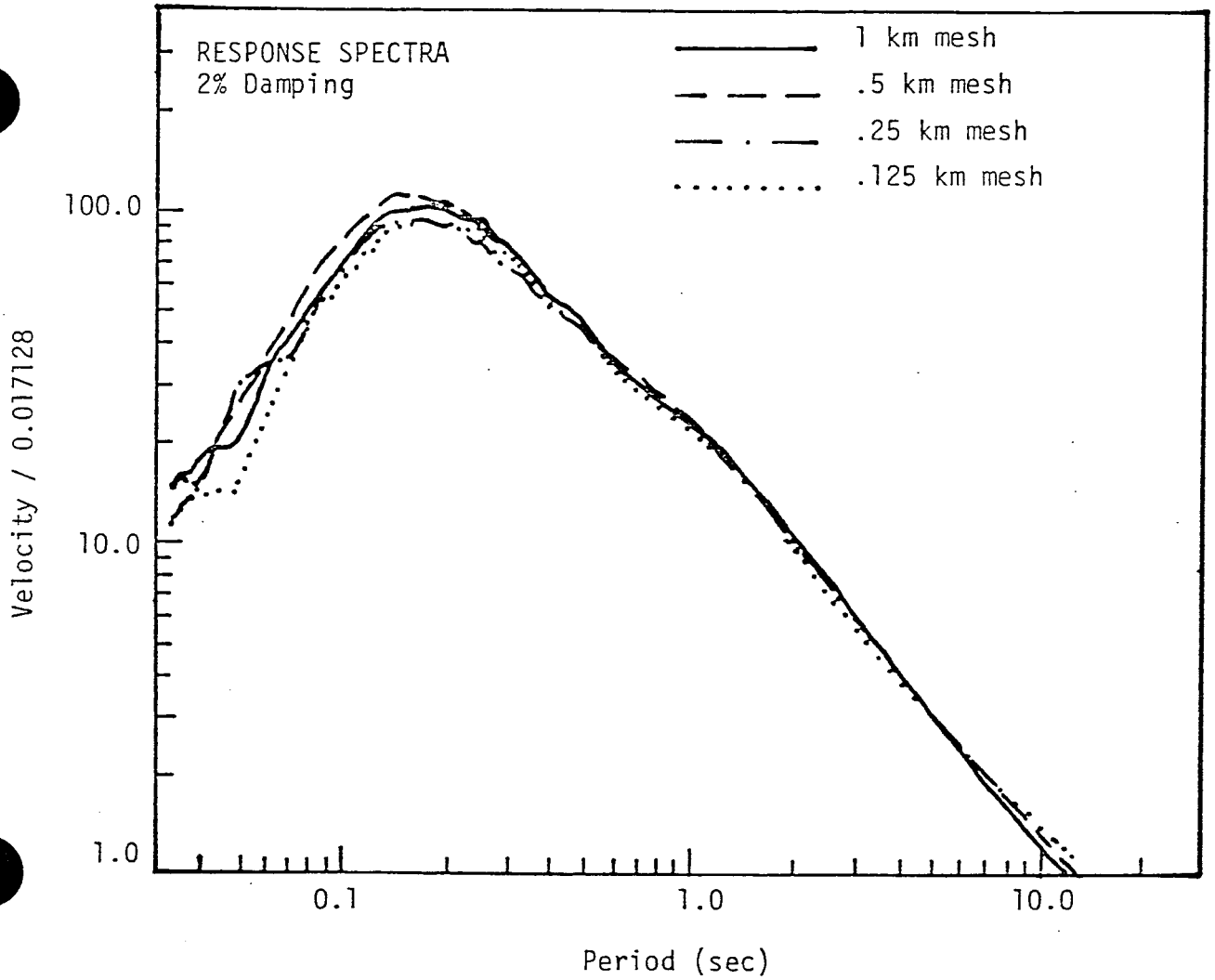

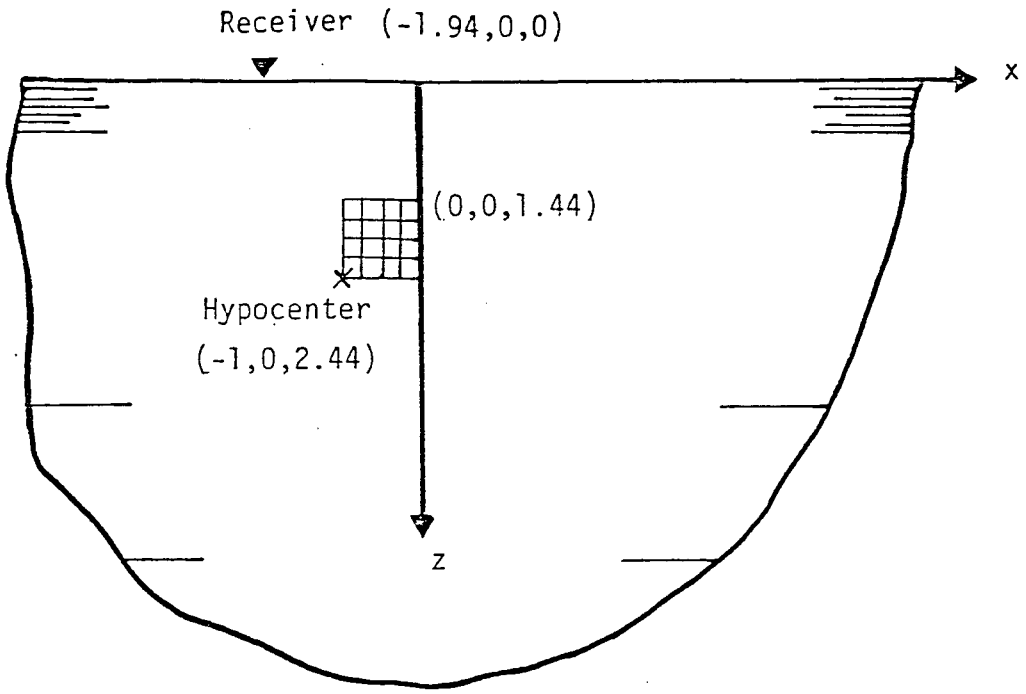

Figure 2-5. Close in mesh size study (defocussed).

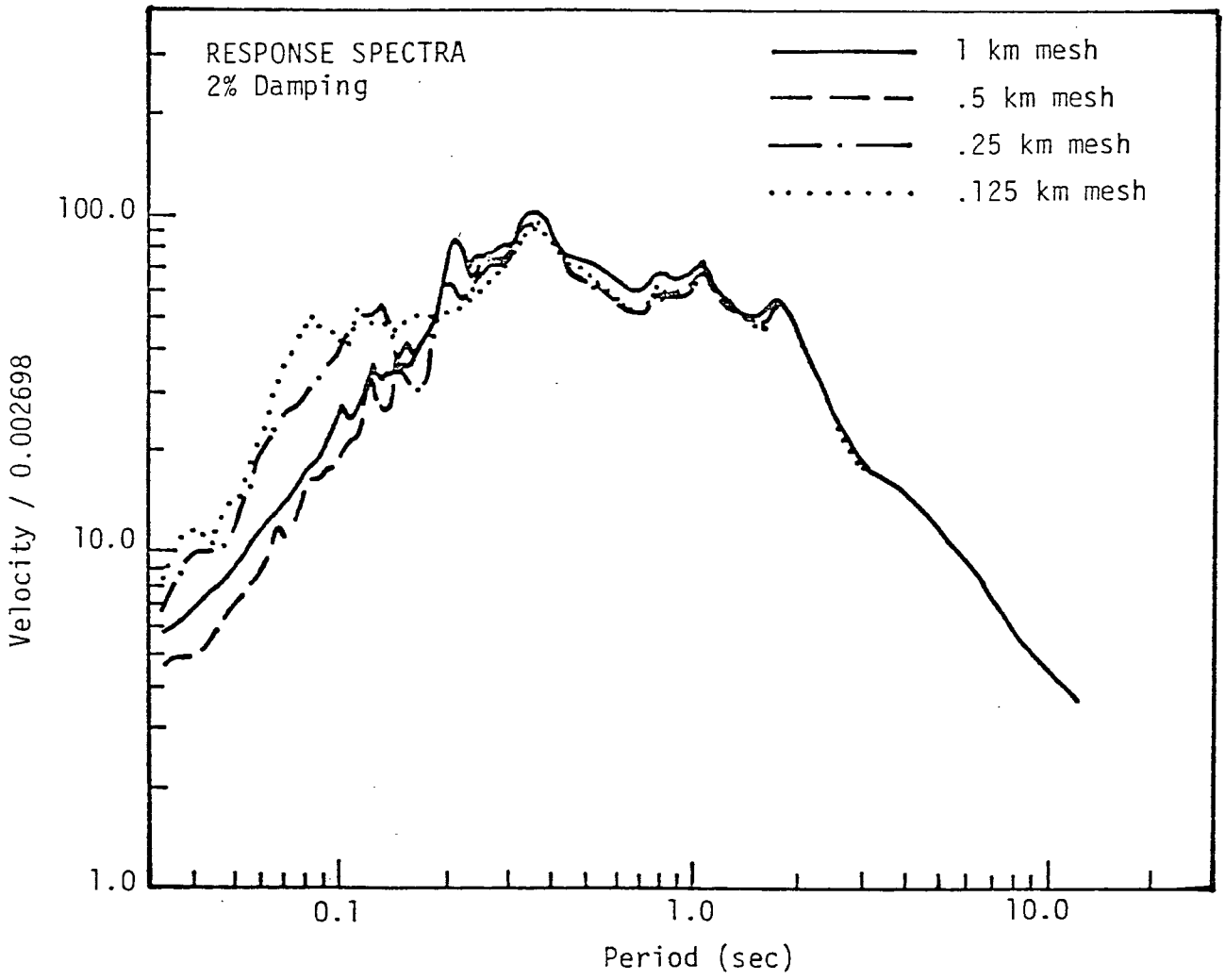

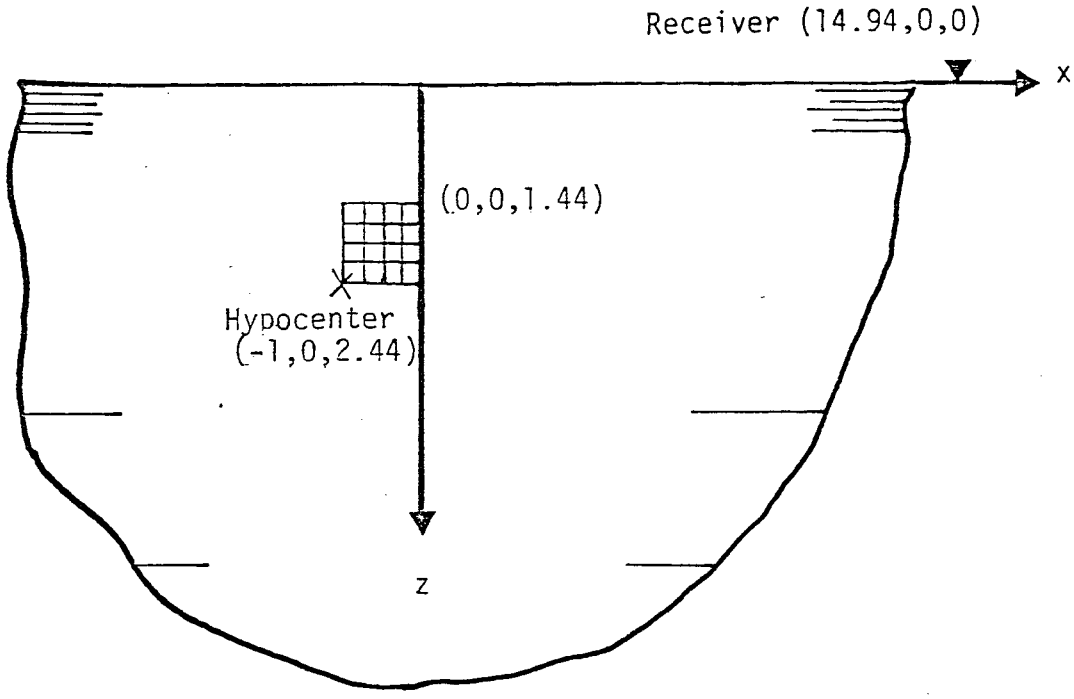

Figure 2-6. Far away mesh size study (focussed).

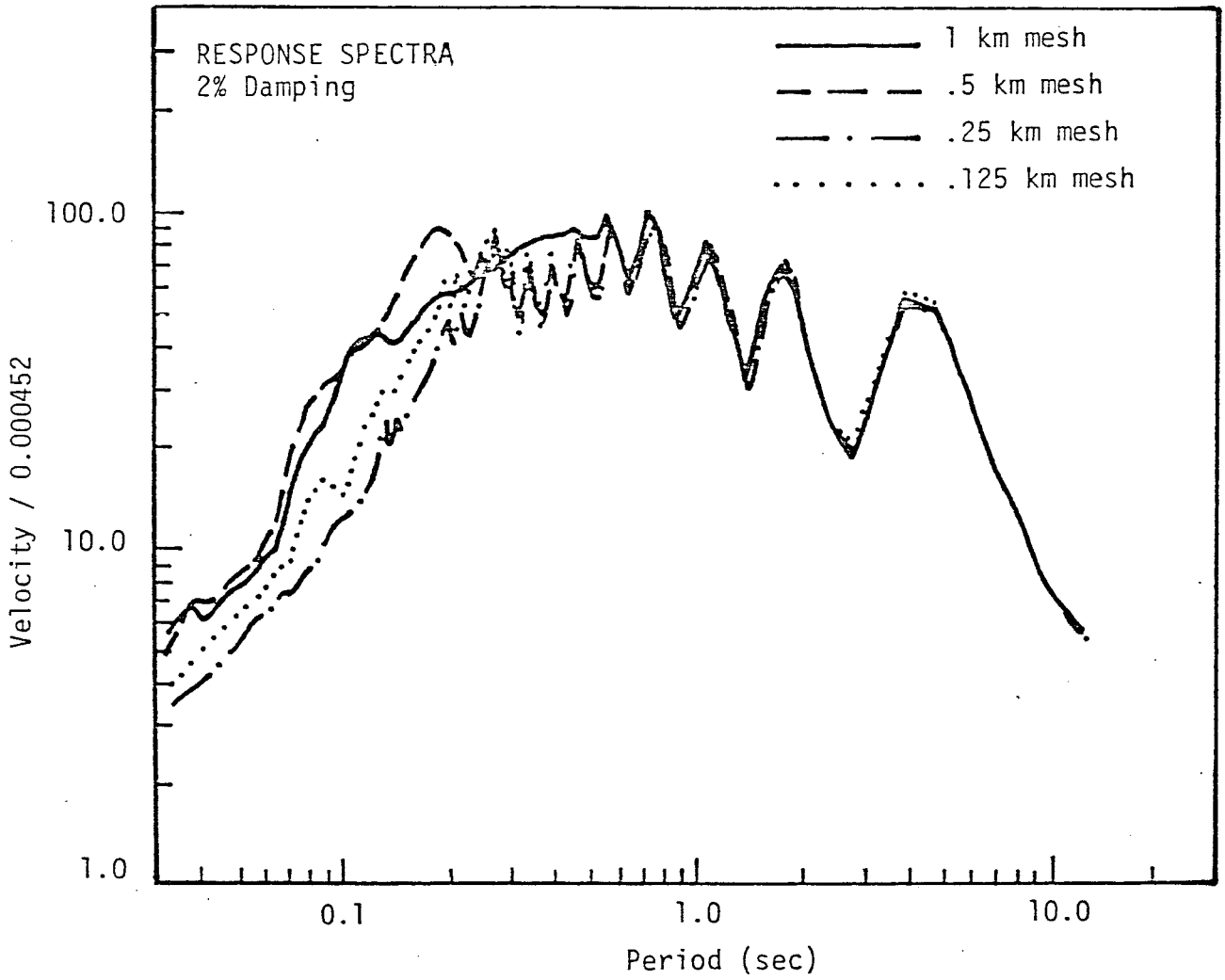

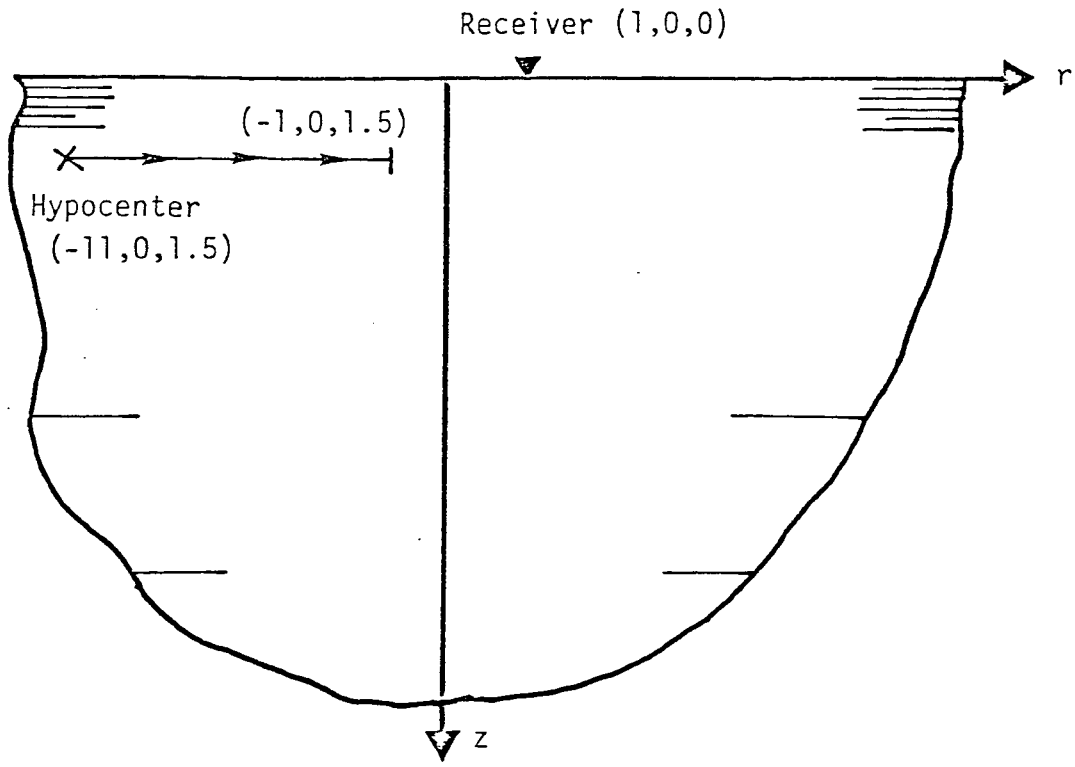

Figure 2-7. Close in horizontal line source study (focussed).

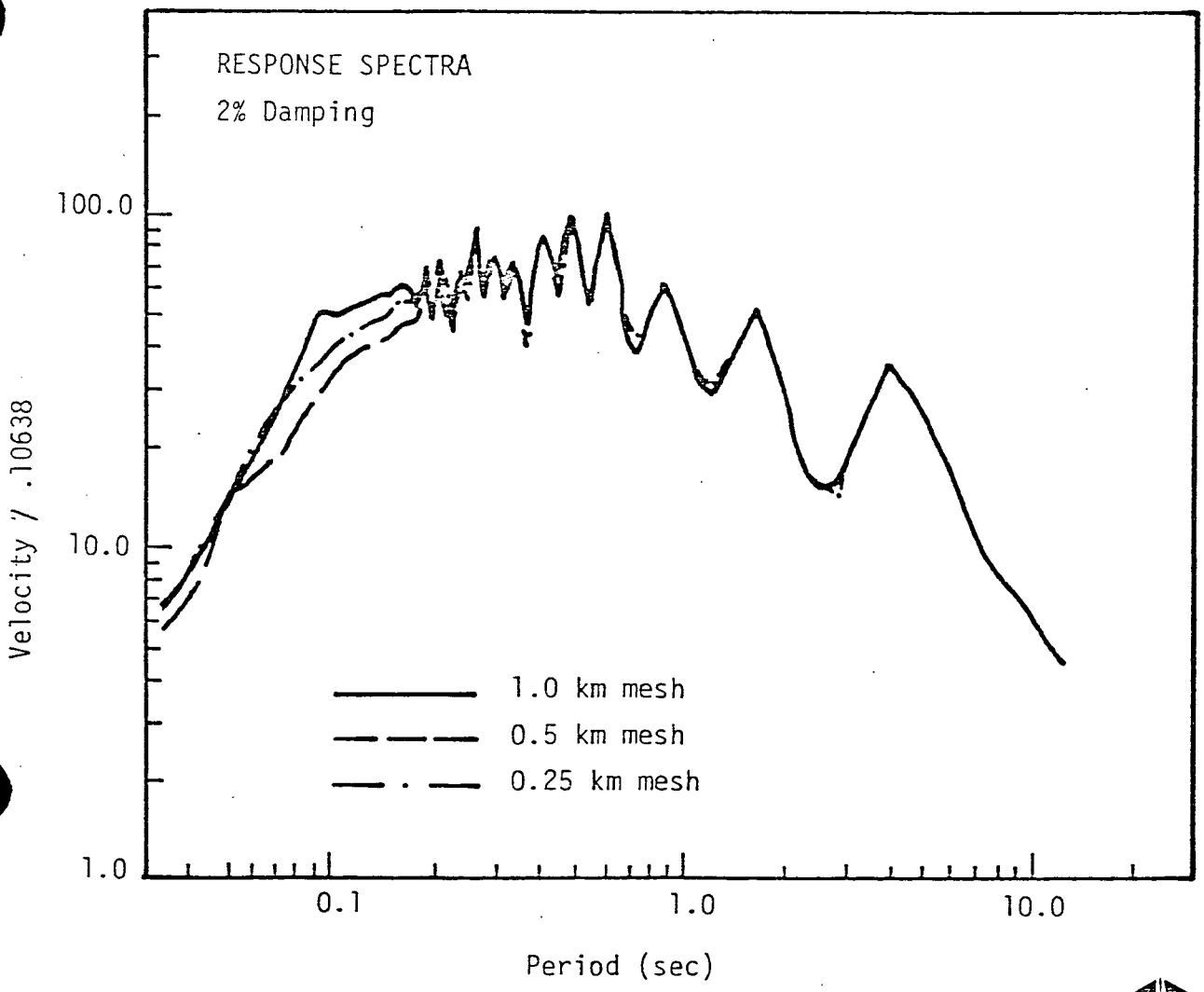

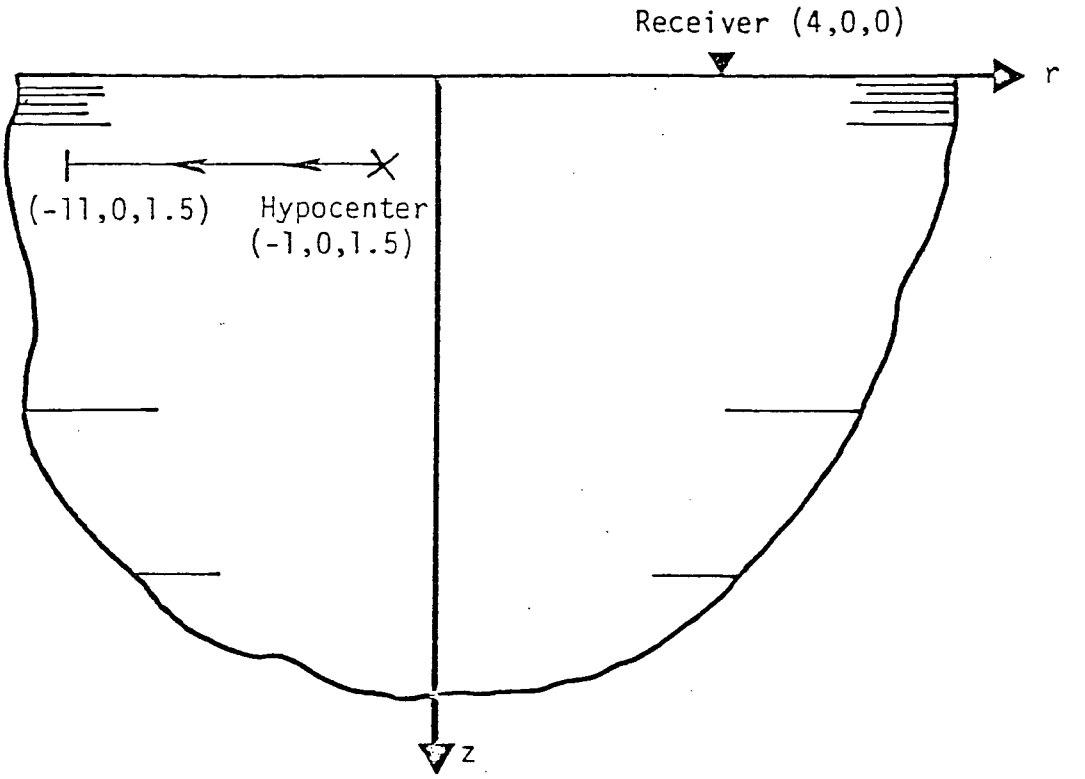

Figure 2-8. Intermediate horizontal source study (defocussed).

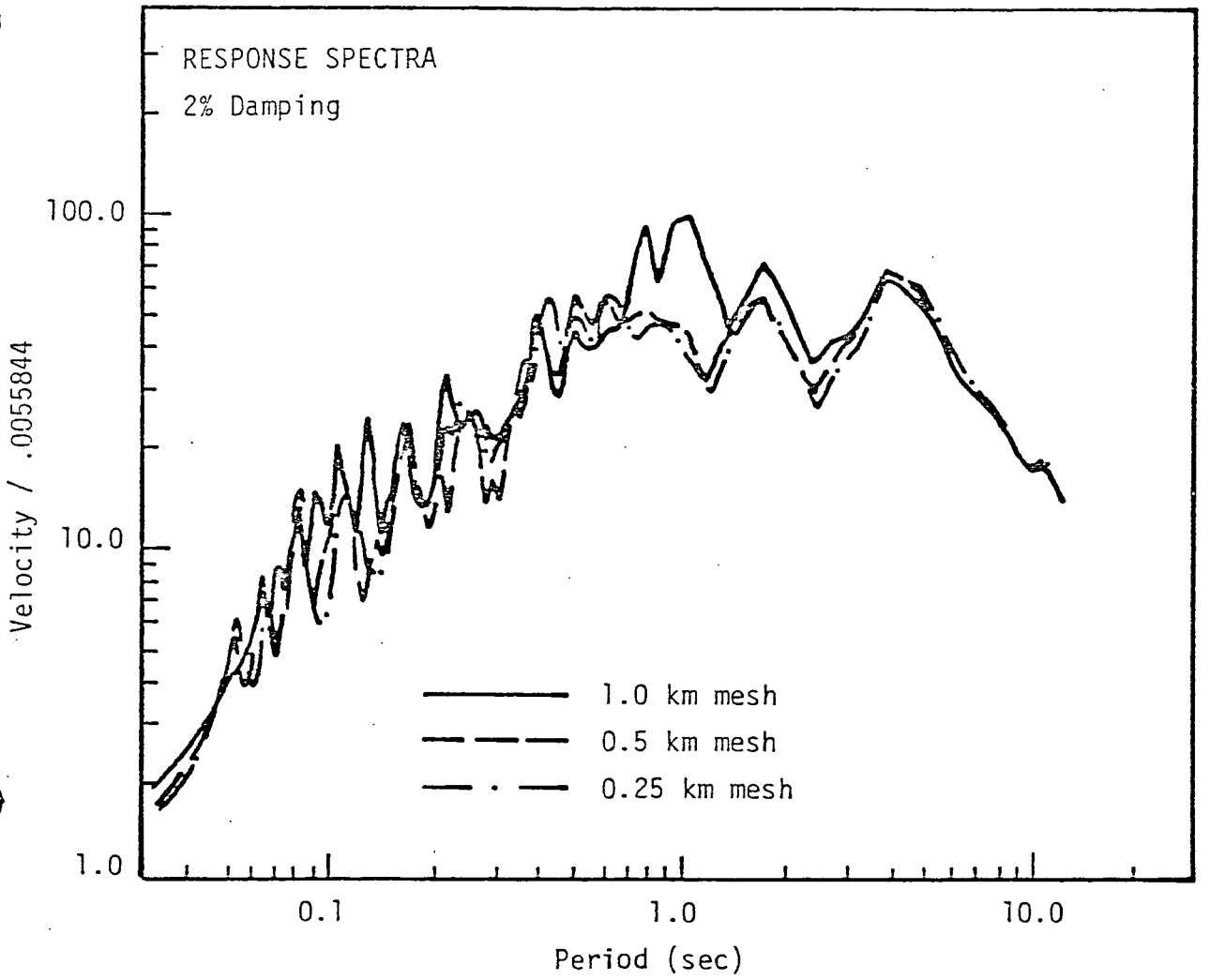

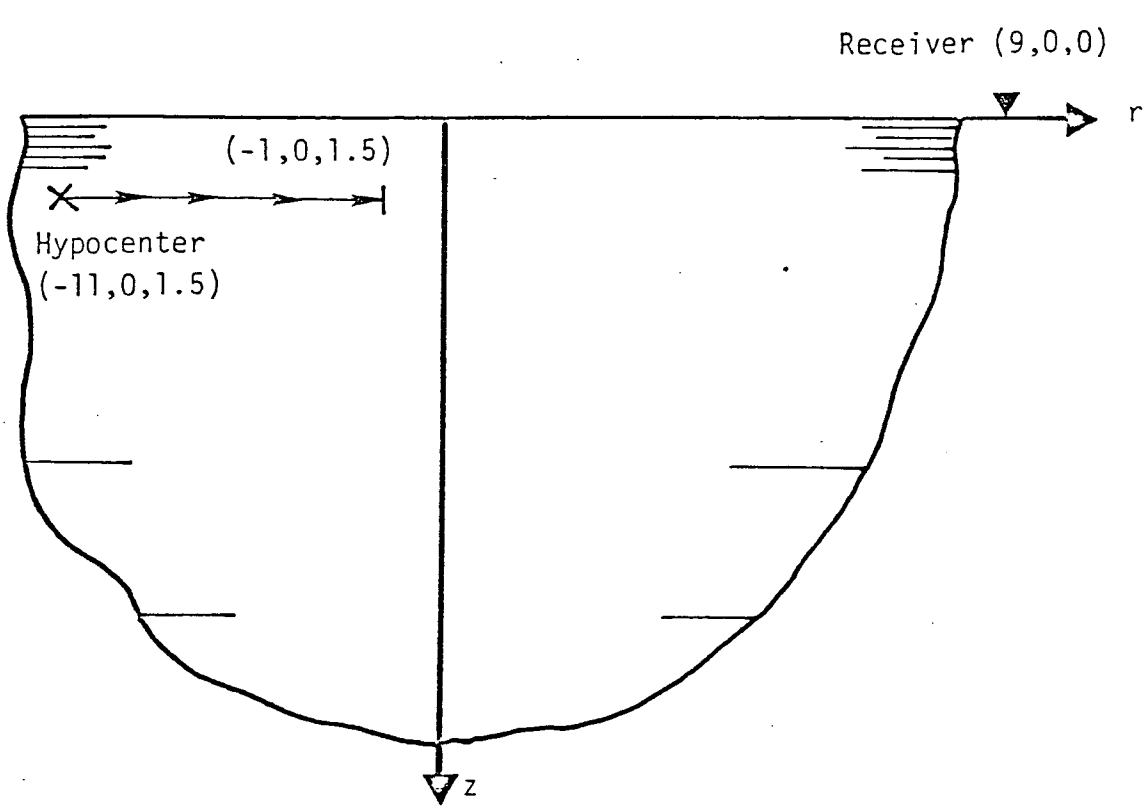

Figure 2-9. Far away horizontal line source study (focussed).

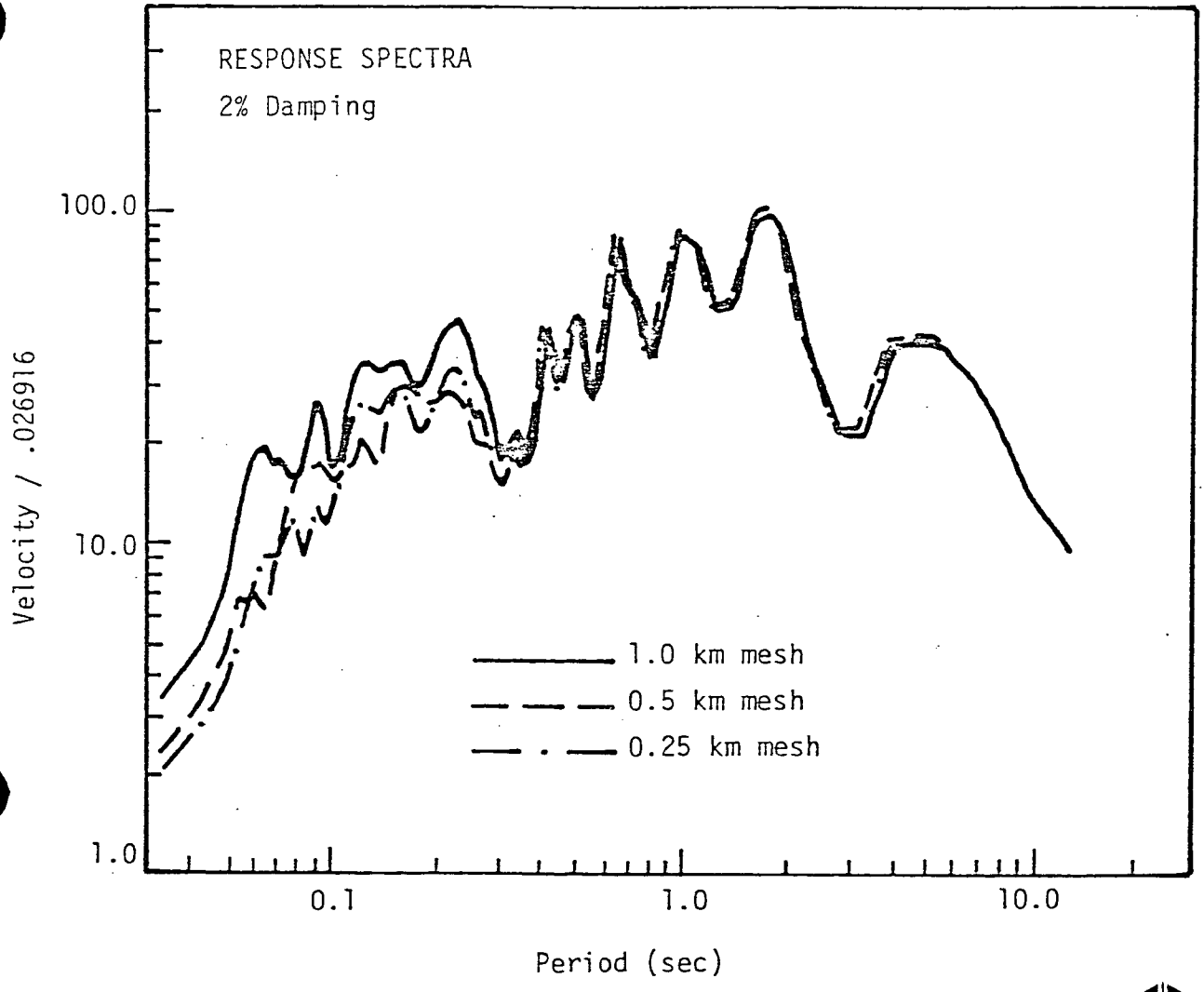

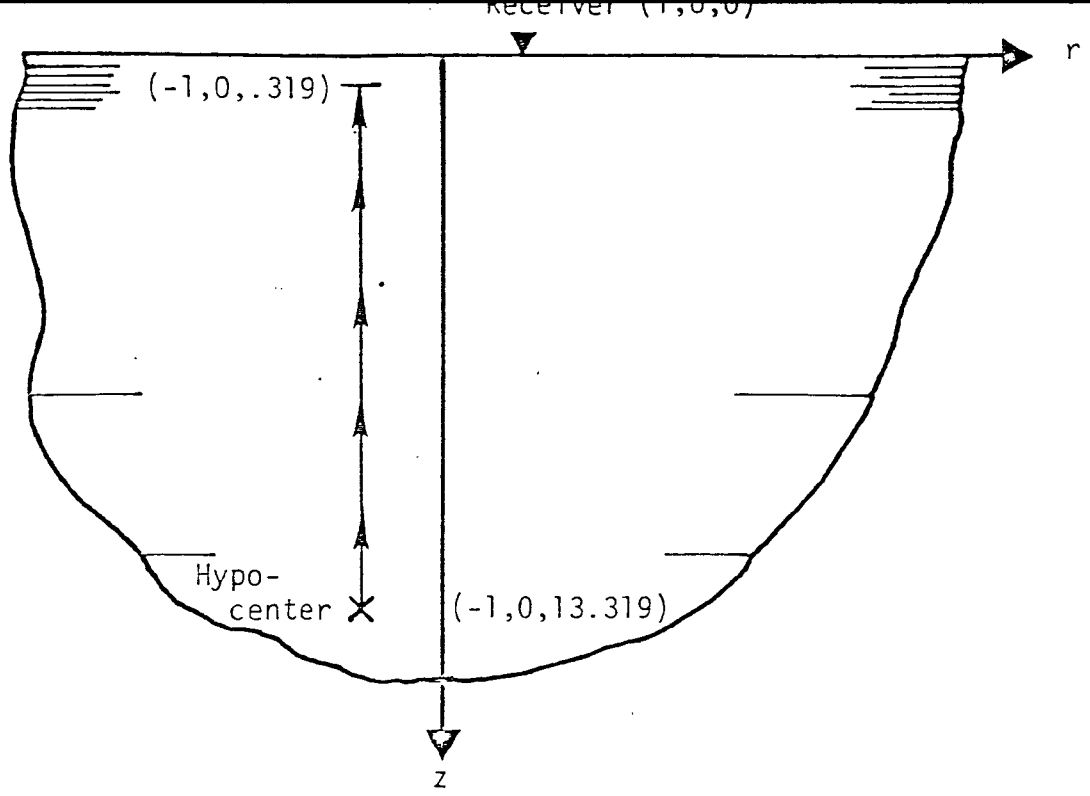

Figure 2-10. Close in vertical line source study (focussed).

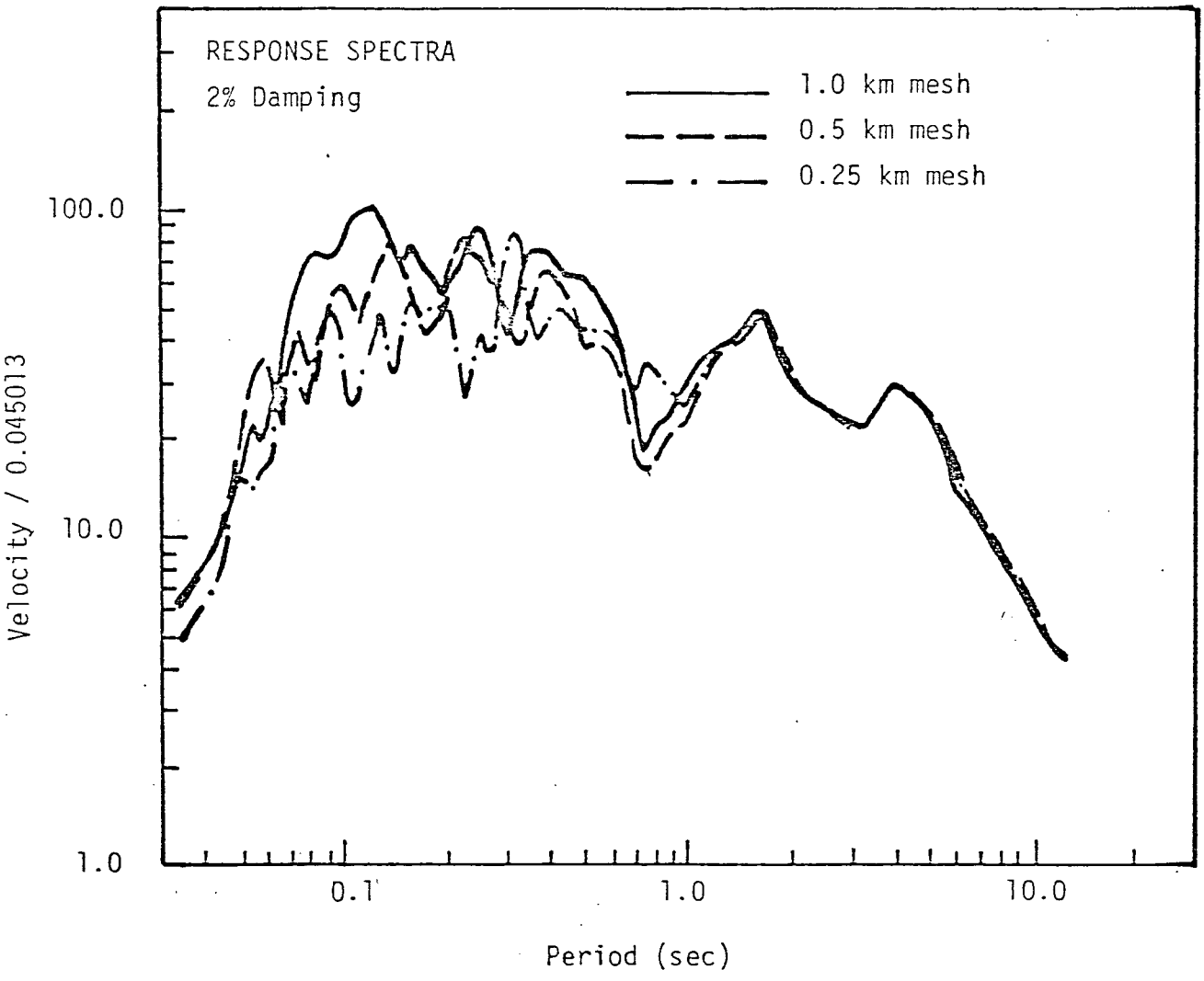

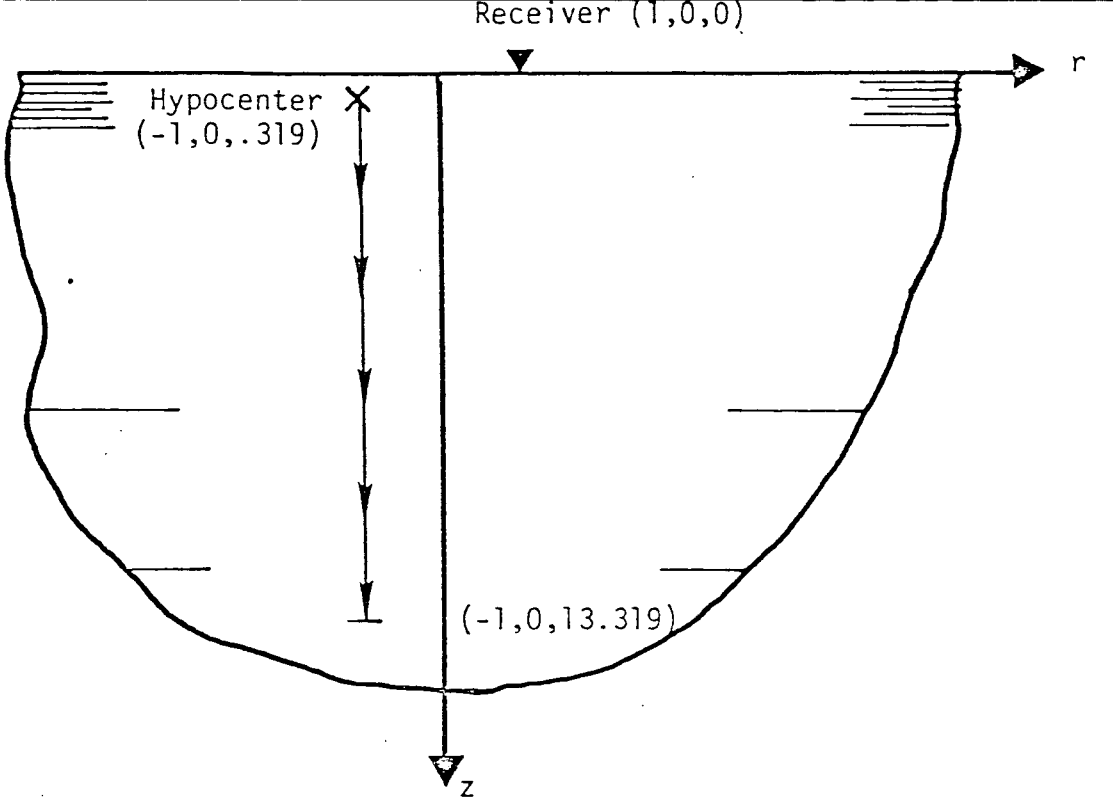

Figure 2-11. Close in vertical line study (defocussed).

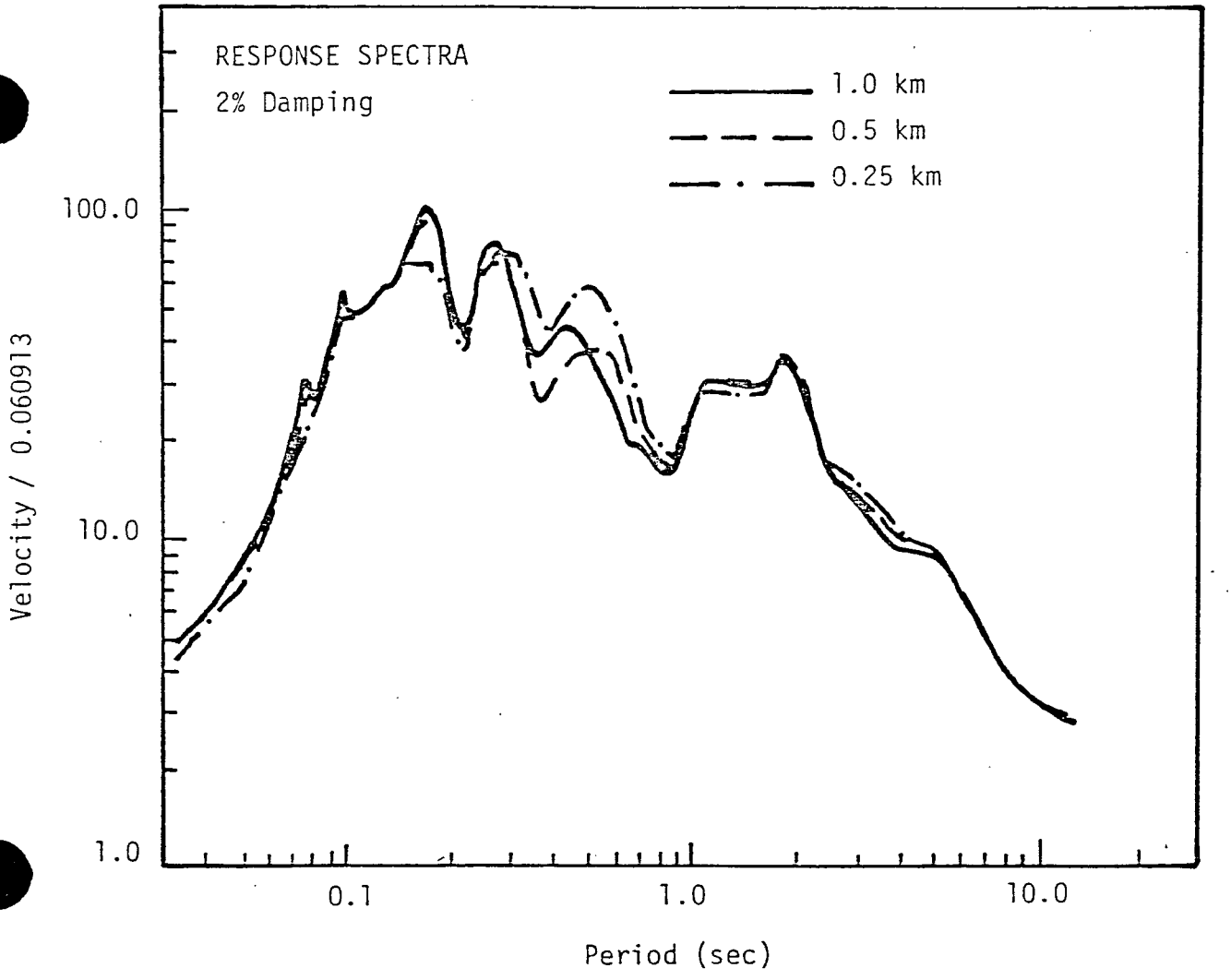

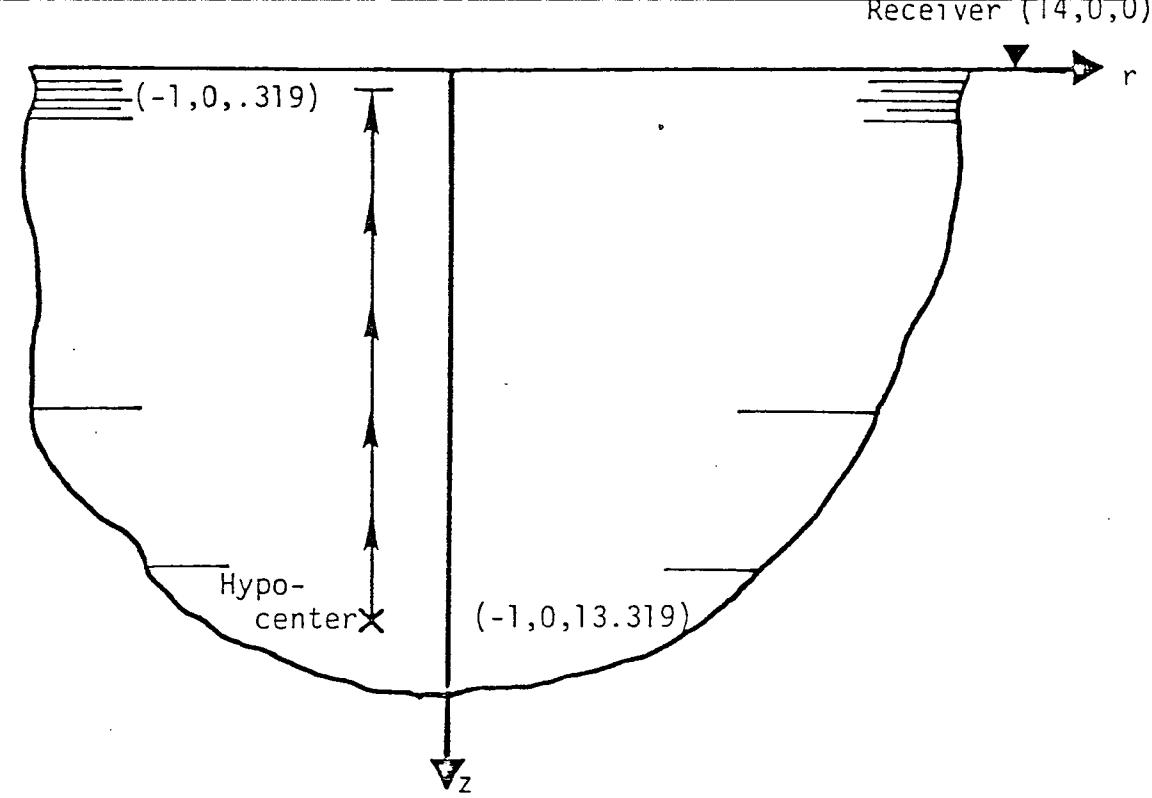

Figure 2-12. Far away vertical line source study (focussed).

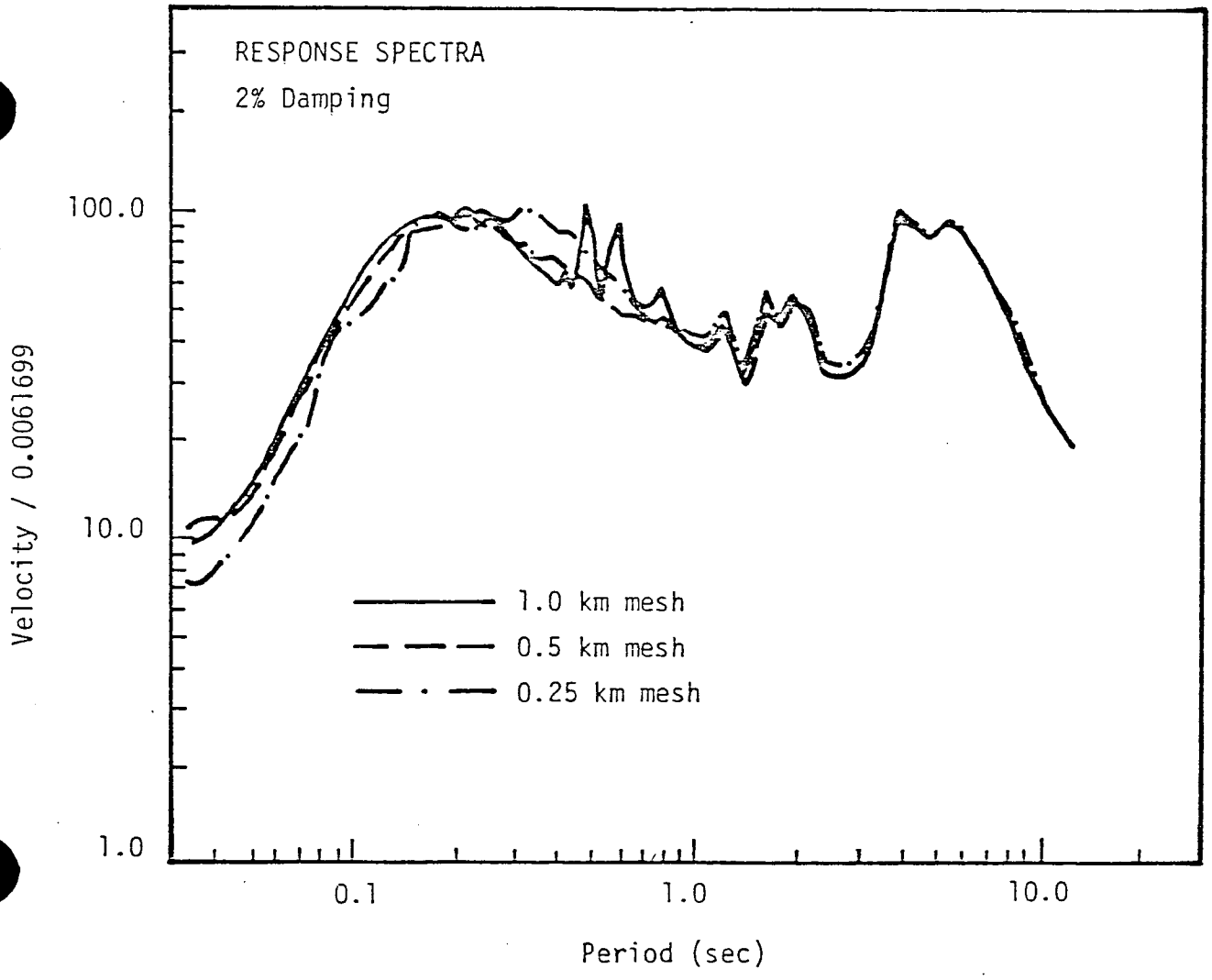

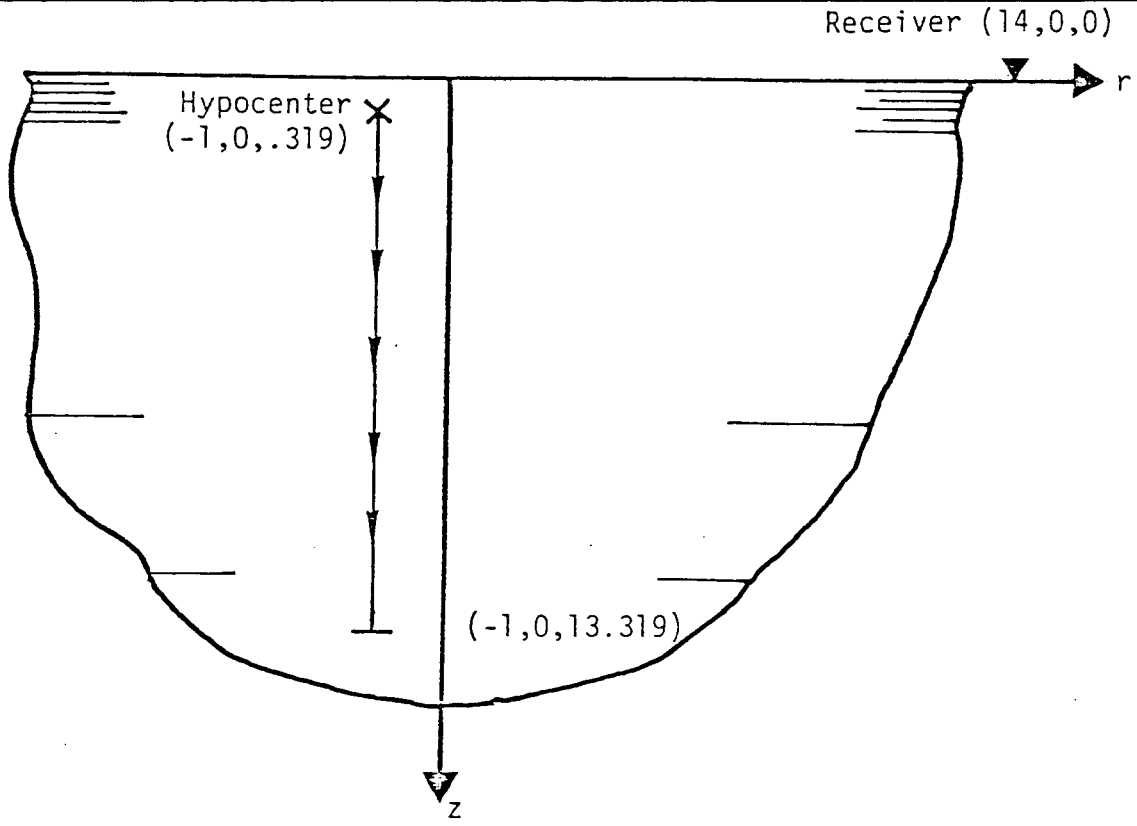

Figure 2-13. Far away vertical line source study (defocussed).

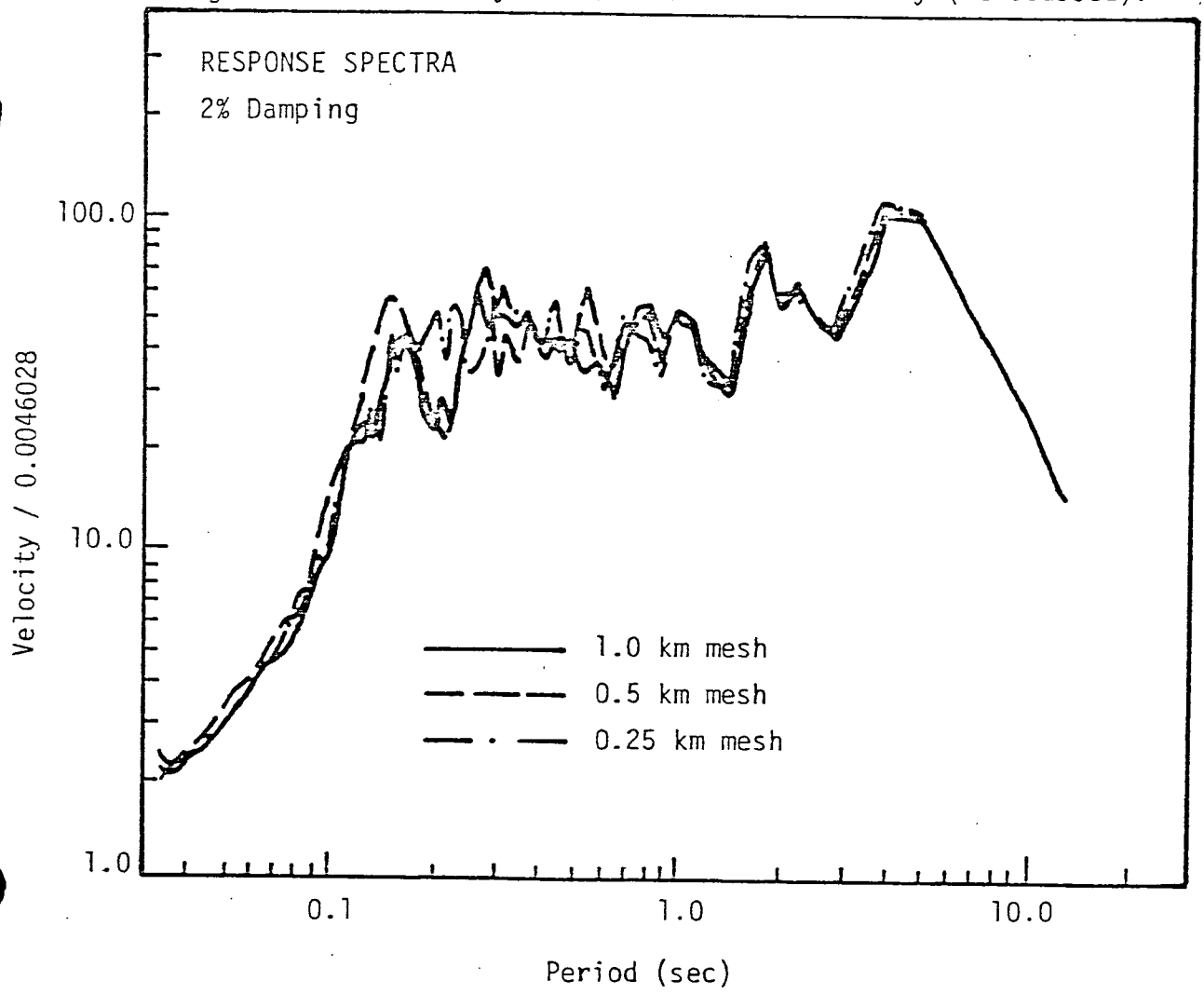

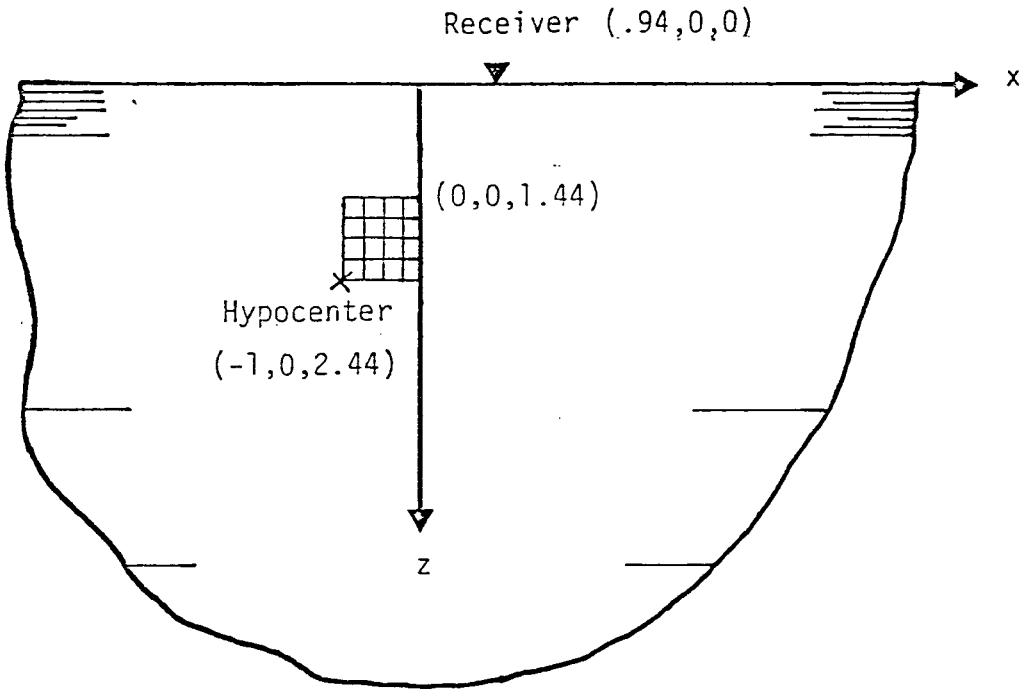

Figure 2-14. Close in mesh size study (focussed).

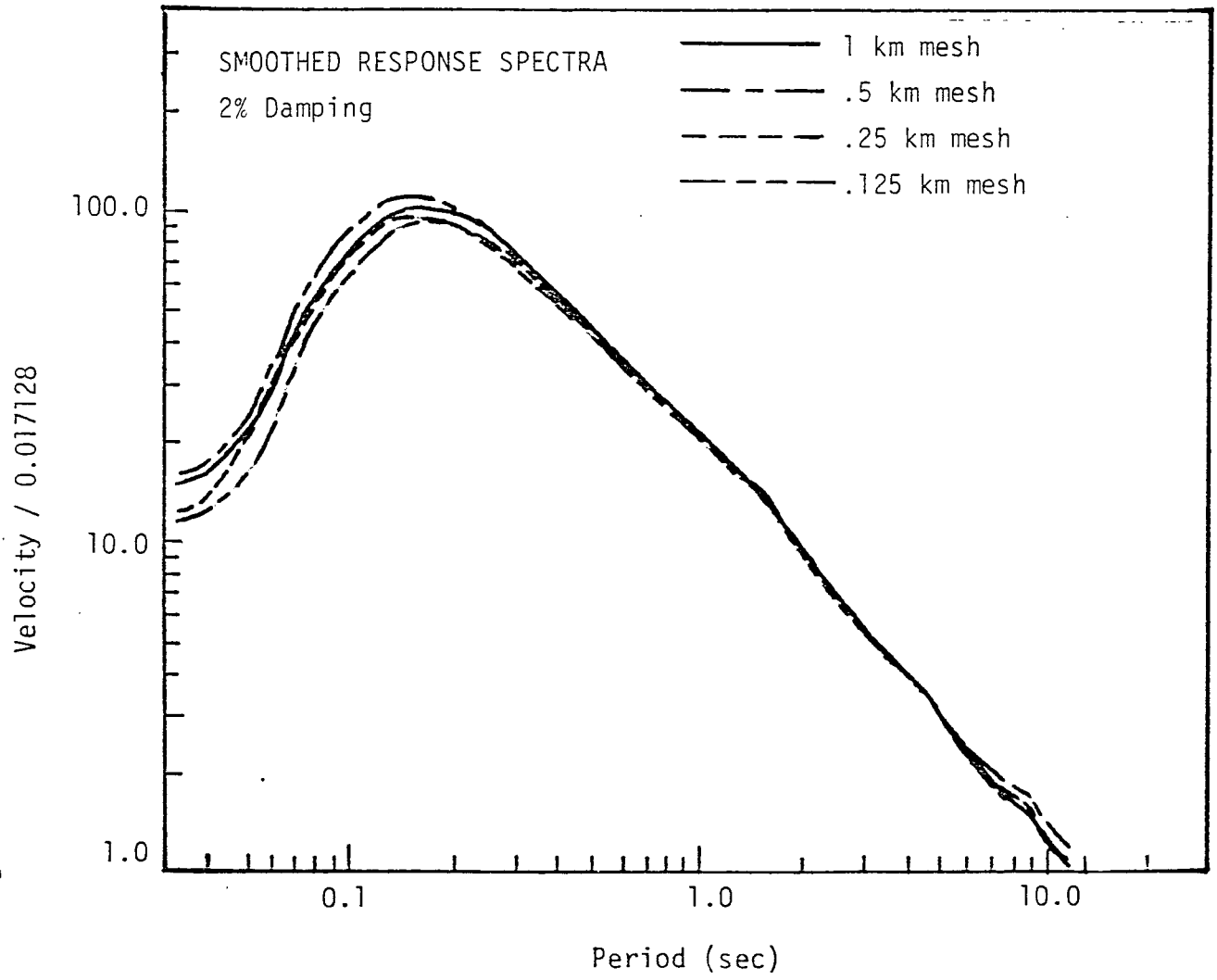

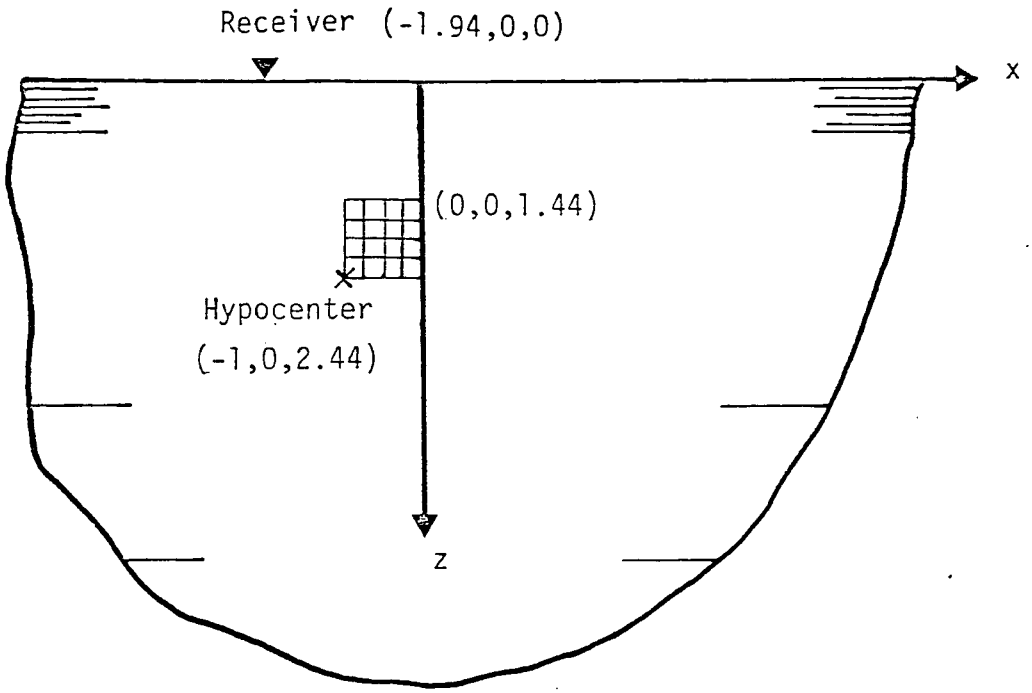

Figure 2-15. Close in mesh size study (defocussed).

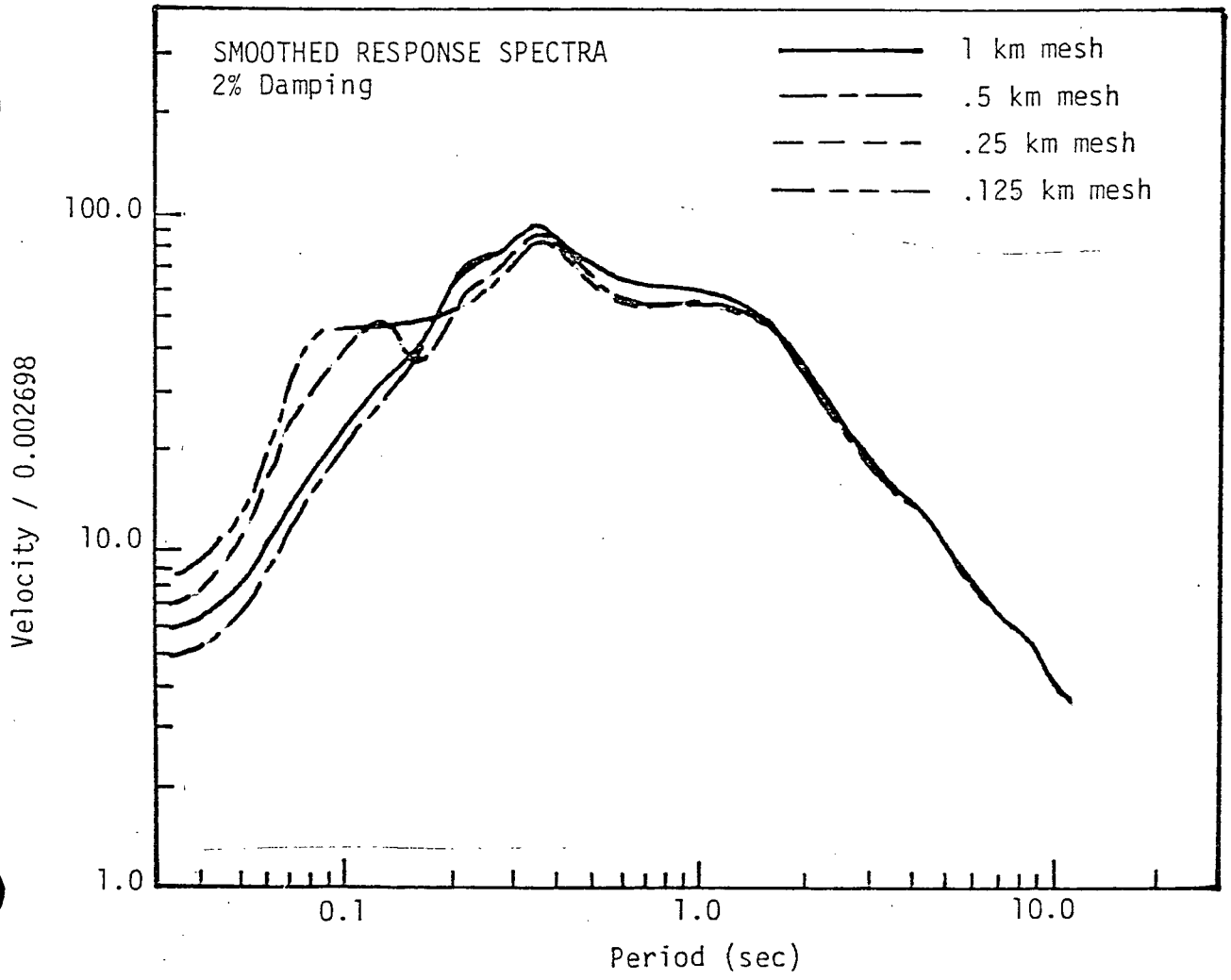

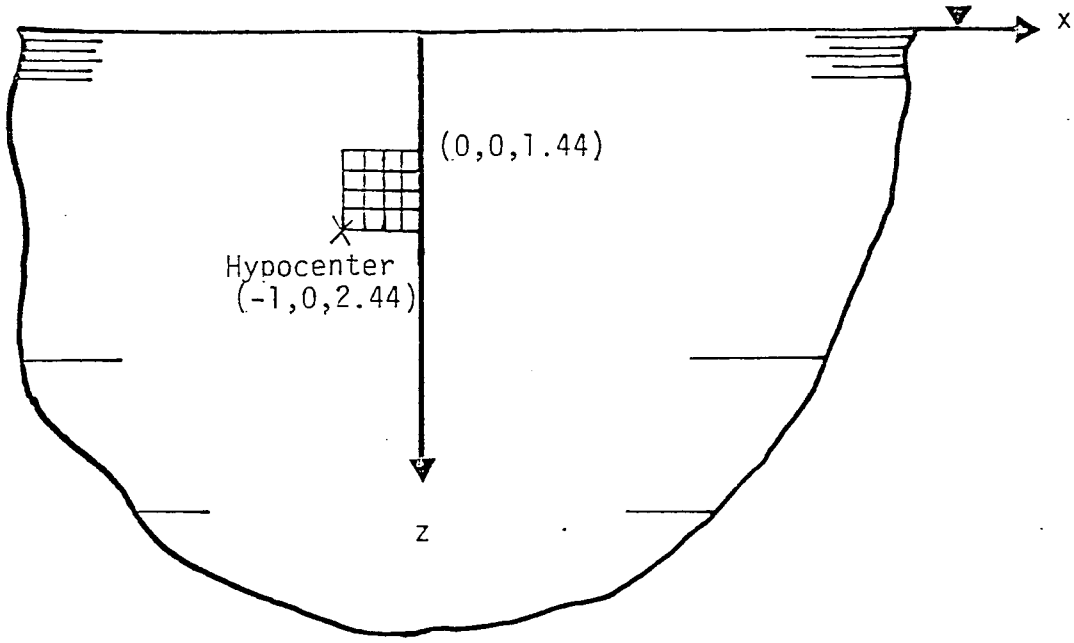

Figure 2-16. Far away mesh size study (focussed).

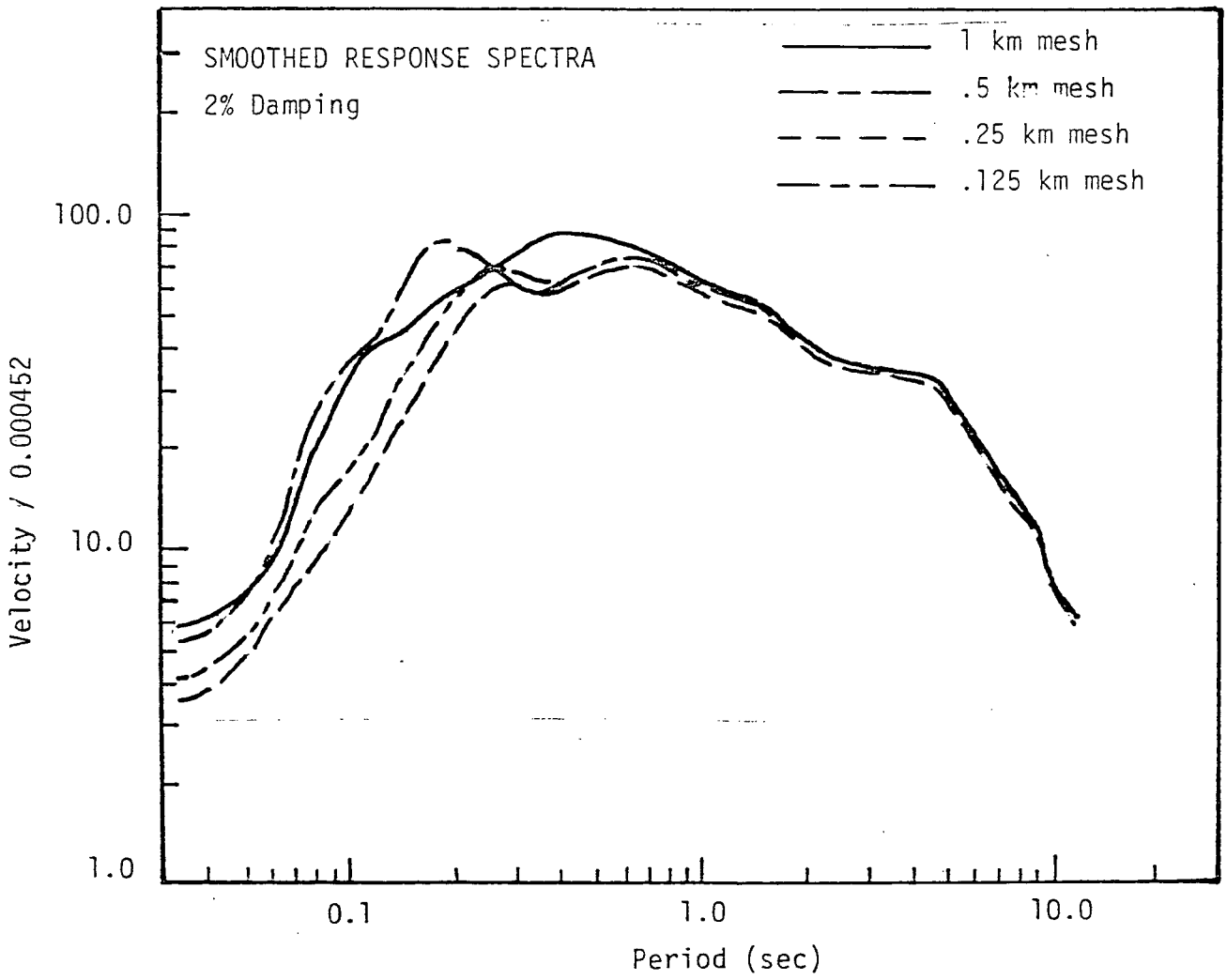

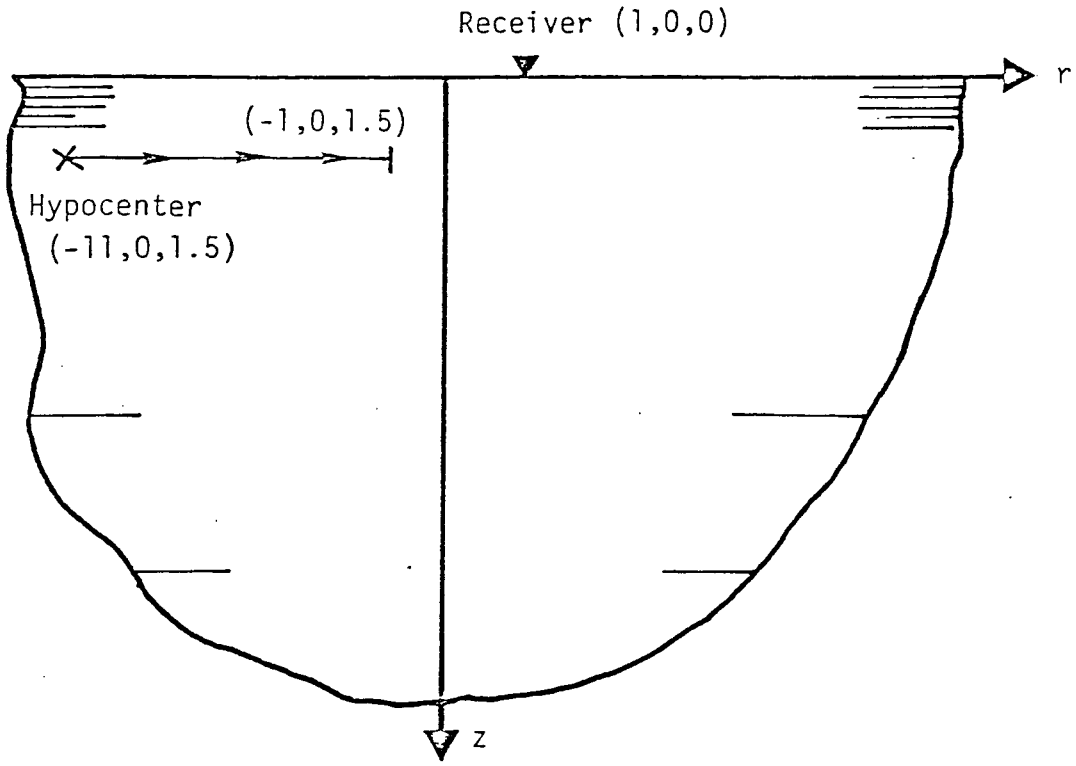

Figure 2-17. Close in horizontal line source study (focussed).

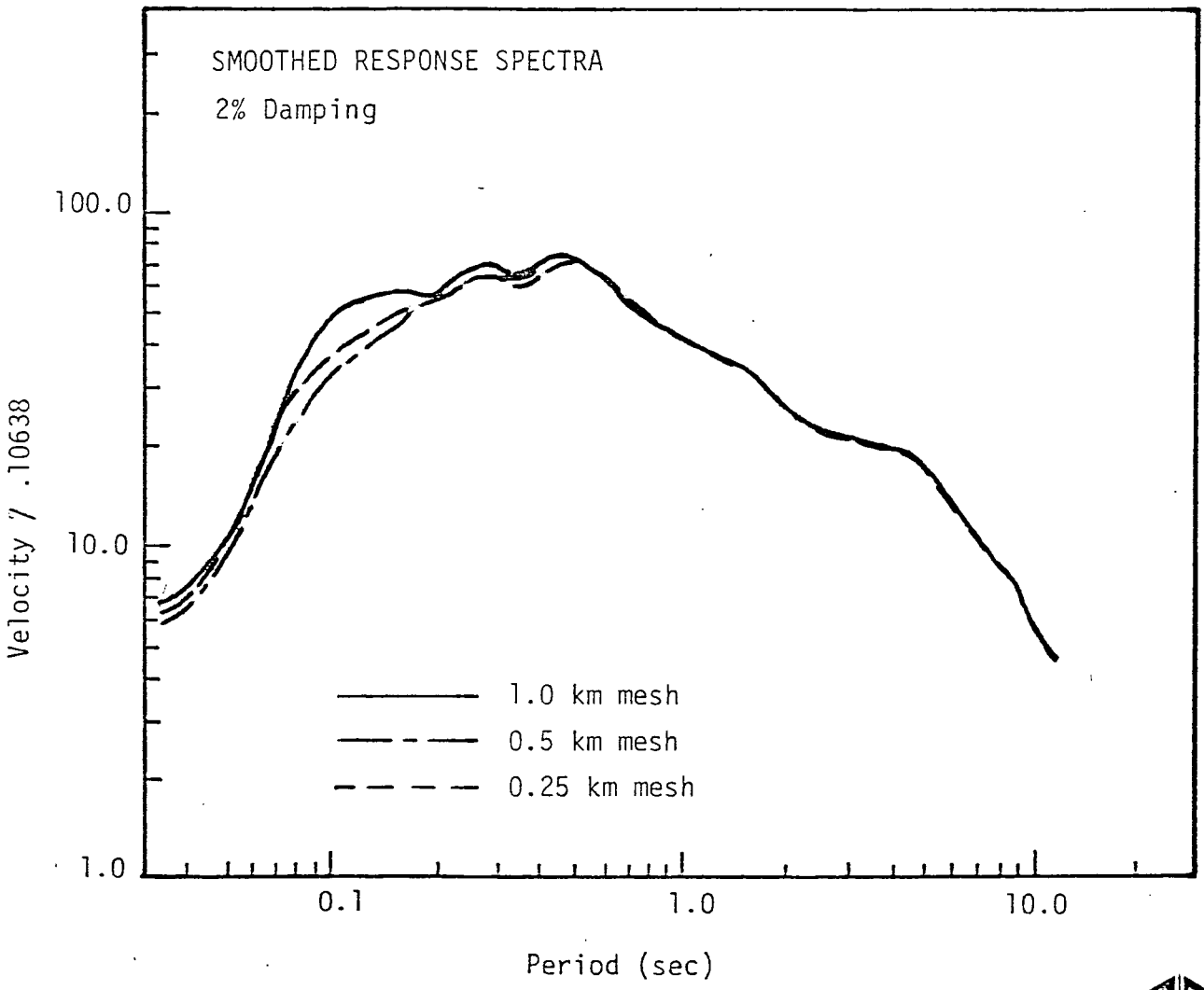

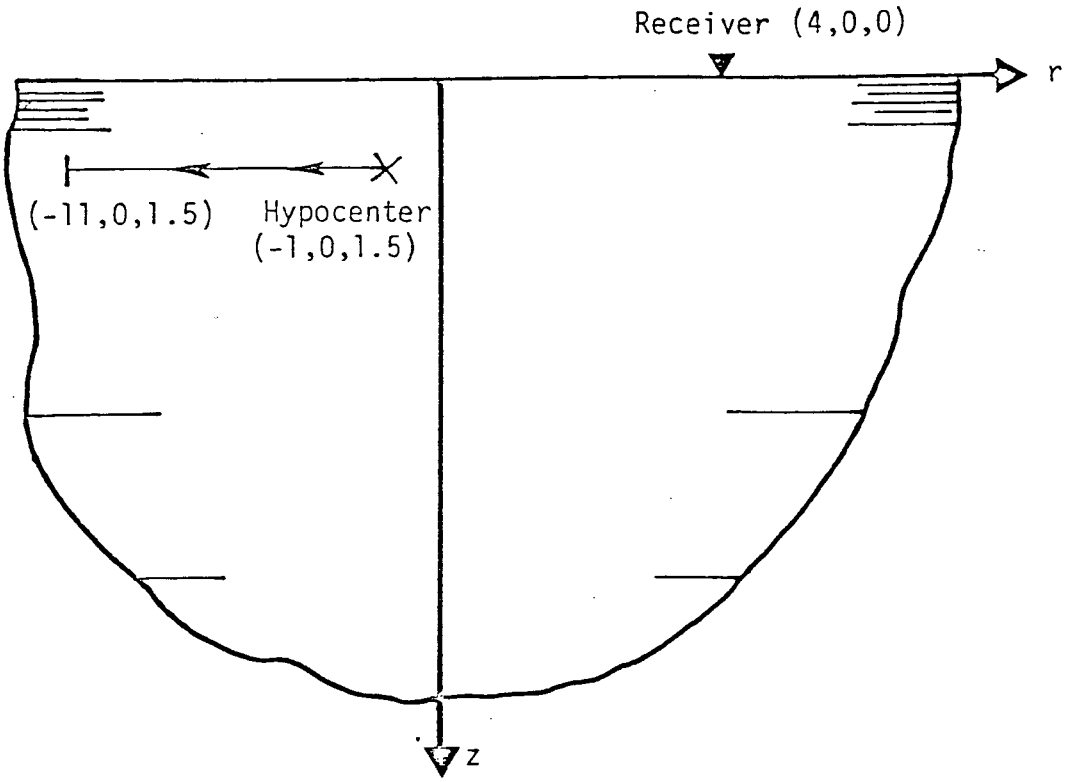

Figure 2-18. Intermediate horizontal source study (defocussed).

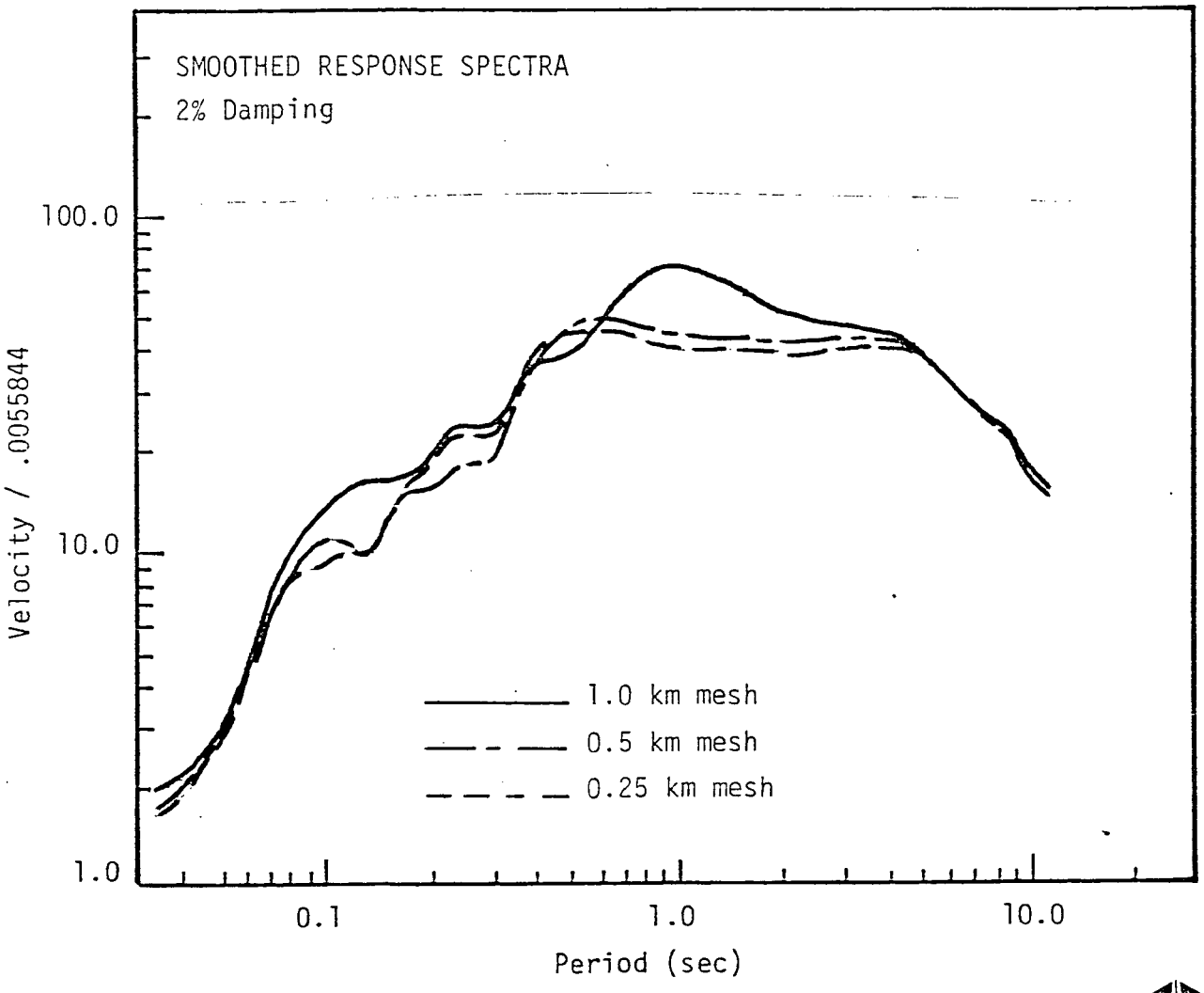

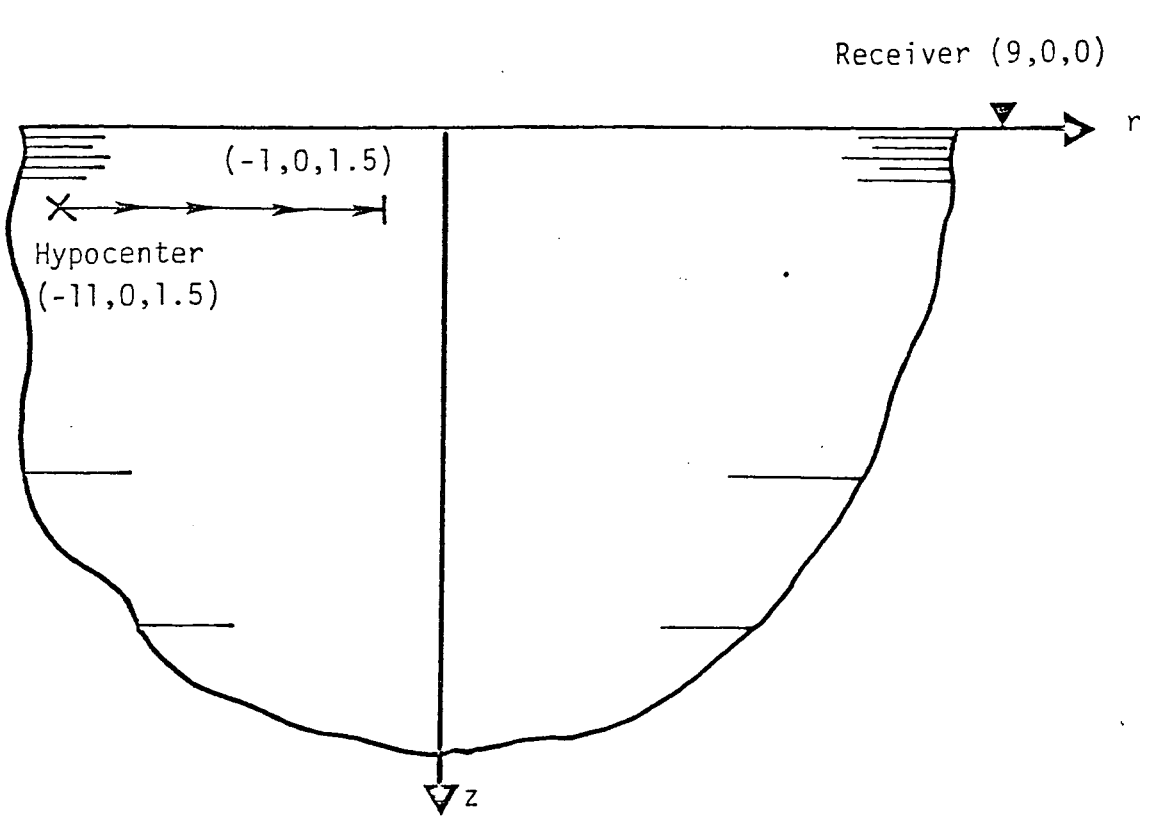

Figure 2-19. Far away horizontal line source study (focussed).

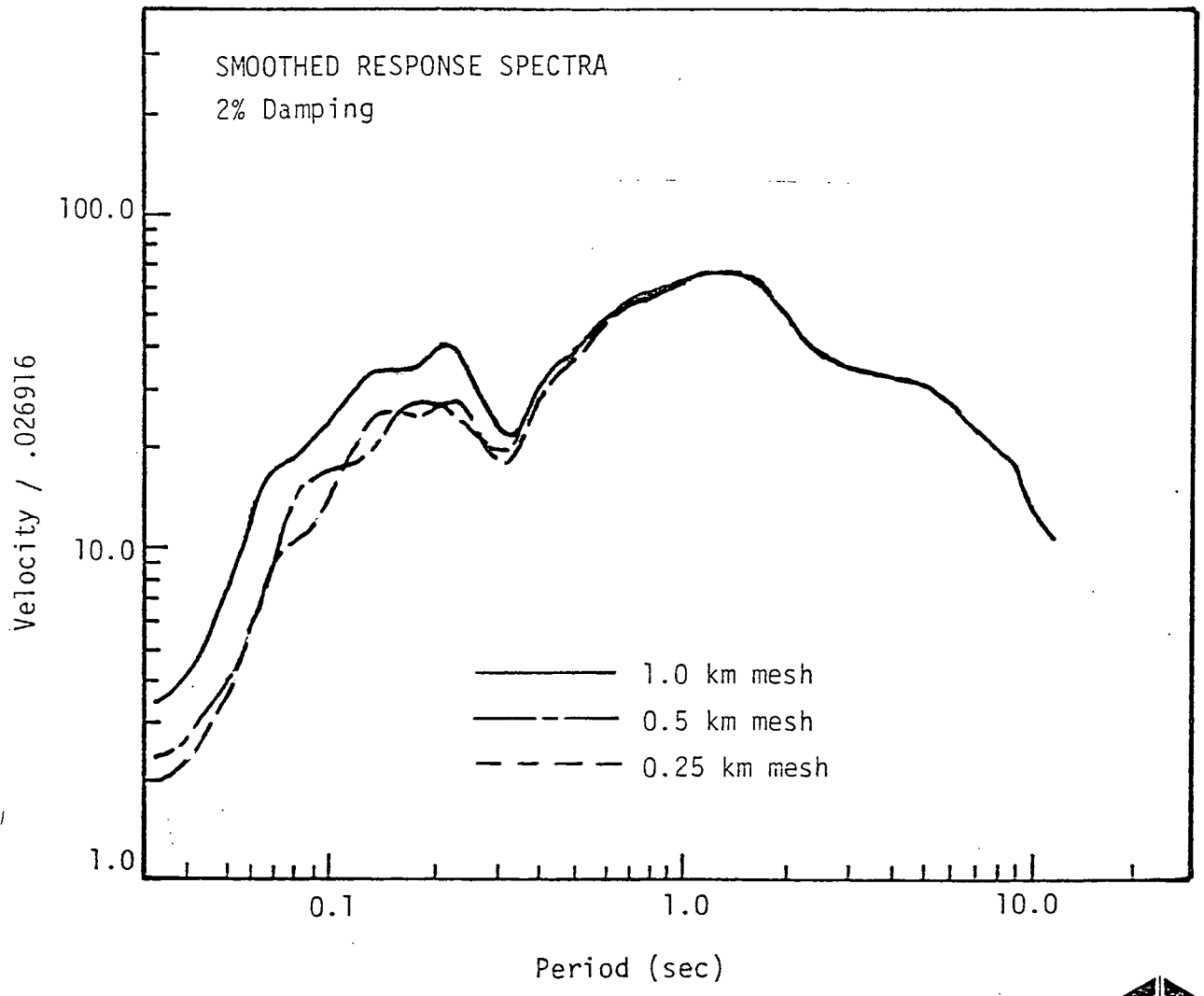

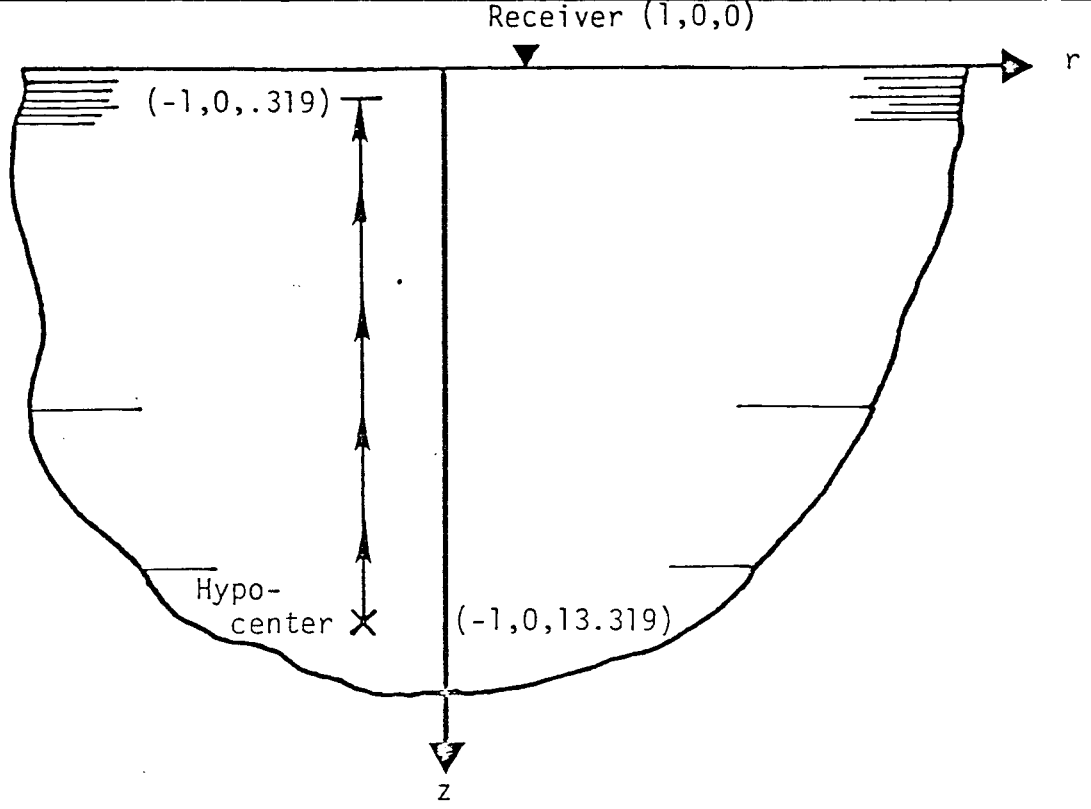

Figure-2-20. Close in vertical line source study (focussed).

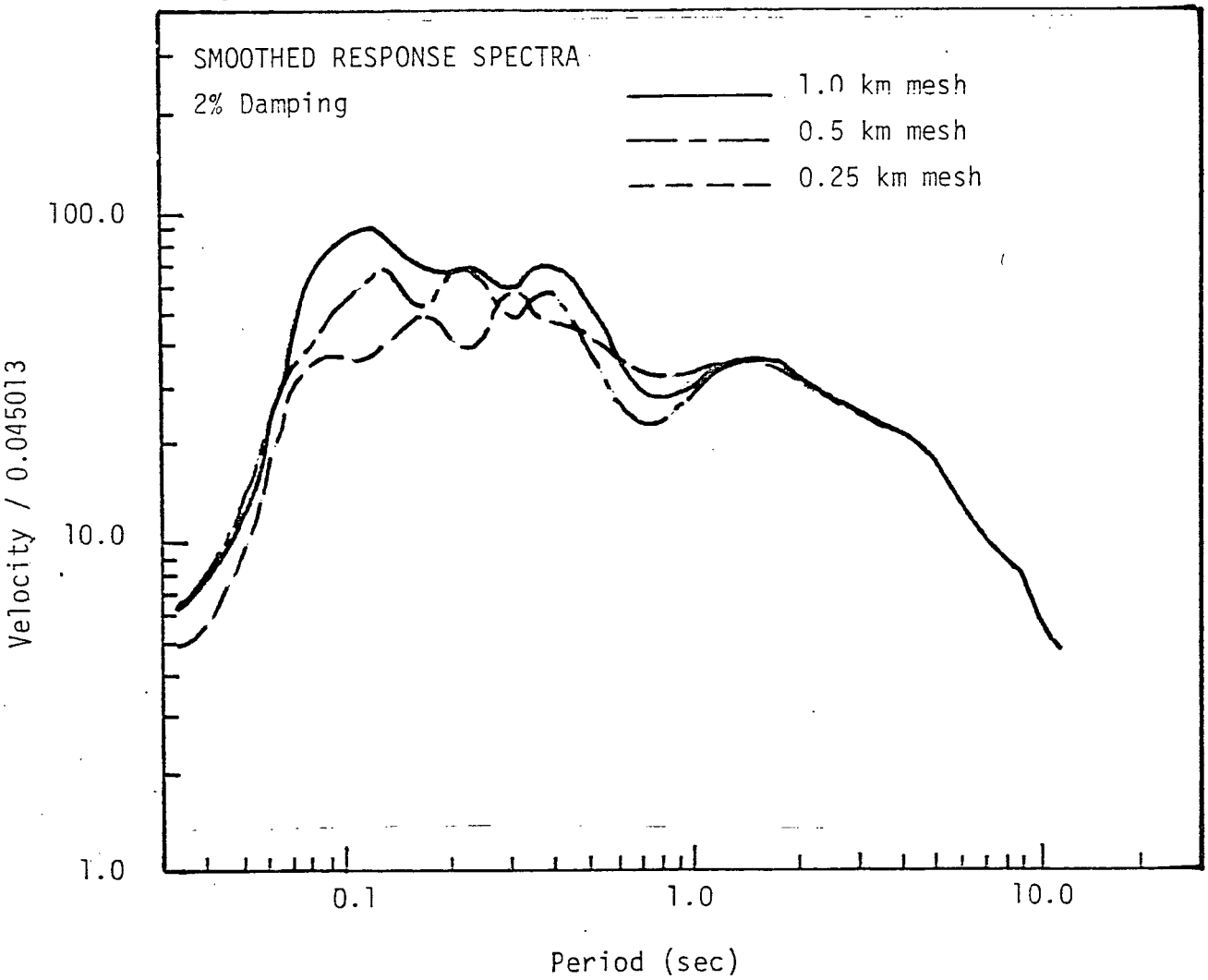

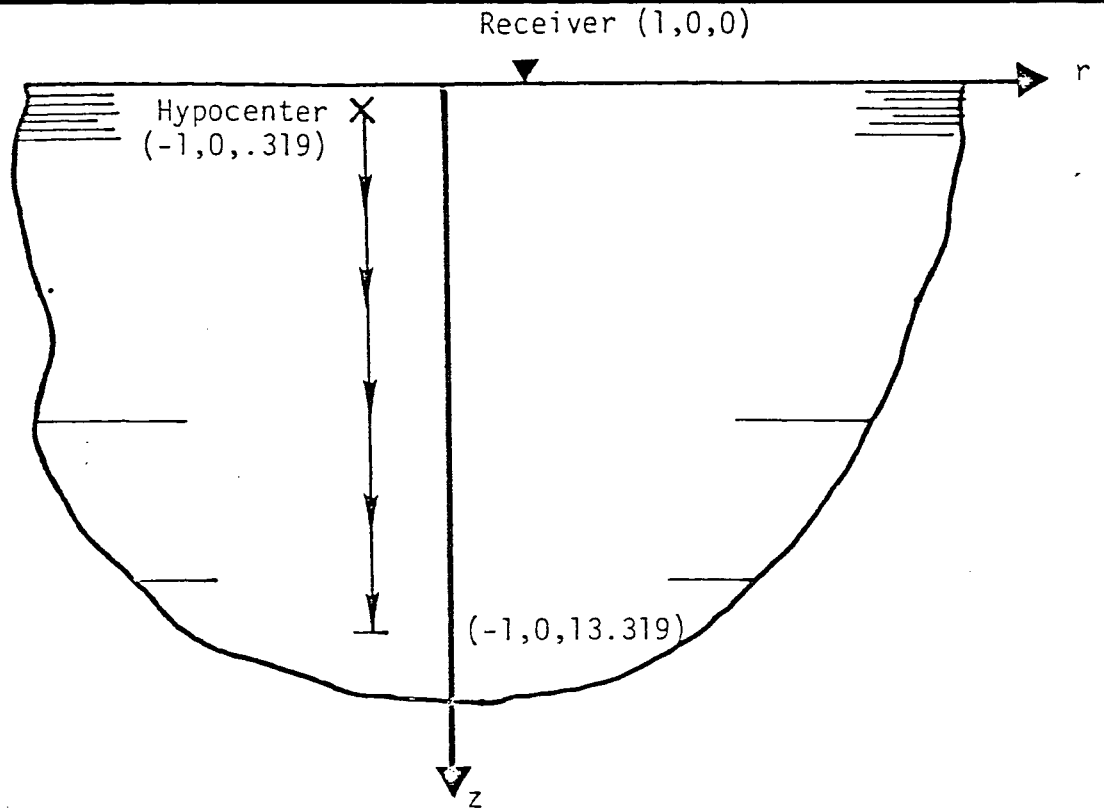

Figure 2-21. Close in vertical line study (defocussed).

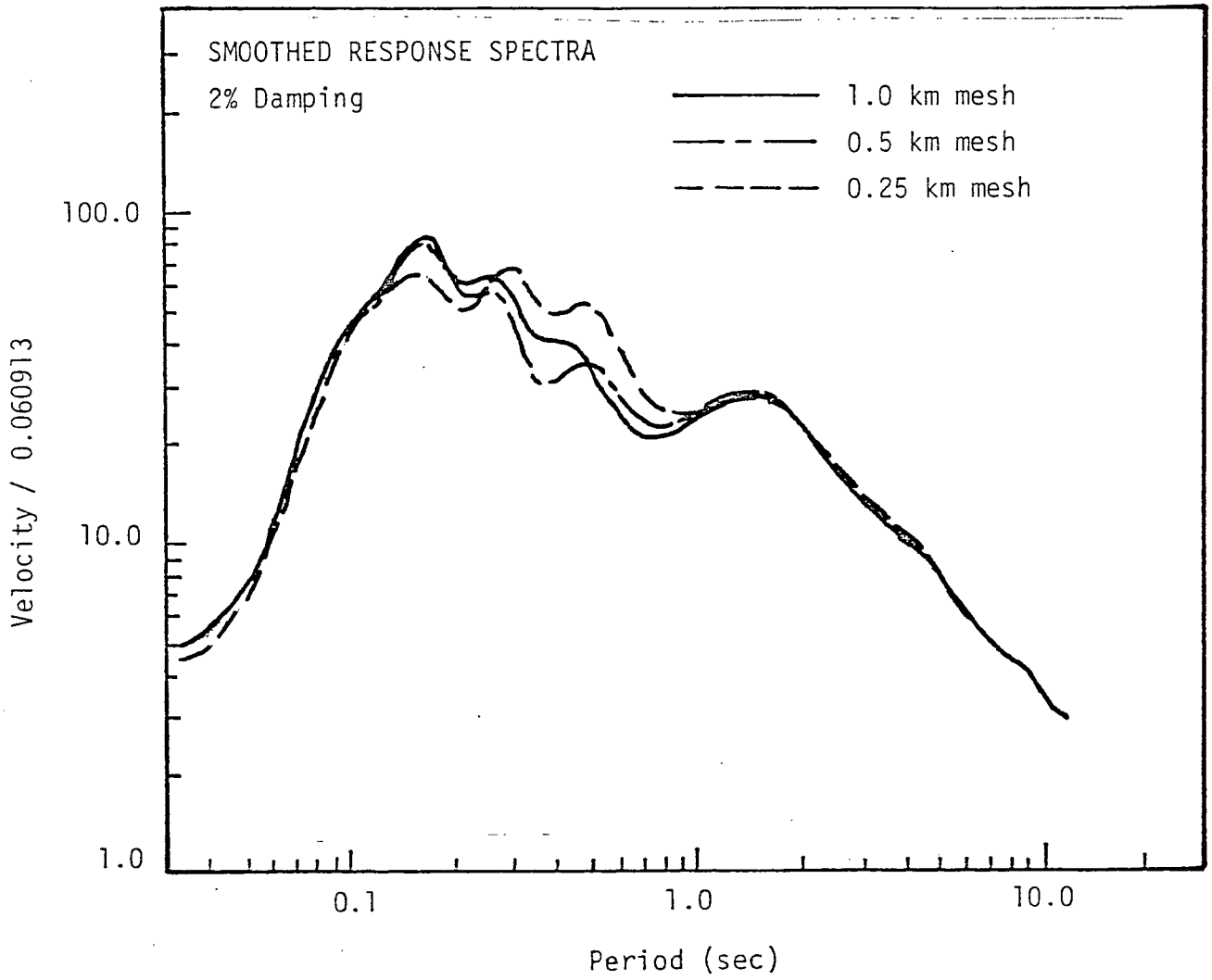

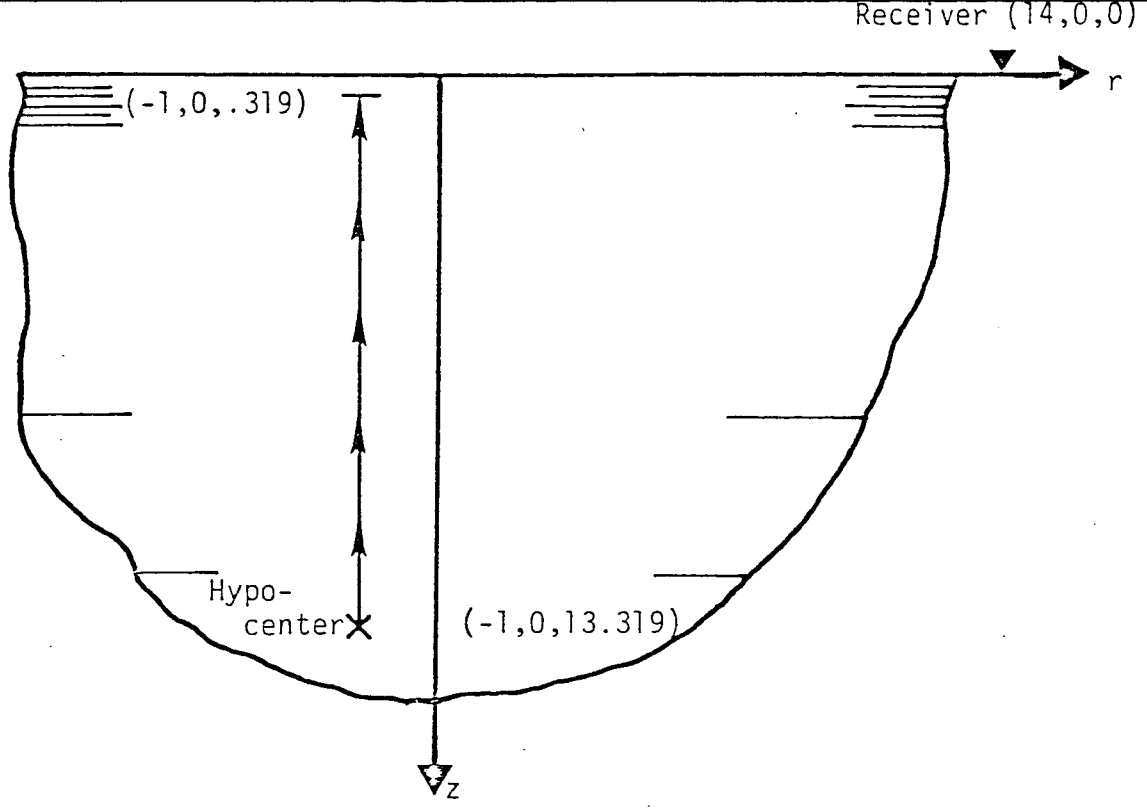

Figure 2-22. Far away vertical line source study (focussed).

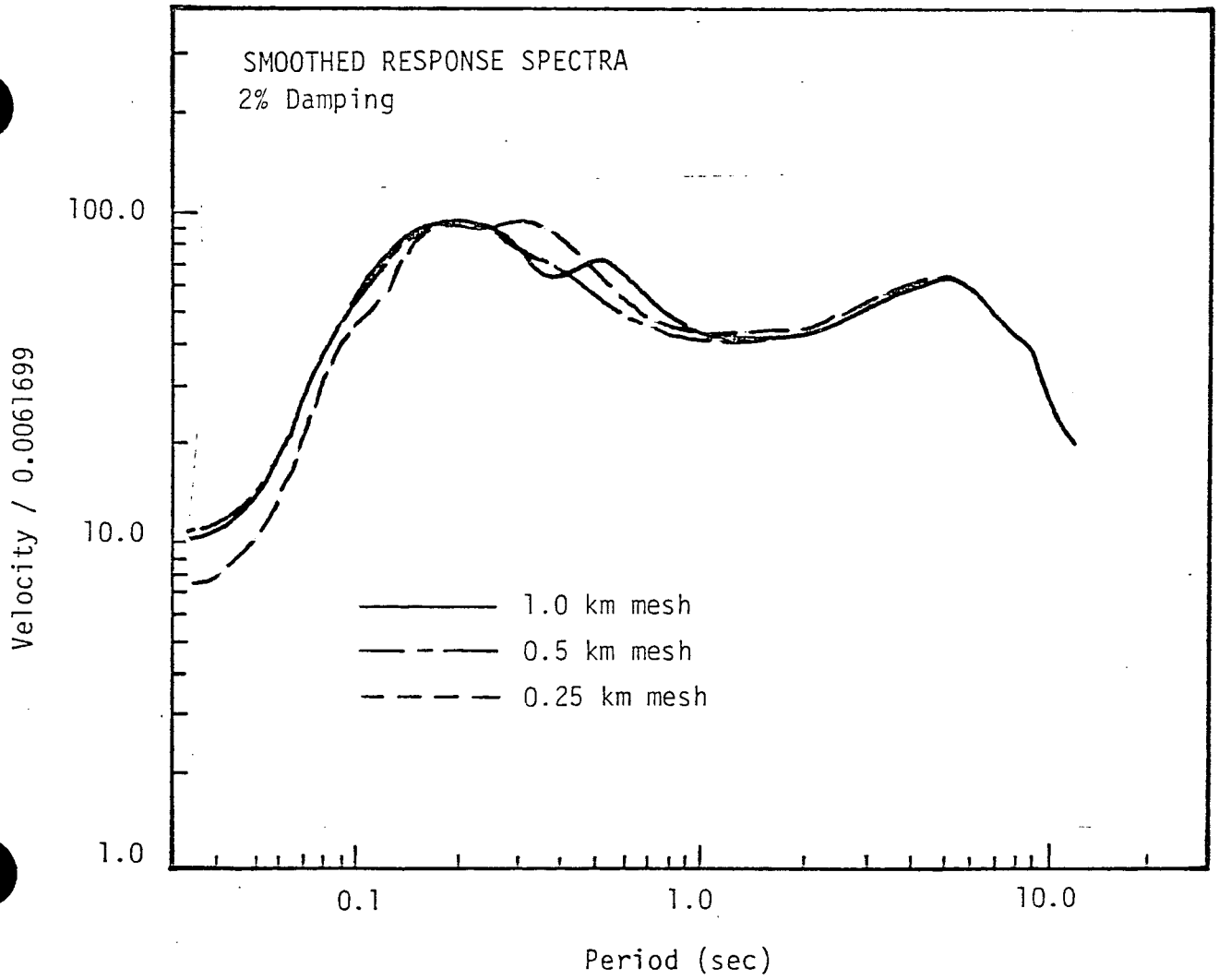

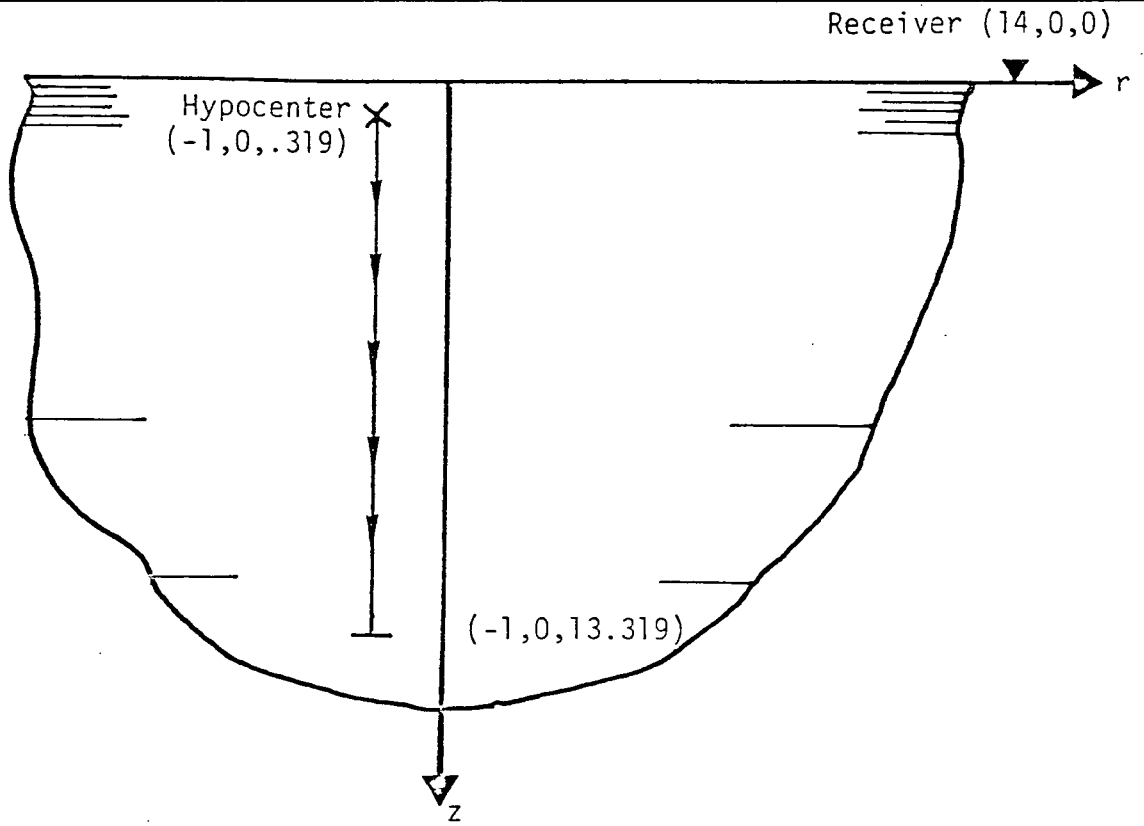

Figure 2-23. Far away vertical line source study (defocussed).

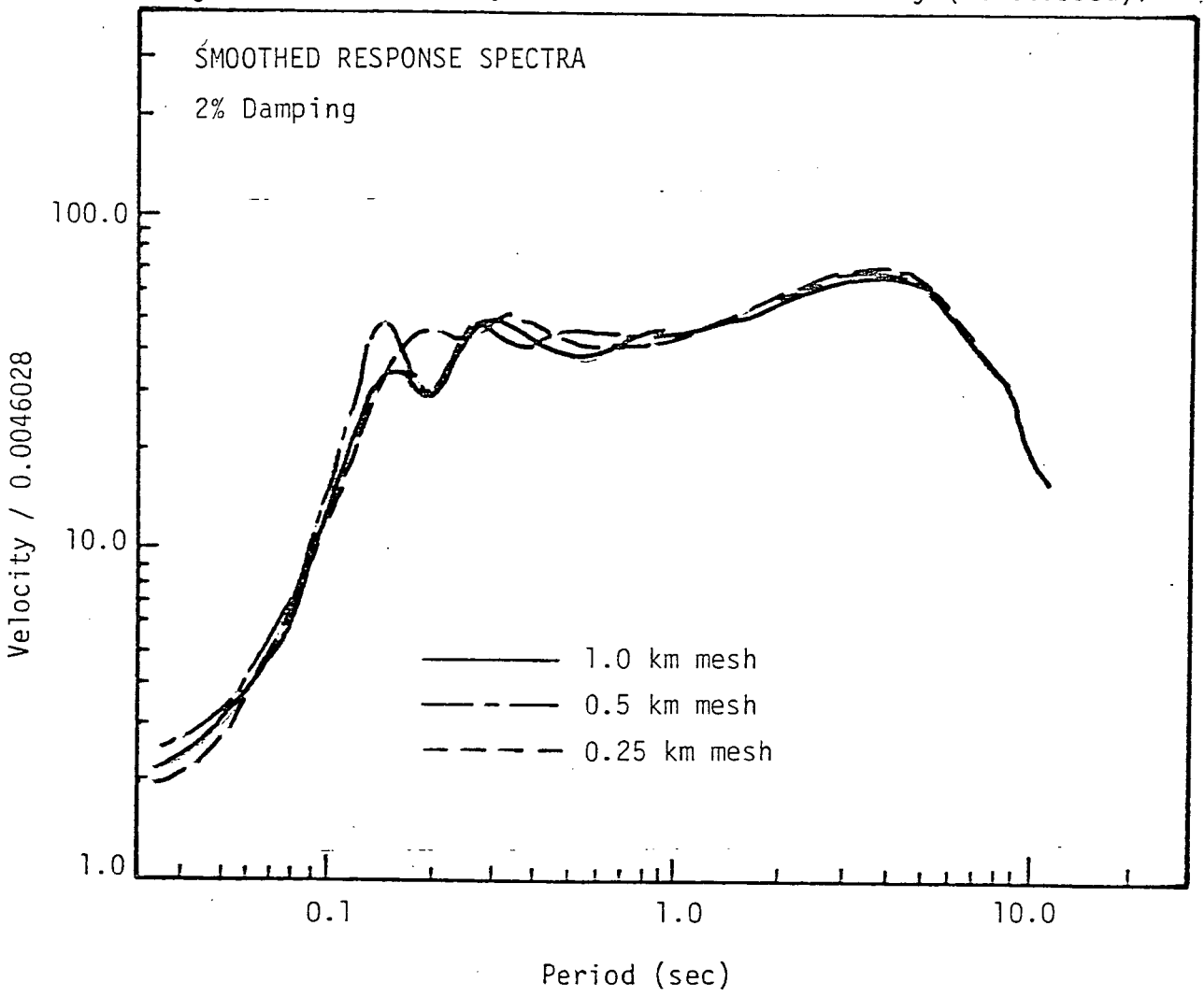

used in all the comparative studies corresponds to the earth model representative of the San Onofre site in TERA/DELTA's report.[3]

The calculated response spectrum for the 1-km-mesh-spacing is depicted by the solid line in each comparative study, while the results for the refined mesh spacings are demarcated as shown. The pseudo velocity response spectral values, in each comparative study, are scaled by the number appearing in the label of the vertical axis. This scaling factor corresponds to the maximum spectral value from the unsmoothed 1 km-spacing curve divided by 100.0.

The comparative studies for the 1 km-square surface of rupture centered at a depth of 1.94 km are presented in Figures 2-4 through 2-6 for the unsmoothed response spectra. In Figures 2-4 and 2-5, the rupture is focused and defocused, respectively, at a close-in receiver; while in Figure 2-6, the rupture is focused at a more distant receiver. The results exhibit no monotonic trend as the period approaches zero, and have previously received approval toward resolving the NRC concerns on the mesh treatment issue. Similar results for vertical and horizontal lines of rupture were deemed necessary by the NRC staff and their consultants for completing the mesh treatment resolution.

The comparative studies for a 10-km-long horizontal band of rupture with a width of 0.2 km and centered at a depth of 1.5 km are presented in Figures 2-7 through 2-9 for the unsmoothed response spectra. In Figure 2-7, the rupture is focused at a close-in receiver; in Figure 2-8, the rupture is defocused away from an intermediate receiver; and in Figure 2-9, the rupture is focused at a far-away receiver. The agreement between the spectral values for the different mesh spacings is as good as the comparisons in Figures 2-4 through 2-6, leaving only the vertical line of rupture to be discussed.

The comparative studies for a 13-km-long vertical band of rupture, having a width of 0.25 km and extending to within 0.32 km of the earth's surface, are presented in Figures 2-10 through 2-13 for the unsmoothed response spectra. In Figures 2-10 and 2-11, the rupture is focused and defocused at a close-in

receiver; while in Figures 2-12 and 2-13, the receiver is far away. Again, no trend is prevalent as a function of mesh spacing.

The unsmoothed response spectra, presented in Figures 2-4 through 2-13, complete the calculation sequence and are considered sufficient to illustrate that no adverse sensitivity exists to mesh spacing when synthesizing earthquake ground motions. The corresponding smoothed response spectra (refer to Appendix A of TERA/DELTA's report[3] for definition of smoothing) are presented in Figures 2-14 through 2-23 and further substantiate that DELTA's computed ground motions are not significantly influenced by the mesh spacing.

3.0 SLIP FUNCTION

3.1 EVIDENCE REGARDING THE CHARACTERIZATION OF FAULT SLIP

Three sources of evidence bear on our characterization of fault slip: numerical and theoretical simulations of the rupture process, laboratory experiments, and recordings of earthquake ground motions. Recordings of earthquake ground motions provide information regarding principally the area of the zone undergoing rupture and the average final offset. Complexities associated with the actual earthquakes make it difficult to extract more detailed information about slip. Under special circumstances, additional information can be obtained regarding the duration of slipping on the fault surface and rupture velocity.

Laboratory experiments and numerical simulations of fault rupture provide additional information that may be representative of actual earthquake behavior. See, for example, Figure 3-1 which is taken from Archuleta and Frazier, 1978. The preponderance of such information supports the following general features of fault slip: the initial slip occurs at a point and spreads at a velocity somewhat less than the shear wave velocity for the material; and the sliding that occurs for points on the rupture surface begins quite abruptly. Under idealized conditions considered in crack mechanics, the initial slip velocity is directly related to the failure strength of the material -- the higher the failure strength, the higher the initial slip velocity. Following the initial brittle fracture, the sliding process decelerates until information regarding barriers to further crack extension arrives back at the point undergoing slip. At this time, provided sufficient barriers are encountered, crack slip ceases. Based on numerical calculations and laboratory experiments, the duration of slip is approximately equal, on the average, to the time it takes for shear waves to traverse the narrowest dimension of the rupture surface.

3.2 IDEALIZED SLIP FUNCTION

The slip function that was used in the May, 1978 report consisted of a doubly ramped function, i.e., the slip velocity was composed of two box functions. The

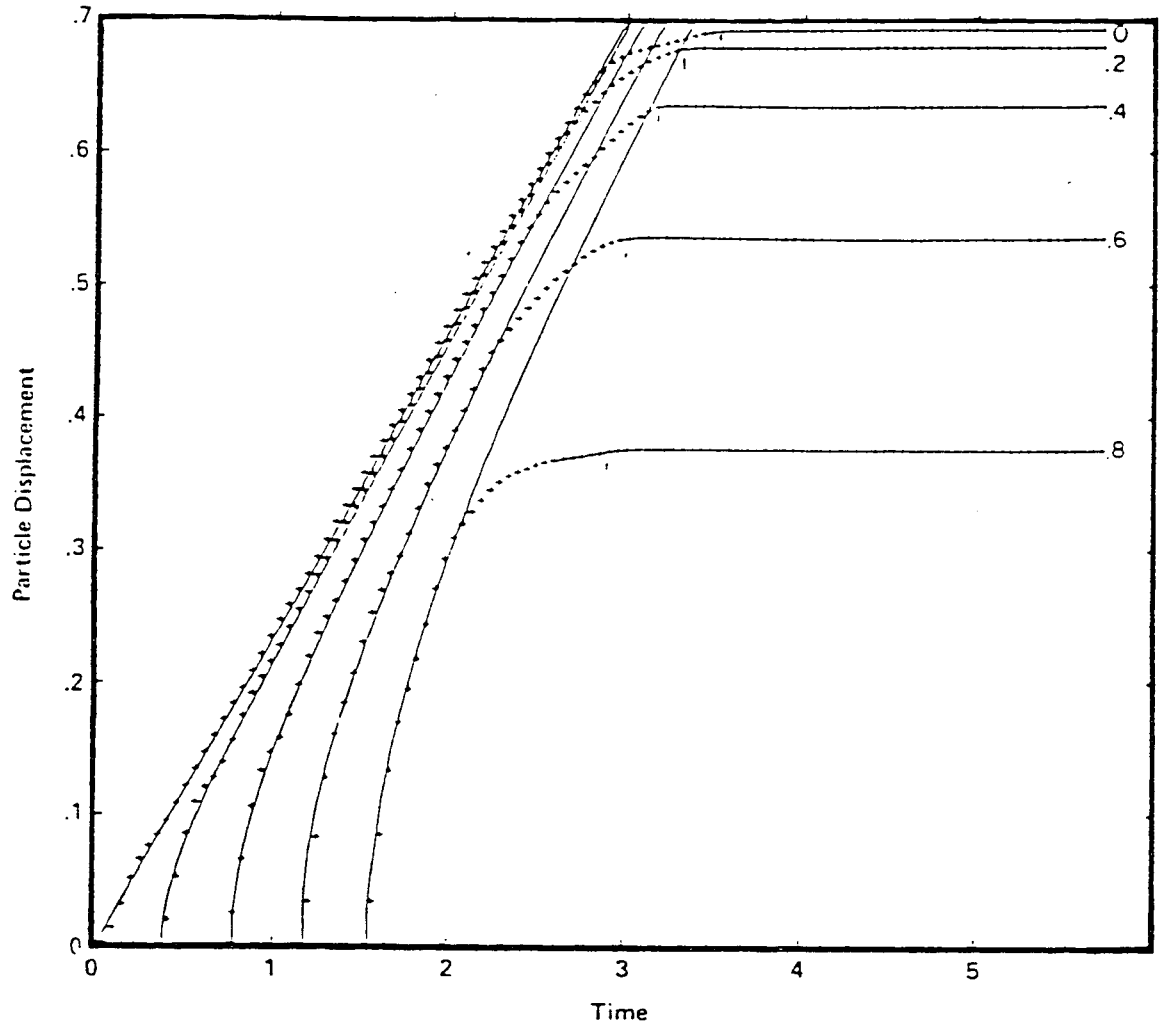

——————— Kostov's Self Similar Rupture[7]

++++++++++++++++++ Archuleta and Frazier's (1978) Finite Element Results

Time histories of particle slip displacement for five points on a circular crack surface of radius r_o, equally spaced along a radial line emanating from the hypocenter.

Figure 3-1. Slip along a circular crack.

initial box function contains the maximum slip velocity and operates for a duration of 1/40 sec, or one time-step in the numerical calculations. The second portion of the slip function has a considerably lower slip velocity which remains constant for the remaining duration of slip at that point on the rupture surface. This function, which is illustrated in Figure 3-2, was designed to contain the principal features illustrated in the numerical calculations presented in Figure 3-1.

Concerns regarding this slip function were apparently not focused on its capacity to characterize slip in numerical and laboratory experiments, in that this slip function has more degrees of freedom for modeling fault slip than the alternate function that was suggested in the October, 1978 meeting. Rather, concerns were expressed regarding the number of parameters required to define the slip function, i.e., there may be more parameters in the slip function than can be uniquely determined from earthquake modeling studies. On the other hand, concerns were also expressed regarding the fact that certain parameters in the slip function were held constant from one earthquake to the next, the major concern being that the maximum slip velocity (which significantly influences high frequency spectra) was held constant. The maximum slip velocity was held constant in the May, 1978 report for two reasons. First, crack mechanics indicates that the maximum slip velocity is directly controlled by material strength, i.e., dynamic stress drop. Assuming that the noncoherent fracture sequence of earthquakes results from irregularities in the tectonic stress condition rather than from strong variations in the strength properties of the gouge materials, leads us to expect maximum slip velocity to remain nearly constant from one earthquake to the next. The second and more prevailing reason was that there appears to be little evidence, from the earthquake modeling studies performed in the earlier report, to indicate that the maximum slip velocity should vary according to earthquake magnitude or stress drop. Additional analyses have been performed in the present study to investigate this in greater detail. Also, alternate slip functions were investigated to satisfy the request for use of a slip function with fewer parameters, namely a ramped step function.

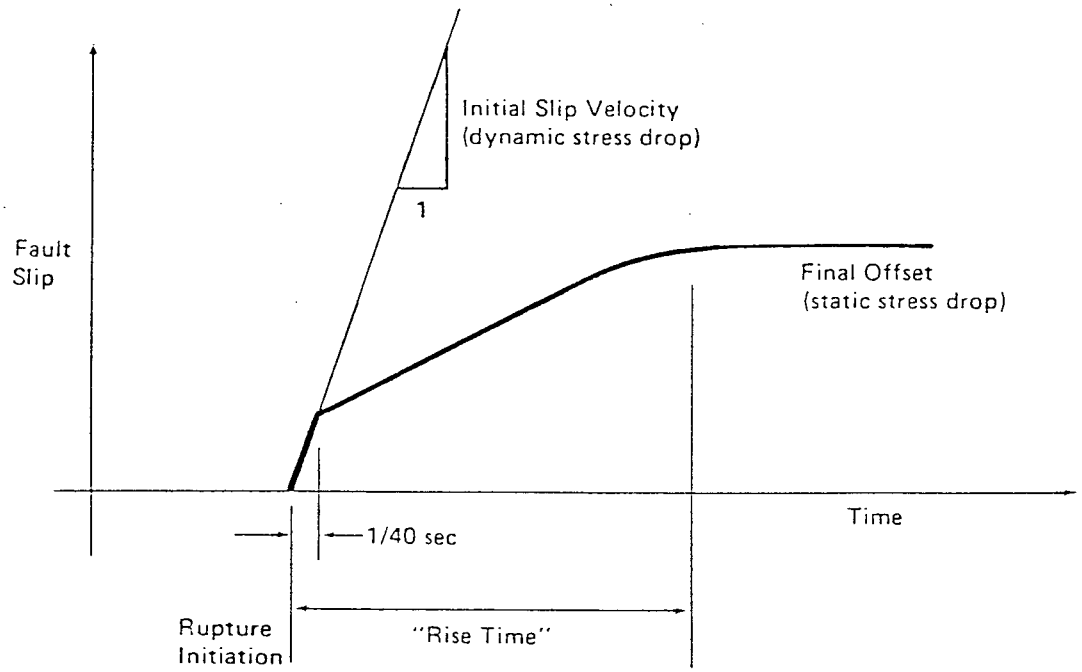

Figure 3-2. Idealized slip function used in May, 1978 report.

Figure 3-3 presents DELTA's recently developed three-parameter slip function. The three parameters are the same as those in the May, 1978 report; namely, initial slip velocity, final offset, and duration of slip (rise time). In the current slip function, however, there is gradual transition from the high initial slip velocity to the final offset. We note two advantages of the current slip function. First, the slip function closely resembles slip obtained from numerical simulations of the earthquake process. Second, the three-parameter slip function reduces to the conventional ramped step two-parameter function as the rise time approaches the final offset divided by the maximum slip velocity. Thus, results for a two-parameter slip function occur as a natural consequence of parameter studies involving the three-parameter slip function.

3.3 SPECTRAL CONSEQUENCES OF VARYING FAULT SLIP

Examination of the spectral amplitude of the slip function is useful to analysis of the way in which changes in the various slip parameters influence these amplitudes. Such information is also useful for interpreting how slip characteristics influence response spectra of computed ground motions. As illustrated in Appendix A of the May, 1978 report, one appropriate procedure is to compute response spectra from slip velocity using the same algorithm that produces response spectra from ground acceleration. The correspondence between slip velocity and ground acceleration at high frequencies is described below.

As depicted in Figure 2-3, computed ground displacement u(t) can be approximated as the convolution of three terms: fault slip s(t), Green's function g(t), and time filter T(t) which has a trapezoidal-like shape for a rectangular zone of rupture. Consequently, the spectral amplitude of ground motion is simply the product of the spectral amplitude of these three terms. For very long periods (low frequency) the pseudo-trapezoidal filter appears as an impulse whose spectral amplitude is independent of frequency; while, at very short periods (high frequency), the filter has the characteristics of a ramp function whose spectral amplitude varies as inverse frequency squared. Similarly, at short periods (high frequency), the spectral amplitude of the Green's function varies linearly with frequency in the absence of material attenuation.

DELTA'S THREE-PARAMETER SLIP FUNCTION

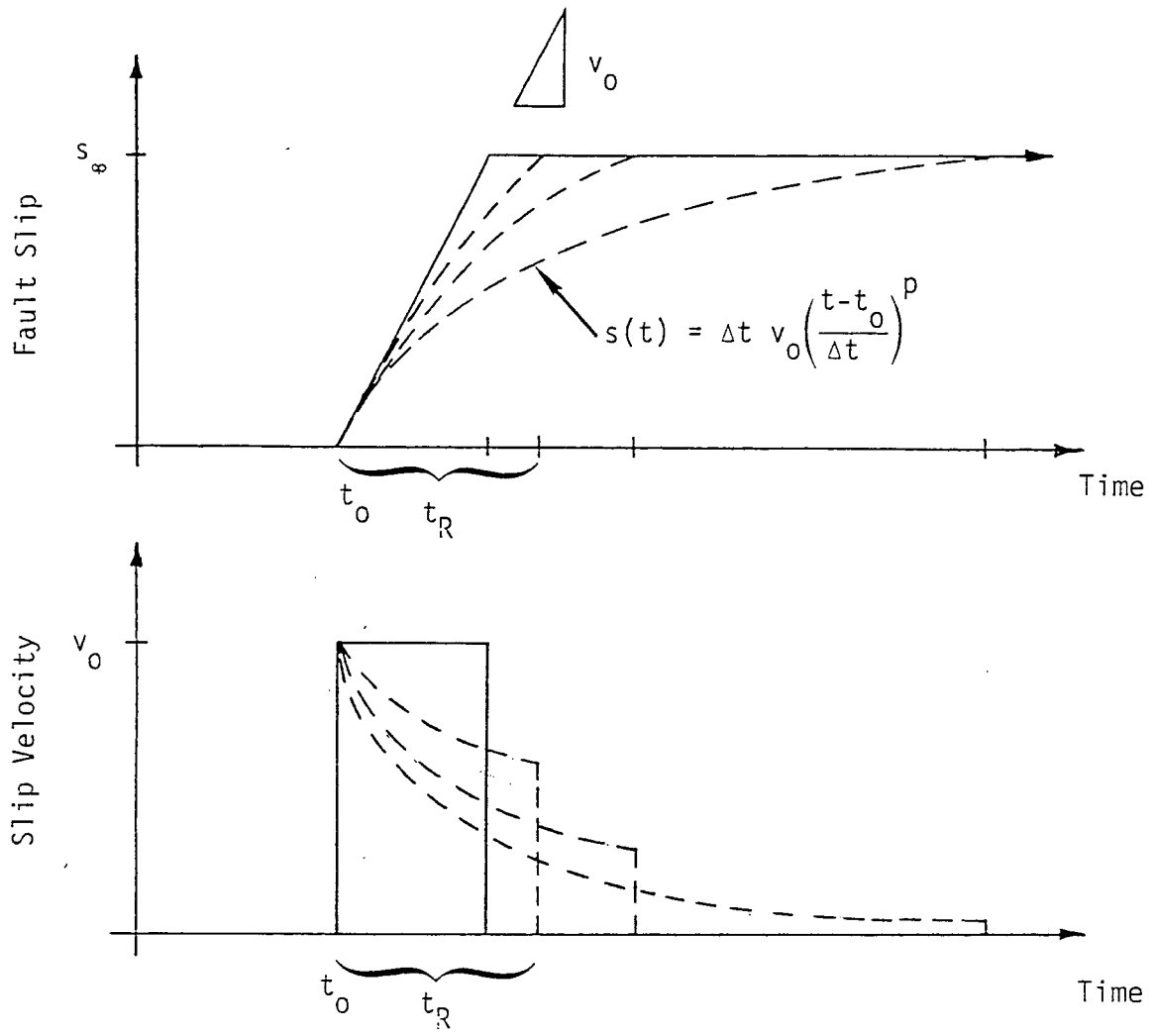

v_o = initial slip velocity ∿ dynamic stress drop

s_∞ = Final fault offset ∿ static stress drop

t_o = time of rupture initiation

t_R = rise time (duration of slip at a point)

$= \frac{s_\infty}{v_o}$ for two-parameter model.

Figure 3-3. Idealized slip function in which $p = [\ln(s_\infty/\Delta t\ v_o)]/\ln(t_R \Delta t)$ is assigned to cause $s(t = t_o + t_R) = s_\infty$. Note that $p = 1$ for $t_R = s_\infty/v_o$, thus yielding the two-parameter slip function.

For short periods, then, the spectral amplitude of the ground motion is given by

$$\hat{\dot{u}}(\omega) \sim \frac{T_o}{\omega^2} \times (\omega g_o) \times \hat{\dot{s}}(\omega)$$

where ω denotes angular frequency, and T_o and g_o denote amplitude scaling factors for the pseudo-trapezoidal filter and the Green's function, respectively. The expression merely states the well-known fact that convolutions with Green's functions tend to differentiate at high frequencies, and the not-so-well-known fact that convolutions with the time filter which accounts for spatially distributed rupture tend to integrate twice at high frequencies. Thus, high frequency ground accelerations vary with frequency in a manner similar to that for slip velocity $\dot{s}(t)$, and response spectra that are computed from slip velocity should resemble response spectra for ground accelerations at high frequencies. In the low frequency limit, the response spectrum computed from slip acceleration resembles that computed from ground acceleration.

Since high frequencies are most relevant to this project, the spectral properties of the slip function are illustrated using response spectra computed from slip velocity. Figures 3-4 through 3-6 show how response spectrum varies with maximum slip velocity (v_o), static offset (s_∞), and rise time (T_R), respectively. Consistent with results in Appendix A of the May, 1978 report, short periods vary linearly with v_o; and long periods vary linearly with s_∞.

Figures 3-7 and 3-8 show how response spectrum varies with rise time and static offset, respectively, for the special case of a ramped step slip function, i.e., $s_\infty = T_R v_o$. The results presented in these two figures are obtained analytically below as a check on the correctness of our numerical scheme for computing response spectra.

The response spectrum is defined to be maximum response experienced by a single-degree-of-freedom oscillator when subjected to specified base motion.

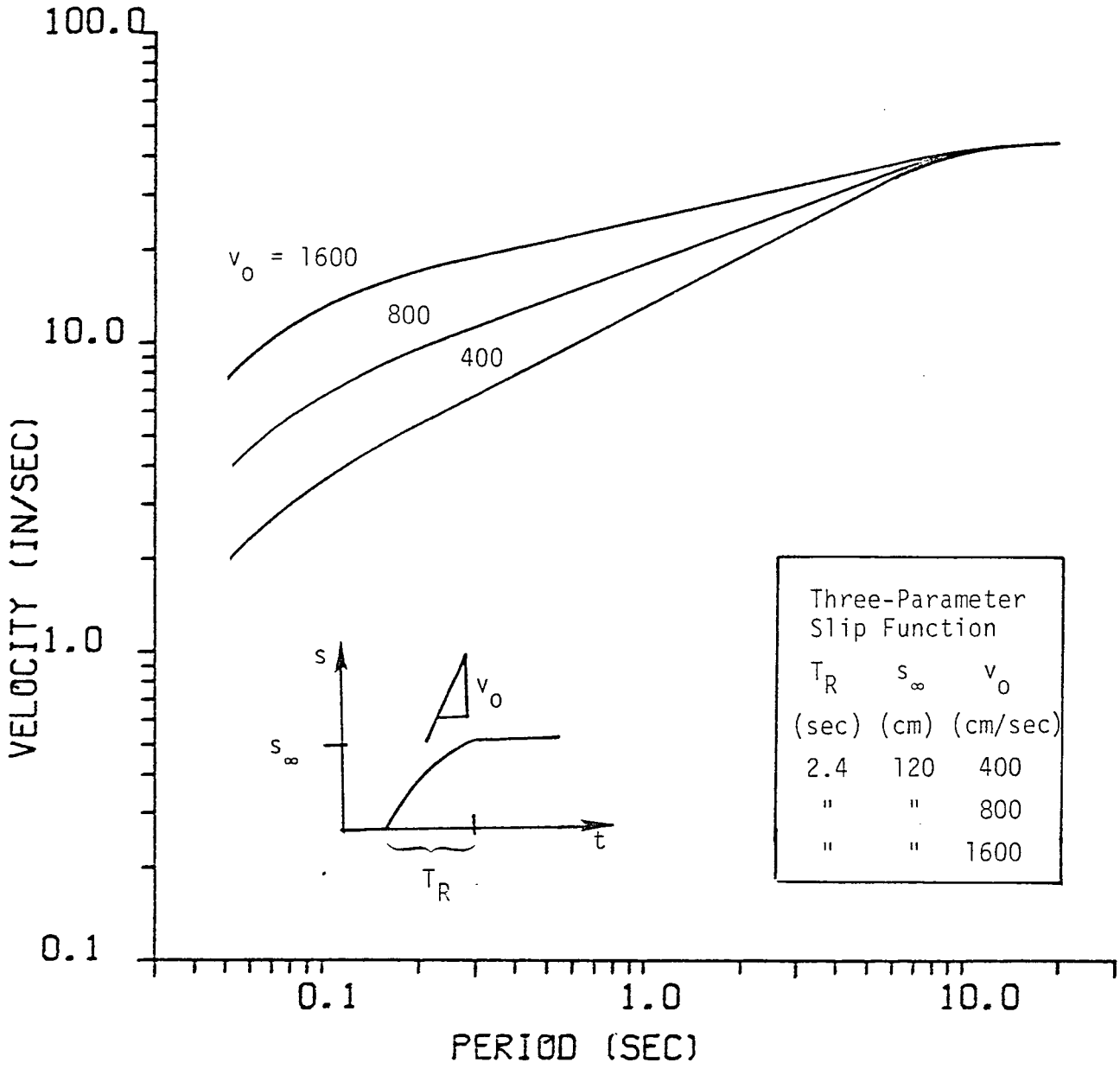

Figure 3-4. Effect of varying initial slip velocity on response spectrum for DELTA's three-parameter slip function.

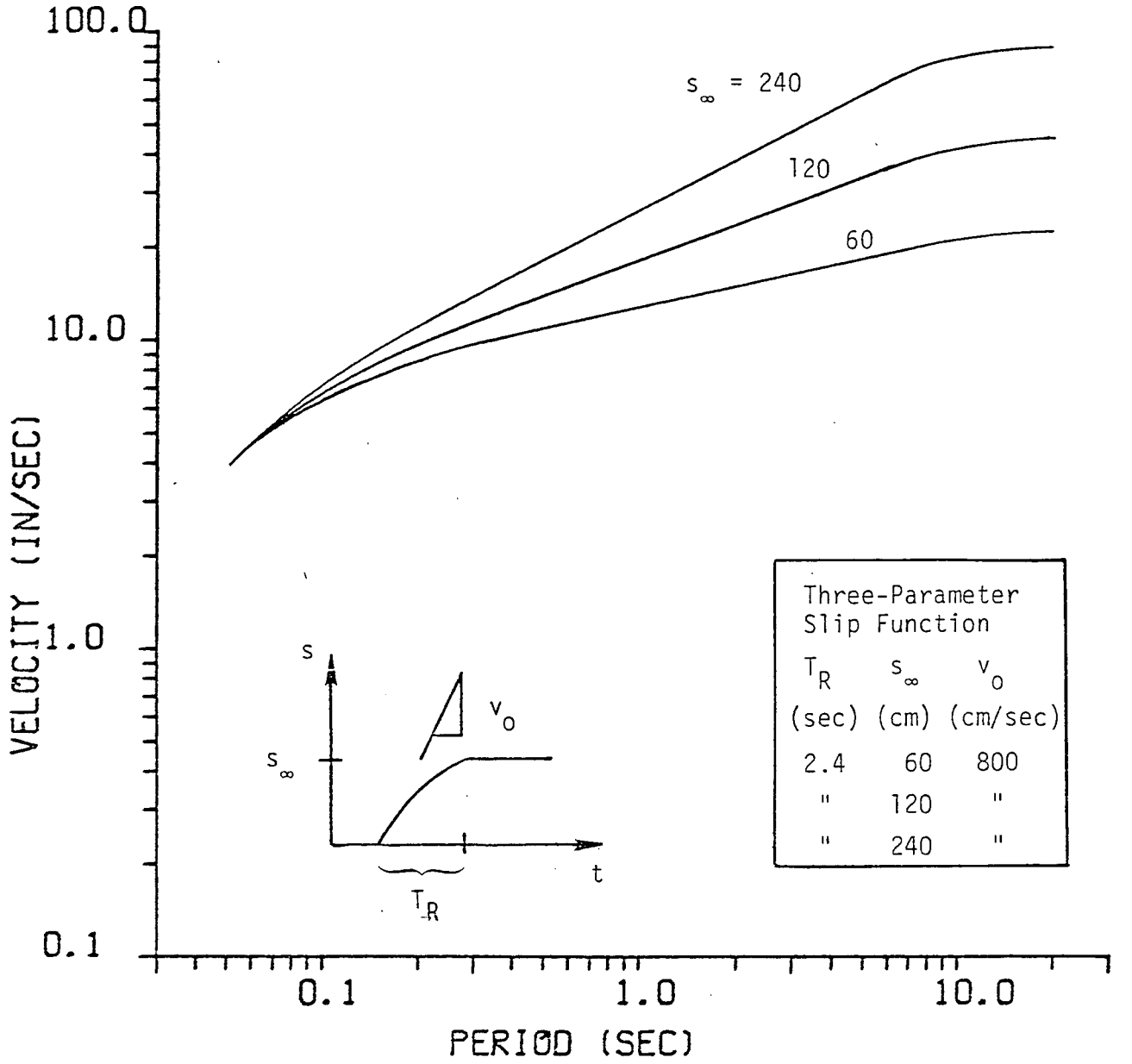

Figure 3-5. Effect of varying final offset on response spectrum for DELTA's three-parameter slip function.

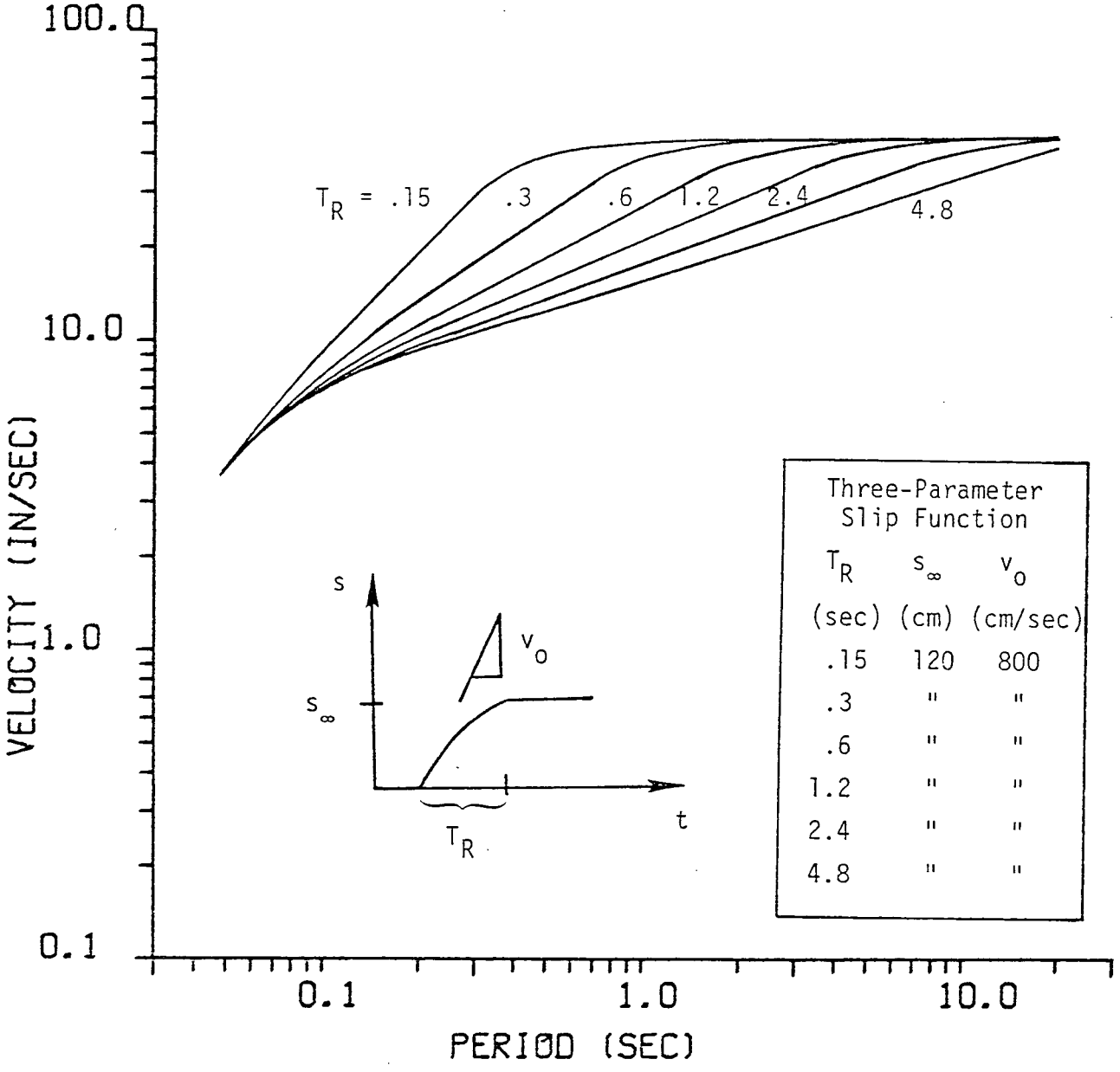

Figure 3-6. Effect of varying rise time on response spectrum for DELTA's three-parameter slip function. Rise time is varied such that the three-parameter slip function approaches the two-parameter function as the rise time becomes 0.15 sec. (s_∞/v_o)

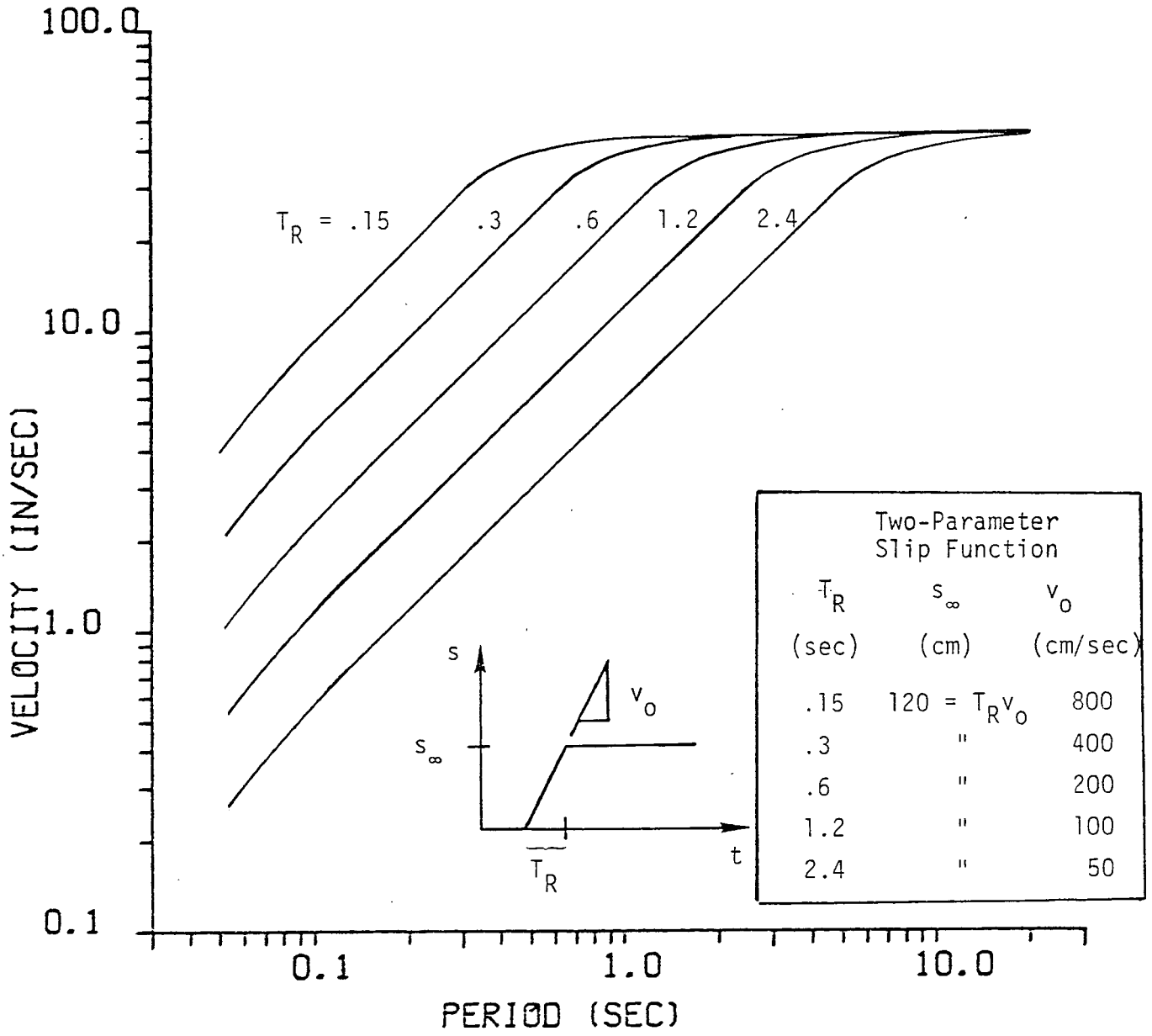

Figure 3-7. Effect of varying slip velocity on response spectrum for two-parameter slip function holding final offset constant.

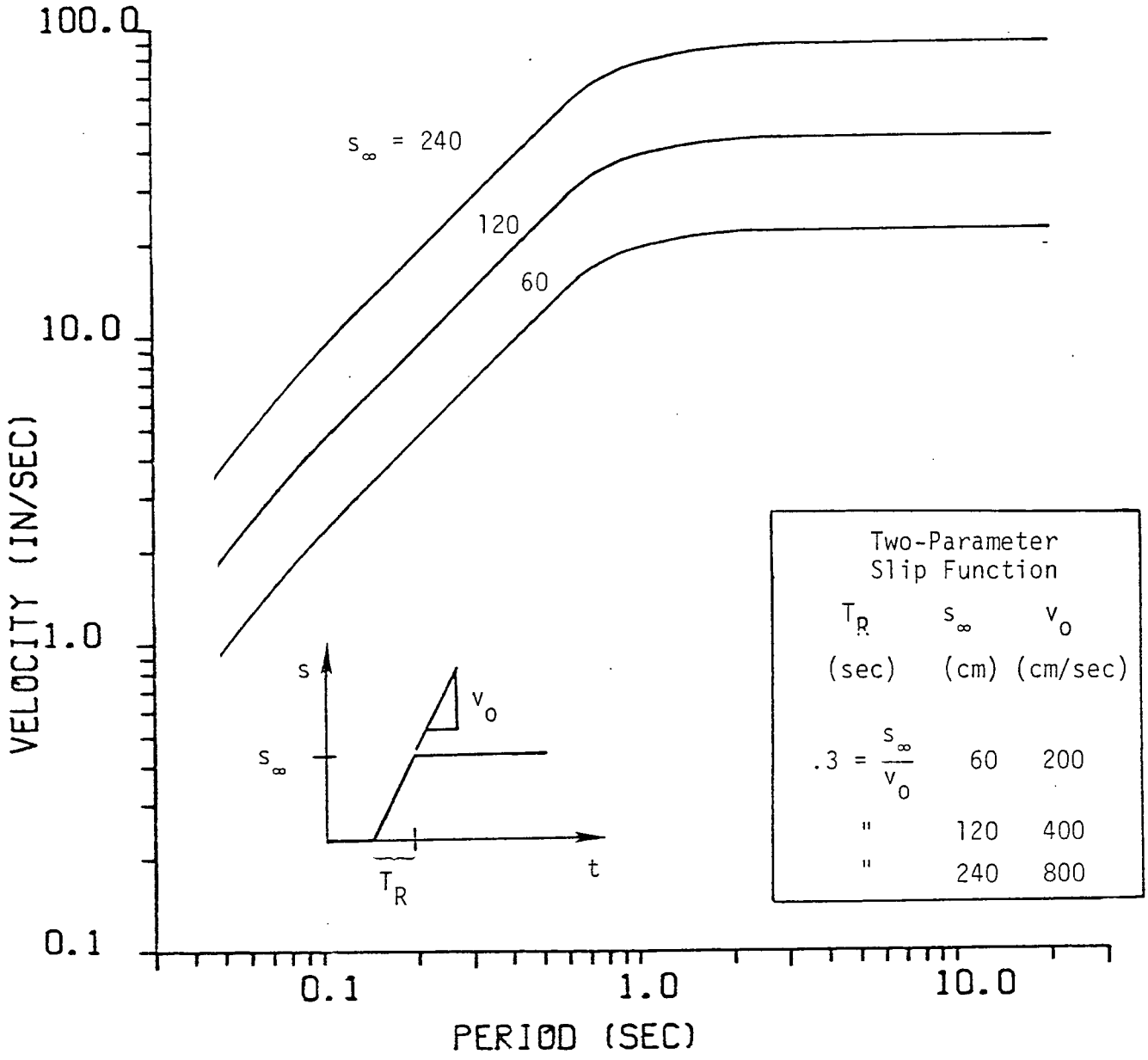

Figure 3-8. Effect of varying final offset on response spectrum for two-parameter slip function holding rise time constant.

The resonant frequency (or period) of the oscillator corresponds to the spectral frequency (or period). Thus, the displacement response spectrum, $d(\omega)$, is the maximum value obtained by

$$v(t,\omega) = - \int_0^t \frac{\ddot{x}(\tau) e^{-\omega\lambda(t-\tau)}}{\omega\sqrt{1-\lambda^2}} \sin \omega\sqrt{1-\lambda^2}\,(t-\tau)\,d\tau$$

where $\ddot{x}$ denotes base acceleration and ω and λ are the resonant frequency and damping coefficient of the oscillator, respectively.[6] For the special case of zero damping ($\lambda = 0$), the response equation becomes

$$v(t, T) = - \frac{T}{2\pi} \int_0^t \ddot{x}(\tau) \sin \frac{2\pi}{T}\,(t-\tau)\,d\tau,$$

where $T = 2\pi/\omega$.

Figures 3-7 and 3-8 are produced for an acceleration pulse which is a boxcar of width = T_R and height = $v_o = s_\infty/T_R$.

$$\ddot{x}(t) = \begin{cases} 0, & \text{for } t < 0 \\ v_o, & \text{for } 0 \leq t \leq T_R \\ 0, & \text{for } t > T_R \end{cases}$$

Substituting this formula for base accelerations into the undamped response equation yields

$$u(t, T) = \left(\frac{T}{2\pi}\right)^2 v_o \begin{cases} \left[1 - \cos\frac{2\pi t}{T}\right] & , \text{for } 0 \leq t \leq T_R \\ \left[\cos\frac{2\pi}{T}(t - W) - \cos\frac{2\pi t}{T}\right] & , \text{for } t > T_R \end{cases}$$

Hence, the displacement response spectrum, which is the maximum value of $u(t, \tau)$ over all $t > 0$, becomes

$$d(T) = \left(\frac{T}{2\pi}\right)^2 2v_o \begin{cases} 1 & , \text{for } 2T_R > T \\ \sin\frac{\pi T_R}{T} & \text{for } 2T_R < T \end{cases}$$

The pseudo velocity response spectrum is simply the product of the displacement response spectrum and the angular frequency of the oscillator, i.e.,

$$v(T) = \left(\frac{2\pi}{T}\right) d(T)$$

$$= \left(\frac{T}{2\pi}\right) 2v_o \begin{cases} 1 & \text{for } 2T_R > T \\ \sin\frac{\pi T_R}{T} & \text{for } 2T_R < T \end{cases}$$

as plotted in Figures 3-7 and 3-8.

4.0 RUPTURE INCOHERENCE

4.1 NEED FOR INCOHERENCE

Most analyses regarding spontaneous growth of earthquake-like cracks have been conducted in ideally homogeneous material. Synthetic seismograms produced by these analyses appear exceedingly simple when compared with recorded earthquake motions. The introduction of the free surface and geologic layers into the analyses produce synthetic seismograms that much more closely resemble those recorded for actual earthquakes. Physically unobserved behavior results, however, when an idealized coherent crack is focused directly at a recording station as is the case in modeling Station 2 of the Parkfield Earthquake. First, the synthetic acceleration record is composed primarily of one isolated spike which is inconsistent with field observations. Second, the transverse component of ground motion (which depicts the arrival of SH waves) is several times greater than the radial component (which responds to P and SV motions). The peak acceleration recorded on the two horizontal components seldom differs by more than 30 to 40 percent, contrary to the synthetic ground motions produced by the ideally coherent rupture. Finally, under conditions of ideally coherent rupture, the peak acceleration in the path of focusing is several times greater than motions obtained at other sites of nearly equal distance from the rupture surface, but not directly in the path of focusing (e.g., Stations 5 and 8 of the Parkfield Earthquake).

These inconsistencies between simulated earthquake ground motions and recorded motions result largely from incoherence in the rupture process of actual earthquakes. Actual earthquake rupture stops, lurches ahead, changes direction and even ruptures several times at one point on the rupture surface. It is this non-regular rupture behavior that breaks up the emission of ideally coherent waves. In addition, as seismic energy leaves the rupture surface en route to the recording station, many paths are followed, not just those paths provided for in ideally horizontally layered structures. These non-coherent and irregular features of actual earthquake rupture are certainly more prevalent at

high frequencies -- frequencies in the range of 5 to 20 Hz -- than for lower frequencies, where most seismologic research is conducted.

As demonstrated in Section 5.3 of the present work, some of these non-coherent or irregular processes must be incorporated into the earthquake modeling procedures in order to simulate earthquake ground motion under all conditions, particularly when directly in the line of focus of the progressing rupture. The complexities of these processes are beyond our ability to model deterministically. Consequently, we have resorted to random processes as a point of departure from the ideally coherent rupture. The particular random processes that have been introduced are described in the subsequent section.

4.2 INCOHERENT FEATURES OF DELTA'S EARTHQUAKE MODEL

Five types of nondeterministic incoherence have been introduced into DELTA's earthquake model: one to account for phenomena on length scales less than 1 km, termed "micro-incoherence," and four to account for phenomena on length scales of 1 km and greater, termed "macro-randomness." First, micro-incoherence will be discussed.

Coherent ruptures expanding at 90 percent of the shear wave velocity over a 1-km-square segment of rupture can, under ideal conditions, produce larger motions at a station directly in the line of focus from that rupture segment than the entire earthquake produces for stations not in line with the focus but much closer to the rupture surface. More simply stated, wavelengths on the order of 100 meters can strongly focus in a distance of 1 km under ideal conditions. Two modifications to the ideally coherent rupture have been investigated for limiting the amount of focusing that can occur from such small segments of rupture. One modification that was investigated, but not employed in the current model, involves the construction of rupture over a 1-km-square segment as a combination of several thousand ruptures over sub-segments with an area of a few hundred square meters each. The time for rupture initiation in each segment was taken as the time for ideally coherent rupture arrival within the sub-segment plus or minus a random number between 0 and 0.1 seconds. This

procedure has the effect of low-pass filtering synthetically produced ground motions at all of the recording stations by the same amount. Since ideally focused stations received more predominantly high frequency energy, the effect was more noticeable on the focused stations.

An alternate and much more direct approach was used to prevent strong focusing for rupture over 1-km distances. Consistent with the method that was employed in the May, 1978 report, a mathematical limit was placed on the degree of focusing to be allowed from any single 1-km-square segment of rupture. Specifically, the direct rays emanating from a 1-km-square rupture were not permitted to arrive at the receiver station in a time frame narrower than one-tenth of a second. This was accomplished by limiting the narrowness of the pseudo-trapezoid previously described in Section 2 of this report.

Macro-randomness has been introduced into the earthquake model to:

(1) delay the time of rupture initiation in each of the 1-km segments,

(2) alter the orientation of the rupture in each segment,

(3) alter the direction in which the rupture progresses through each rupture segment, and

(4) alter the orientation of particle motions that arrive at the receiver from each rupture segment.

Each of these sources of incoherence has been introduced through the use of a Gaussian random number generator. The time for rupture initiation in each segment has been delayed beyond that indicated by the arrival of the gross crack by a random number with a two-thirds confidence of not exceeding one second. The tip of the crack migrates through each 1-km-square segment in a direction that deviates from the gross direction of rupture propagation by a random number with a two-thirds confidence not in excess of 30 degrees. The orientation of the strike of each rupture segment has been modified by a random number with a two-thirds confidence of not exceeding 20 degrees. And finally,

horizontal particle motion computed at the receiver station from each rupture segment is altered in direction by a random number with a two-thirds confidence of not exceeding 30 degrees.

These five types of randomness and their ranges are summarized in Table 4-1. The influence that each type of randomness has on computed results is presented in Section 6.2.5 as additional parameter studies. Section 5 presents comparisons between ground motions computed using the randomness and not using the randomness to demonstrate the need for incoherency in the computer model when simulating recorded earthquake data.

4.3 EFFECTS OF RANDOMNESS ON COMPUTED RESULTS

The random processes that have been introduced cause the results to vary somewhat between repetitious calculations. The particular degree of variance is depicted in Figures 4-1 through 4-6 for the site specific smoothed response spectra.

In Figure 4-1, the four solid curves represent the southeast horizontal component of the site-specific response for precisely the same earthquake (offshore San Onofre Earthquake "D" using DELTA's model as defined in Table 5-1) as generated using four independent random number sequences. The variance is approximately $\pm$ 20 percent for frequencies between 5 Hz and 20 Hz. Similar variance is revealed for the northeast and vertical components in Figures 4-2 and 4-3, respectively.

The effect is more clearly visualized when varying the random number sequence thirteen times for the same earthquake, as shown in Figures 4-4 through 4-6. In addition, it is possible to derive the mean Earthquake "D" and the standard deviation from the mean using such studies, as presented in Figures 4-7 through 4-9.

TABLE 4-1

RANDOM PARAMETERS

I. MICRO-INCOHERENCE (within 1-km zones of rupture)

(1) Single zones of rupture produce at least 0.1 sec of signal spread at the receiver.

II. MACRO-RANDOMNESS (between 1-km zones of rupture)

(2) Initiation time randomness

= gross rupture arrival + 0 to 1 sec of randomness.

(3) Rupture direction randomness

= gross direction of rupture extension $\pm$ 30° of randomness.

(4) Fault orientation randomness

= gross strike orientation $\pm$ 20° of randomness.

(5) Receiver orientation randomness

= direction of particle motion at recording station $\pm$ 30° of randomness.

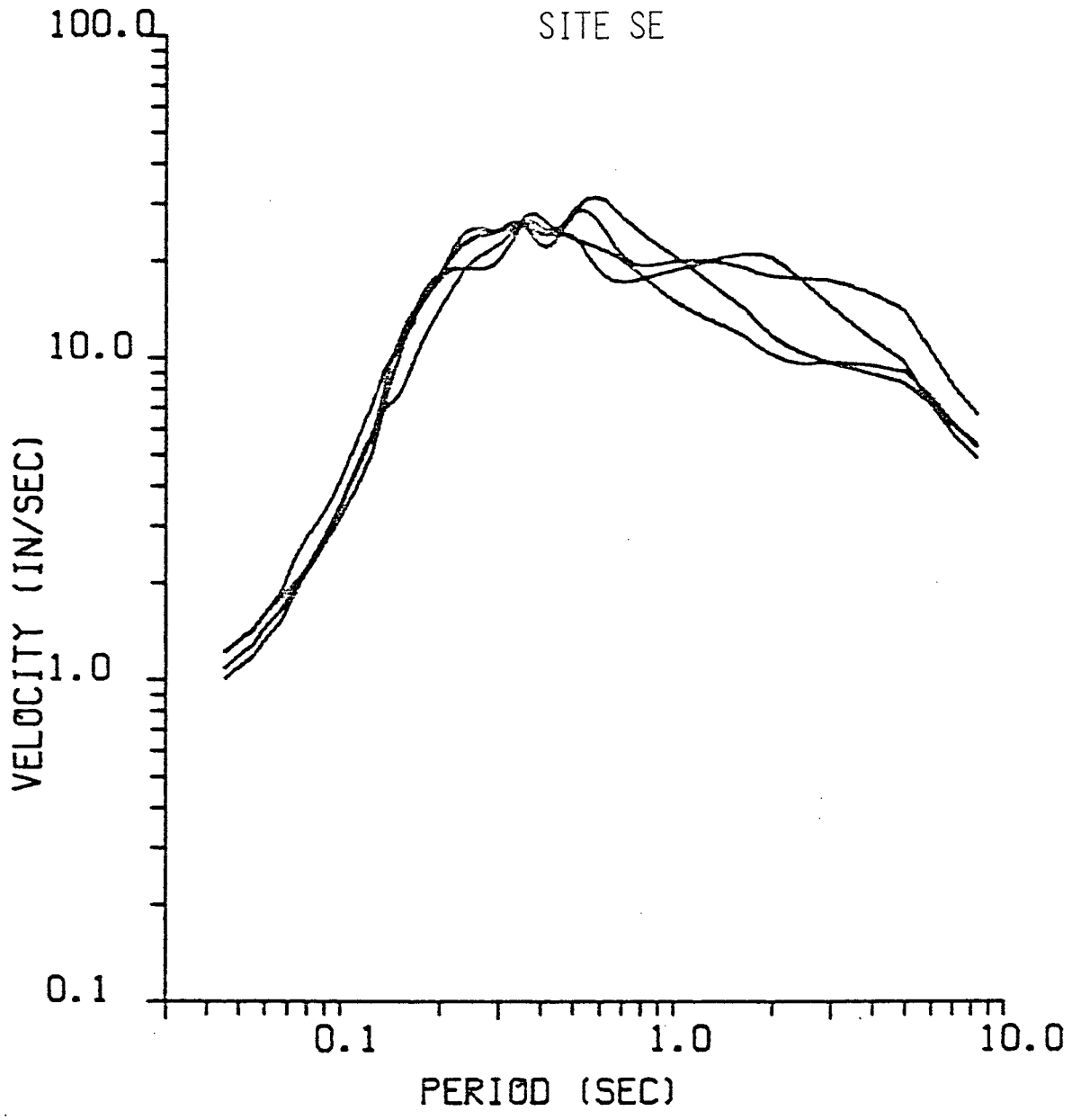

Figure 4-1. Effect of varying random number sequence four times on site specific response for southeast component.

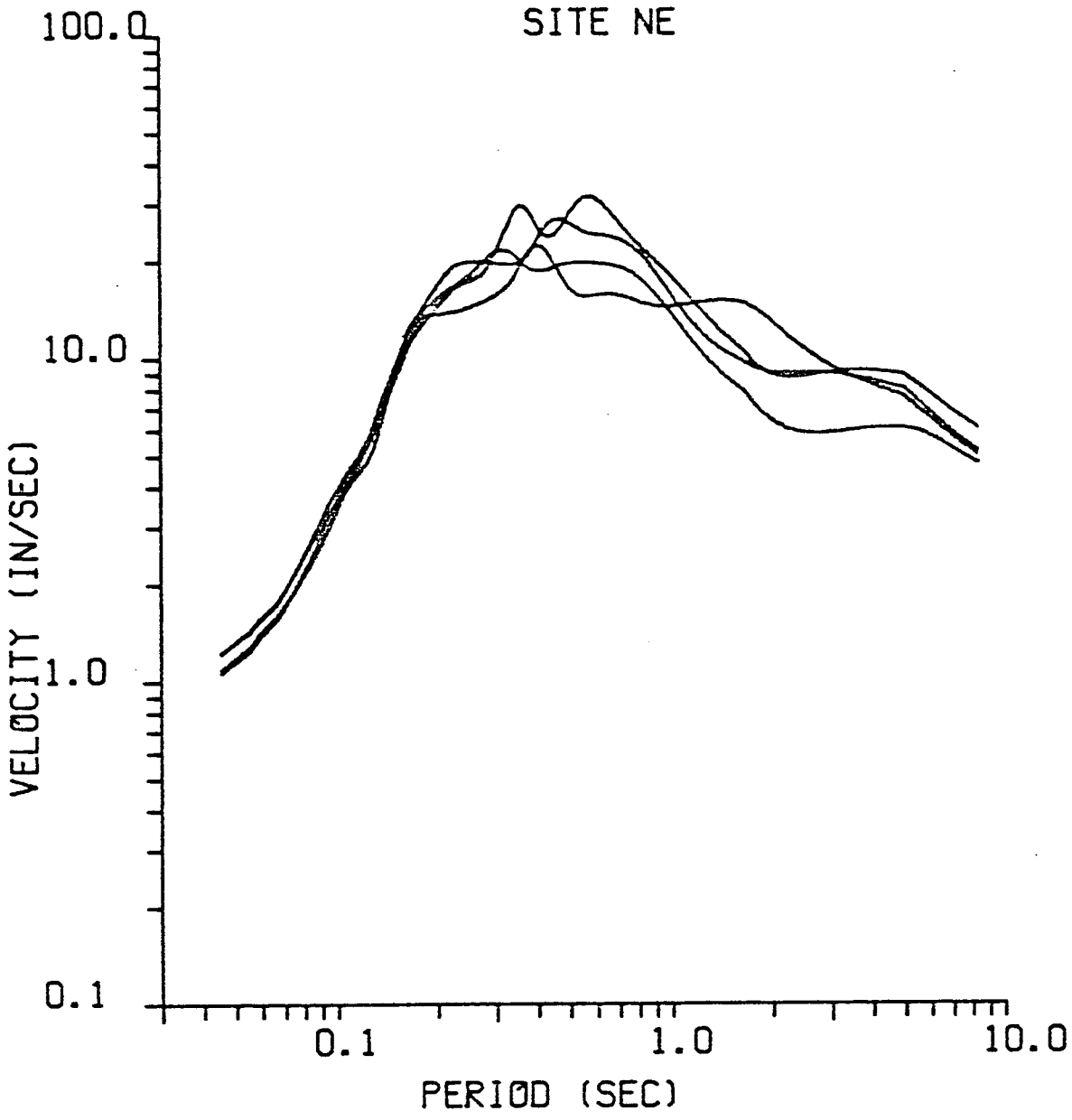

Figure 4-2. Effect of varying random number sequence four times on site specific response for northeast component.

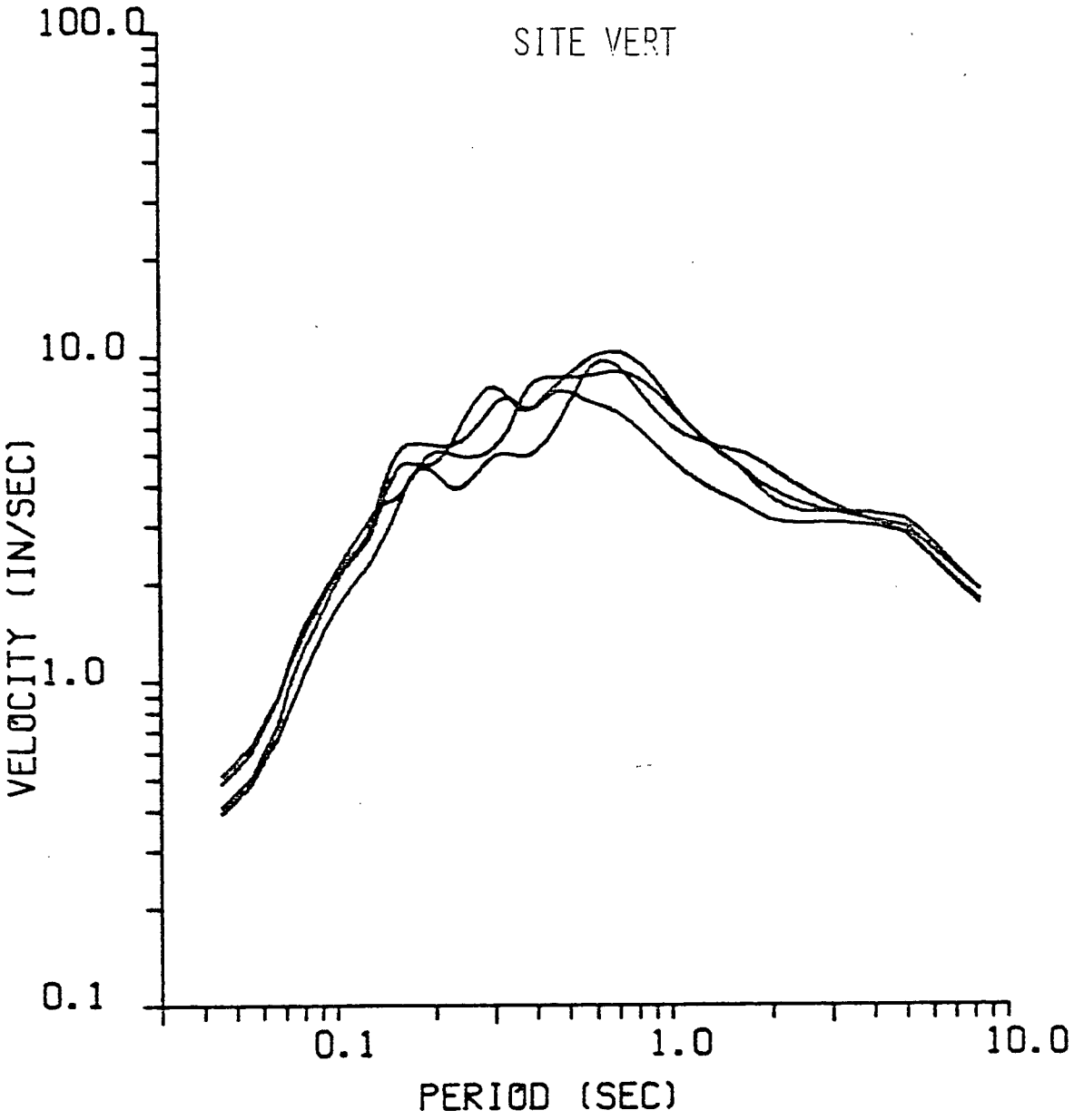

Figure 4-3. Effect of varying random number sequence four times on site specific response for vertical component.

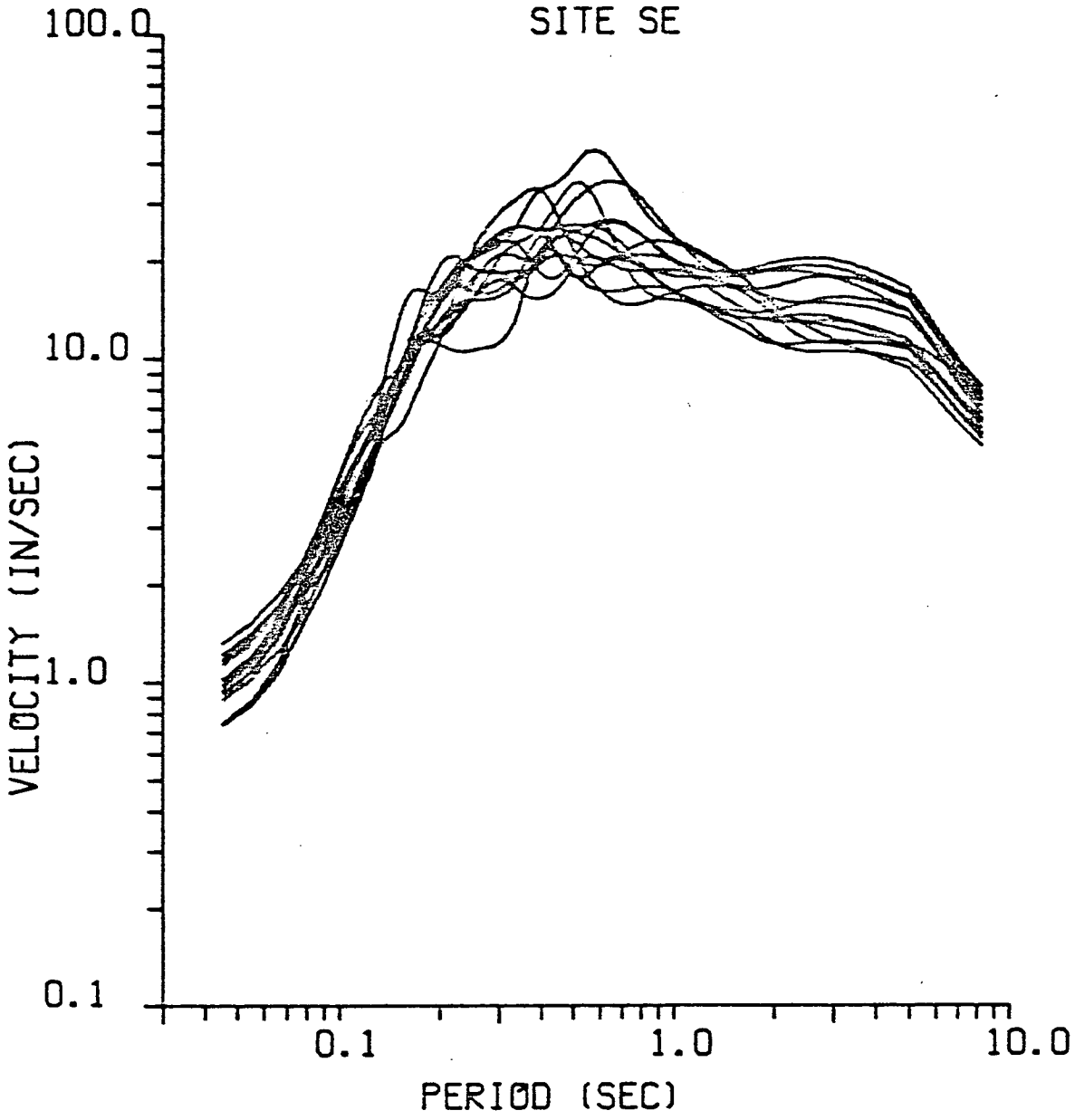

Figure 4-4. Effect of varying random number sequence thirteen times on site specific response for southeast component.

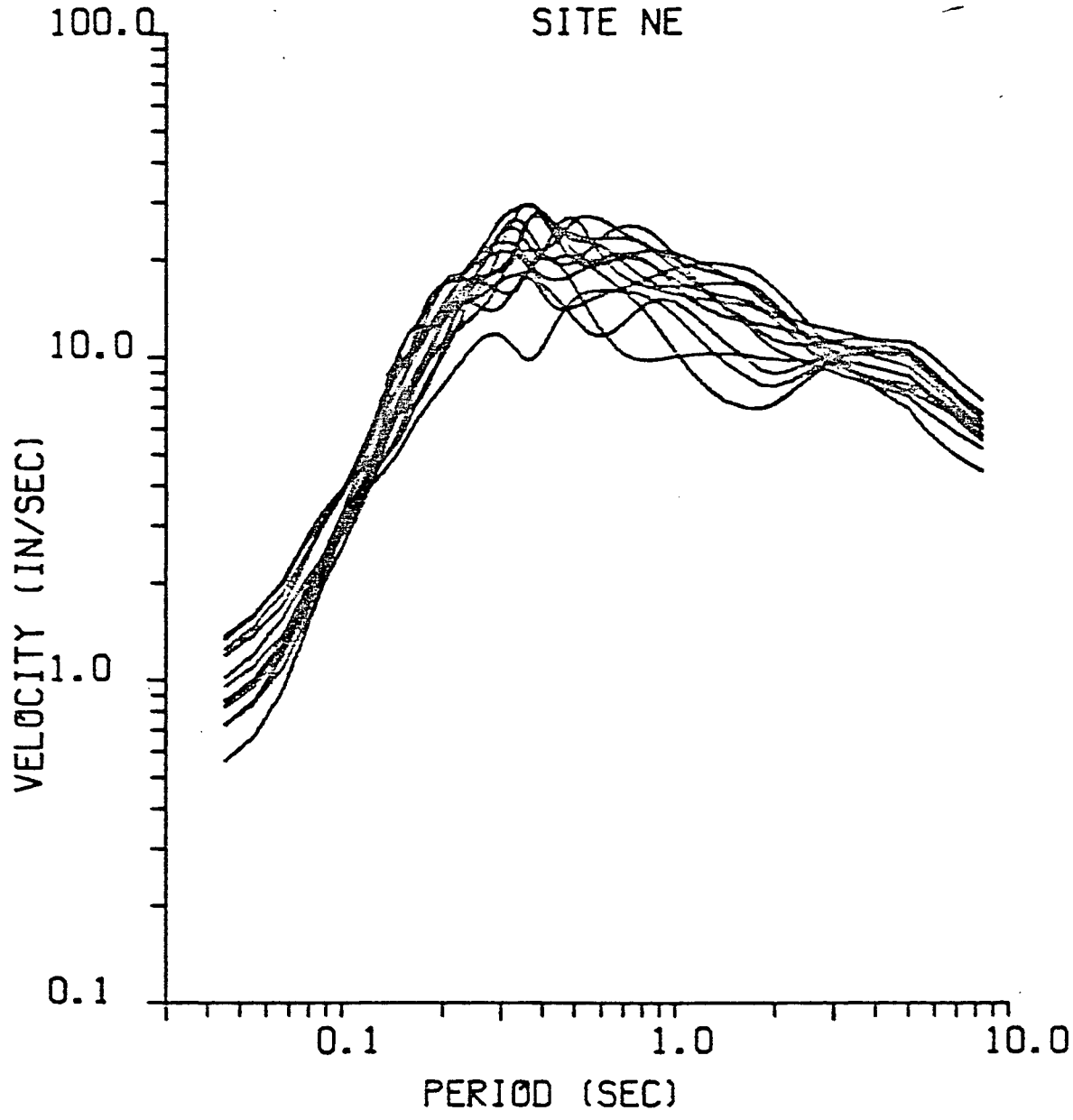

Figure 4-5. Effect of varying random number sequence thirteen times on site specific response for northeast component.

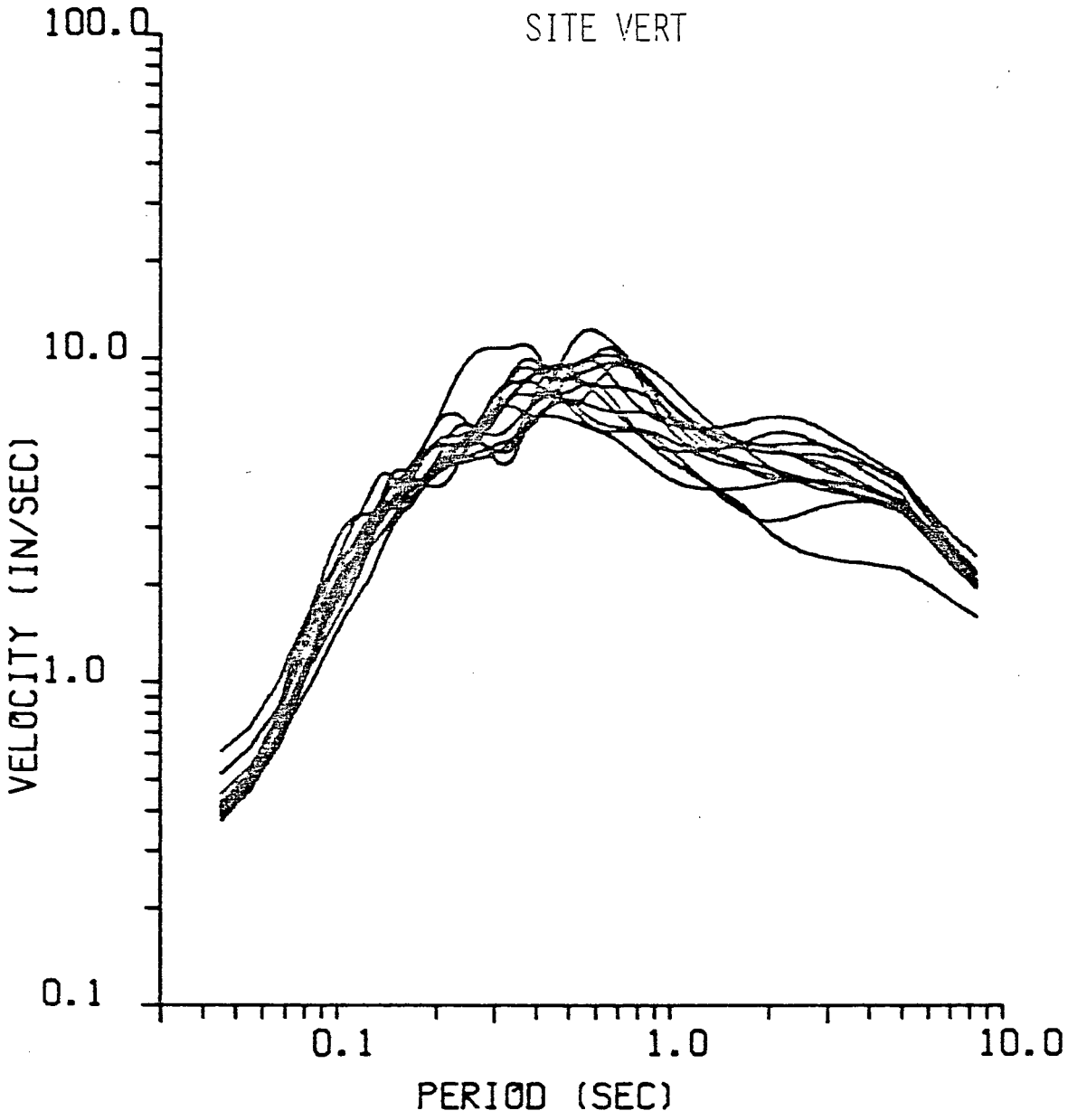

Figure 4-6. Effect of varying random number sequence thirteen times on site specific response for vertical component.

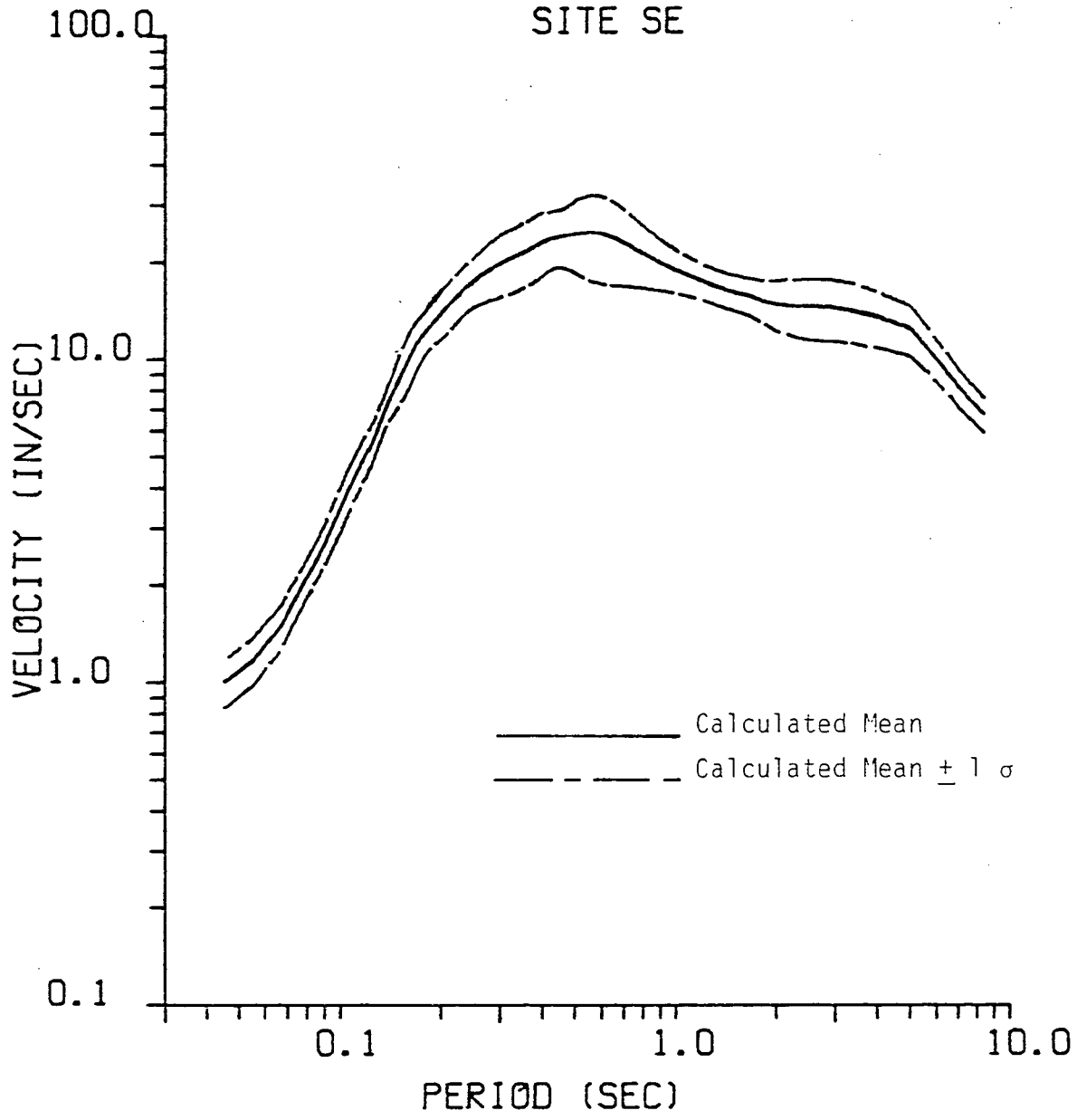

Figure 4-7. Calculated mean plus or minus one standard deviation for southeast component of site specific response as shown in Figure 4-4.

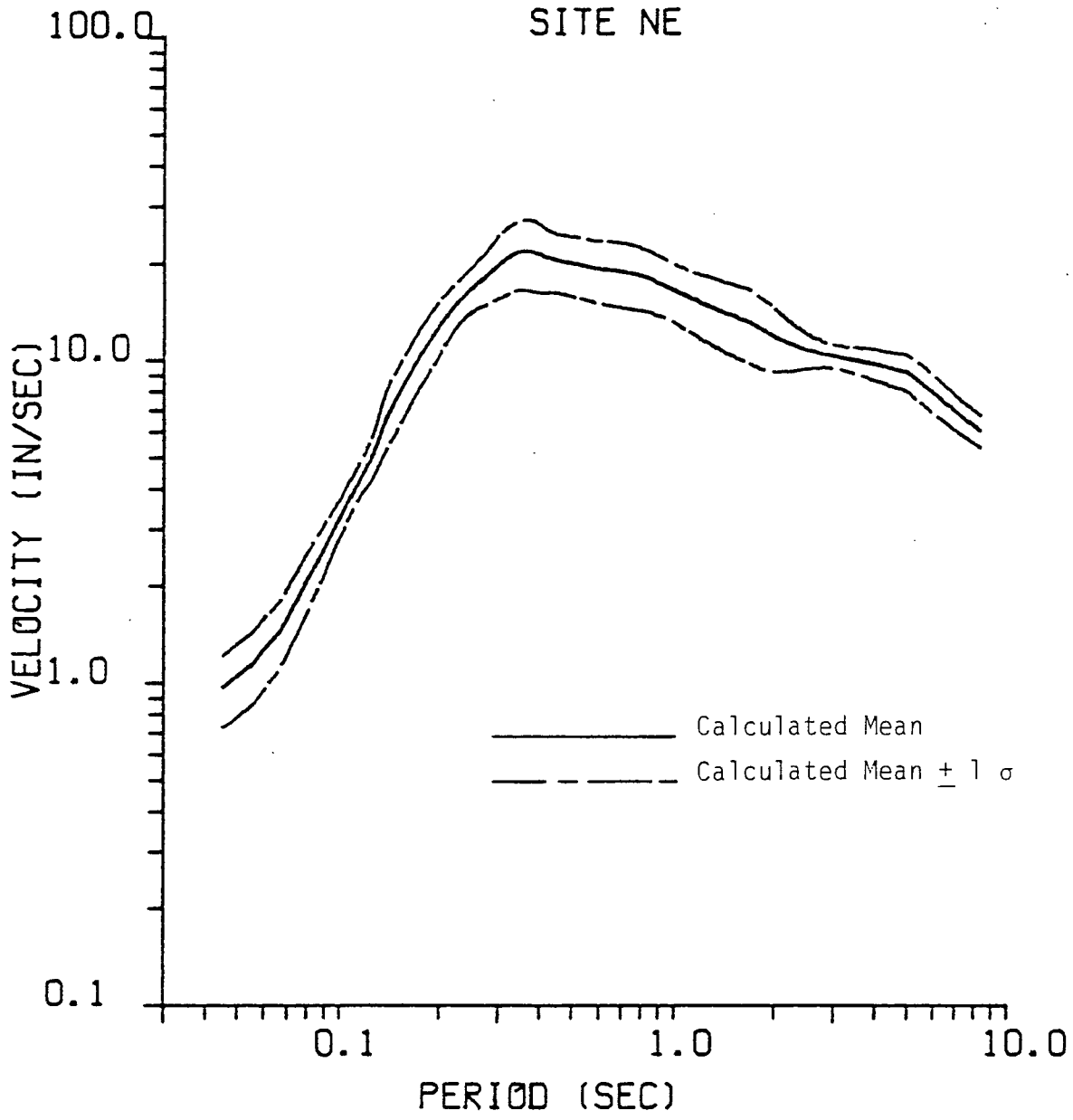

Figure 4-8. Calculated mean plus or minus one standard deviation for northeast component of site specific response as shown in Figure 4-5.

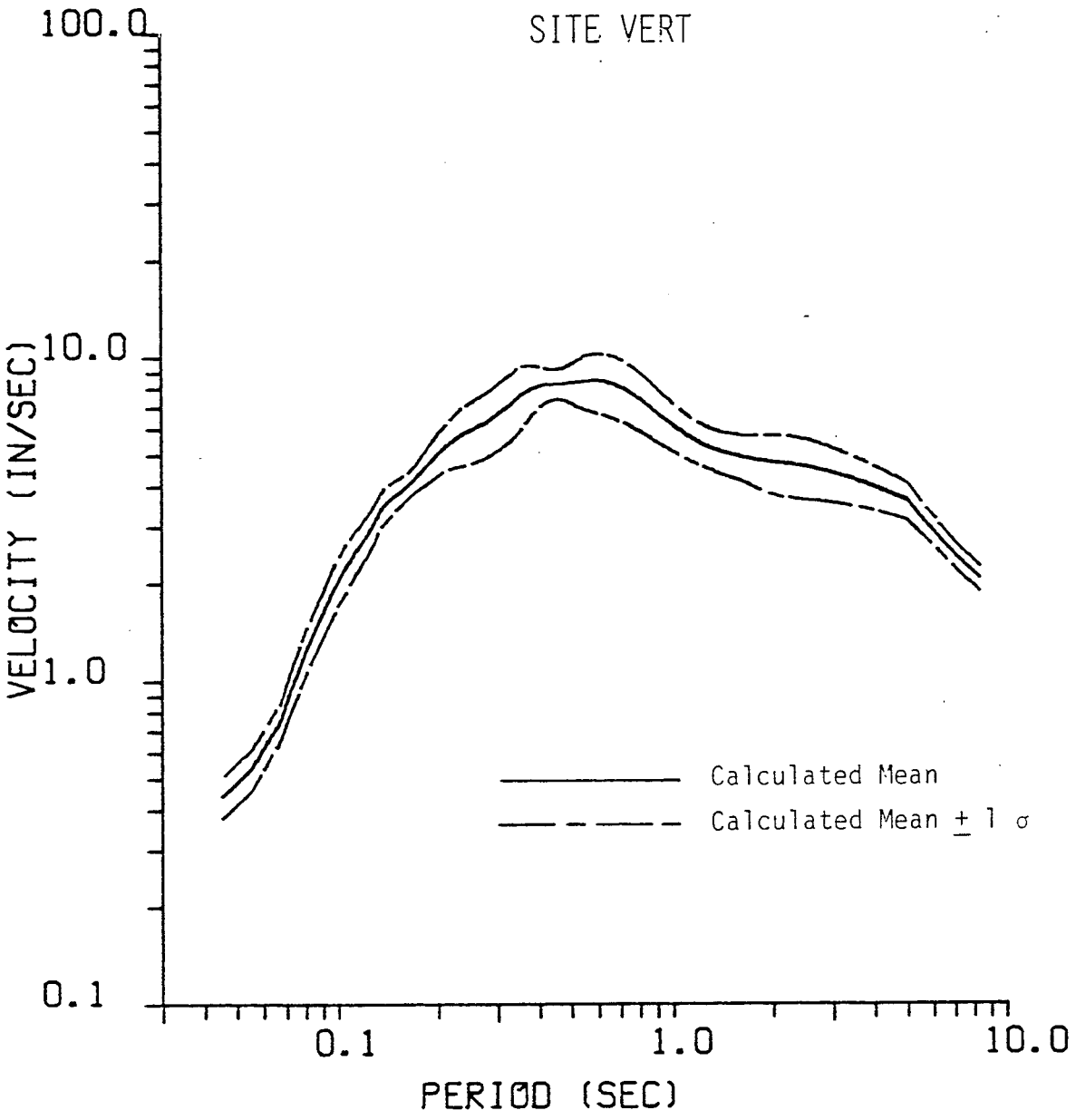

Figure 4-9. Calculated mean plus or minus one standard deviation for vertical component of site specific response as shown in Figure 4-6.

5.0 RESULTS OF EARTHQUAKE MODELING STUDIES

5.1 EARTHQUAKES STUDIED

The 1940 Imperial Valley Earthquake and the 1966 Parkfield Earthquake are studied in order to calibrate various earthquake models for use in extrapolating site specific ground motion. Both earthquakes underwent strike-slip motion (similar to the hypothesized motion at San Onofre in the event of an offshore earthquake) and both were located in Southern California.

The 1940 Imperial Valley Earthquake is the largest recorded strike-slip earthquake to date in Southern California. However, the recorded data is insufficient to precisely describe the rupture phenomena -- the station at El Centro (see Figure 5-1) provides all the close-in strong motion recordings. Yet, Trifunac and Brune[8] suggest that the aggregate rupture process was composed of a sequence of small ruptures. Such a hypothesis is most likely attributable to the broken fault trace as shown in Figure 5-1.

The earth model used to represent the Imperial Valley geology consists of five viscoelastic layers overlying a semi-infinite viscoelastic half-space similar to the published model of Heaton and Helmberger.[5] Empirical relations given in the May, 1978 report are used to prescribe the material attenuation factors. The individual parameters characterizing the layers are delineated in Table 5-1.

In contrast to the 1940 Imperial Valley Earthquake, five strong motion stations were operating within 15 km of the 1966 Parkfield earthquake rupture as shown in Figure 5-2. Fourteen strong motion accelerograms are available from the five stations, providing good coverage of the distribution of accelerations in the radiation pattern of the rupture. The N25W recording at Station 2 was inoperative. Considering that Station 2 is only 0.2 km from the hypothesized rupture front, the maximum accelerations on the N65E recording seem relatively low. Several explanations are plausible:

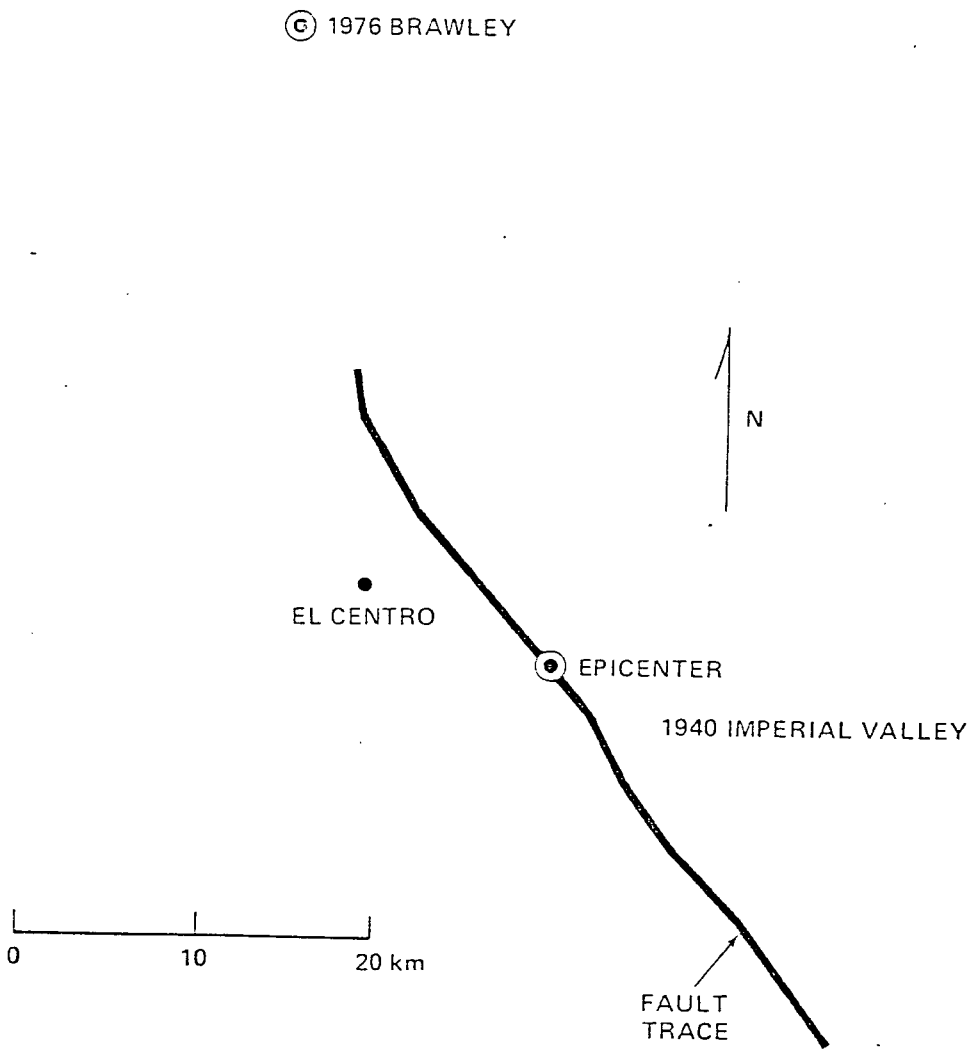

Figure 5-1. Map of the Imperial Valley.

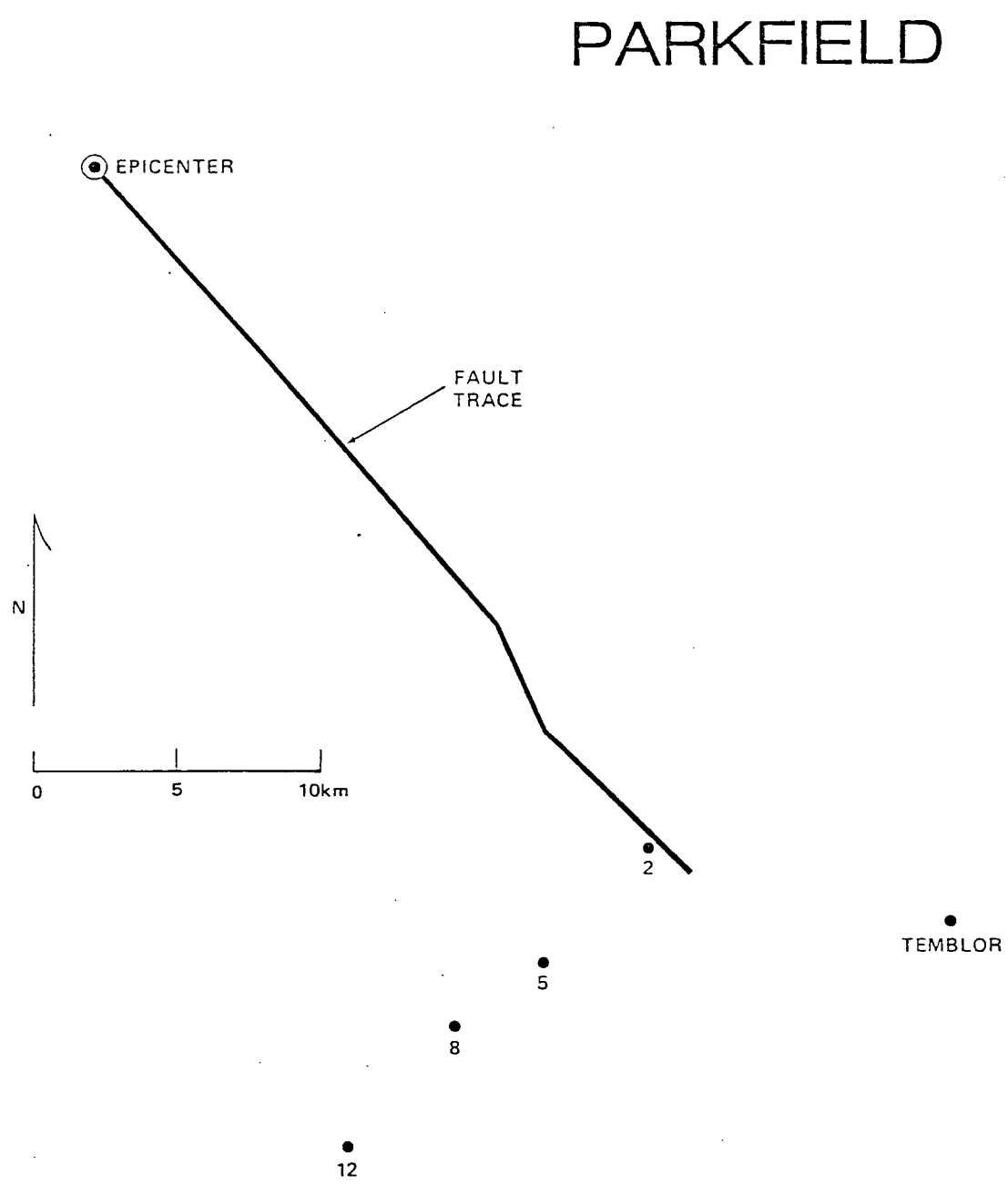

Figure 5-2. Map of the San Andreas Fault near Parkfield.

TABLE 5-1

VISCOELASTIC PARAMETERS FOR THE GEOLOGIC STRUCTURE FOR IMPERIAL VALLEY

Depth to Top of Layer (km)	Layer Thickness (km)	α P-wave Velocity (km/sec)	β S-wave Velocity (km/sec)	ρ Density (g/cc)	Q_p Compressional Quality Factor	Q_s Shear Quality Factor
0.	0.45	1.70	0.75	1.50	81	21
0.45	0.50	2.10	0.92	1.90	106	27
0.95	1.15	2.60	1.50	2.35	112	50
2.10	1.20	3.70	2.30	2.50	165	85
3.40	2.50	4.10	2.60	2.60	185	99
5.90	--	6.40	3.70	2.80	346	154

1. Nearby stations are affected more strongly by complexities in the rupture process than distant stations.

2. The brittle rupture did not reach Station 2.

3. Significant non-linear deformation occurred in the earth underlying Station 2.

4. The recording was inaccurate at Station 2.

These observations should be considered when later interpreting the fit to the data for all five Parkfield stations, simultaneously.

The earth model used to represent the Parkfield geology consists of six viscoelastic layers overlying a viscoelastic semi-infinite half-space similar to the published model of Eaton, et al.[4] The layer properties are specified in Table 5-2. The effects of using layers which are an order of magnitude thicker than the wavelengths of interest are discussed in Section 6.3 and by Apsel (1979, Section 5.3.4).

5.2 MODELS USED AND OVERVIEWS

Site-specific ground motions are extrapolated from numerical calibrations of the Parkfield and Imperial Valley Earthquakes using three different characterizations of fault slip. The three models considered correspond to:

1. DELTA's three-parameter slip function with randomness

2. Two-parameter slip function with randomness

3. DELTA's three-parameter slip function without randomness

Each prescription of fault slip is calibrated to best match the high frequencies recorded for the Parkfield and Imperial Valley Earthquakes. The important consequence of such calibrations is that the site-specific response spectra for an offshore San Onofre earthquake are rather independent of alternate interpretations of fault slip for frequencies greater than 2 Hz.

TABLE 5-2

VISCOELASTIC PARAMETERS FOR THE GEOLOGIC STRUCTURE
SOUTHEAST OF PARKFIELD

Depth to Top of Layer (km)	Layer Thickness (km)	α P-wave Velocity (km/sec)	β S-wave Velocity (km/sec)	ρ Density (g/cc)	Q_p Compressional Quality Factor	Q_s Shear Quality Factor
0.	0.116	0.99	0.57	1.50	34	15
0.116	0.164	1.71	0.99	1.50	66	30
0.28	1.27	2.81	1.62	1.62	124	55
1.55	2.19	5.04	2.91	2.21	257	114
3.74	11.25	6.02	3.48	3.46	320	143
14.99	10.00	6.86	3.95	3.93	378	167
24.99	--	8.09	4.67	4.64	464	206

The parameters used to define DELTA's three-parameter slip function are tabulated in Table 5-3 and comprise what will be referred to as DELTA's Earthquake Model. The two-parameter slip function is extracted from Table 5-3 by redefining the slip duration, t_R, to be the final offset divided by the maximum slip velocity for each earthquake. To calibrate the high frequencies at Parkfield and Imperial Valley, it was necessary to reduce the maximum slip velocity to 480 cm/sec for the two-parameter slip function and to increase the maximum slip velocity to 1,000-1,200 cm/sec for the three-parameter slip function without randomness.

As a general overview of the calibration exercises, DELTA's Earthquake Model provides the best fit to the observed response spectra across the broad frequency band and at all recording stations. The two-parameter slip function model performs equally well at high frequencies. However, the match for frequencies of one Hz and below is highly inferior due to the constraint of the relatively short slip duration ($t_R = s_\infty/v_o$). Results using the two-parameter model could be brought into line at low frequencies using about 20 percent of the static offset that was observed in the field and deduced from distant seismic observations.

Finally, the three-parameter model without randomness suffers considerably at modeling all the earthquake data due to the shortcomings of using an ideally coherent rupture model (as discussed in Chapter 4).

Tables comparing the observed and calculated maximum values of acceleration, velocity and displacement preface the comparisons of the observed and calculated response spectra for each of the three models considered in the following three sections, respectively. The solid lines in the spectral comparisons represent the observed spectra while the dashed lines correspond to the calculated spectra. At the end of each section, the calibrated rupture parameters are extrapolated to San Onofre for use in generating the site-specific spectra. A summary of the site-specific spectra for the alternate slip functions is presented in Figures 1-1 through 1-3.

TABLE 5-3

DELTA EARTHQUAKE MODEL

1. Gross Rupture Velocity
   = V_R = 0.9 x shear-wave velocity
2. Maximum Slip Velocity
   = v_o = 800 cm/sec
3. Fault Offset
   = s_∞ = 60 for Parkfield (stress drop = 30 bars)
   = 50 to 500 cm for Imperial Valley (stress drop = 90 bars)
   = 130 cm for Offshore San Onofre (stress drop = 100 bars)
4. Slip Duration
   = t_R = fault width/shear-wave velocity
   = 2.7 for Parkfield
   = 3.8 for Imperial Valley
   = 2.9 for San Onofre
5. Random Parameters
   (refer to Table 4-1).
6. Rupture extent (km)

	Imperial Valley	Parkfield	San Onofre "D"
Length	48	26	40
Width	11	9	9
Shallowest Extent	1	1.5	1
Deepest Extent	12	10.5	10
Hypocentral Depth	12	10.5	10

In the final section of this chapter, several representative time domain comparisons are presented with two objectives in mind. First, to display typical matches to the observed acceleration, velocity and displacement records, even though it is beyond the scope of the present work to obtain "wiggle for wiggle" validations with the data. Second, to further clarify the need for including incoherence in the rupture model.

5.3 PREFERRED MODEL WITH RANDOMNESS

Using DELTA's Earthquake Model with randomness (see Table 5-3), the gross properties of the Imperial Valley and Parkfield ruptures are used to best fit the synthetic response spectra to the corresponding spectra computed from the recorded data. The resulting maximum accelerations, velocities and displacements are also compared to the corresponding maxima from the recorded data.

As summarized in Table 5-4, the fit to the maxima is quite good for the displacements and velocities as well as the accelerations. The largest discrepancy appears in the acceleration fit for the horizontal component N65E at Parkfield Station 2, where either the recording was unreliable or the earthquake model needs more stringent provisions for reducing the idealized focusing effect. Other differences include the excessive accelerations in the horizontal components at Parkfield Station 12 and the deficient accelerations at Temblor. The misfit at Temblor is probably attributable to either the rupture stopping too short or differences in the geologic structure between the NE and SW sides of the fault. Unreliable low-frequency recordings are probably responsible for some of the discrepancies in the maximum displacements.

Due primarily to the refined mesh treatment, the fit for the vertical components no longer uniformly exceeds the maxima for the recorded data and, in fact, matches very well. The maxima for earthquake "D" at San Onofre are also displayed in Table 5-4. Since the fits for El Centro and Parkfield Stations 5 and 8 are so good, it is not surprising that the "extrapolated" results at San Onofre are reasonable (since the rupture geometry is most similar to these stations).

TABLE 5-4

MAXIMUM VALUES OF ACCELERATION, VELOCITY AND DISPLACEMENT

Station	Component	Acceleration (g)		Velocity (cm/sec)		Displacement (cm)	
		Obs.	Calc.	Obs.	Calc.	Obs.	Calc.
El Centro	South	0.35	0.49	30	33	10	20
	West	0.25	0.19	38	24	20	49
	Vertical	0.2	0.15	10	13	6	11
Parkfield 2	N65E	0.5	1.20	80	77	26	20
	N25W	--	0.64	--	25	--	9
	Vertical	0.2	0.23	12	15	4	2
Parkfield 5	N85E	0.45	0.47	28	26	7	11
	N05W	0.35	0.40	22	26	5	9
	Vertical	0.14	0.15	7	8	3.5	1.6
Parkfield 8	N50E	0.25	0.23	10	19	5	6
	N40W	0.30	0.32	12	13	4	7
	Vertical	0.08	0.14	5	8	2	2
Parkfield 12	N50E	0.06	0.14	7	6	4	5
	N40W	0.07	0.15	8	9	6	6
	Vertical	0.05	0.06	5	6	3	1
Parkfield Temblor	N65W	0.30	0.14	15	10	4	4
	S25W	0.35	0.23	20	20	6	8
	Vertical	0.15	0.06	4.5	3.4	1.4	1.3
San Onofre "D"	SE	--	0.34	--	29	--	17
	NE	--	0.39	--	31	--	16
	Vertical	--	0.11	--	8	--	4

DELTA'S EARTHQUAKE MODEL WITH RANDOMNESS

Maximum Slip Velocity = 800 cm/sec

Rupture Velocity = 0.9 of shear wave velocity

The comparisons between the calculated and "observed" response spectra are shown in Figure 5-3 for the 1940 Imperial Valley Earthquake and in Figures 5-4 through 5-8 for the 1966 Parkfield Earthquake. The two horizontal components appear at the top of each figure and the vertical component appears at the bottom. Superimposed in the box under each comparison are the maximum acceleration, velocity and displacement values, extracted from Table 5-4.

The fit for the horizontal components at Imperial Valley is excellent at all periods shown in Figure 5-3. The calculated vertical response spectrum exceeds the observed curve at intermediate periods and is deficient at short periods. The distinctively flat shape of the observed vertical component indicates that either the rupture sequence in the 1940 earthquake was more complex than that used in the computer model, or the simple approximations to the geologic structure were inadequate.

Figures 5-4 through 5-8 show the smoothed two-percent response spectra for Parkfield Stations 2, 5, 8, 12 and Temblor, respectively. As predicted by the maximum values in Table 5-4, the fit for all components is generally excellent at all periods considered. The shape of the spectra is fairly consistent except that the calculated response tends to exceed the observed response for periods between 0.2 and 0.8 seconds. The deficiencies in some of the comparisons may be explained in terms of the previous discussion of the deficiencies presented in Table 5-4.

Since good fits to Parkfield Station 5 and 8 and El Centro are crucial for a successful extrapolation to San Onofre, it is reassuring to have achieved such a good match to the data, especially at these stations. In Figure 5-9, DELTA's Earthquake Model is used to synthesize response spectra at San Onofre for a hypothesized earthquake, 8 km offshore from the site. The rupture characteristics correspond to Earthquake "D" as defined in Chapter 6. In Figures 4-7 through 4-9 the mean plus one standard deviation synthetic response spectrum is shown. The results shown in Figure 5-9 correspond to one particular random number sequence for earthquake "D." See Figures 1-1, 1-2 and 1-3 to compare the three-parameter model, the two-parameter model and the coherent model.

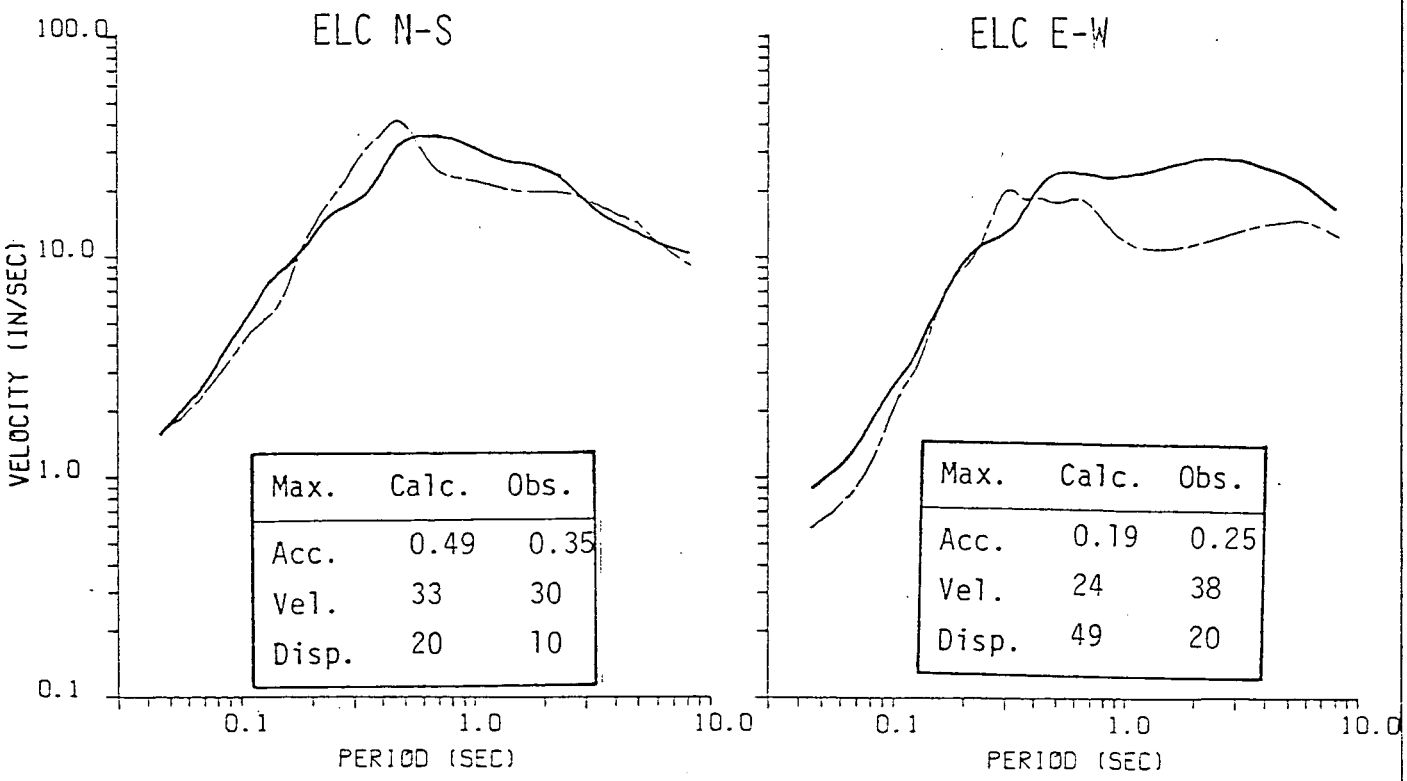

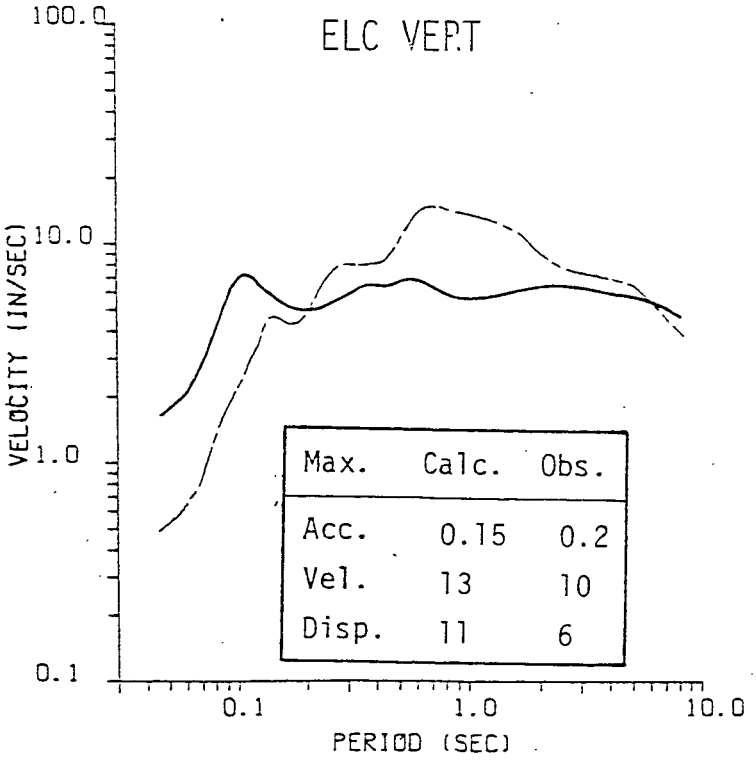

——— – ——— Calculated

——————— Observed

Comparison of the smoothed 2% velocity response spectra of the 1940 Imperial Valley Earthquake using DELTA's three-parameter slip function with randomness.

Figure 5-3

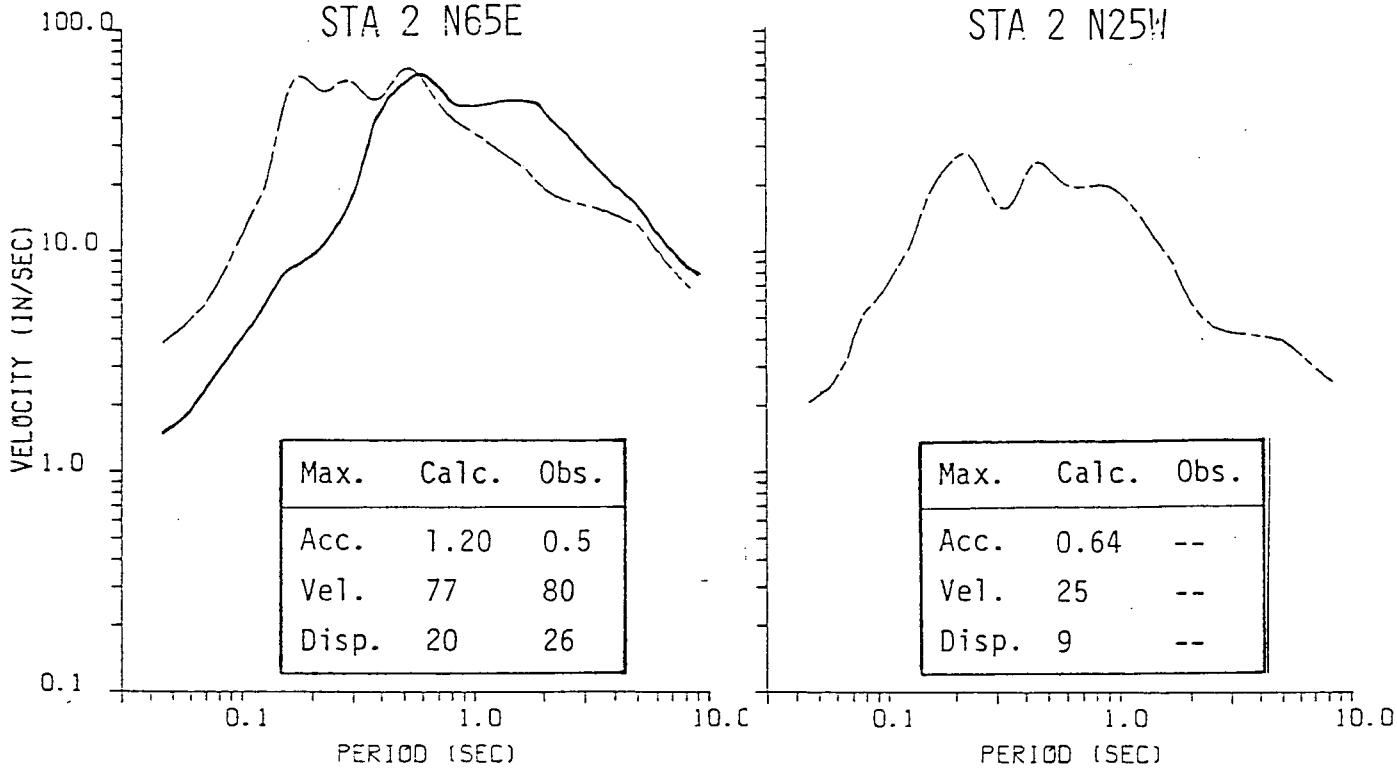

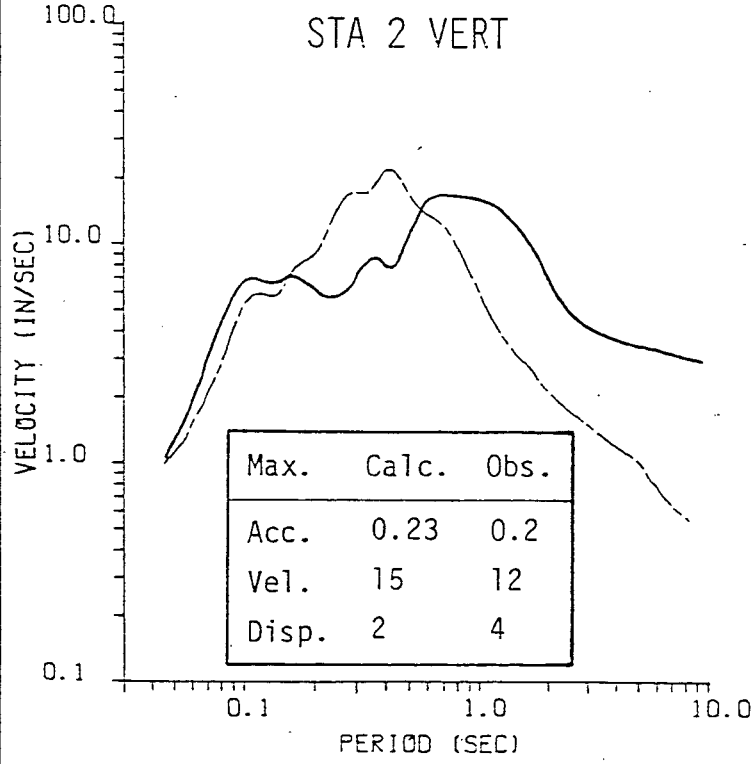

Calculated

Observed

Comparison of the smoothed 2% velocity response spectra recorded at Station 2 of the 1966 Parkfield Earthquake using DELTA's three-parameter slip function with randomness.

Figure 5-4

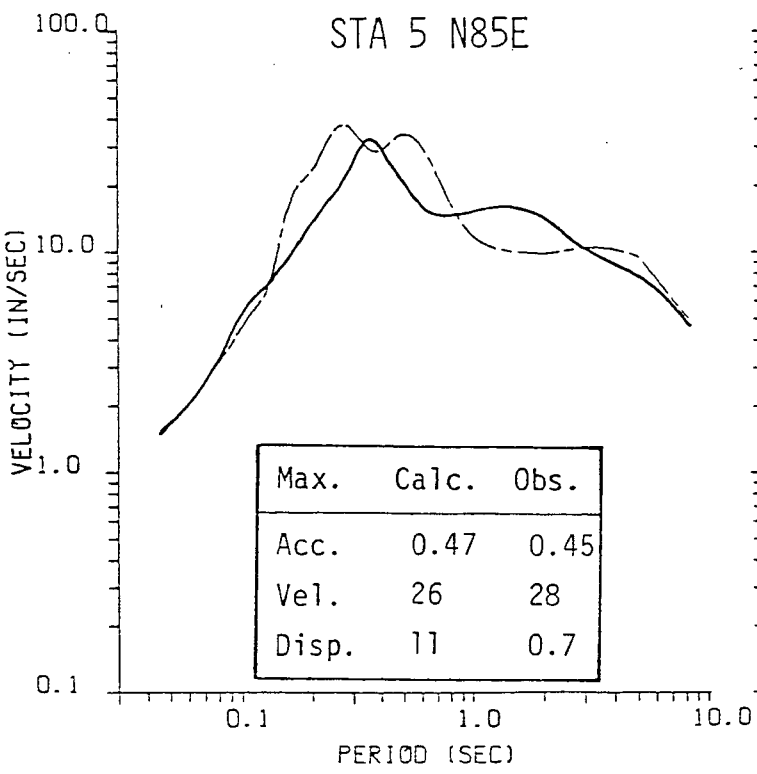

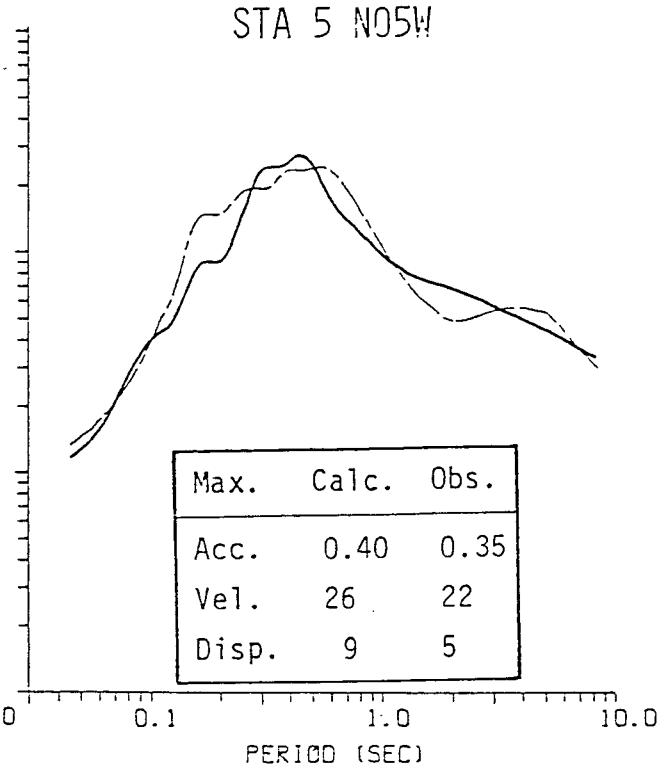

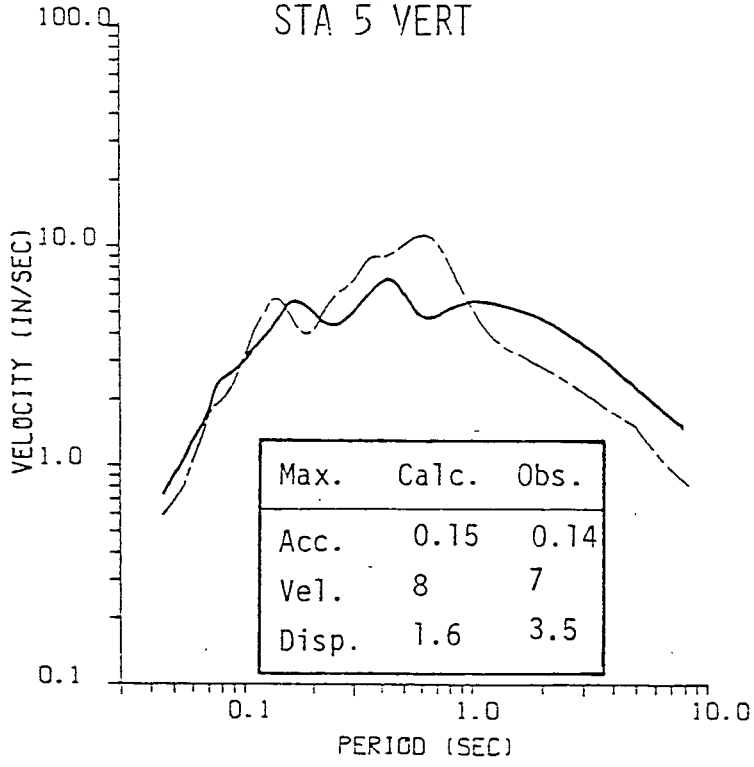

Comparison of the smoothed 2% velocity response spectra recorded at Station 5 of the 1966 Parkfield Earthquake using DELTA's three-parameter slip function with randomness.

Figure 5-5

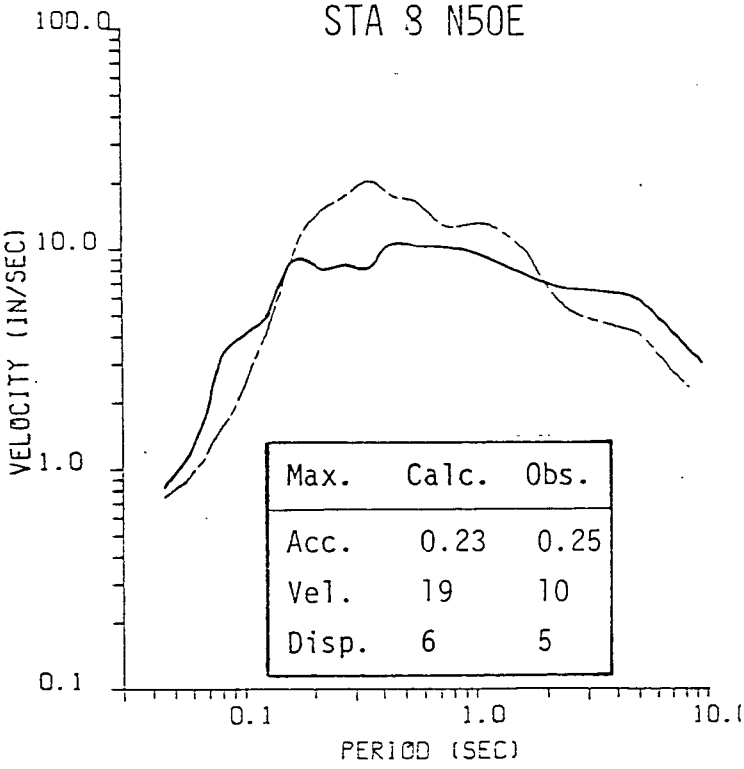

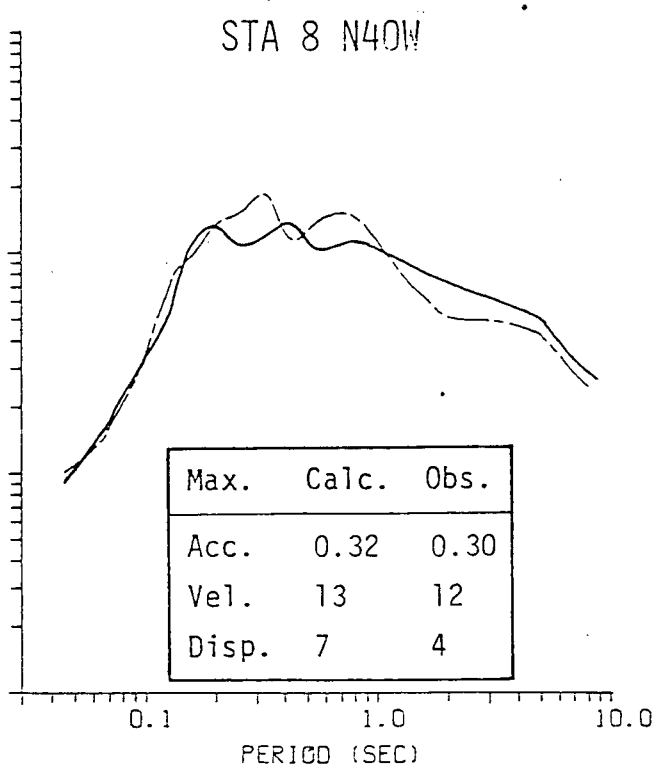

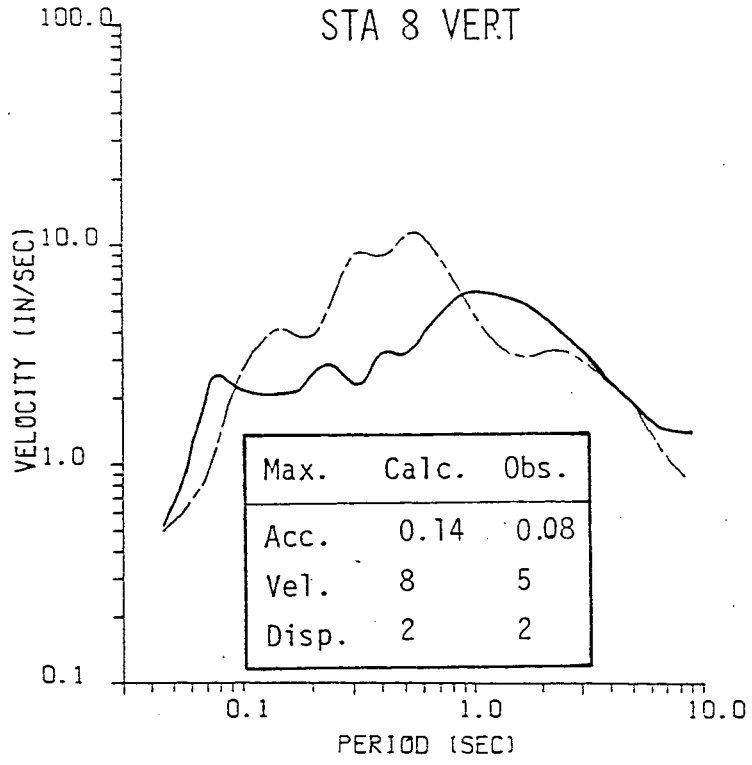

Calculated

Observed

Comparison of the smoothed 2% velocity response spectra recorded at Station 8 of the 1966 Parkfield Earthquake using DELTA's three-parameter slip function with randomness.

Figure 5-6

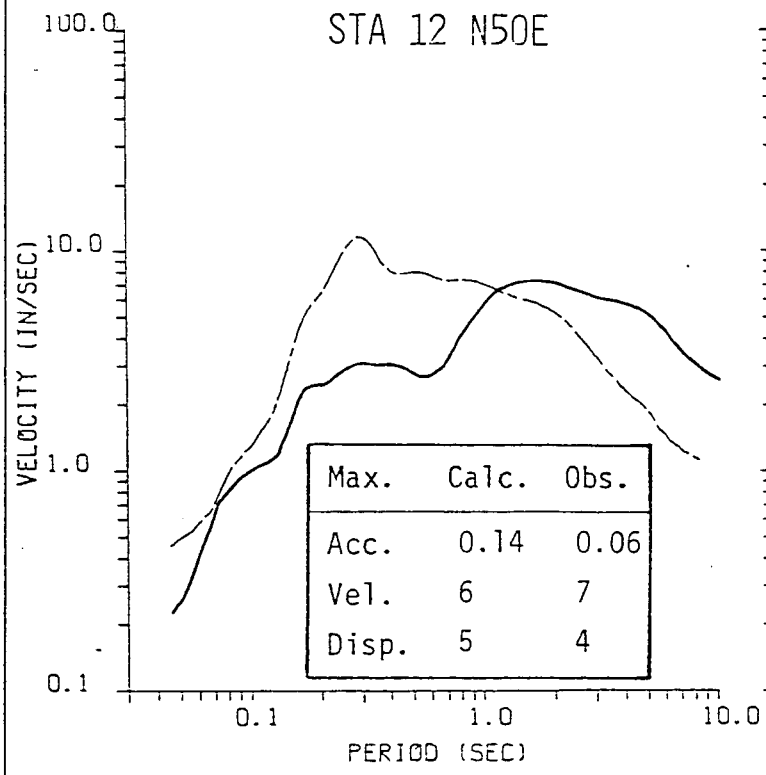

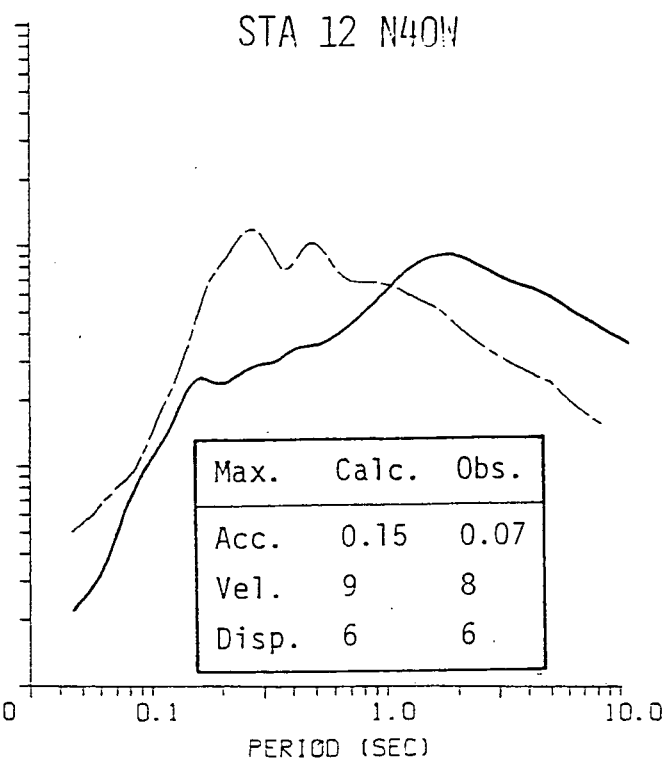

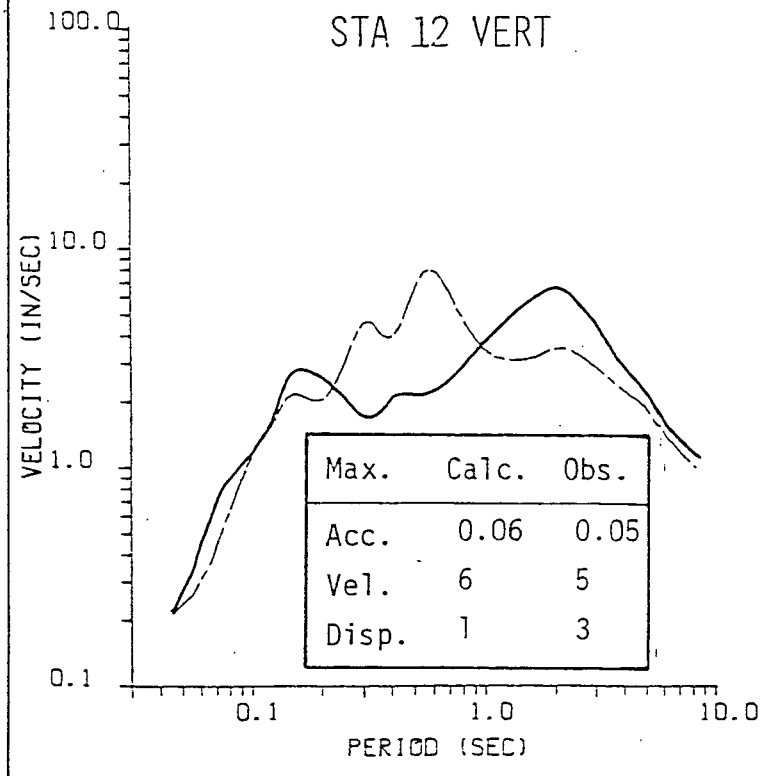

Comparison of the smoothed 2% velocity response spectra recorded at Station 12 of the 1966 Parkfield Earthquake using DELTA's three-parameter slip function with randomness.

Figure 5-7

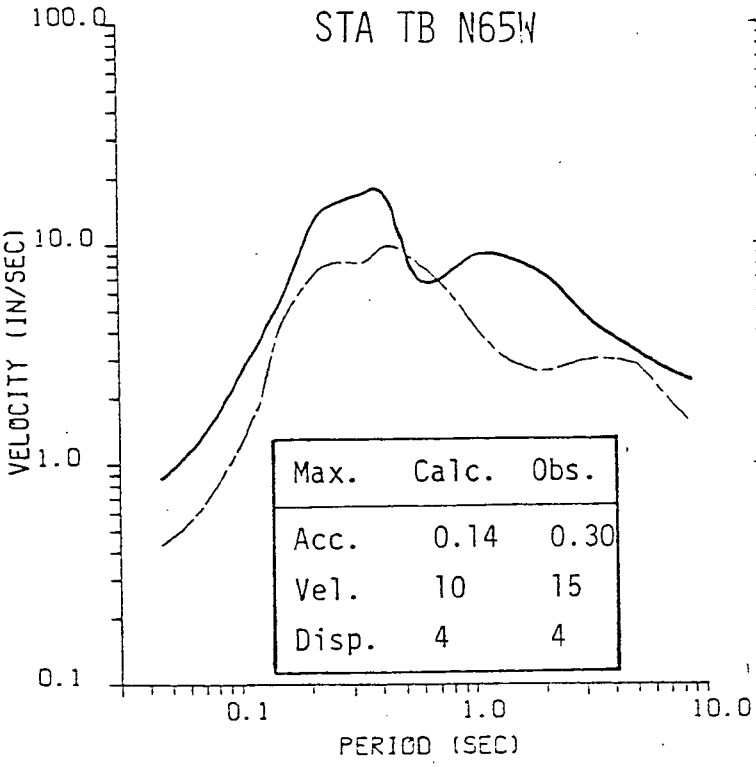

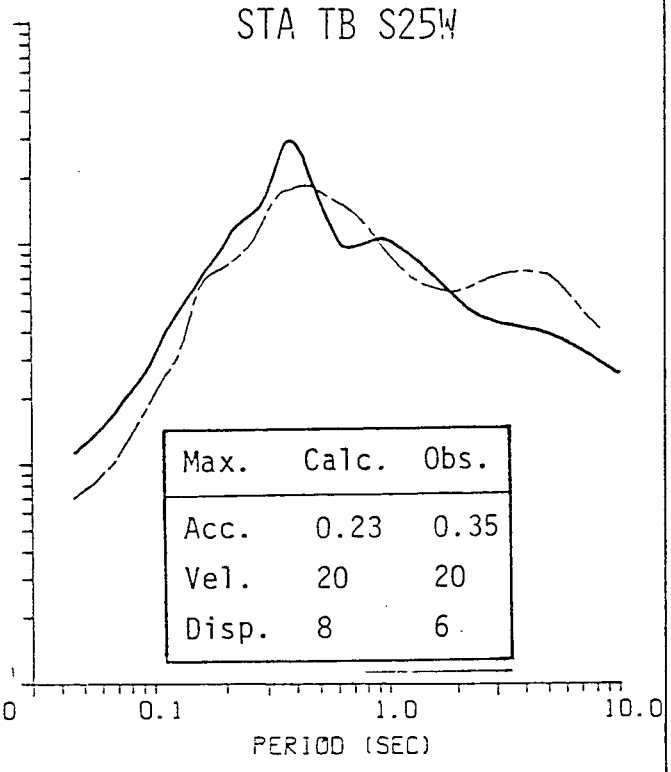

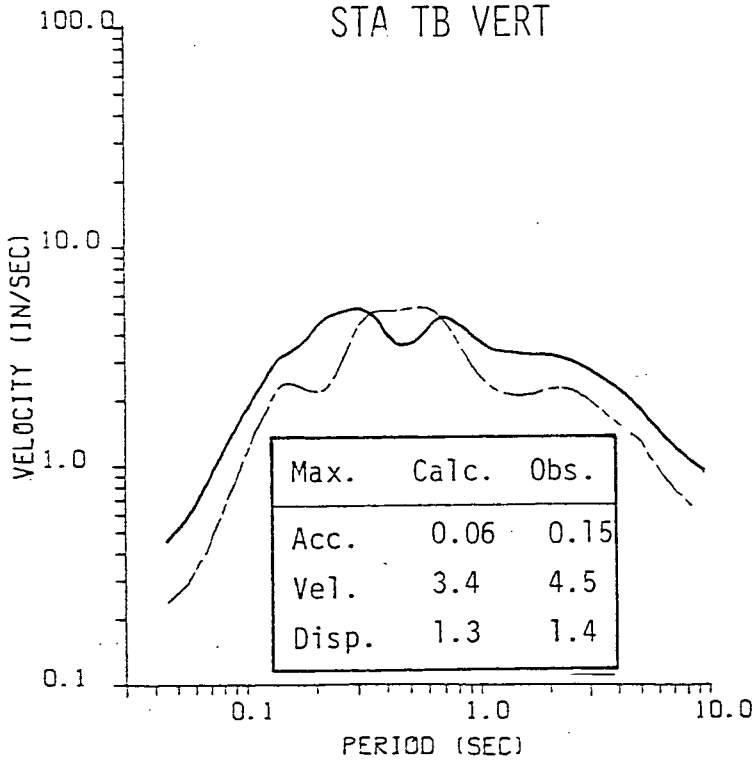

——— – ——— Calculated

——————— Observed

Comparison of the smoothed 2% velocity response spectra recorded at Station TB of the 1966 Parkfield Earthquake using DELTA's three-parameter slip function with randomness.

Figure 5-8

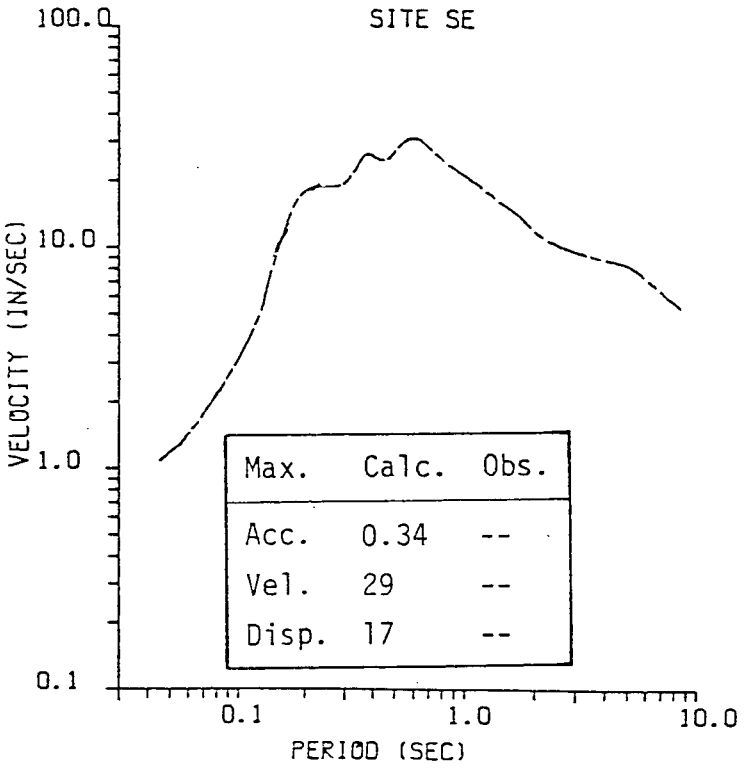

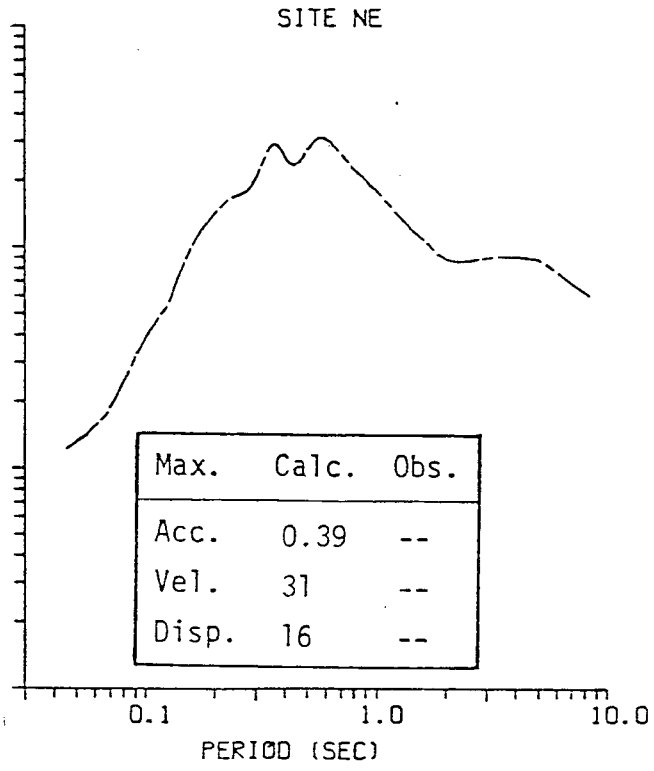

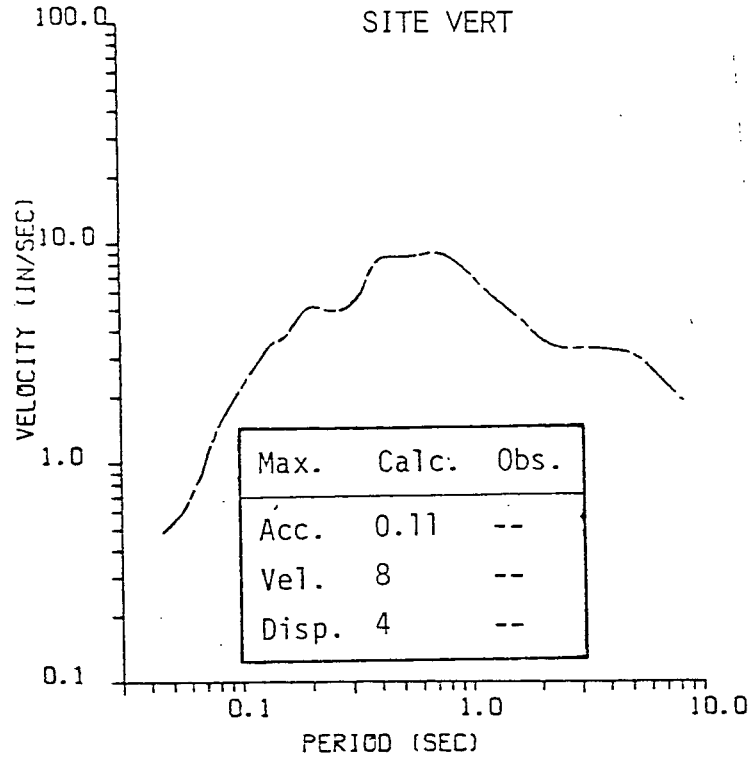

Smoothed 2% velocity response spectra using DELTA's three-parameter slip function with randomness.

Figure 5-9

5.4 TWO-PARAMETER SLIP MODEL WITH RANDOMNESS

In this section, the synthesized response is generated using the two-parameter slip function and is displayed in the same format as the previous section. The two-parameter slip function is a special case of DELTA's three-parameter slip function in which the slip duration, t_R, is constrained to be equal to the final displacement offset divided by the maximum slip velocity for each earthquake. The individual parameters used to define the two-parameter slip function/earthquake model are extracted from Table 5-3 with the following alterations: 1) the maximum slip velocity is reduced to 480 cm/sec in order to match the high frequencies in the recorded data for the Imperial Valley and Parkfield earthquakes; and 2) the constraint on the slip duration at a point leads to values of t_R = 0.125, 0.5, and 0.25 seconds for Parkfield, Imperial Valley, and San Onofre, respectively.

The fit to the maximum accelerations, velocities and displacements is shown in Table 5-5. The match to the high frequency accelerations at El Centro and the five Parkfield stations is comparable to the match obtained using the three-parameter slip model in the previous section. However, the match to the lower frequency displacements and velocities is highly inferior due to the constraint on the slip duration at a point. In order to reduce the calculated low-frequency response to the level of the observed response, it would be necessary to reduce the static offset in the two-parameter model to values corresponding to about 20 percent of the static offset observed in the field and deduced from distant seismic observations. Even so, it would be difficult to match the broad band frequency dependence of the observed spectra since the constrained rise time would be at most one or two time-steps (thus affecting the resolution at high frequency).

The comparisons between the calculated and "observed" response spectra are shown in Figure 5-10, for the 1940 Imperial Valley Earthquake, and in Figures 5-11 through 5-15 for the 1966 Parkfield Earthquake. As predicted by the maximum values in Table 5-5, the fits are generally excellent at short periods

TABLE 5-5

MAXIMUM VALUES OF ACCELERATION, VELOCITY AND DISPLACEMENT

Station	Component	Acceleration (g)		Velocity (cm/sec)		Displacement (cm)	
		Obs.	Calc.	Obs.	Calc.	Obs.	Calc.
El Centro	South	0.35	0.59	30	82	10	384
	West	0.25	0.30	38	128	20	549
	Vertical	0.2	0.15	10	40	6	74
Parkfield 2	N65E	0.5	1.20	80	294	26	176
	N25W	--	0.66	--	115	--	74
	Vertical	0.2	0.29	12	27	4	22
Parkfield 5	N85E	0.45	0.59	28	123	7	129
	N05W	0.35	0.44	22	77	5	244
	Vertical	0.14	0.16	7	23	3.5	25
Parkfield 8	N50E	0.25	0.34	10	60	5	158
	N40W	0.30	0.31	12	68	4	237
	Vertical	0.08	0.16	5	22	2	18
Parkfield 12	N50E	0.06	0.14	7	38	4	197
	N40W	0.07	0.18	8	50	6	172
	Vertical	0.05	0.11	5	21	3	17
Parkfield Temblor	N65W	0.30	0.18	15	35	4	141
	S25W	0.35	0.35	20	87	6	105
	Vertical	0.15	0.06	4.5	14	1.4	13
San Onofre "D"	SE	--	0.44	--	87	--	264
	NE	--	0.55	--	88	--	192
	Vertical	--	0.11	--	24	--	37

TWO-PARAMETER SLIP FUNCTION WITH RANDOMNESS

Maximum Slip Velocity = 480 cm/sec

Rupture Velocity = 0.9 of shear wave velocity

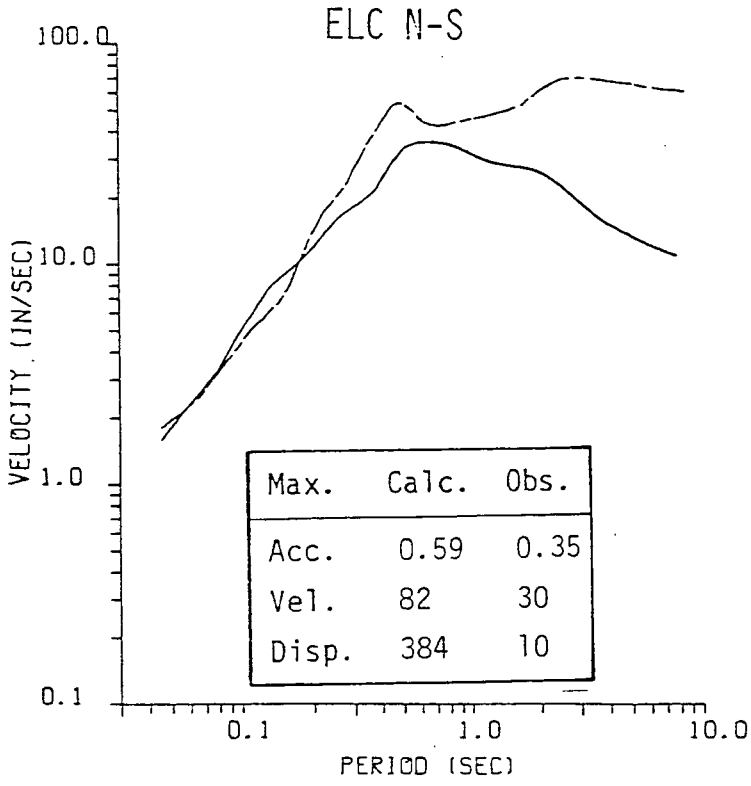

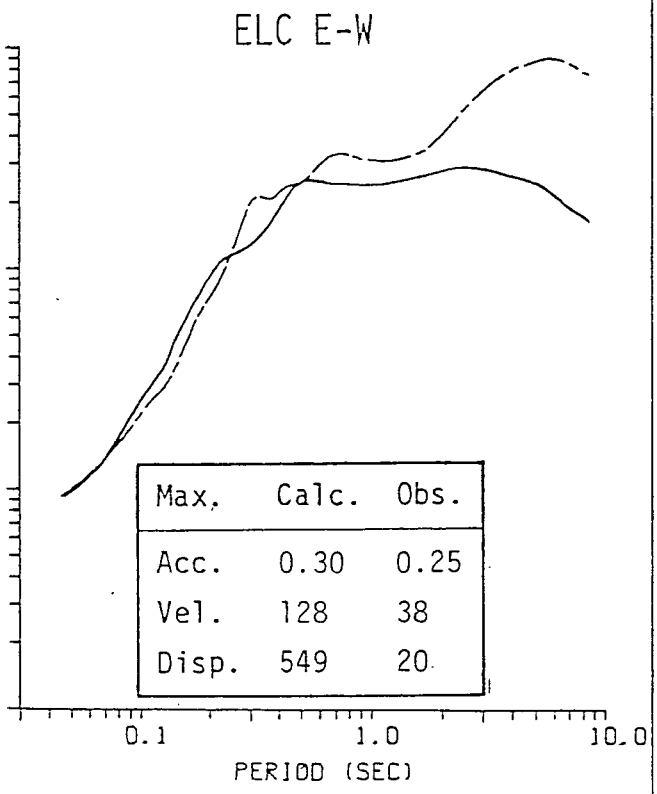

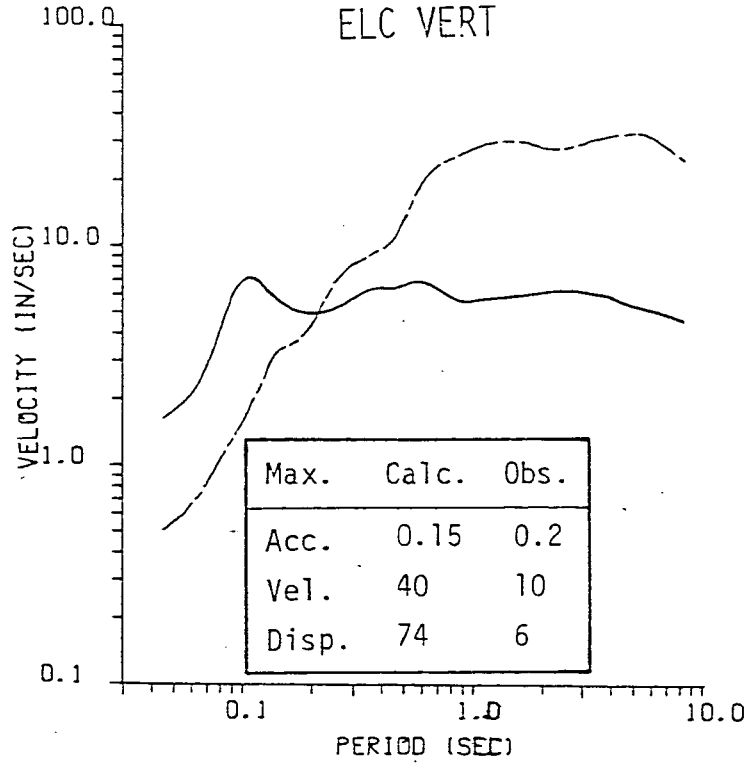

——— – ——— Calculated

——————— Observed

Comparison of the smoothed 2% velocity response spectra of the 1940 Imperial Valley Earthquake using two-parameter slip function ($T_R = s_\infty/v_o$) with randomness.

Figure 5-10

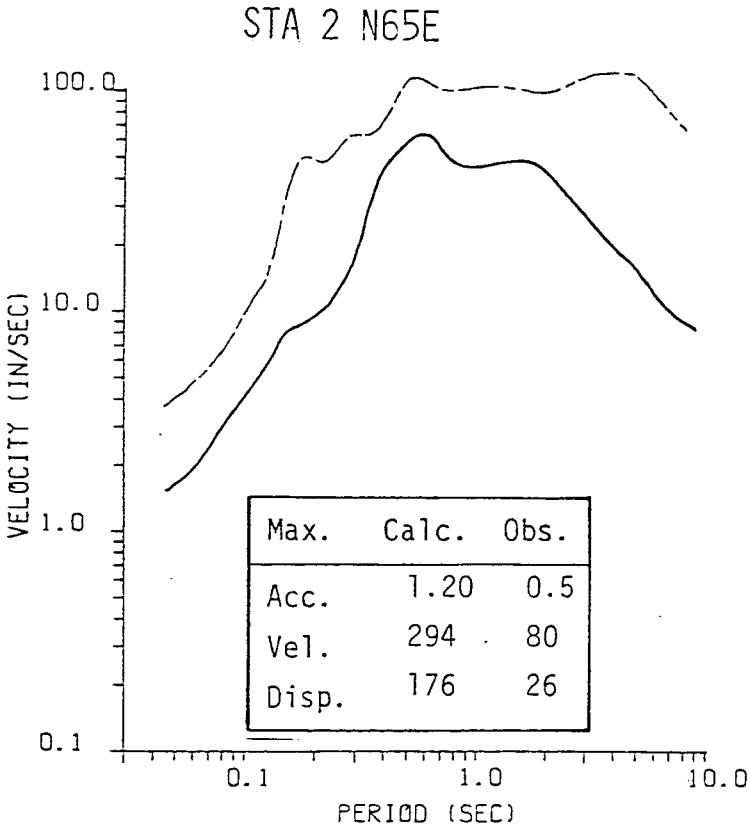

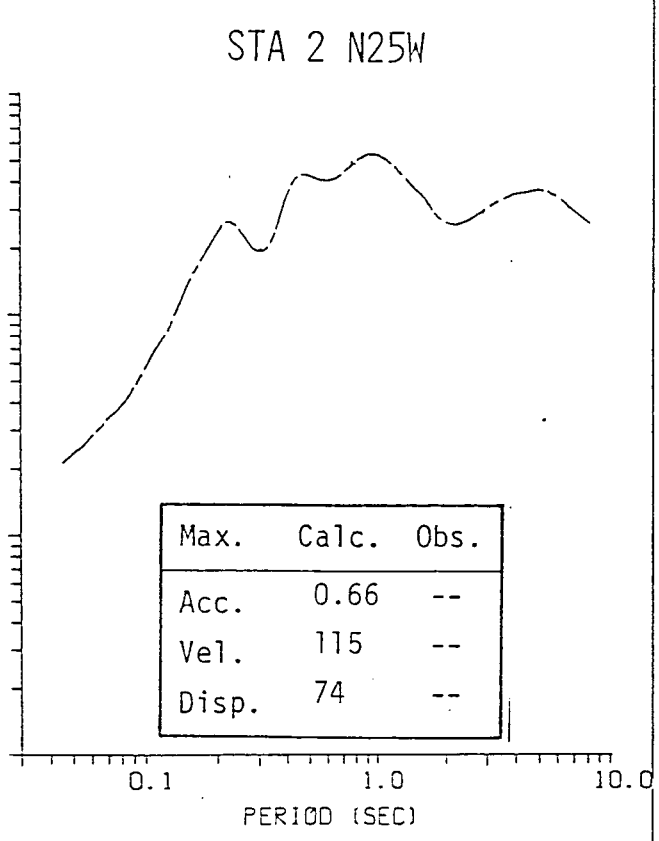

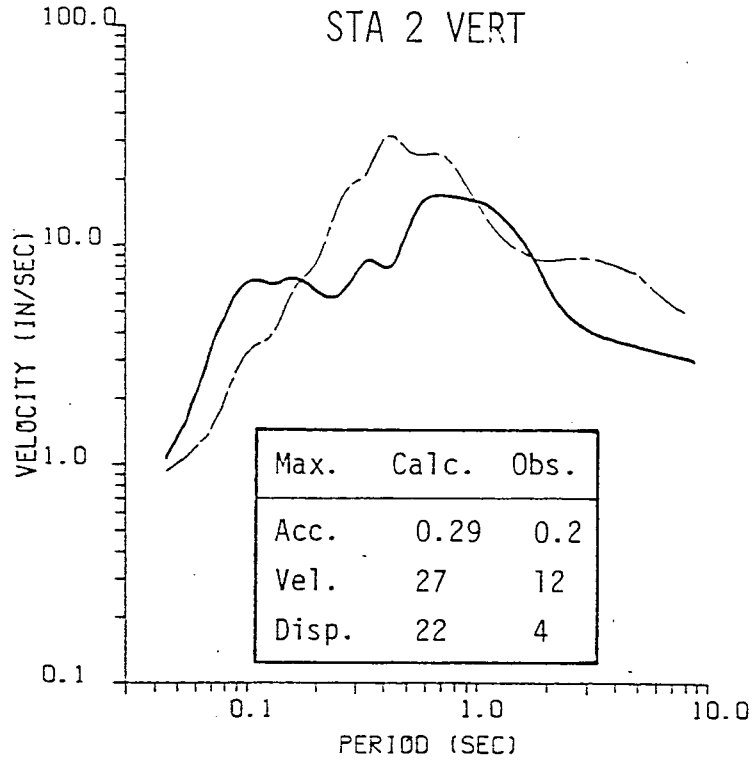

——— – ——— Calculated

——————— Observed

Comparison of the smoothed 2% velocity response spectra recorded at Station 2 of the 1966 Parkfield Earthquake using two-parameter slip function ($T_R = s_\infty/v_o$) with randomness.

Figure 5-11

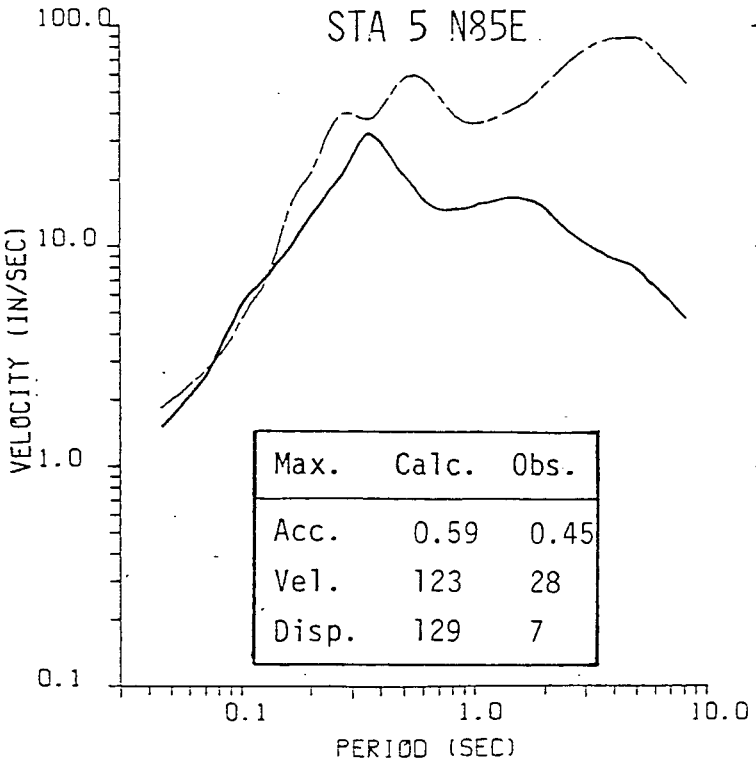

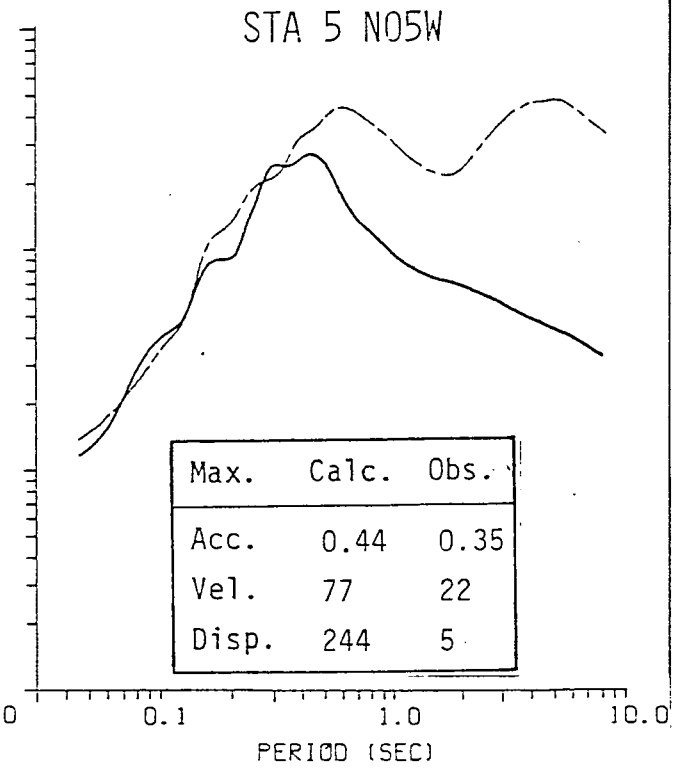

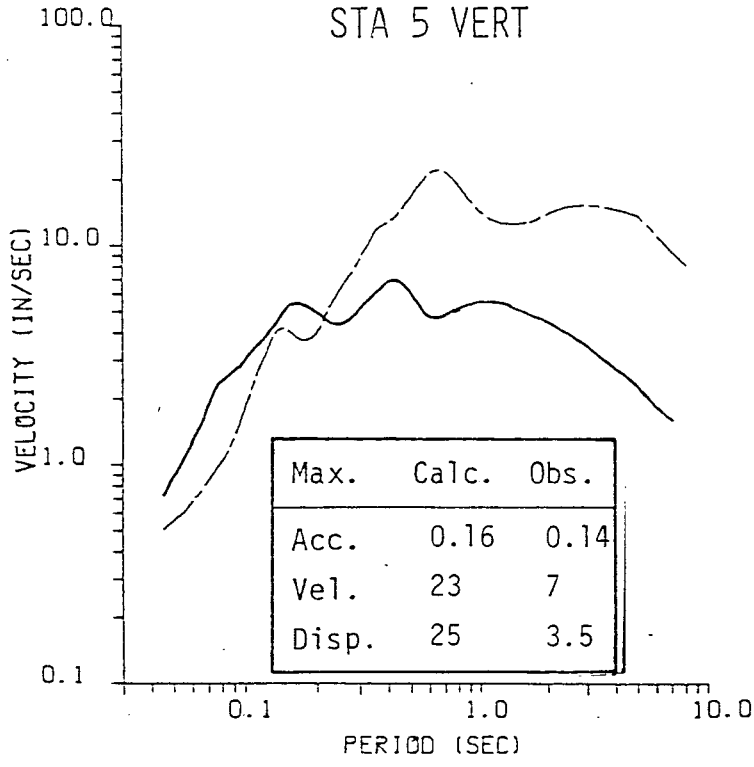

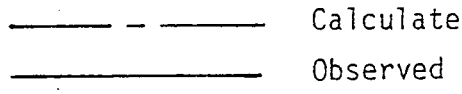

Comparison of the smoothed 2% velocity response spectra recorded at Station 5 of the 1966 Parkfield Earthquake using two-parameter slip function ($T_R = s_\infty/v_o$) with randomness.

Figure 5-12

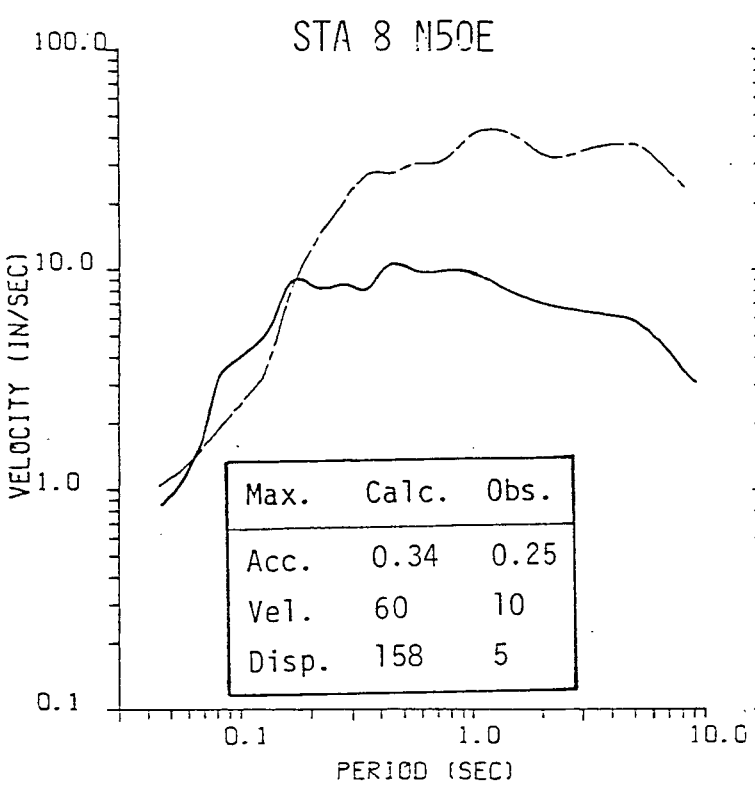

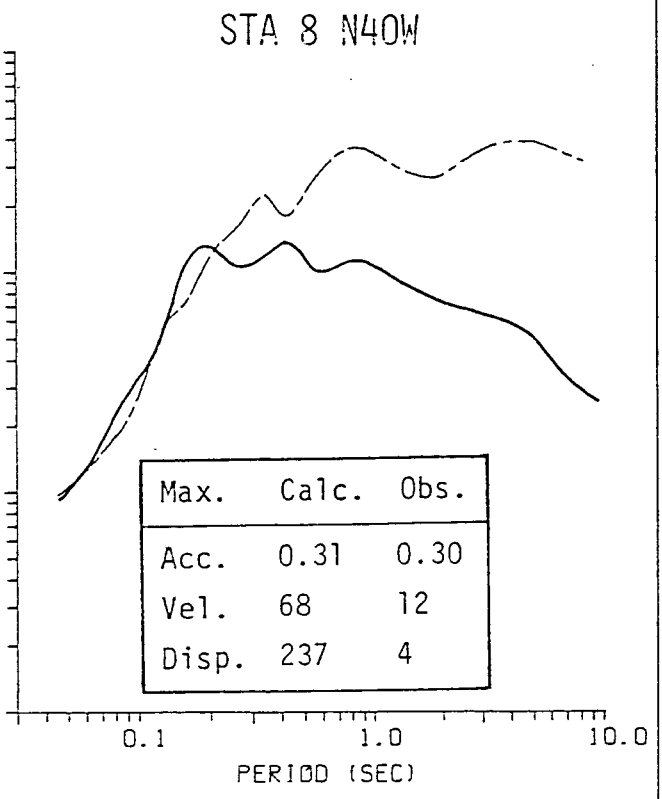

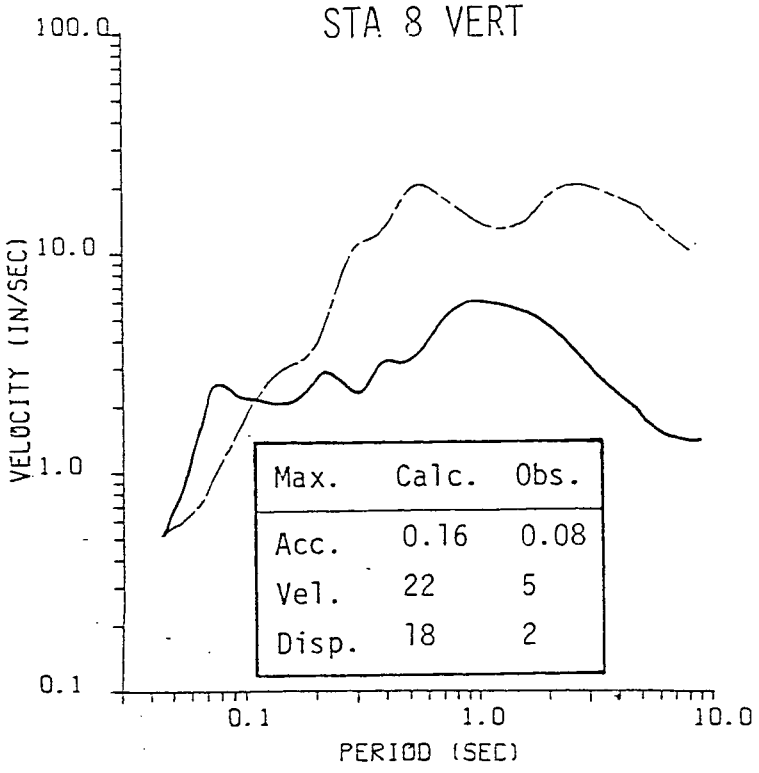

Calculated

Observed

Comparison of the smoothed 2% velocity response spectra recorded at Station 8 of the 1966 Parkfield Earthquake using two-parameter slip function ($T_R = s_\infty/v_o$) with randomness.

Figure 5-13

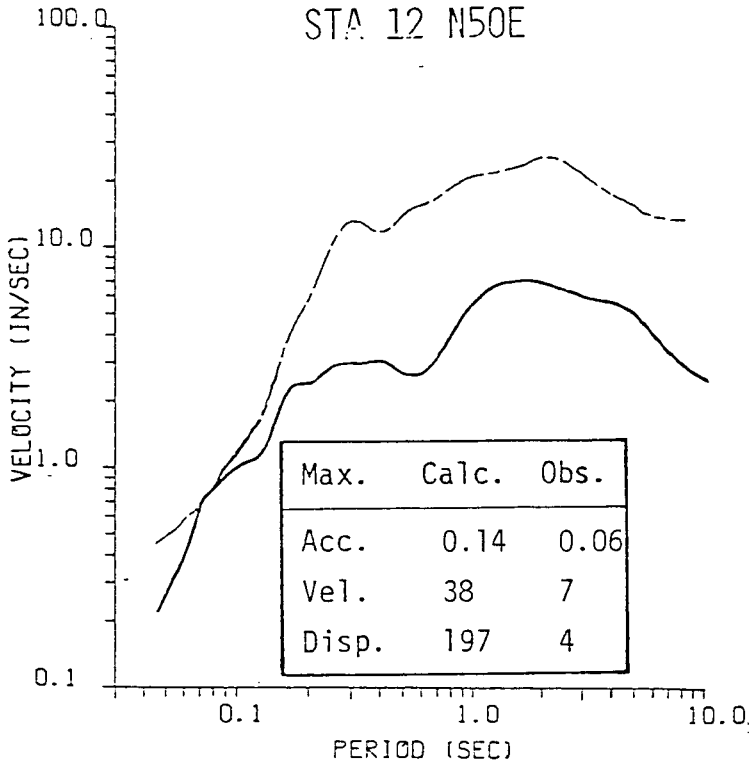

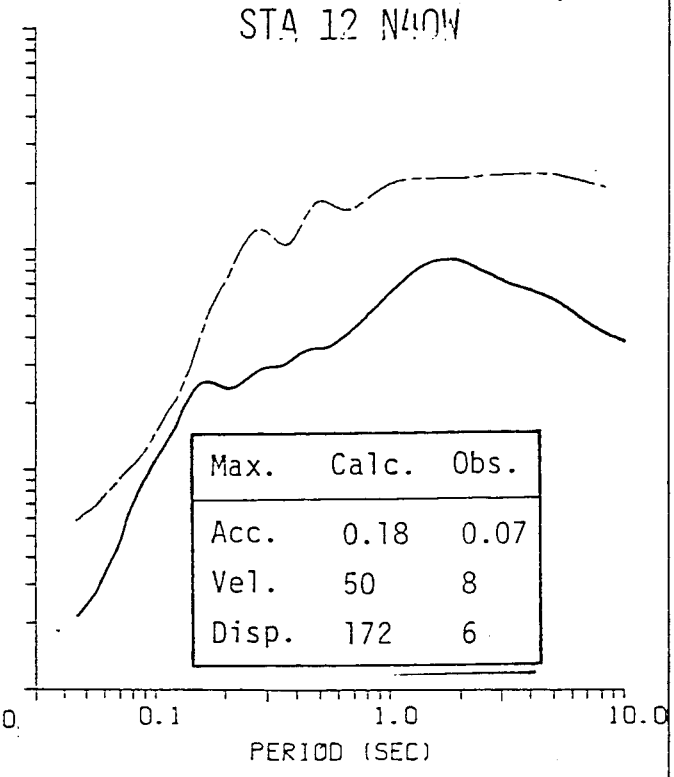

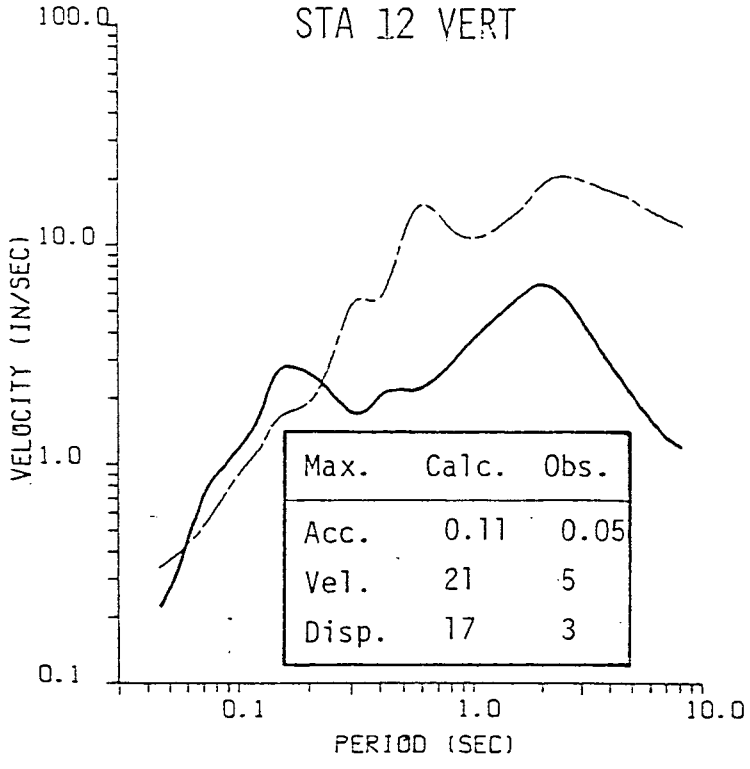

——— – ——— Calculated

——————— Observed

Comparison of the smoothed 2% velocity response spectra recorded at Station 12 of the 1966 Parkfield Earthquake using two-parameter slip function ($T_R = s_\infty/v_o$) with randomness.

Figure 5-14

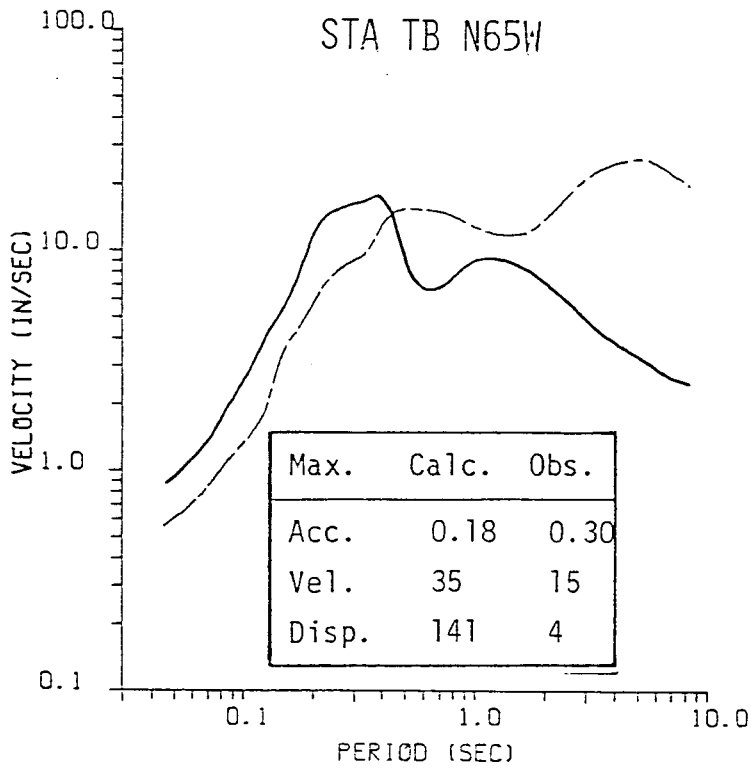

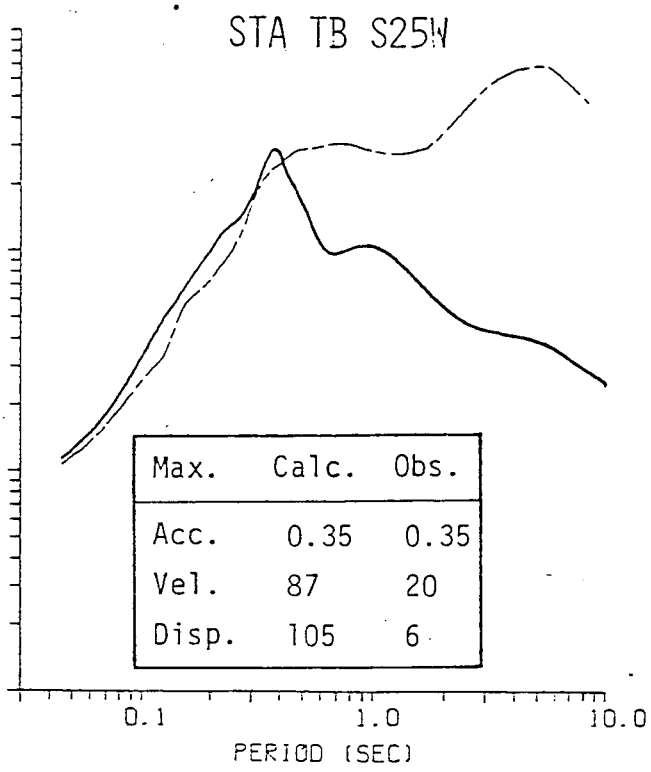

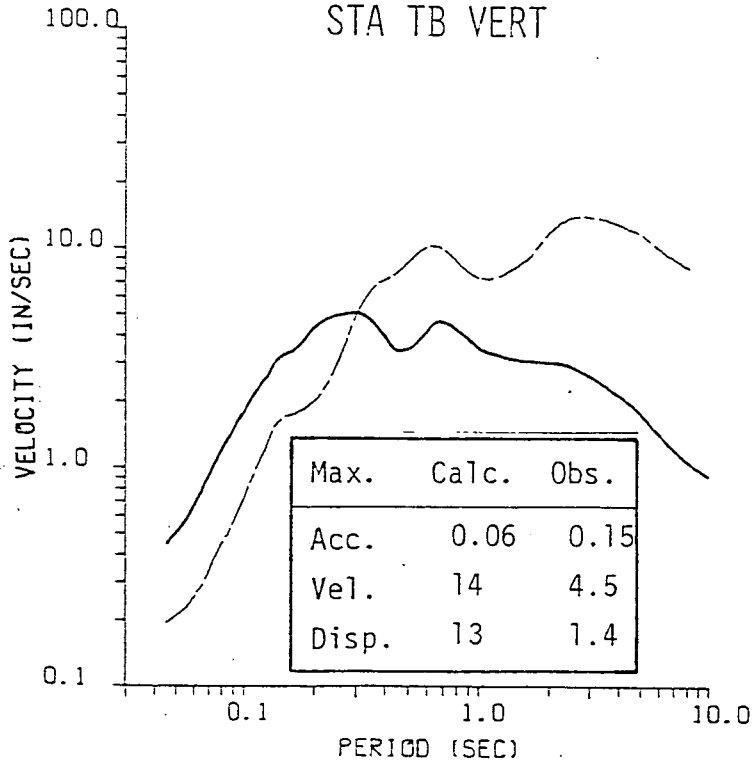

Calculated

Observed

Comparison of the smoothed 2% velocity response spectra recorded at Station TB of the 1966 Parkfield Earthquake using two-parameter slip function ($T_R = s_\infty/v_o$) with randomness.

Figure 5-15

and highly excessive at periods longer than about 0.4 seconds. The discrepancies between the observed and calculated high frequencies at Parkfield Stations 2, 12 and Temblor are analogous to the mismatches obtained with the three-parameter model. The extrapolated site-specific response spectra for earthquake "D" are shown in Figure 5-16. See Figures 1-1, 1-2 and 1-3 to compare the three-parameter model, the two-parameter model and the coherent model.

5.5 COHERENT MODEL

In this section, the synthesized response is generated using the three-parameter slip function without randomness and is displayed in the same format as the previous two sections. In order to calibrate the coherent model to the high frequencies in the recorded data for the Imperial Valley and Parkfield Earthquakes, the maximum slip velocity is rescaled to 1,000 cm/sec for Parkfield and 1,200 cm/sec for Imperial Valley. The extrapolated model for the site-specific calculations assumes a maximum slip velocity of 1,200 cm/sec.

The maximum values of acceleration, velocity and displacement are given in Table 5-6 and the response spectra are displayed in Figures 5-17 through 5-23. See Figures 1-1, 1-2 and 1-3 to compare the three-parameter model, the two-parameter model and the coherent model. As discussed in Chapter 4, the shortcomings of using an ideally coherent rupture model lead to highly unrealistic results. For instance, the focusing of the rupture at Parkfield Stations 2 and even Station 5 causes gross exaggerations of the results at those stations over the entire frequency band of interest.

Being most similar to the site-specific/fault configuration, El Centro and Parkfield Station 8 serve to most reliably calibrate the coherent model at high frequency for purposes of extrapolation to San Onofre. The relatively low response at San Onofre is probably due to the idealized rupture of earthquake "D" propagating past the site without dispensing much energy toward the site (similar to the reduction at Parkfield Station 12). Correspondingly, the increased response at Station Temblor is directly attributable to the increase in focusing toward Temblor.

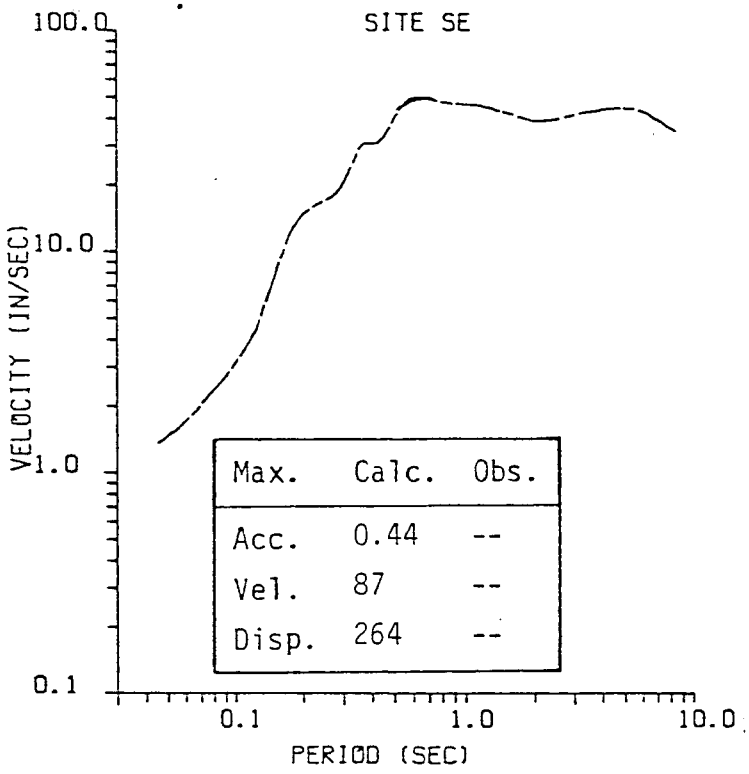

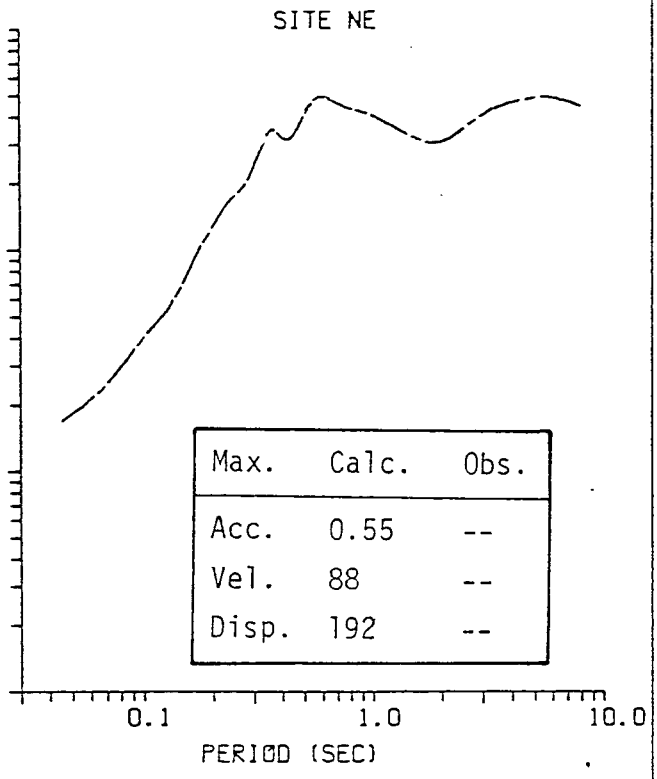

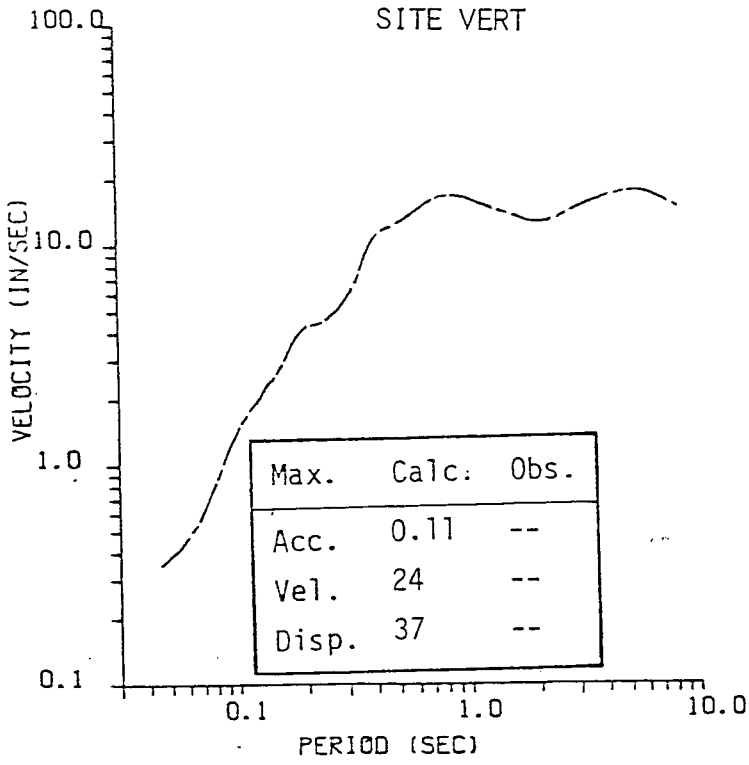

——— – ——— Calculated

Smoothed 2% velocity response spectra using two-parameter slip function ($T_R = s_\infty/v_o$) with randomness.

Figure 5-16

TABLE 5-6

MAXIMUM VALUES OF ACCELERATION, VELOCITY AND DISPLACEMENT

Station	Component	Acceleration (g)		Velocity (cm/sec)		Displacement (cm)	
		Obs.	Calc.	Obs.	Calc.	Obs.	Calc.
El Centro	South	0.35	0.45	30	55	10	32
	West	0.25	0.35	38	72	20	94
	Vertical	0.2	0.35	10	20	6	19
Parkfield 2	N65E	0.5	6.57	80	201	26	55
	N25W	--	1.38	--	47	--	16
	Vertical	0.2	0.27	12	12	4	3
Parkfield 5	N85E	0.45	1.26	28	82	7	30
	N05W	0.35	0.35	22	22	5	14
	Vertical	0.14	0.28	7	12	3.5	3
Parkfield 8	N50E	0.25	0.30	10	26	5	11
	N40W	0.30	0.35	12	23	4	14
	Vertical	0.08	0.23	5	13	2	3
Parkfield 12	N50E	0.06	0.10	7	10	4	7
	N40W	0.07	0.16	8	13	6	8
	Vertical	0.05	0.09	5	9	3	3
Parkfield Temblor	N65W	0.30	0.16	15	13	4	7
	S25W	0.35	0.53	20	59	6	19
	Vertical	0.15	0.13	4.5	6.5	1.4	2.0
San Onofre "D"	SE	--	0.21	--	32	--	38
	NE	--	0.26	--	21	--	24
	Vertical	--	0.12	--	10	--	6

DELTA MODEL WITHOUT RANDOMNESS

Maximum Slip Velocity = 1000 cm for Parkfield
Maximum Slip Velocity = 1200 cm/sec for Imperial Valley and Site Specific

Rupture Velocity = 0.9 of shear wave velocity

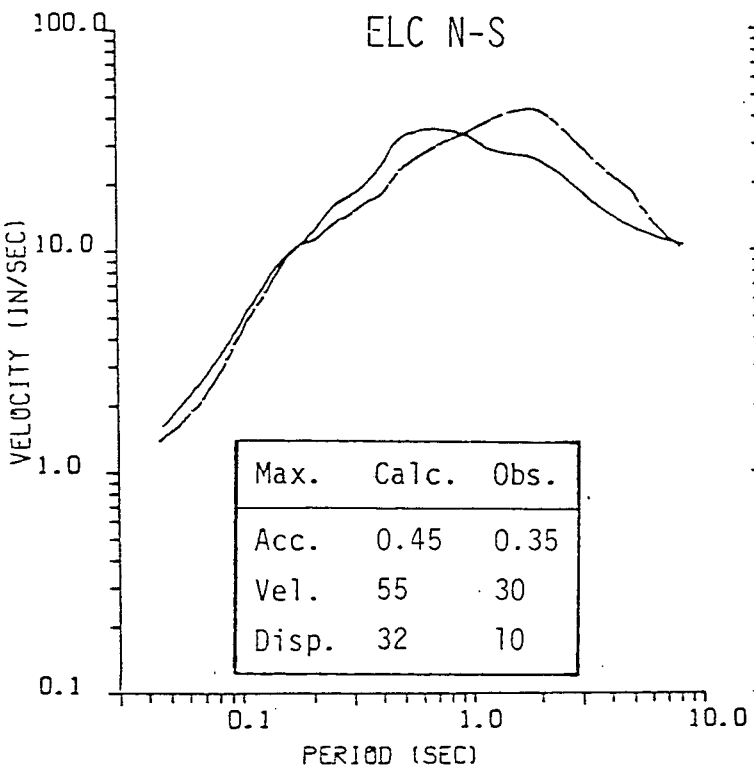

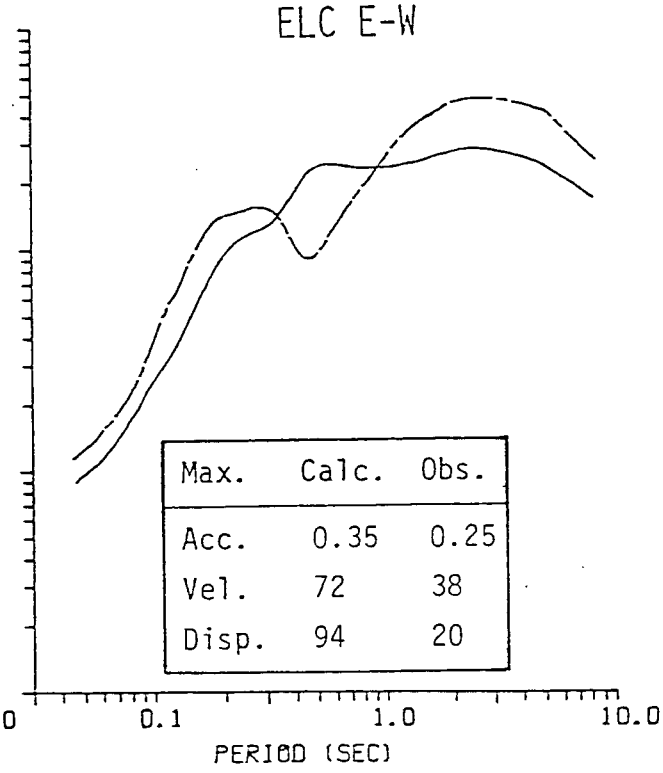

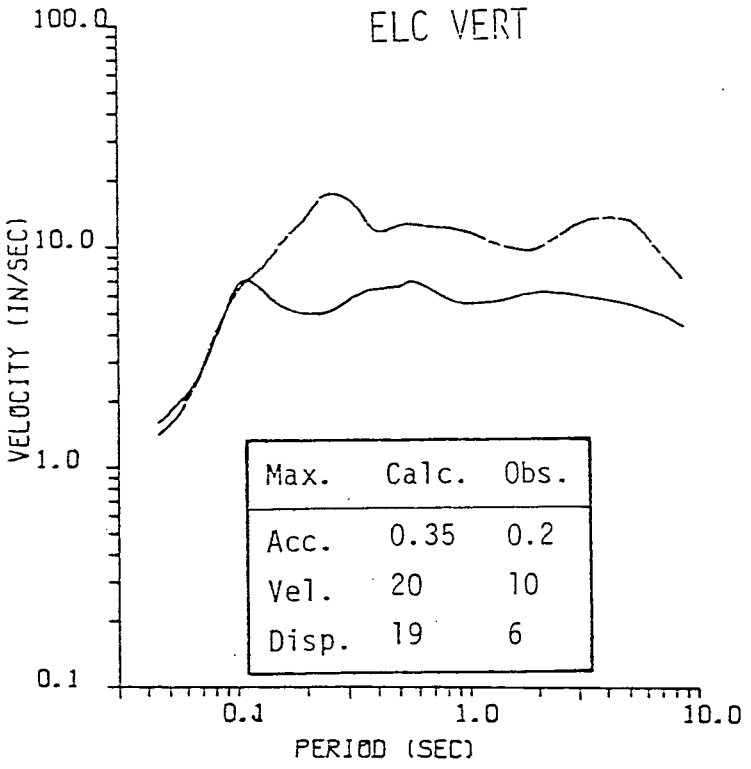

Calculated

Observed

Comparison of the smoothed 2% velocity response spectra of the 1940 Imperial Valley Earthquake using DELTA's three-parameter slip function without randomness.

Figure 5-17

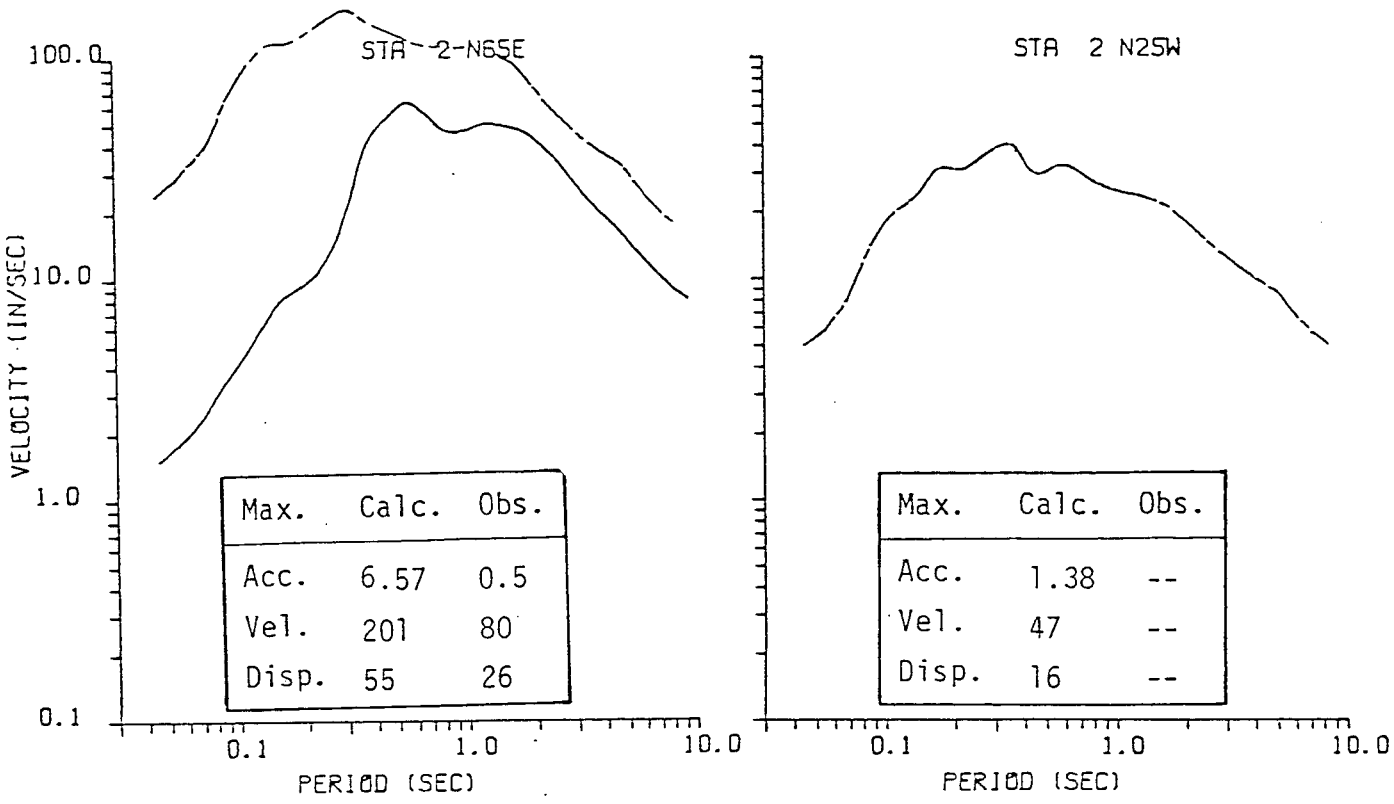

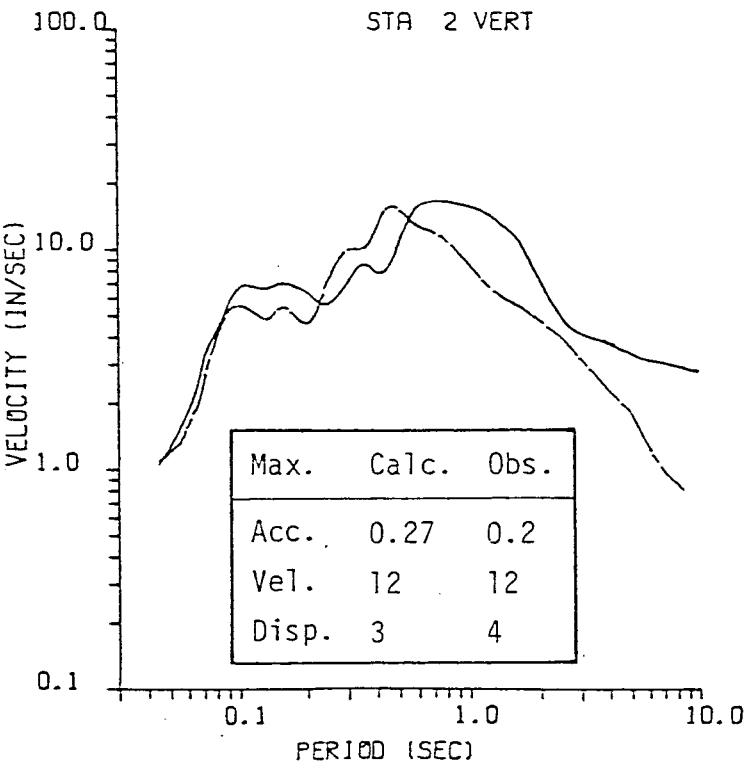

——— – ——— Calculated

——————— Observed

Comparison of the smoothed 2% velocity response spectra recorded at Station 2 of the 1966 Parkfield Earthquake using DELTA's three-parameter slip function without randomness.

Figure 5-18

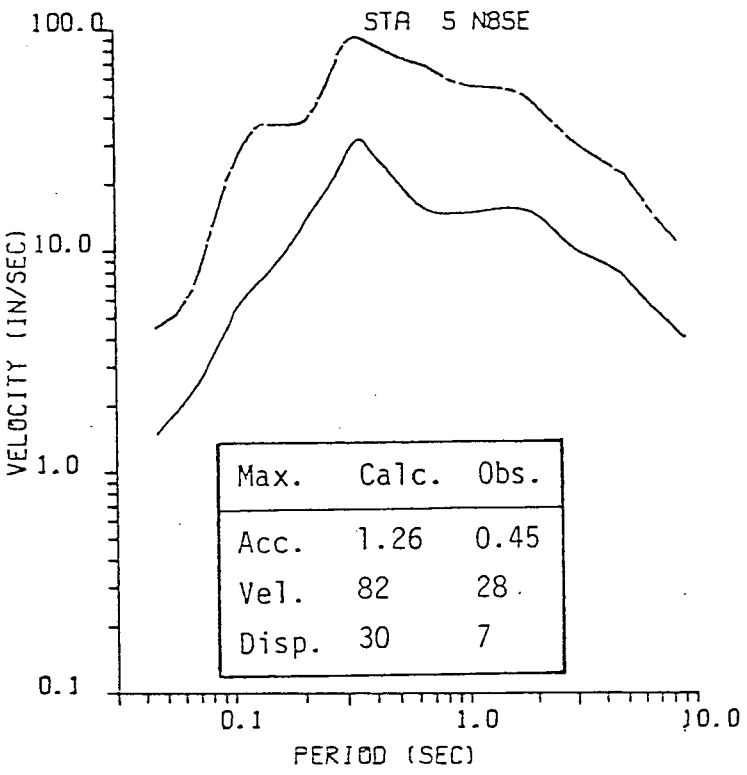

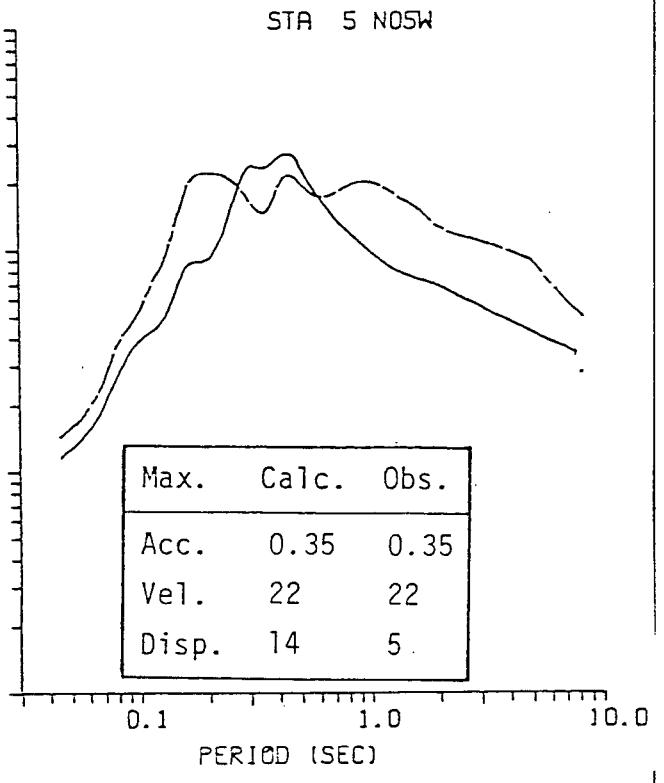

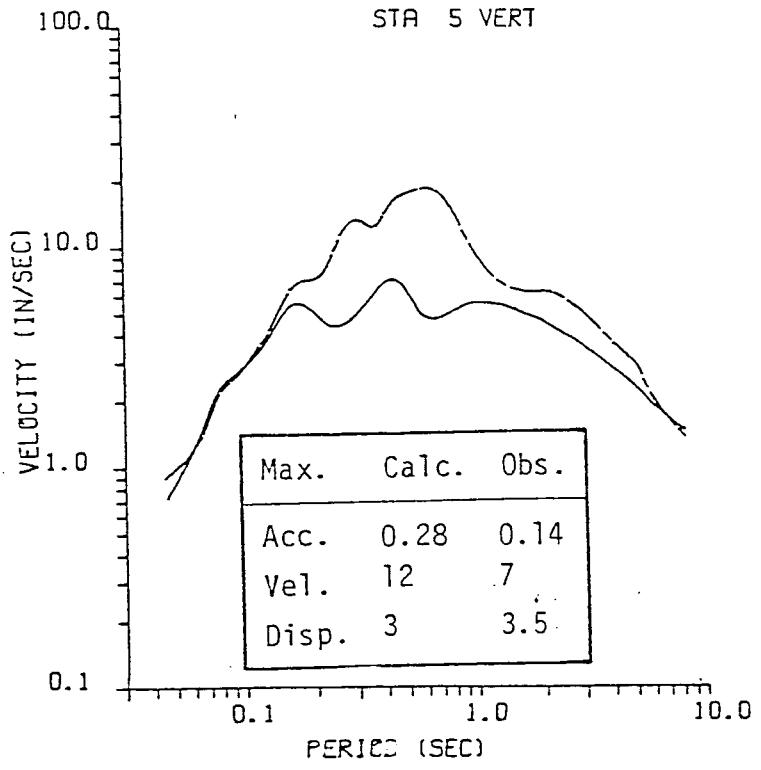

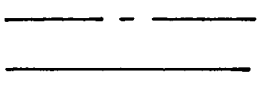

Comparison of the smoothed 2% velocity response spectra recorded at Station 5 of the 1966 Parkfield Earthquake using DELTA's three-parameter slip function without randomness.

Figure 5-19

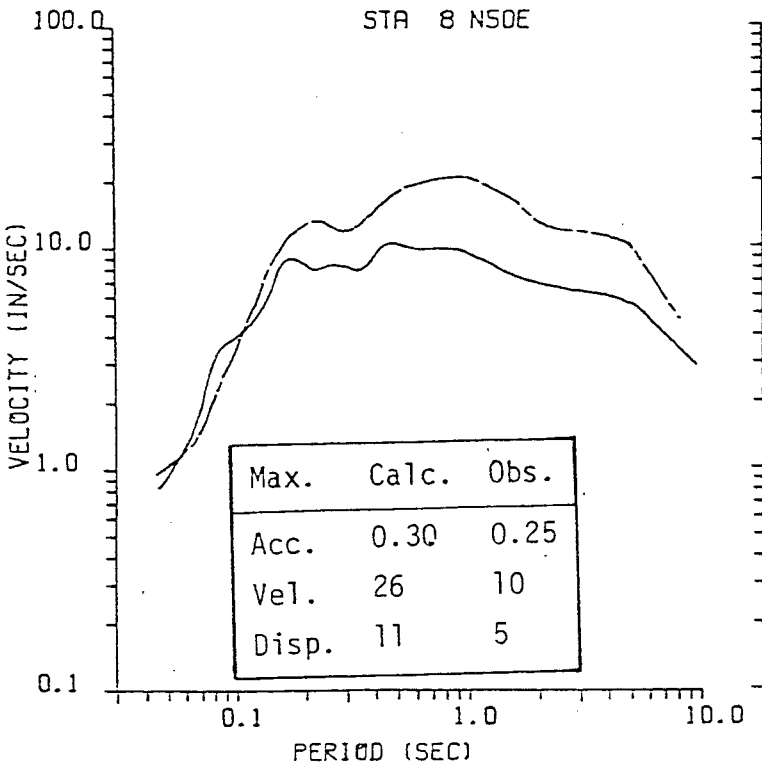

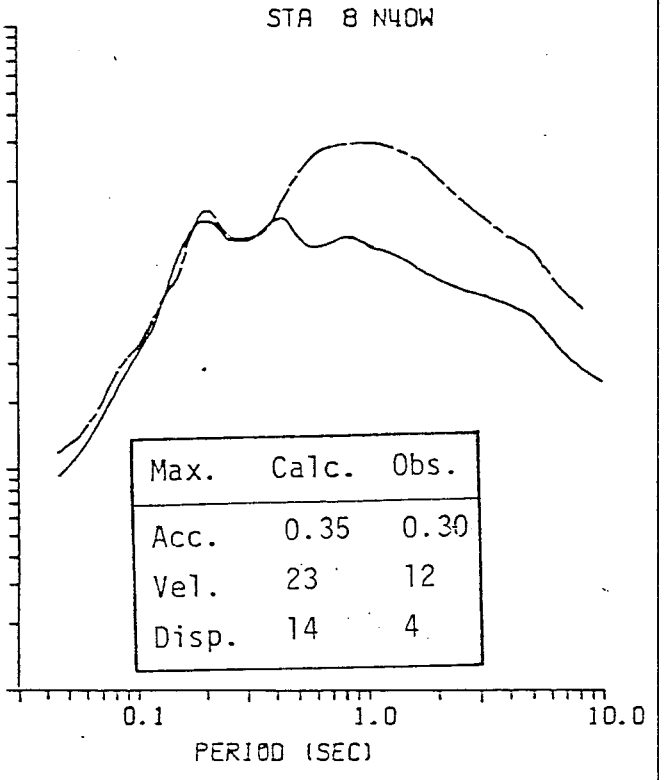

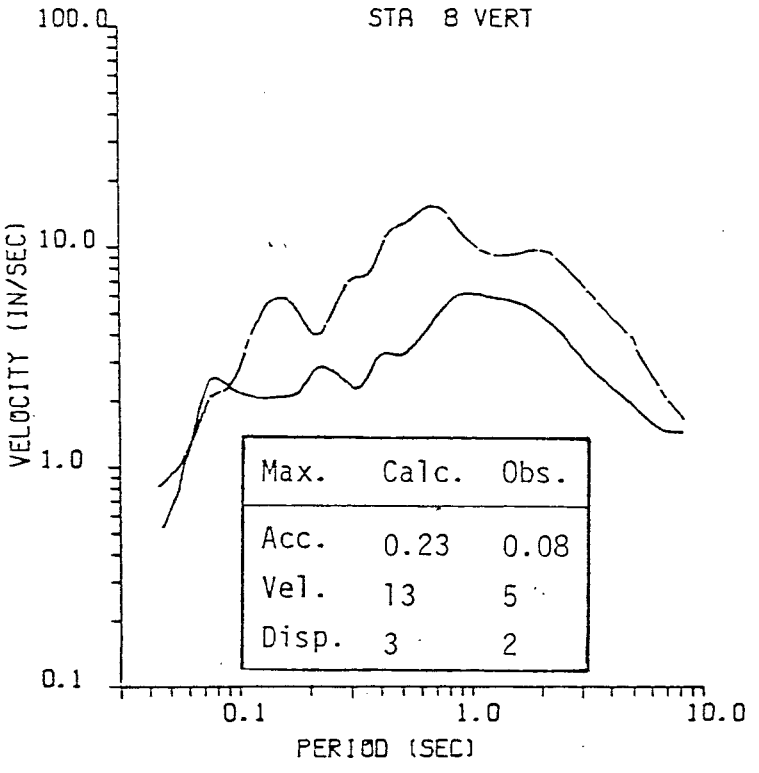

Calculated

Observed

Comparison of the smoothed 2% velocity response spectra recorded at Station 8 of the 1966 Parkfield Earthquake using DELTA's three-parameter slip function without randomness.

Figure 5-20

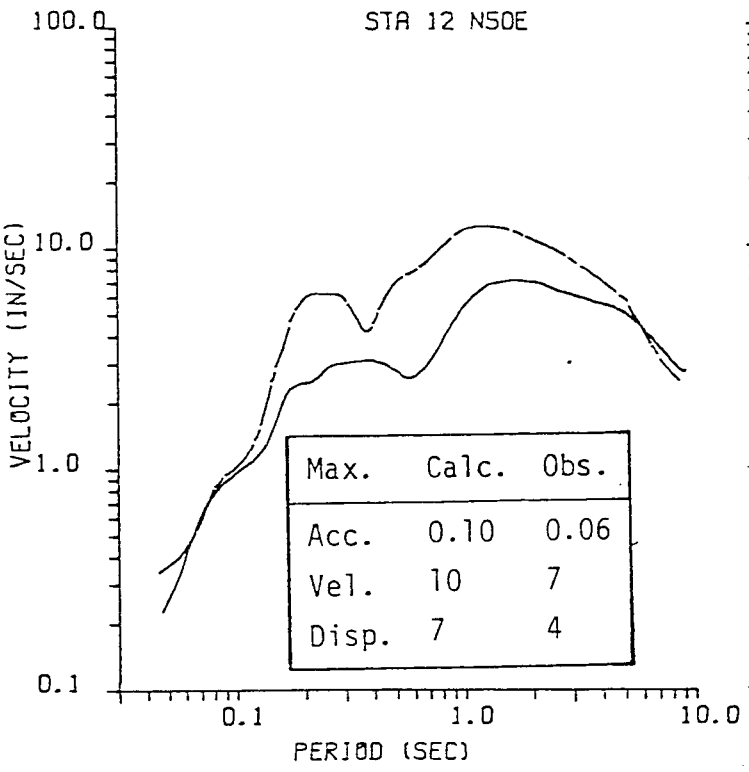

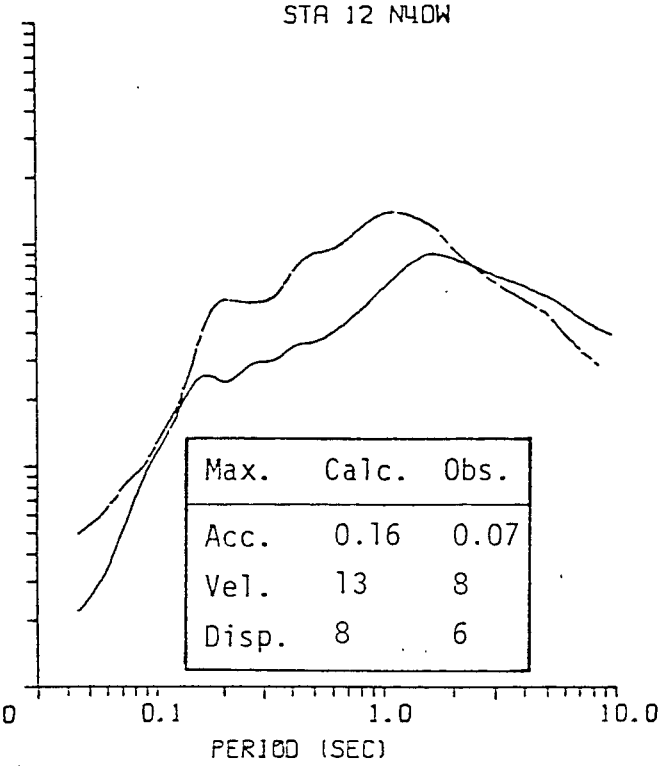

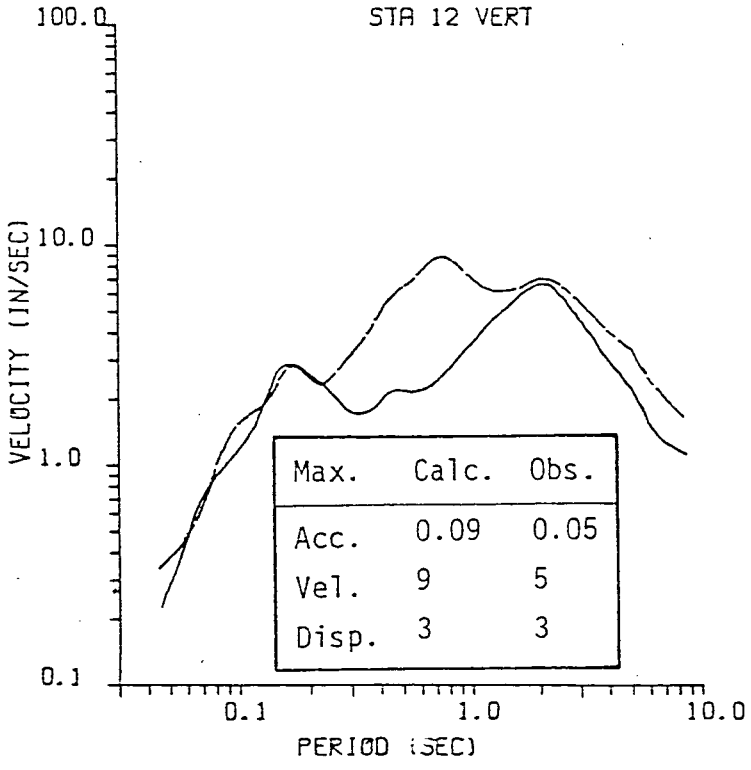

——— – ——— Calculated

——————— Observed

Comparison of the smoothed 2% velocity response spectra recorded at Station 12 of the 1966 Parkfield Earthquake using DELTA's three-parameter slip function without randomness.

Figure 5-21

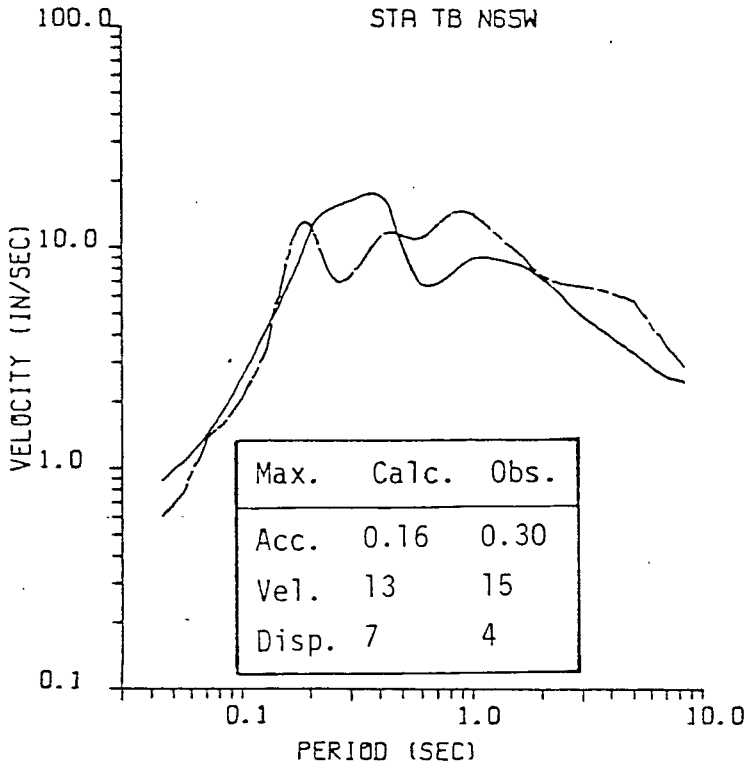

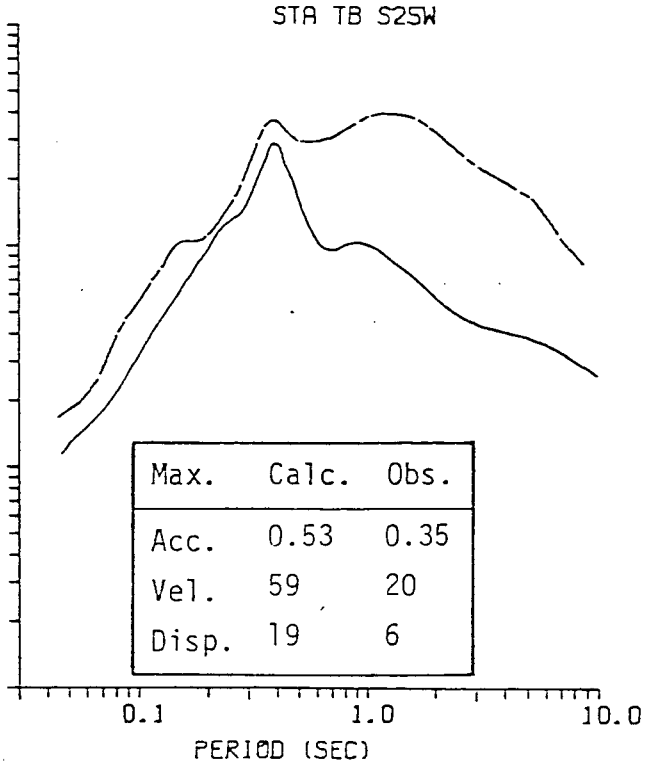

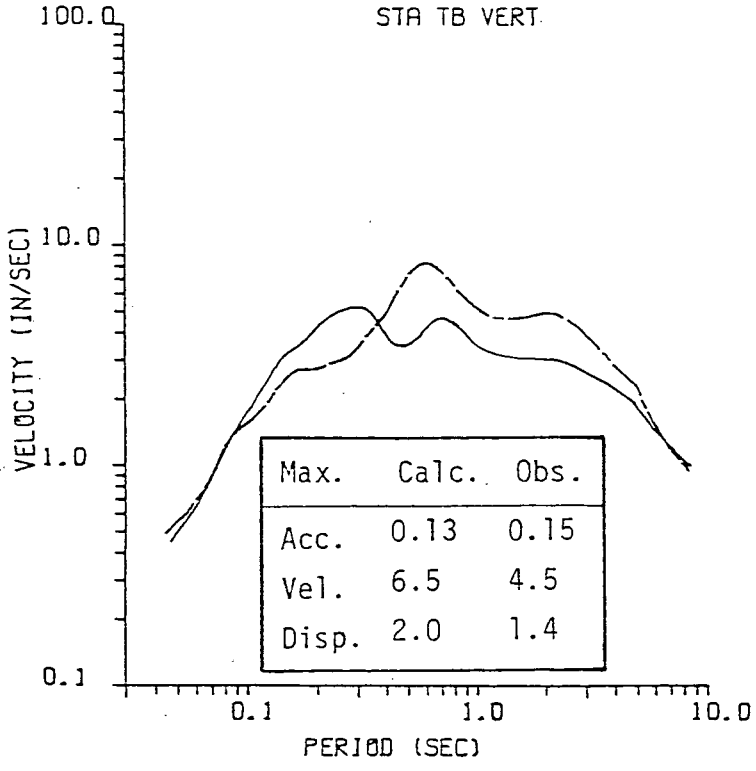

——— Calculated

——— Observed

Comparison of the smoothed 2% velocity response spectra recorded at Station TB of the 1966 Parkfield Earthquake using DELTA's three-parameter slip function without randomness.

Figure 5-22

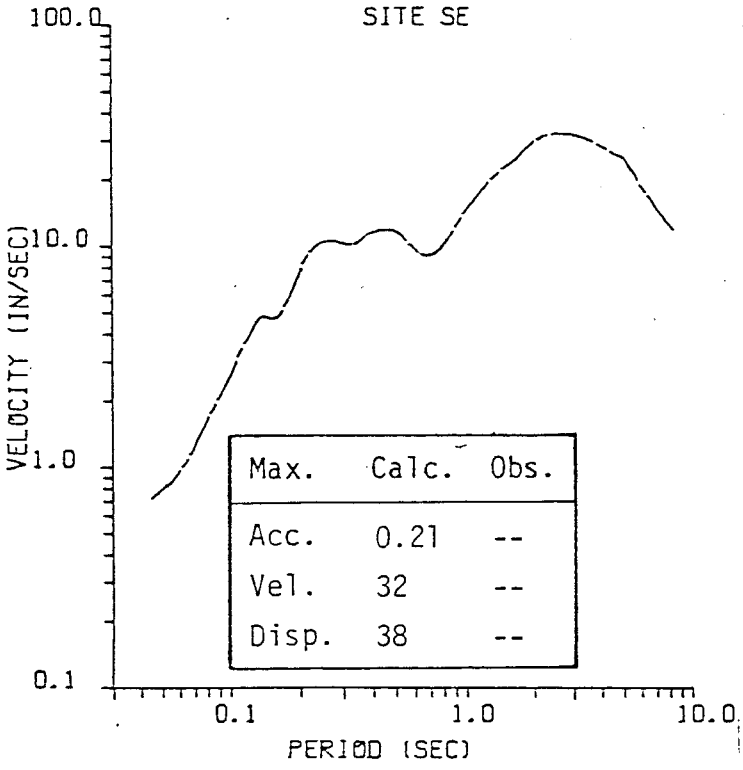

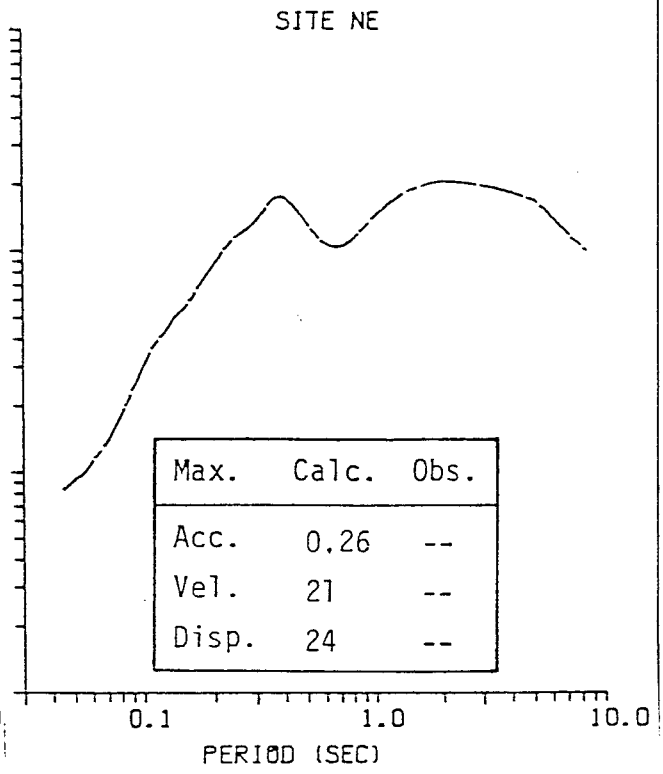

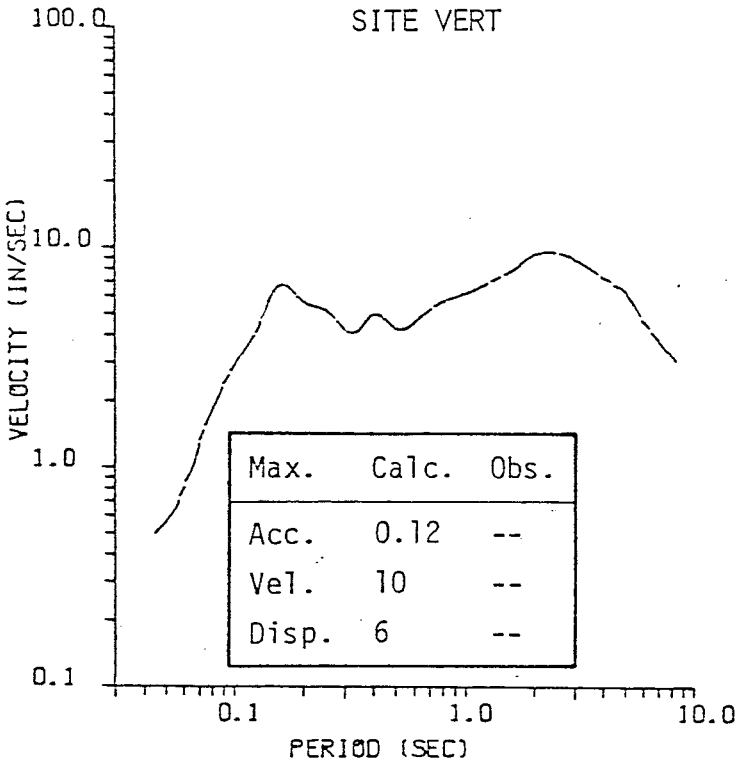

——— - ——— Calculated

Smoothed 2% velocity response spectra using DELTA's three-parameter slip function without randomness.

Figure 5-23

The next section further demonstrates the unrealistic results obtained using a coherent model by comparing the corresponding synthetic seismograms to the recorded time series.

5.6 SEISMOGRAMS

Even though the direct result of the earthquake ground motion computations (using program FALTUNG) is a set of three component seismograms, it was not the objective of the present work to obtain "wiggle-for-wiggle" fits to the recorded data. Such an undertaking would involve selecting more complex rupture sequences as well as more detailed geologic specifications and is beyond the scope of this study. Instead, the objective was to reproduce the important features of ground motion (overall duration of motion as well as modeling the maximum accelerations, velocities and displacements) using fairly simple rupture models.

Typical seismograms are displayed in Figures 5-24 through 5-26 for horizontal component N65E at Parkfield Station 2 and in Figures 5-27 through 5-29 for horizontal component N50E at Parkfield Station 8. In all of the figures, positive horizontal displacement signifies outward motion (positive vertical displacement would signify upward motion).

In Figure 5-24, the acceleration, velocity and displacement seismograms calculated using DELTA's Earthquake Model with randomness are displayed as a function of time from 0 to 50 seconds. The corresponding time series calculated using DELTA's Earthquake Model without randomness are shown in Figure 5-25. Finally, the recorded time series for the N65E horizontal component at Parkfield Station 2 are presented in Figure 5-26. Before interpreting the comparisons between the three figures, it must be pointed out that the time delays in the synthetic seismograms relative to the observed seismograms are caused by the different reference times. In the computed seismograms, the reference time corresponds to the time at which rupture first initiates at the hypocenter; in the

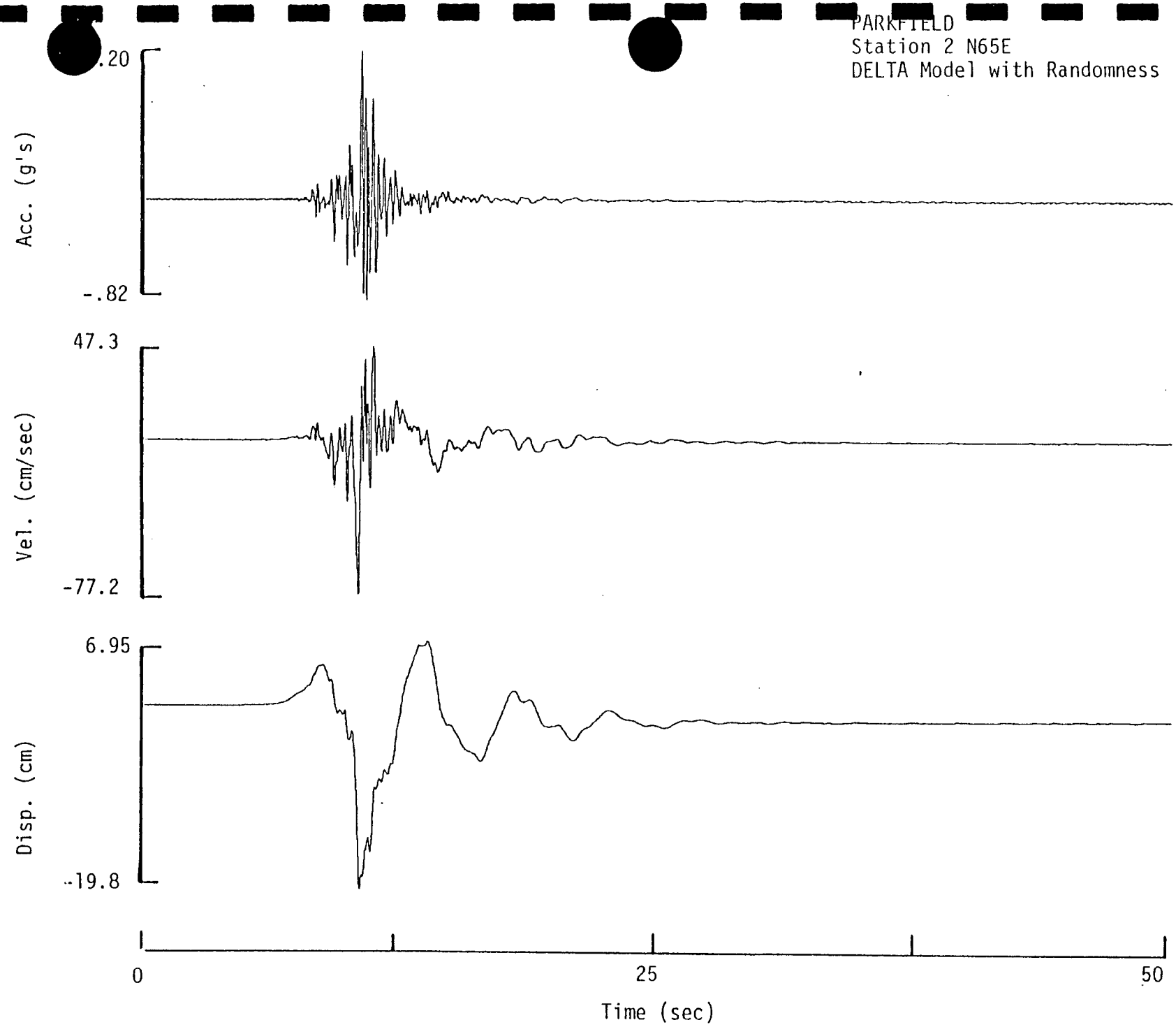

Figure 5-24. Time histories computed for horizontal component N65E at Parkfield Station 2 using DELTA's Earthquake Model with randomness.

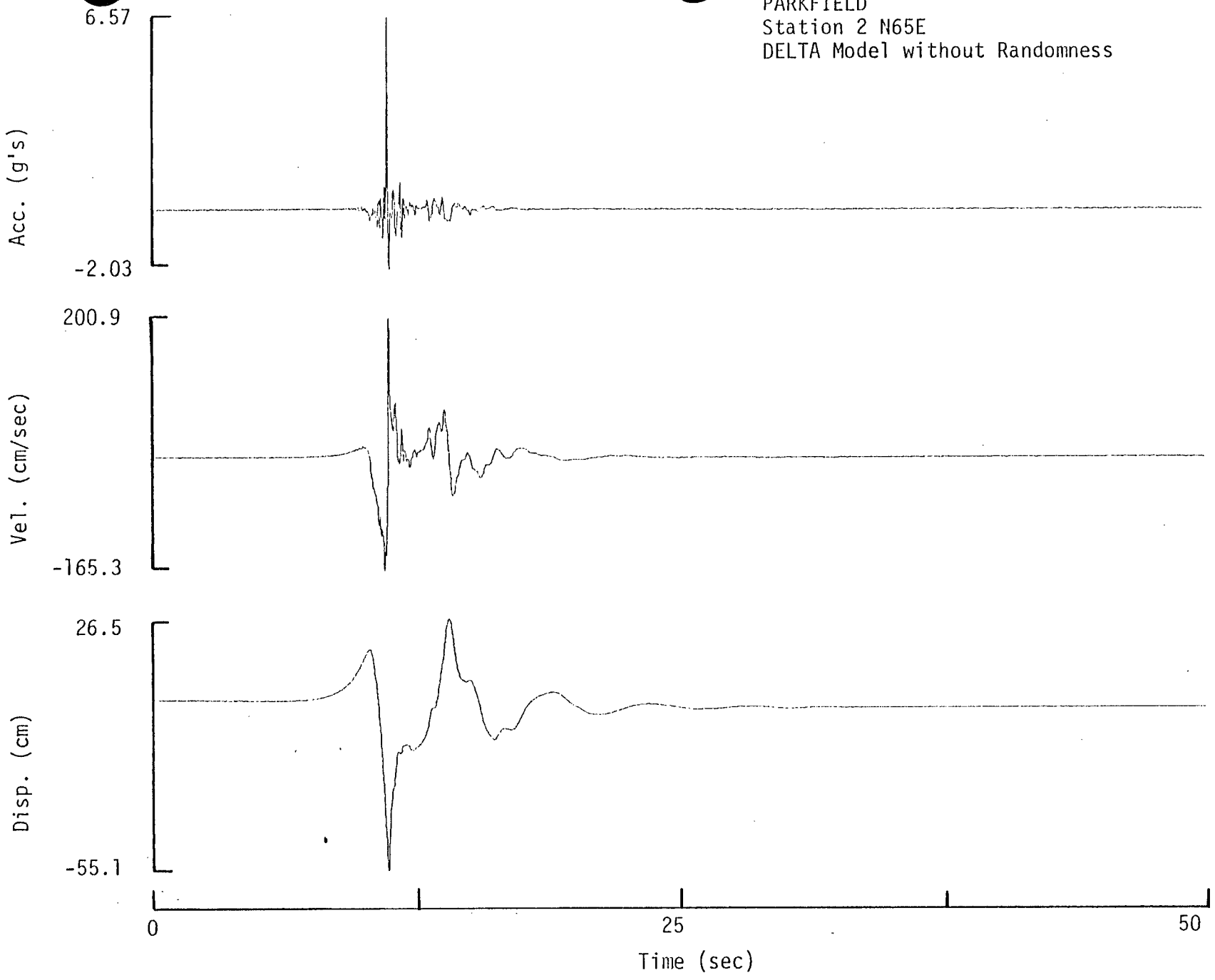

Figure 5-25. Time histories computed for horizontal component N65E at Parkfield Station 2 using DELTA's Earthquake Model without randomness.

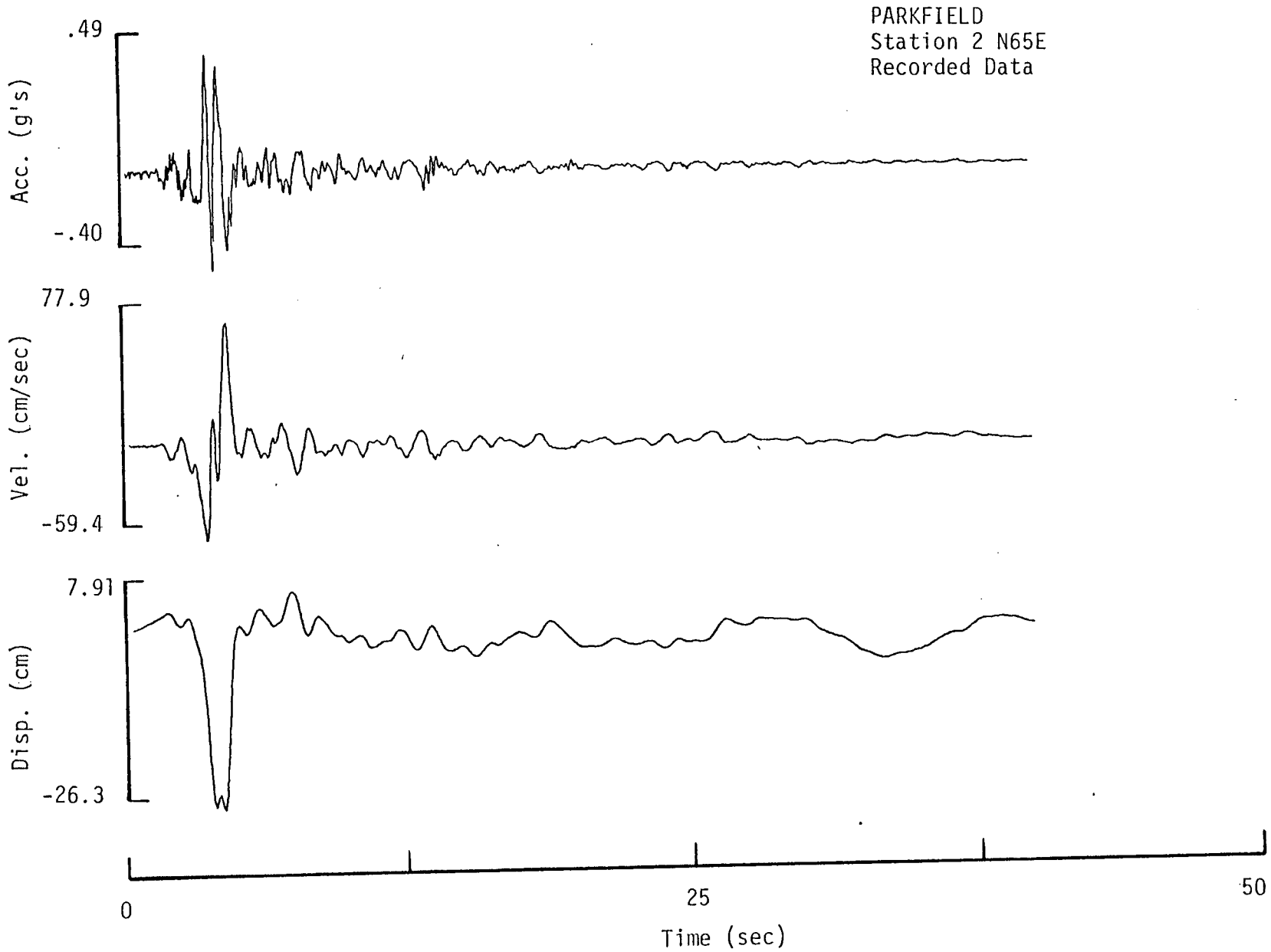

Figure 5-26. Time histories recorded for horizontal component N65E at Parkfield Station 2.

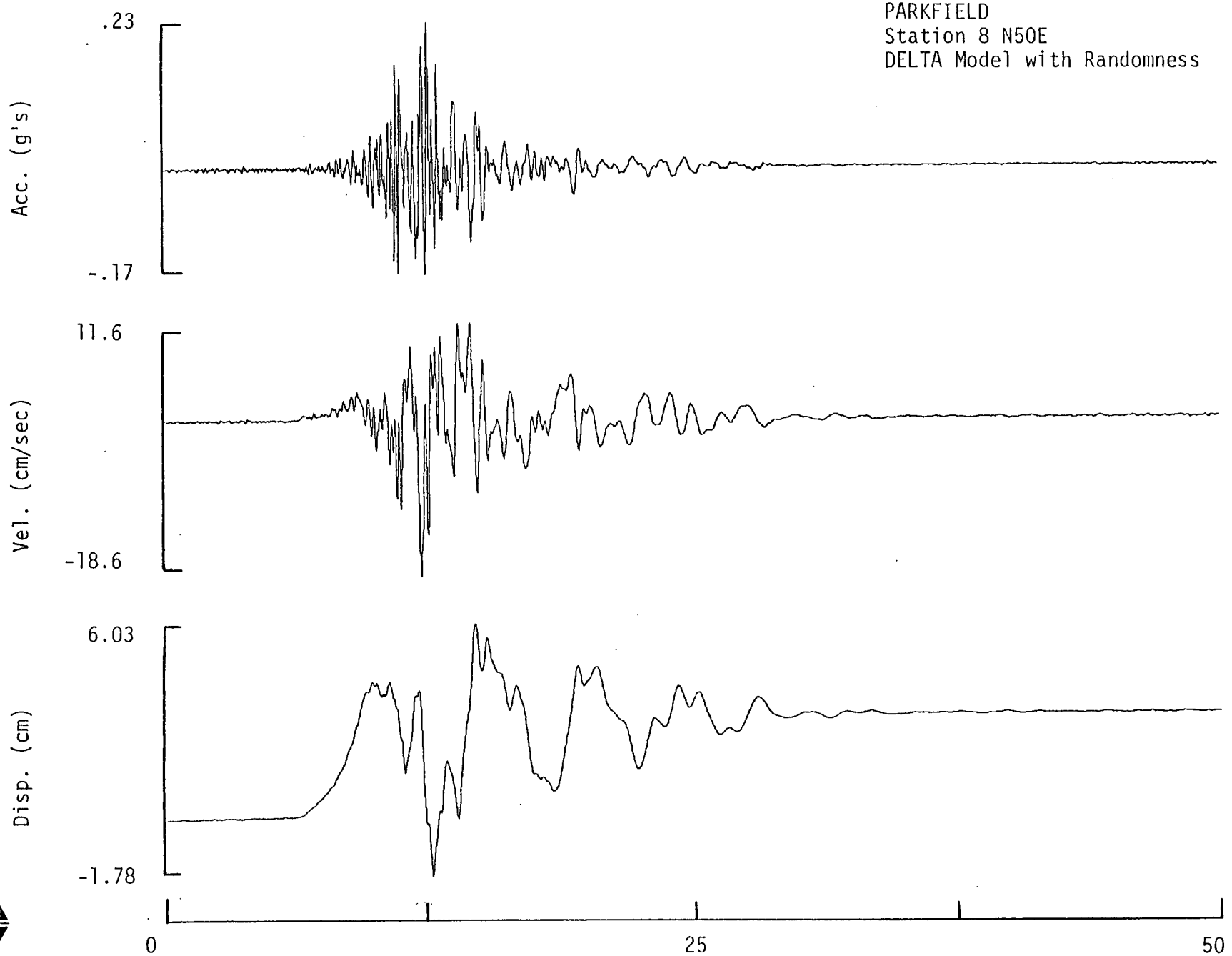

Figure 5-27. Time histories computed for horizontal component N50E at Parkfield Station 8 using DELTA's Earthquake Model with randomness.

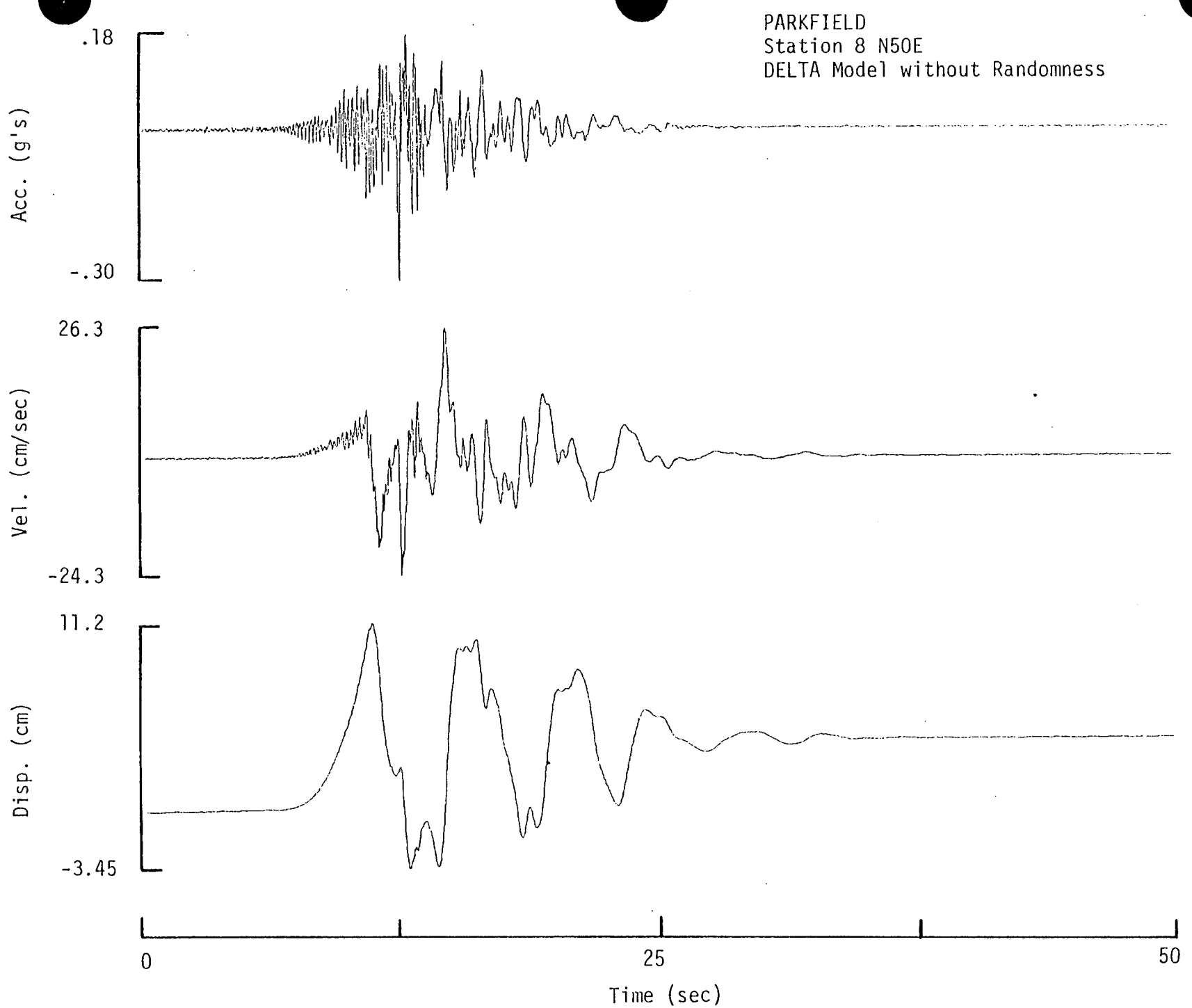

Figure 5-28. Time histories computed for horizontal component N50E at Parkfield Station 8 using DELTA's Earthquake Model without randomness.

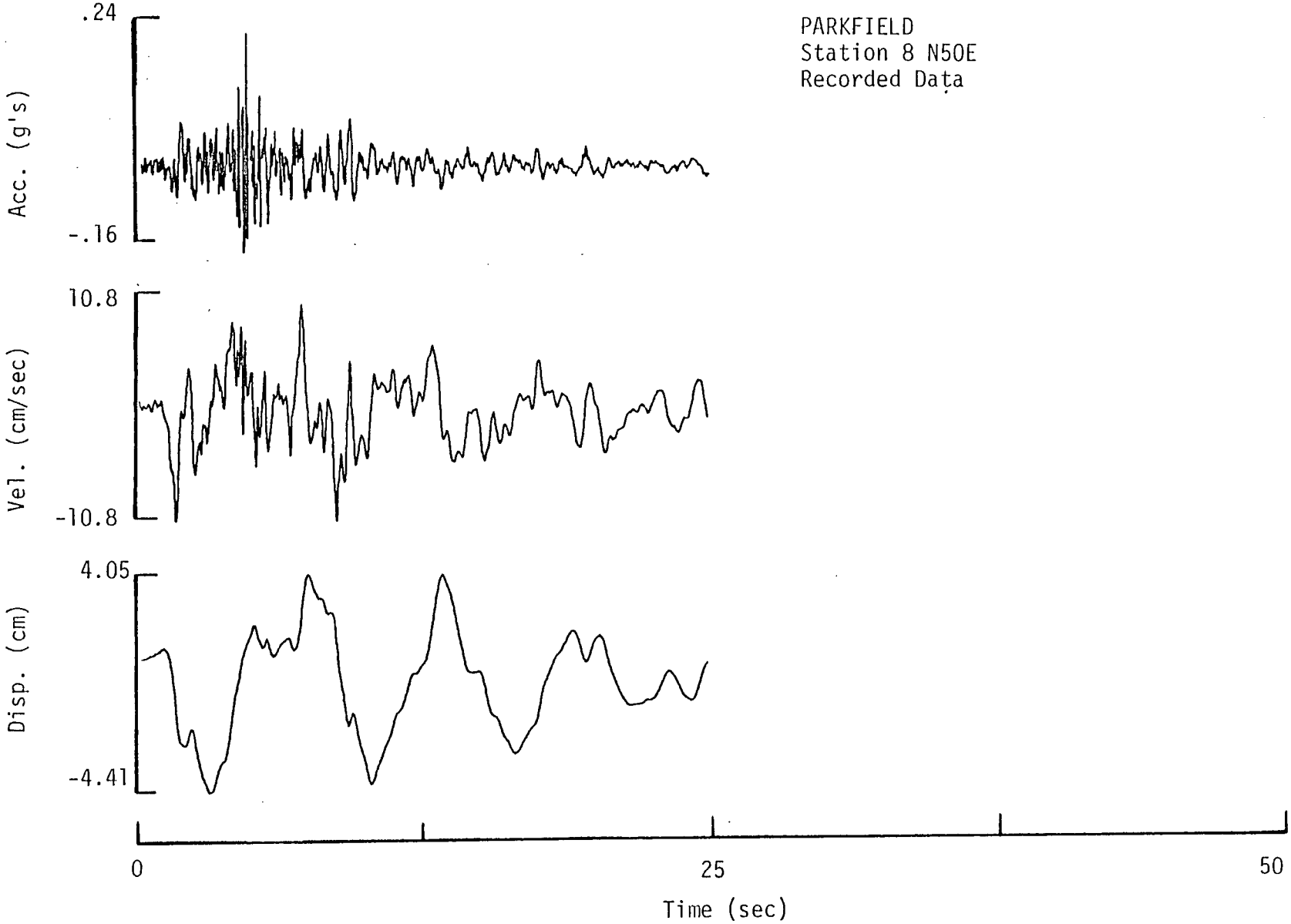

Figure 5-29. Time histories for horizontal component N50E at Parkfield Station 8.

recorded seismograms, the reference time corresponds to the time at which the motion was strong enough to trigger the strong motion recording device. Therefore, the calculated response will always appear delayed.

The coda length and the important phases are quite similar between DELTA's model with randomness and the recordings. Even the amplitudes match in the displacements and velocities. The need for introducing incoherence is immediately evident by noticing how the isolated spike appearing in Figure 5-25 (DELTA's Model without randomness) dominates the entire time signal -- amplitude and coda length. Analyzing the differences between Figures 5-24 and 5-25 in reference to the recordings (Figure 5-26), it may be concluded that a near perfect match is attainable with a slightly more incoherent model. However, incoherence introduced in the guise of randomness does not replace the need to further understand the complexities of the rupture and propagation processes.

The corresponding comparisons for the horizontal N50E component at Parkfield Station 8 are shown in Figures 5-27 through 5-29. Now, with the focusing effects less severe, the dependence on randomness is less pronounced, although similar conclusions to the discussion of Station 2 may be drawn.

In summary, of all the fault slip characterizations considered, DELTA's Earthquake Model with randomness best models the recorded peak accelerations, velocities and displacements; the broad frequency band of the observed response spectra; and the coda length and general appearance of the recorded seismograms. In addition, it may be concluded that the extrapolations to San Onofre are conservative estimates of ground motion at the site in the event of a hypothetical earthquake 8 km offshore.

6.0 SENSITIVITY STUDIES

The previous section illustrates the way in which the site-specific extrapolation of response spectra from the Parkfield and Imperial Valley earthquakes depends on certain details of the rupture model. This section illustrates how sensitive the site-specific response spectrum is to the various model parameters. Parameters pertaining to fault/site geometry, rupture characteristics, and earth parameters are examined in Sections 6.1, 6.2 and 6.3, respectively.

All sensitivity studies are performed with respect to the standard offshore model consisting of a 40-km rupture (earthquake "D" of Figure 6-1) located 8 km from the San Onofre Nuclear Generating Station. The standard rupture extends from a depth of 1.189 km to 10.0 km, with the hypocenter positioned at the deepest point of rupture at the northwestern extreme. The gross rupture characteristics, as presented in Table 5-3, consist of a rupture that spreads from the hypocenter at 90% of the local shear wave velocity. The maximum slip velocity is 800 cm/sec; the duration of slip is 2.9 sec, and the static offset is 130 cm. Randomness is applied to these rupture parameters in the manner described in Table 4-1. The layer properties are presented in Table 6-1.

6.1 FAULT GEOMETRY

One of the outstanding features of the earthquake modeling approach is the capability for examining a suite of postulated earthquakes to isolate particular configurations that produce the strongest shaking. Such a study is presented in Figures 6-1 through 6-20.

Figures 6-2 through 6-4 illustrate the way in which fault location and rupture direction influence response spectra. Clearly, focusing due to rupture direction is significant, as demonstrated by the relative amplitudes created by earthquakes "A" and "G," which differ only in terms of the direction of rupture with respect to the site. The rupture direction is from North to South and the earthquake G response is much less than the other responses as the rupture does not focus toward the site.

TABLE 6-1

VISCOELASTIC PARAMETERS FOR THE GEOLOGIC STRUCTURES
AT THE SAN ONOFRE SITE

Depth to Top of Layer (km)	Layer Thickness (km)	α P-wave Velocity (km/sec)	β S-wave Velocity (km/sec)	ρ Density (g/cc)	Q_p Compressional Quality Factor	Q_s Shear Quality Factor
0.0	0.021	1.88	0.62	2.16	114	17
0.021	0.044	1.95	0.64	2.16	120	17
0.065	0.032	2.03	0.66	2.16	126	18
0.097	0.113	2.13	0.79	2.10	122	22
0.210	0.11	2.28	0.93	2.10	123	27
0.32	0.33	2.48	1.16	2.10	124	36
0.65	0.27	2.75	1.39	2.24	133	45
0.92	0.27	2.85	1.47	2.24	137	49
1.19	0.10	3.10	1.66	2.47	148	57
1.29	0.10	3.20	1.71	2.47	154	59
1.39	2.12	4.80	2.94	2.60	231	115
3.51	6.97	5.70	3.49	2.76	286	143
10.48	---	6.10	3.73	2.76	312	156

FAULT LOCATION PARAMETER STUDY

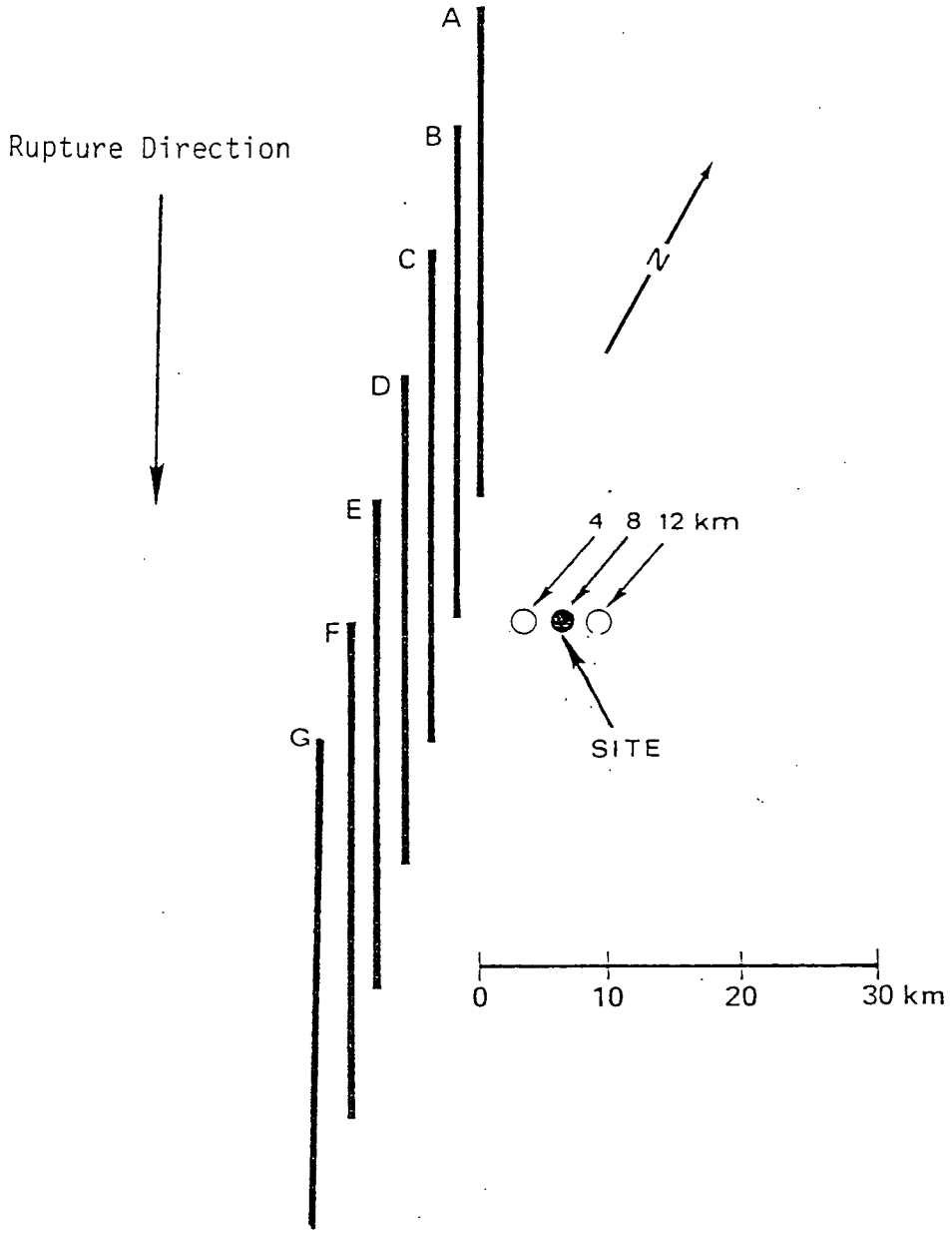

The rupture plots were separated for purposes of illustration only. All of the earthquakes are aligned with Earthquake A, 8 km from the site.

Figure 6-1. Map of seven 40-km earthquakes used to study the effect of earthquake location.

A DIVISION OF TERA CORPORATION

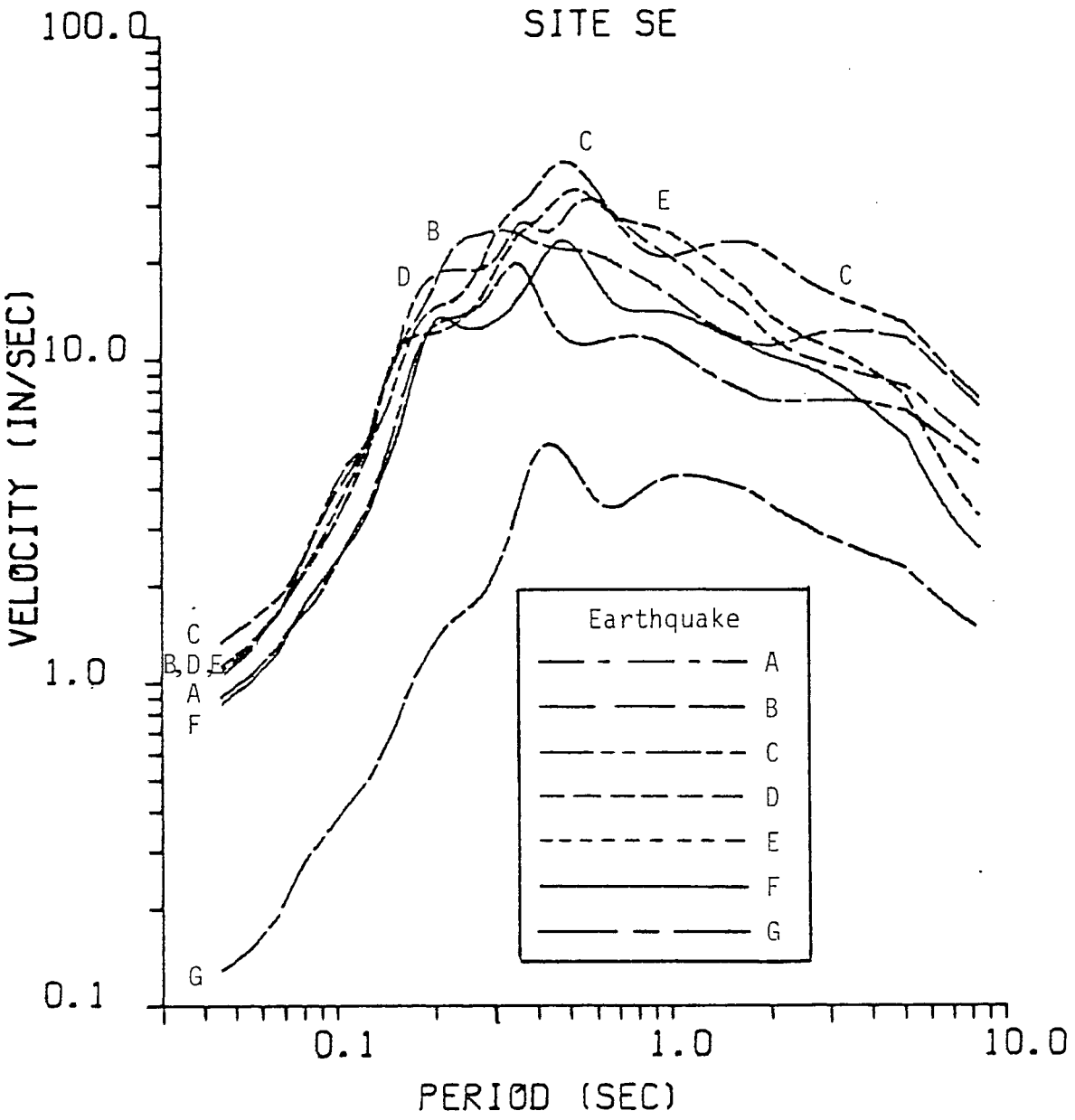

Figure 6-2. Effect of fault location on site specific response for southeast component for earthquakes mapped in Figure 6-1.

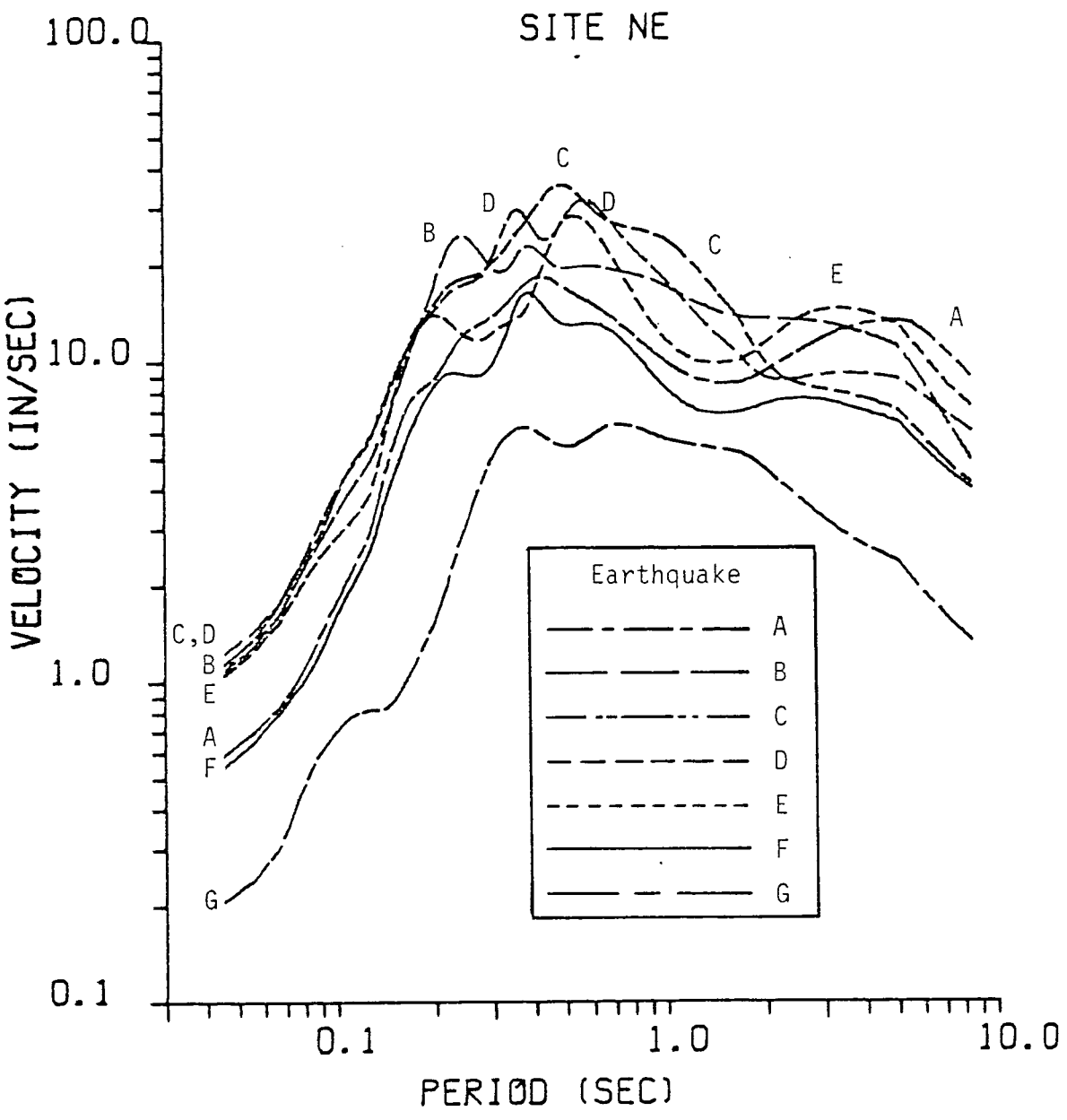

Figure 6-3. Effect of fault location on site specific response for northeast component for earthquakes mapped in Figure 6-1.

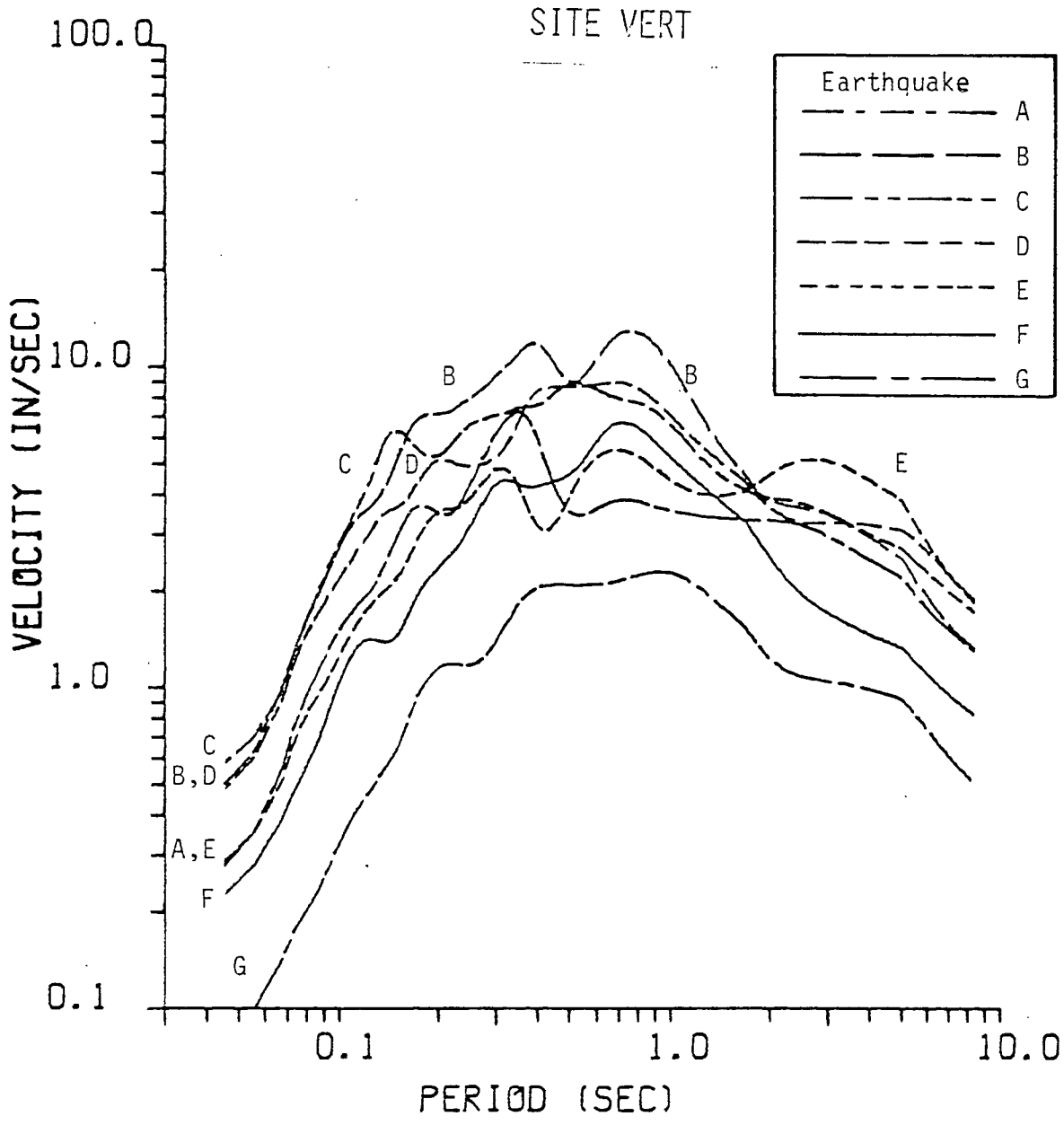

Figure 6-4. Effect of fault location on site specific response for vertical component for earthquakes mapped in Figure 6-1.

FAULT LENGTH PARAMETER STUDY

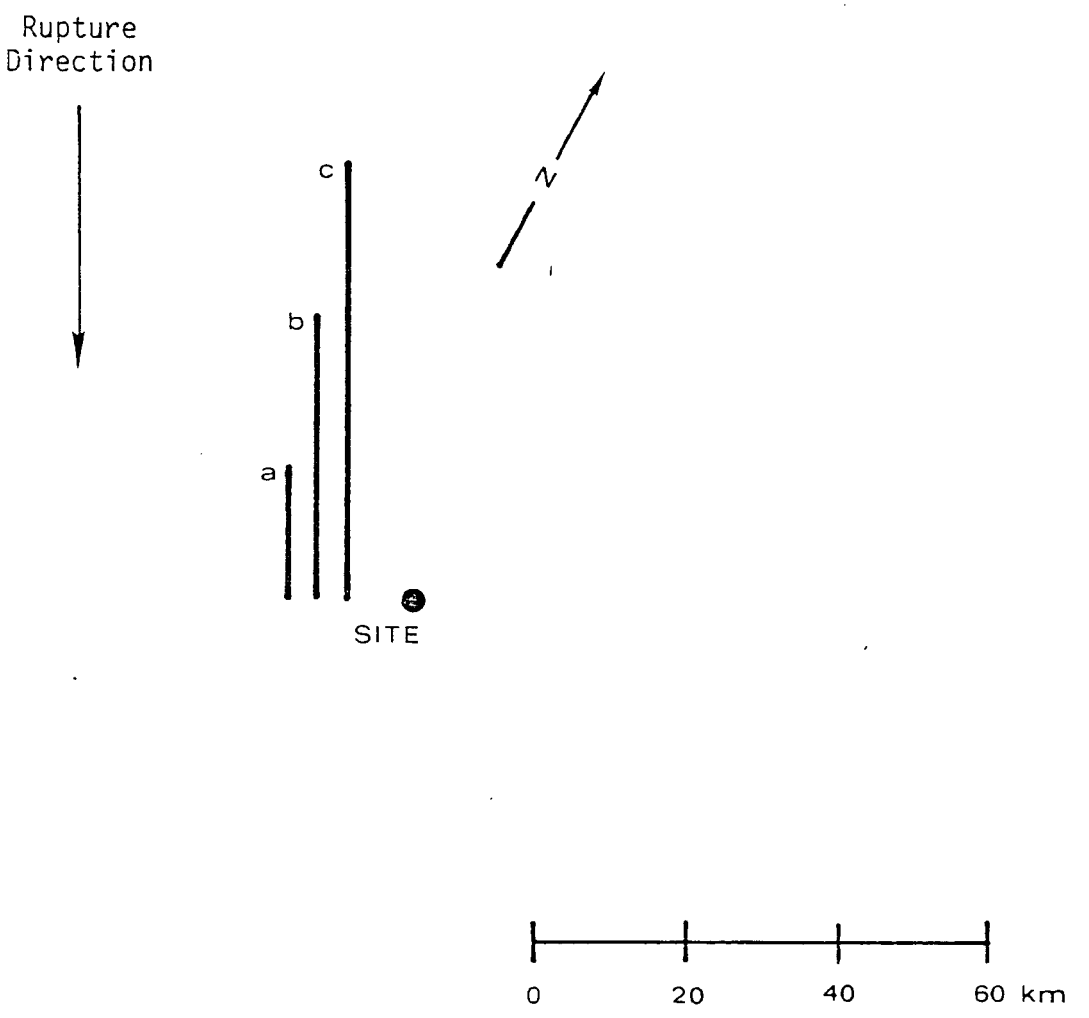

The rupture plots were separated for purposes of illustration only. All of the faults are located 8.0 km from the site with the epicentral location at the northwest extreme.

Figure 6-5. Map of three earthquakes used to study the effect of fault length.

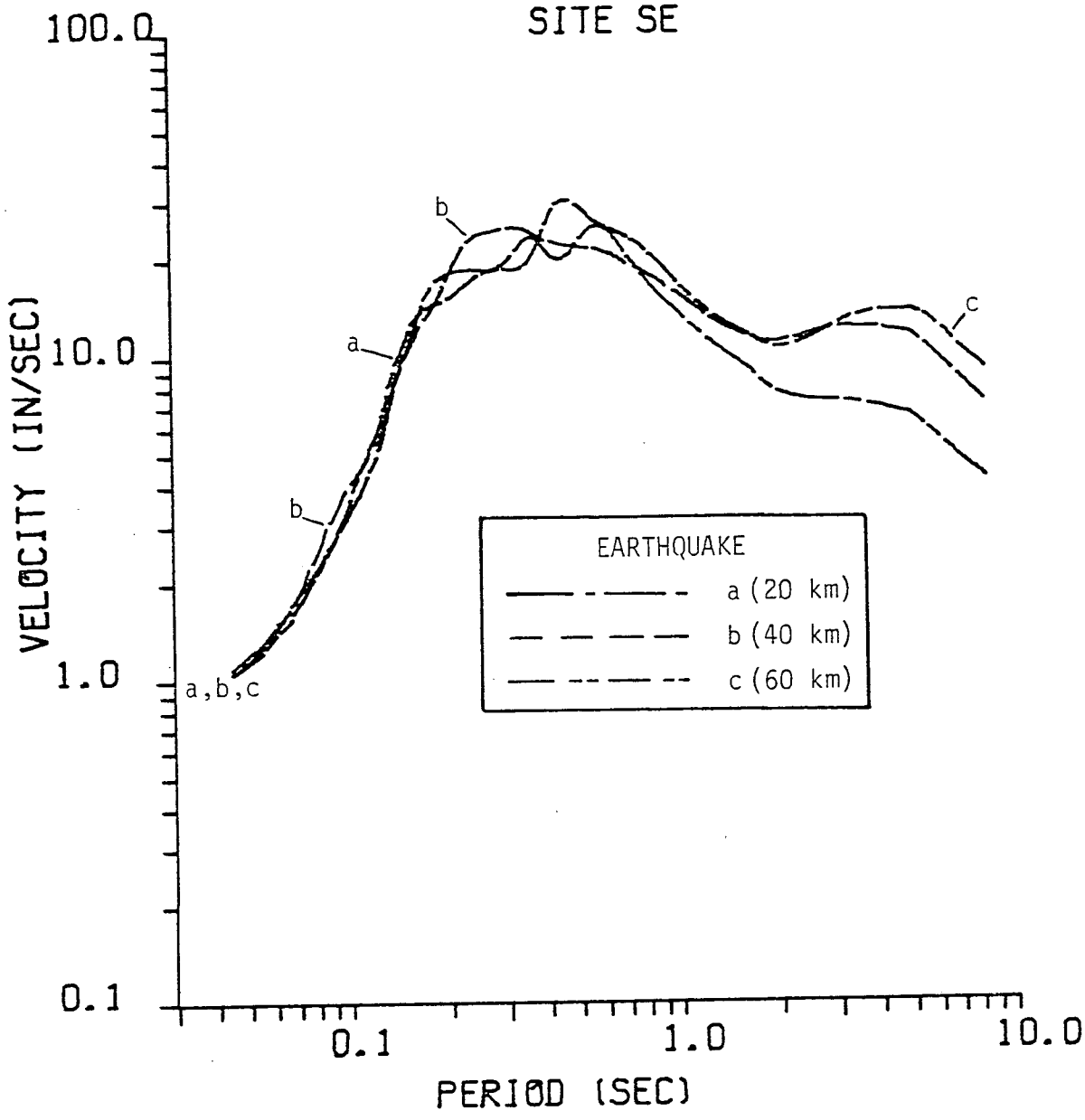

Figure 6-6. Effect of fault length on site specific response for southeast compnent for earthquakes mapped in Figure 6-5.

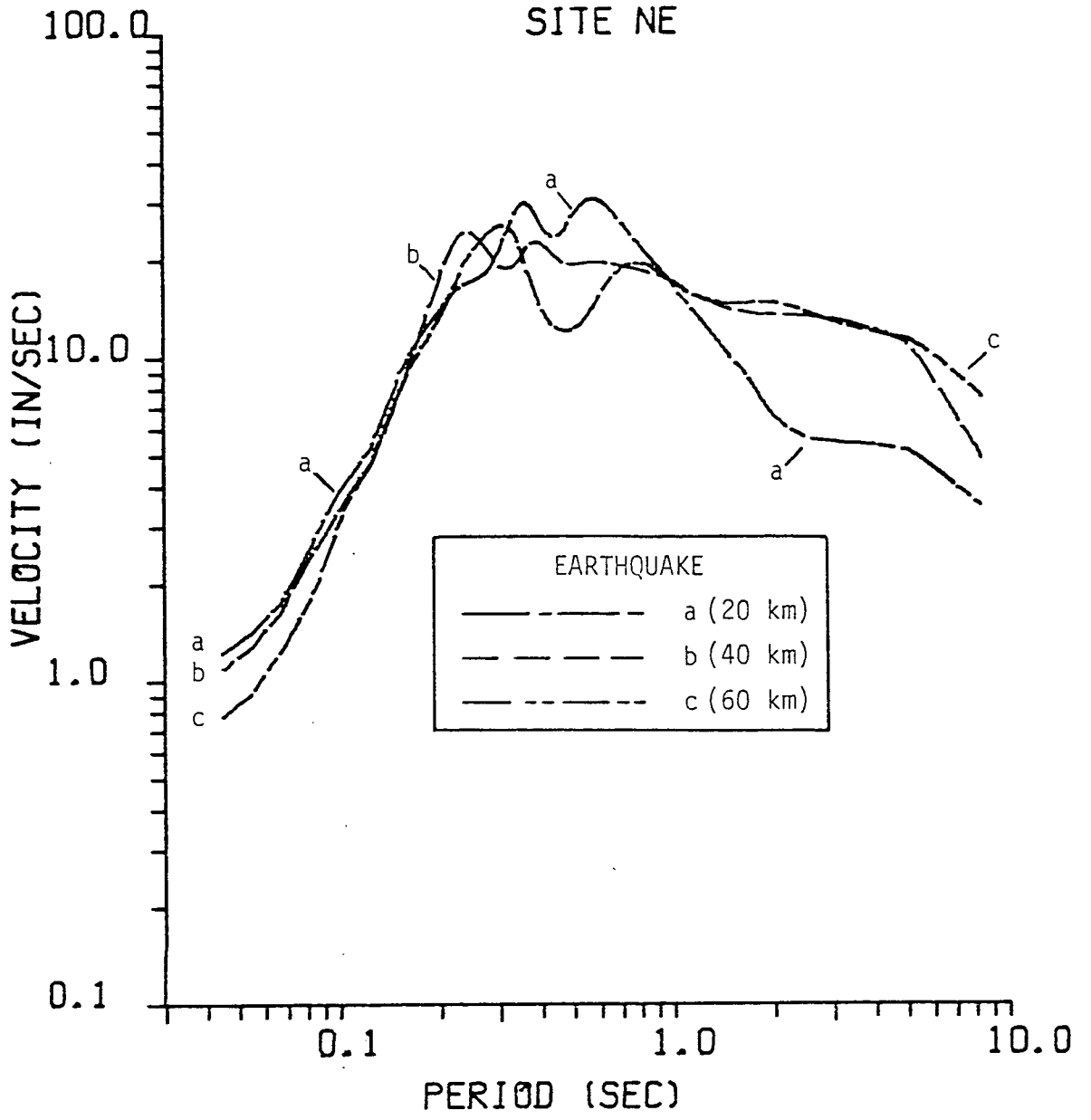

Figure 6-7. Effect of fault length on site specific response for northeast component for earthquakes mapped in Figure 6-5.

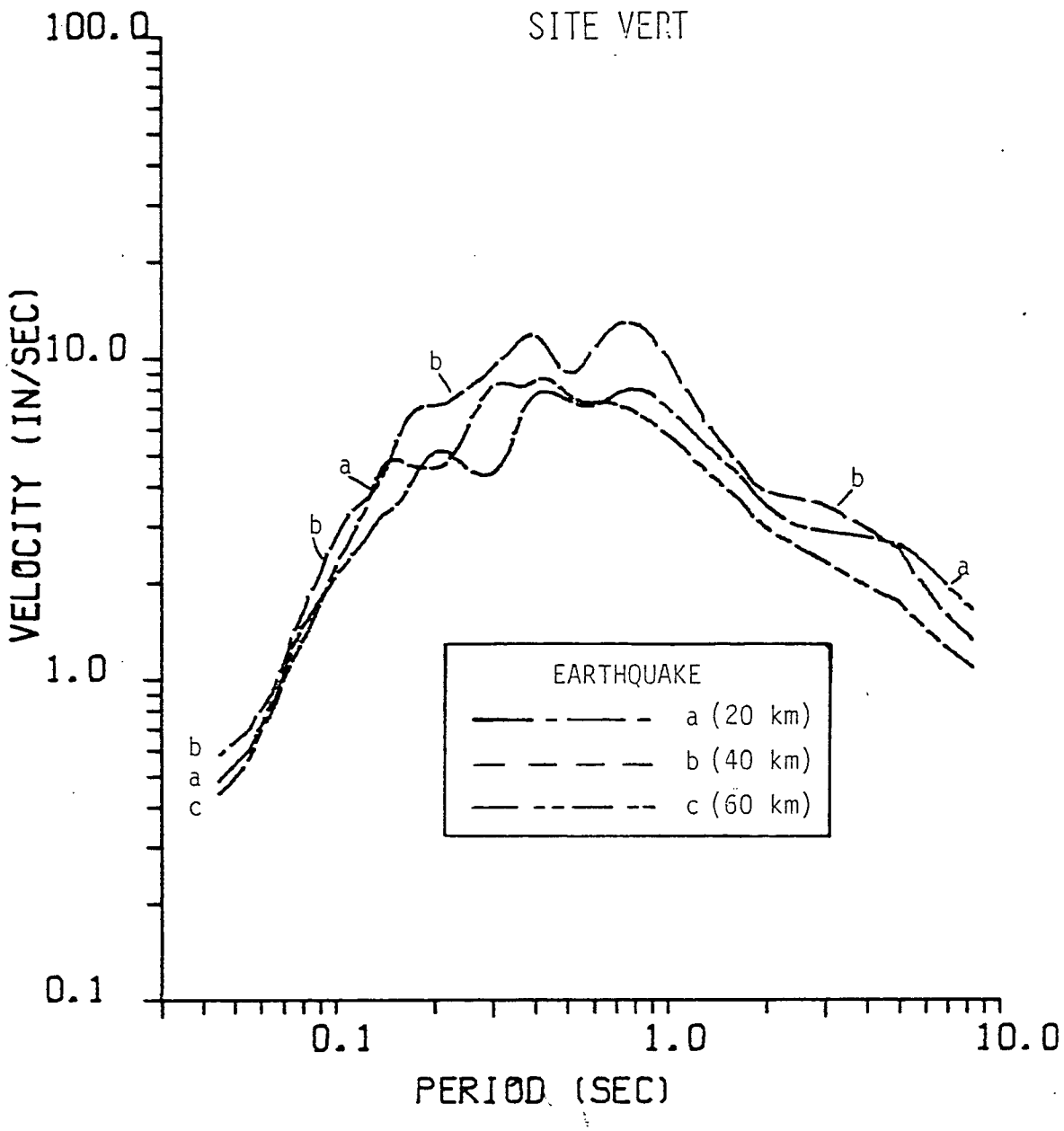

Figure 6-8. Effect of fault length on site specific response for vertical component for earthquakes mapped in Figure 6-5.

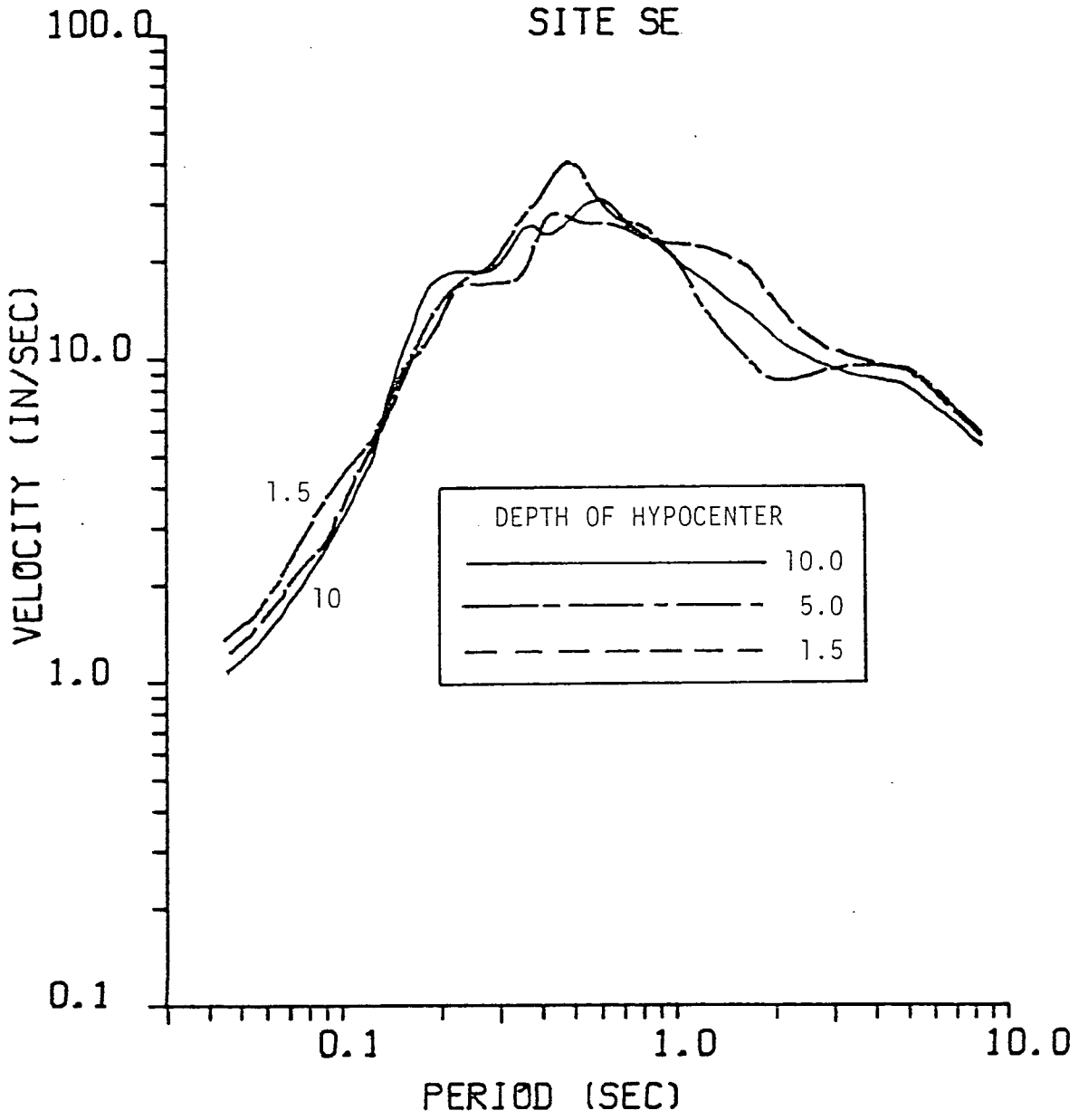

Figure 6-9. Effect of hypocentral depth on site specific response for southeast component.

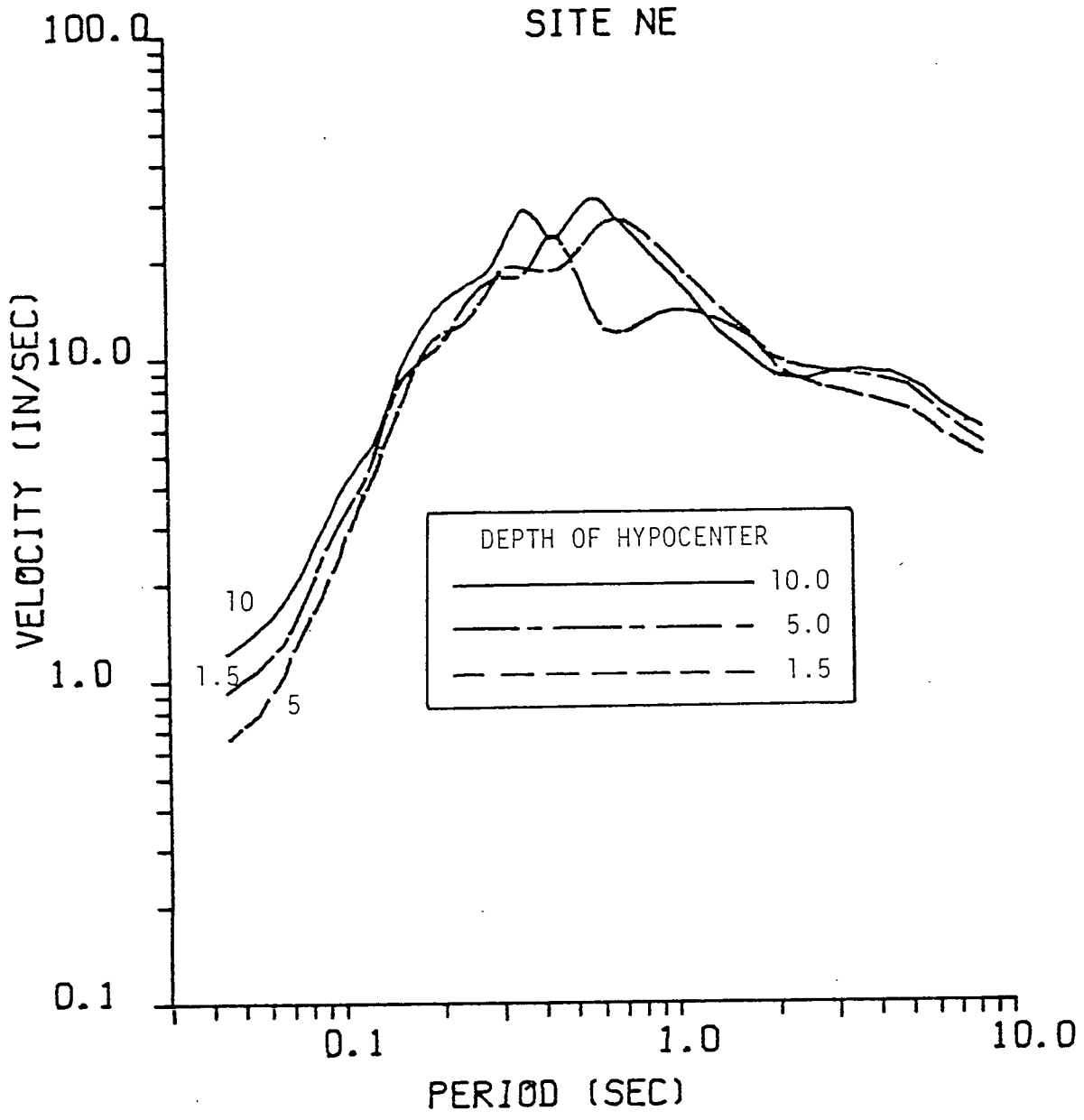

Figure 6-10. Effect of hypocentral depth on site specific response for northeast component.

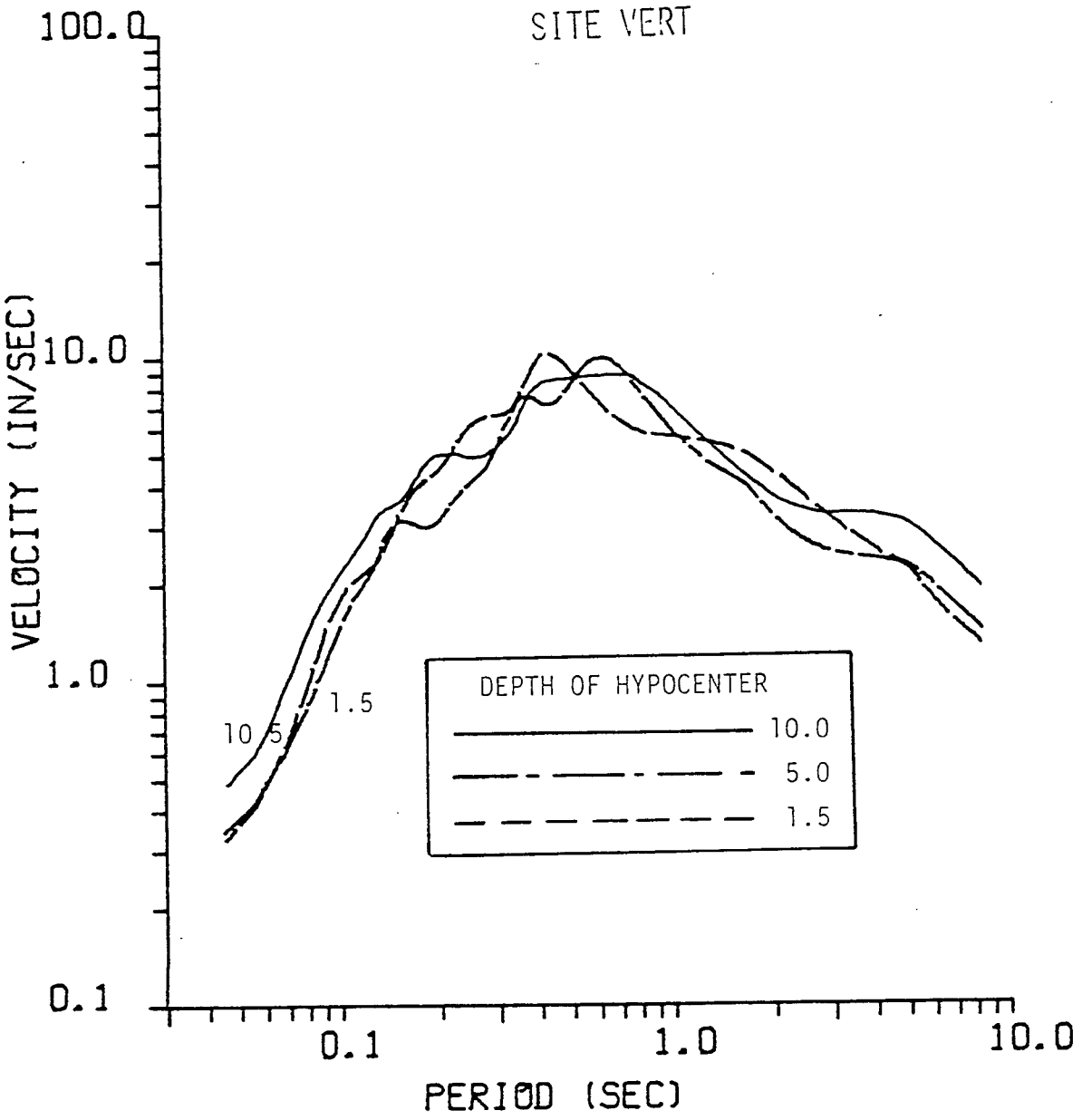

Figure 6-11. Effect of hypocentral depth on site specific response for vertical component.

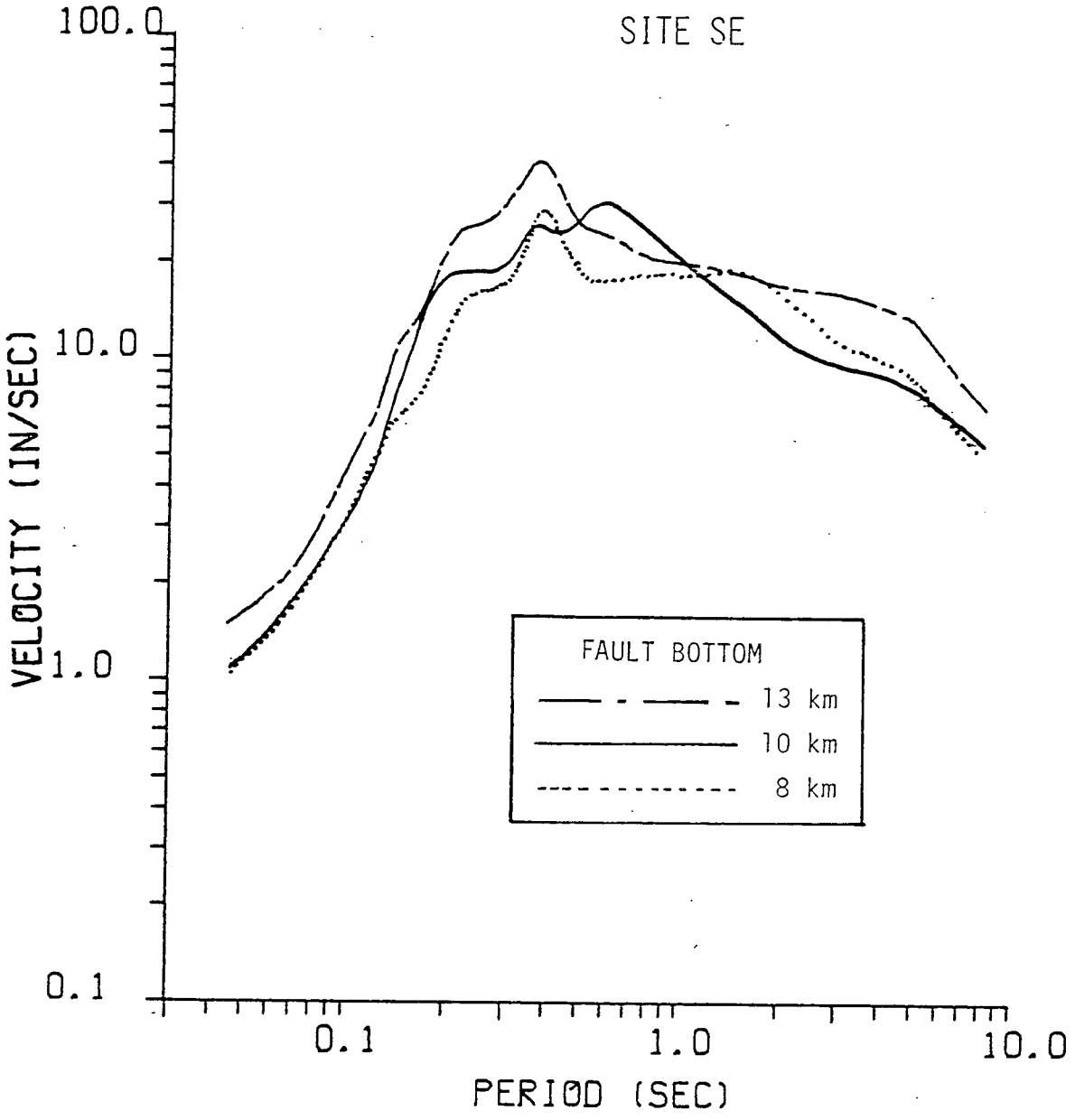

Figure 6-12. Effect of depth of fault bottom on site specific response for southeast component. Note, the hypocenter is located at the respective fault bottoms.

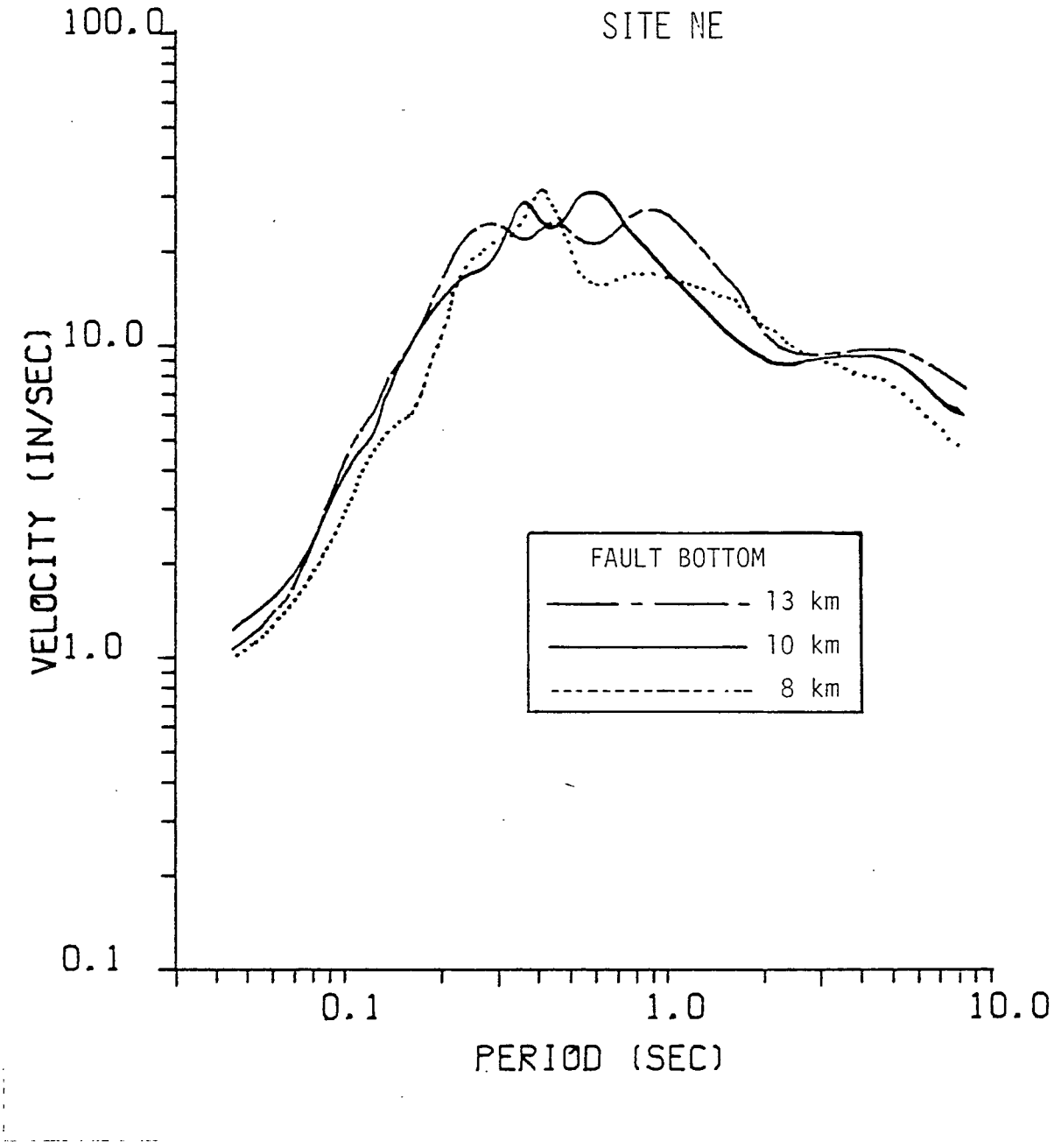

Figure 6-13. Effect of depth of fault bottom on site specific response for northeast component. Note, the hypocenter is located at the respective fault bottoms.

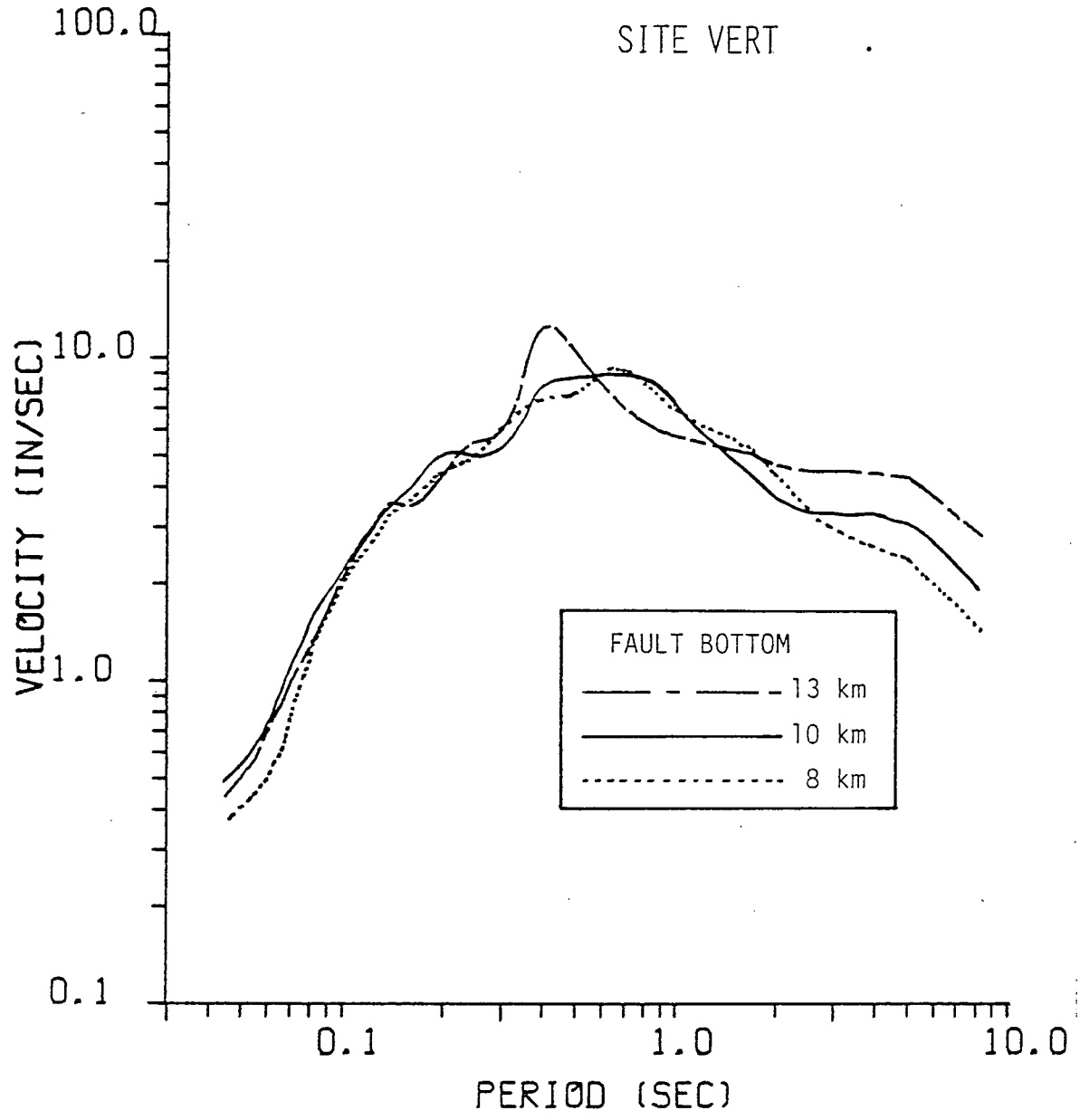

Figure 6-14. Effect of depth of fault bottom on site specific response for vertical component. Note, the hypocenter is located at the respective fault bottoms.

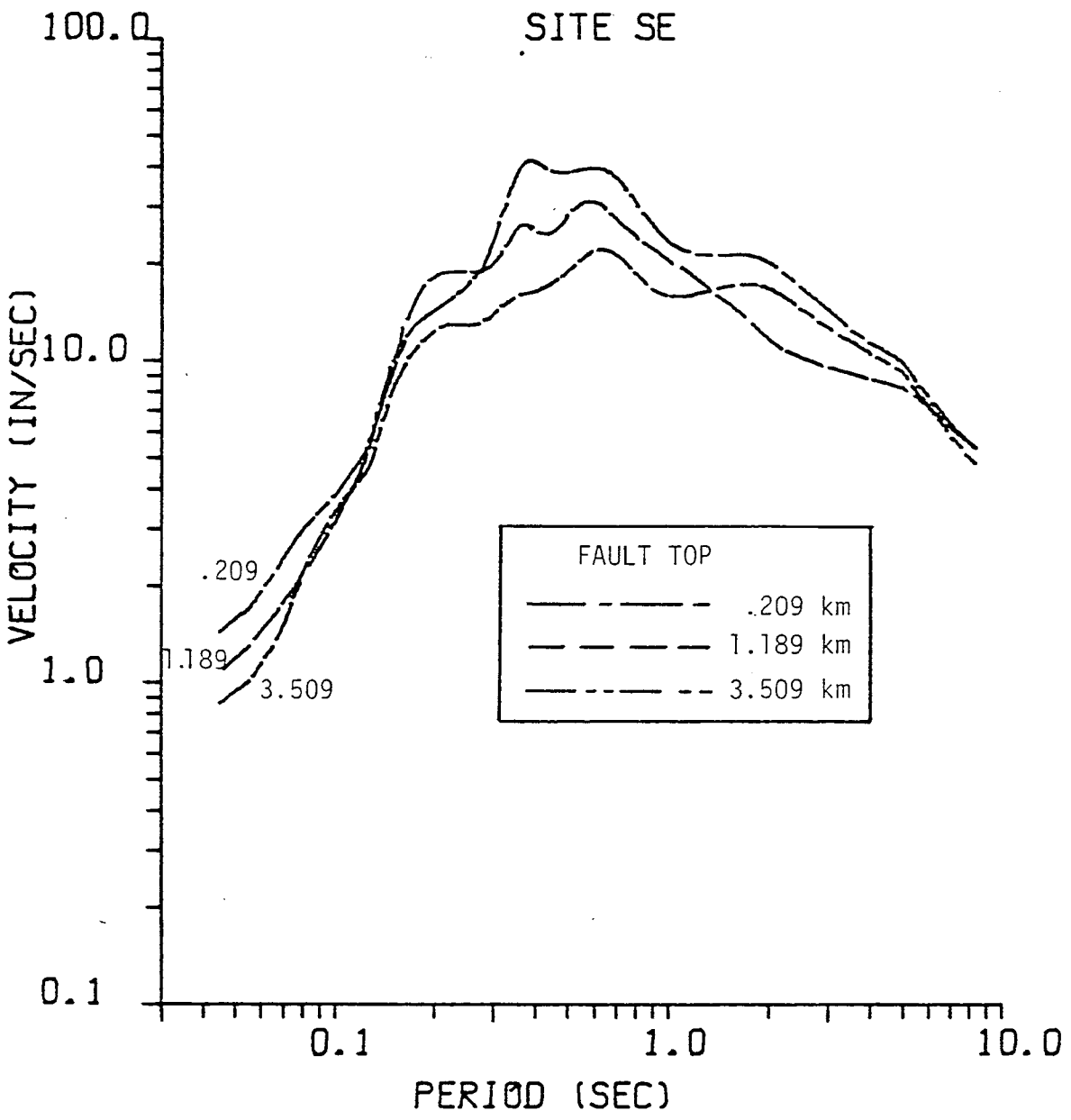

Figure 6-15. Effect of depth of fault top on site specific response for southeast component.

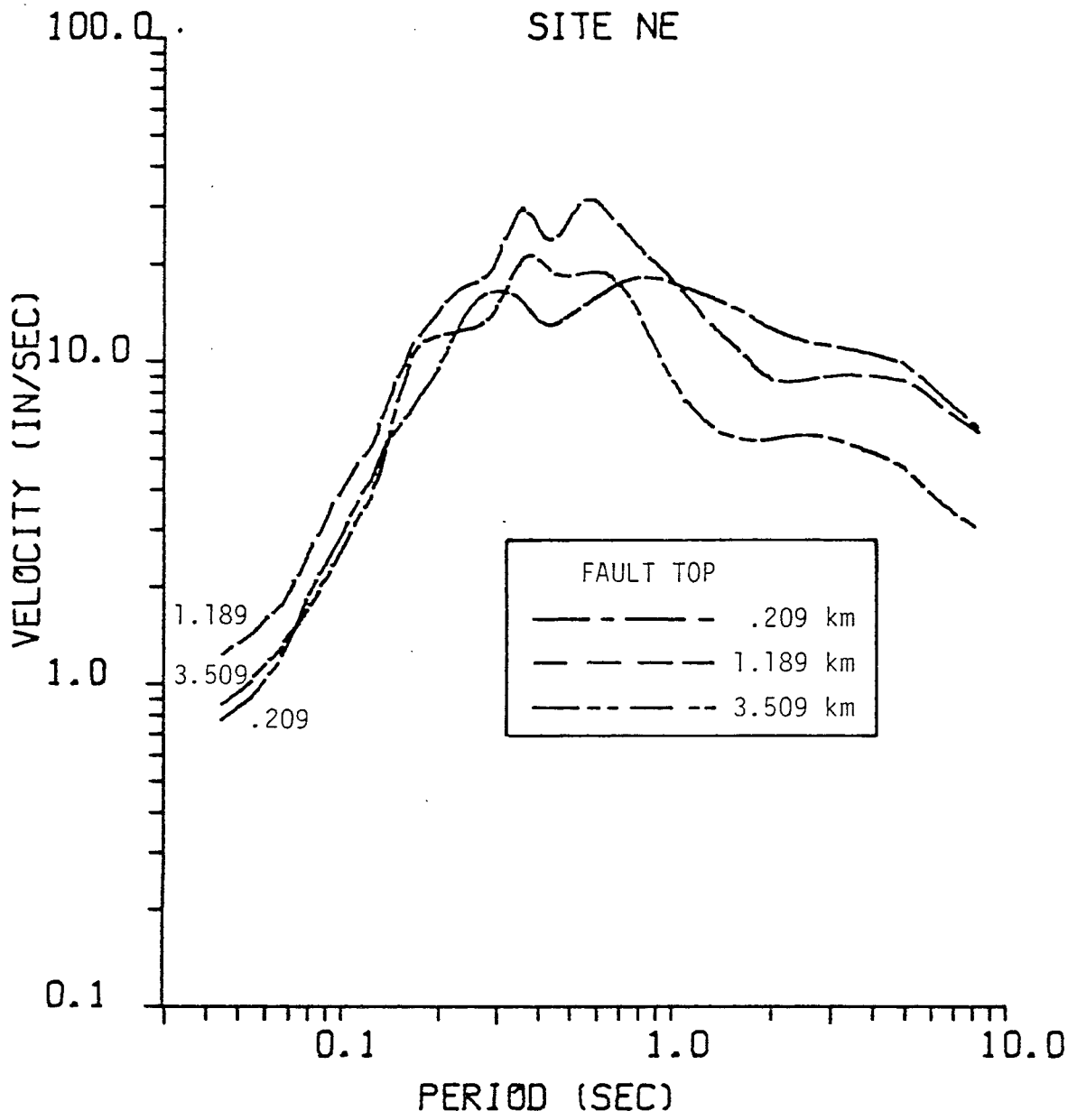

Figure 6-16 Effect of depth of fault top on site specific response for northeast component.

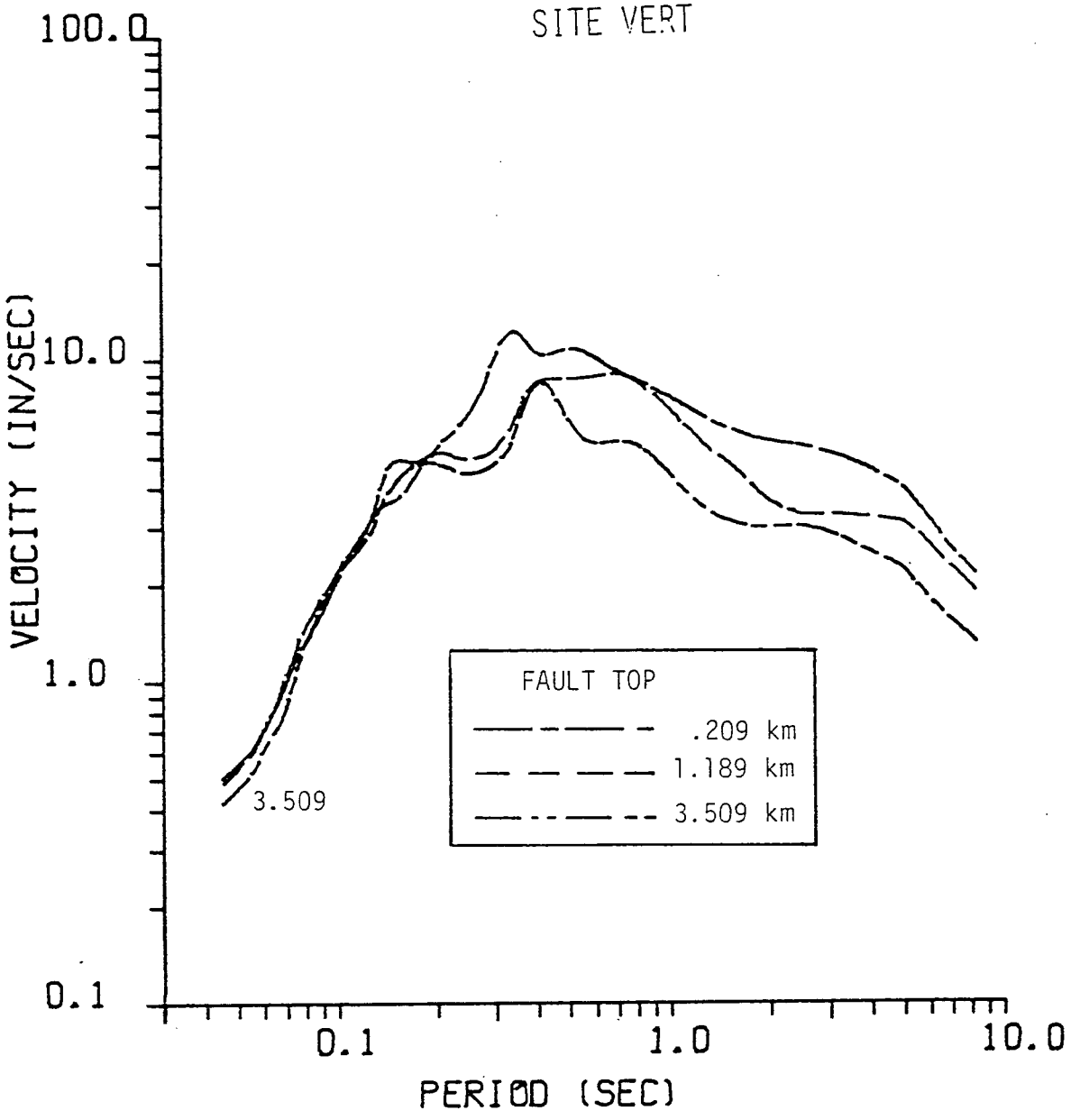

Figure 6-17. Effect of depth of fault top on site specific response for vertical component.

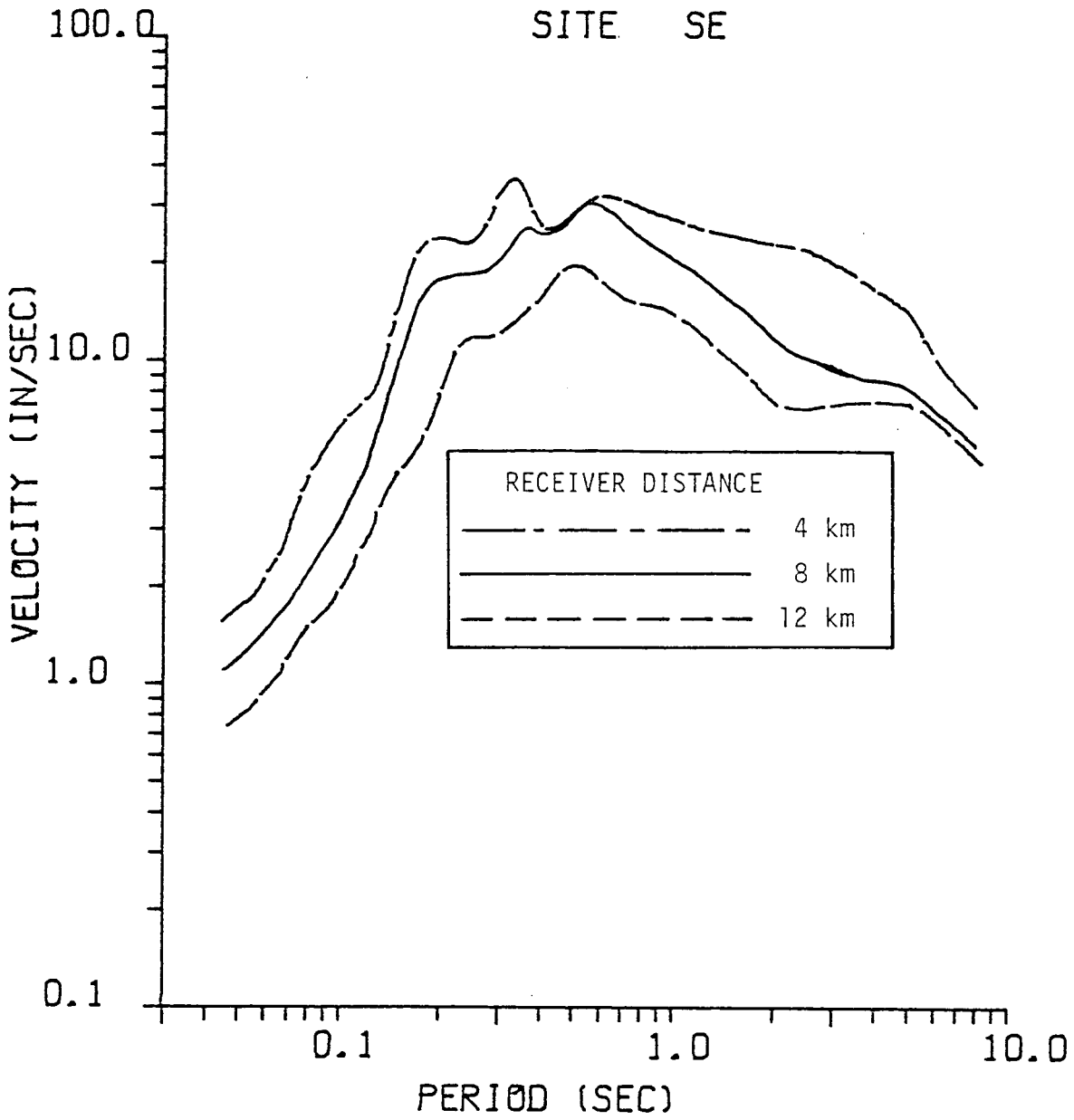

Figure 6-18. Effect of receiver distance from Earthquake "D" on site specific response for southeast component as mapped in Figure 6-1.

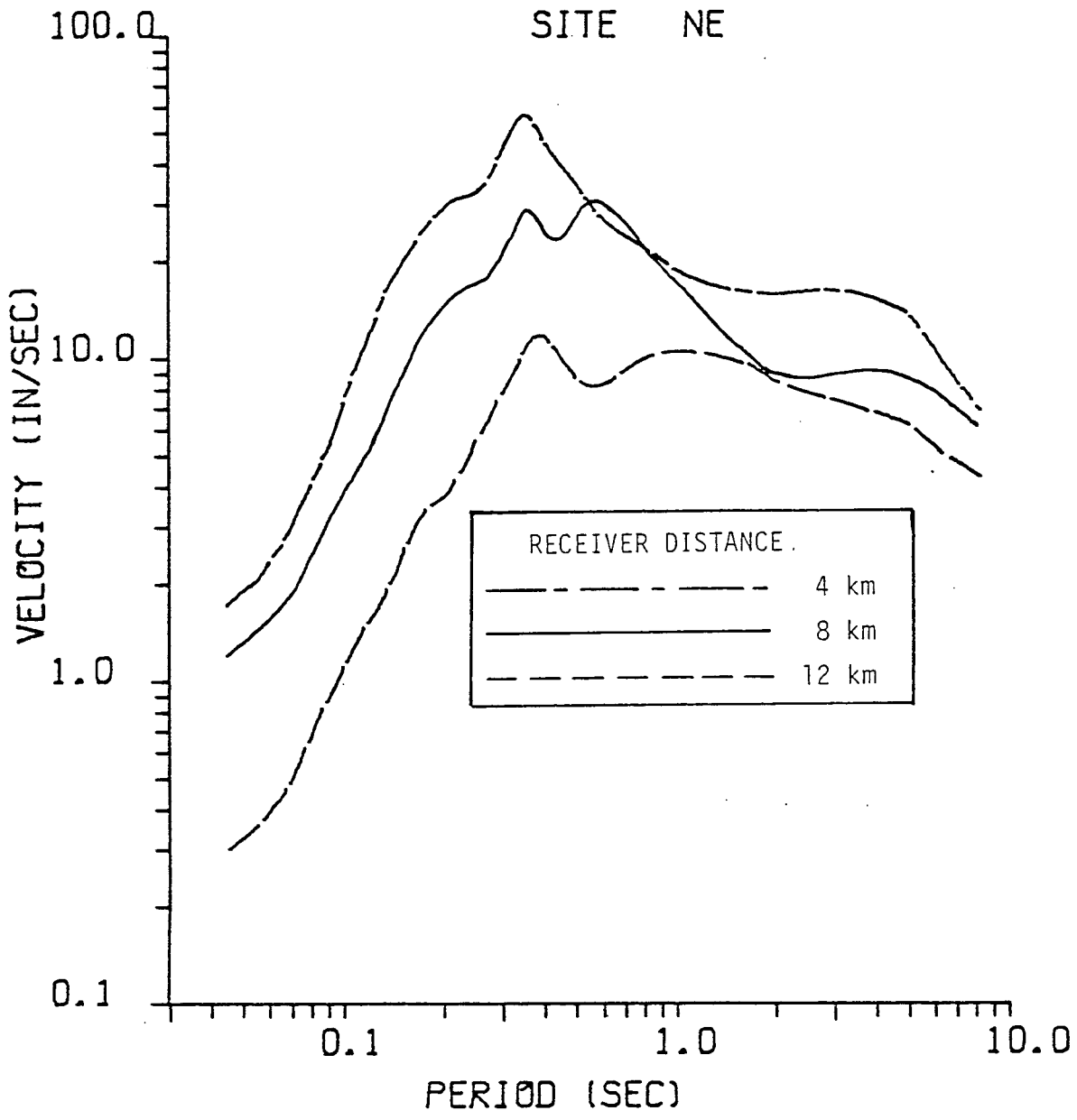

Figure 6-19. Effect of receiver distance from Earthquake "D" on site specific response for northeast component as mapped in Figure 6-1.

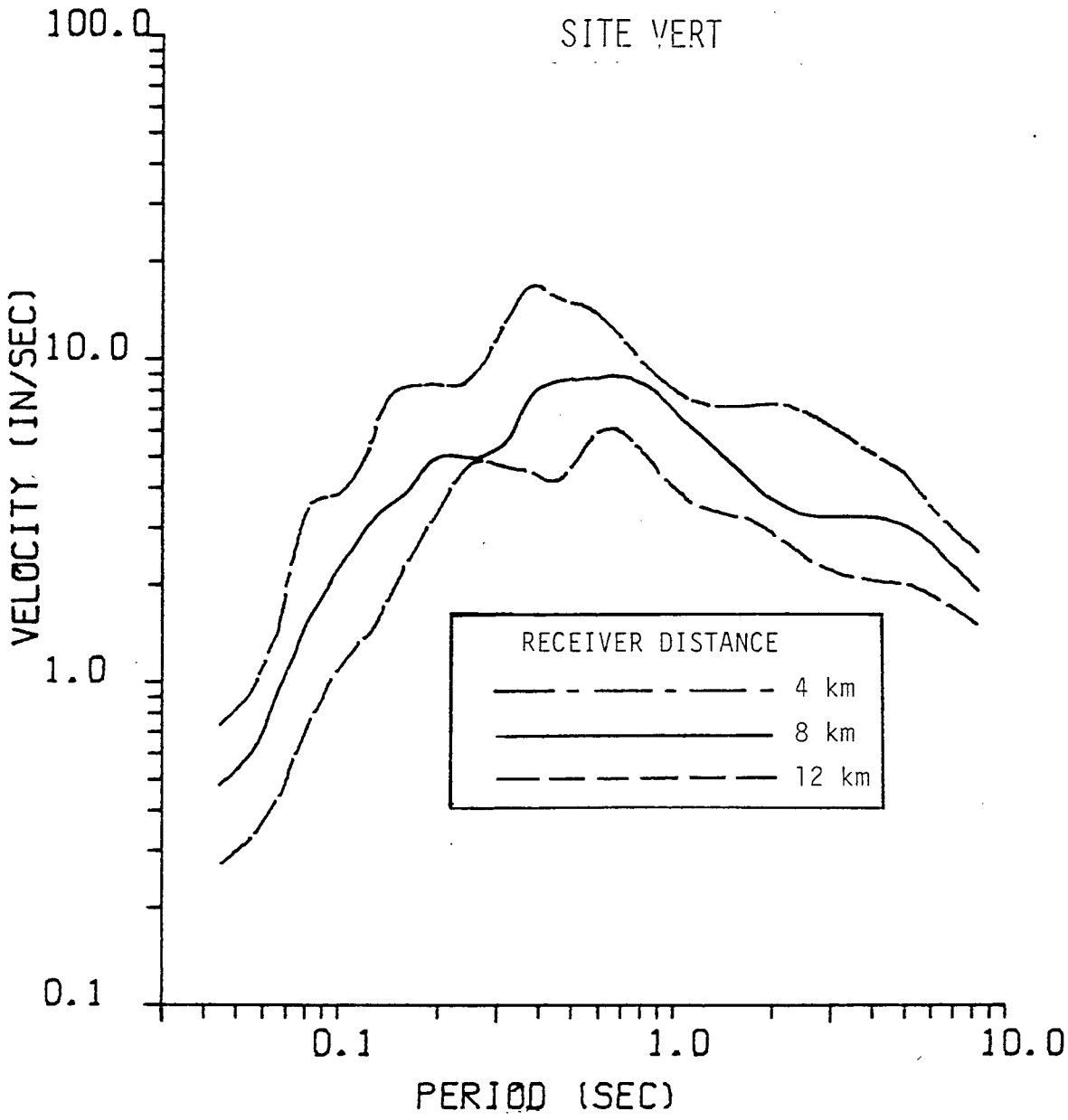

Figure 6-20. Effect of receiver distance from Earthquake "D" on site specific response for vertical component as mapped in Figure 6-1.

The influence that fault length has on response spectra is illustrated in Figures 6-6 through 6-8. As illustrated in Figure 6-5, rupture lengths of 20, 40, and 60 km are considered. The rupture propagates toward the site to simulate the most severe earthquakes. For periods longer than about 1.0 sec, the spectral amplitude increases with increasing rupture length, whereas, no trend is apparent for shorter periods. It should be pointed out that different random numbers were used in the characterization of rupture for these three earthquakes.

Some explanation is needed to guard against misinterpretation of these results. This study does not strictly indicate that observed peak accelerations within 10 km of the rupture should be independent of magnitude for magnitudes greater than 6.0, which is approximately the magnitude of the 20-km rupture. Rather, this study indicates that a magnitude 6.0 is capable of producing just as large peak accelerations as a much larger magnitude earthquake. The probability is higher for getting larger ground acceleration from larger magnitude earthquakes, since there is a greater likelihood of having the rupture focus at the recording station for larger zones of rupture. The three rupture zones used in this study were positioned so as to produce maximum ground shaking at the site.

Figures 6-9, 6-10 and 6-11 illustrate the sensitivity (or lack of sensitivity) of response spectra to hypocentral depth. The lack of sensitivity is probably, to some extent, due to randomness in the direction of rupture through individual segments of rupture; that is, because the rupture does not spread uniformly from the hypocenter, its location is less significant.

Figures 6-12, 6-13 and 6-14 illustrate the sensitivity (or lack of sensitivity) of response spectra to depth of rupture, in that there appears to be a small increase in spectral amplitude with deepening rupture. It should be stated that the hypocenter was positioned at the deepest extent of rupture in each earthquake simulation.

Figures 6-15, 6-16 and 6-17 illustrate the sensitivity of response spectra to the shallowness of rupture. As depicted in these figures, there is no clear trend. A stronger trend would be expected of sites closer to the rupture surface. High

frequency seismic waves must propagate through deeper layers and emerge rather steeply at the site to avoid the hysteretic losses associated with shallow layers. Also, the deeper rupture is somewhat more energetic than shallow rupture due to an increase in shear modulus with depth. Consequently, there is a tendency for rupture which occurs at depths between 2 and 8 km to be the most influential for intense accelerations at the site.

Figures 6-18, 6-19 and 6-20 illustrate the importance of site distance from the zone of rupture.

6.2 RUPTURE CHARACTERIZATION

The sensitivity of response spectra to the rupture characterization is examined presently. The rupture characterization of DELTA's Earthquake Model includes rupture velocity, maximum slip velocity, slip duration, static offset and incoherence. The influence of incoherence on ground motions computed for Stations 2 and 8 at Parkfield is depicted in Table 6-2; the influence of the other four parameters on ground motion computed for earthquake "D" at San Onofre is illustrated in Figures 6-21 through 6-32.

Figures 6-21 through 6-23 study the sensitivity of the site-specific response spectra to changes in rupture velocity. Lowering the rupture velocity below 80 percent of the shear wave velocity tends to reduce the response at all periods. For rupture velocities between 80 and 95 percent of the shear wave velocity, the trend is less pronounced. DELTA's Earthquake Model assumes a rupture velocity ratio of 0.90 for all the earthquakes studied.

The effect of varying the maximum slip velocity (which is related to the dynamic stress drop) is shown in Figures 6-24 through 6-26 for the site-specific event. An increase in the maximum slip velocity leads to a linear increase of the short period response. The effect diminishes for longer periods. DELTA's Earthquake Model assumes a maximum slip velocity of 800 cm/sec for all the earthquakes studied.

TABLE 6-2

INFLUENCE OF RANDOMNESS FOR PARKFIELD EARTHQUAKE

DELTA Model	Station 2			Station 8			RATIO Sta 2/Sta 8	
	N65E	N25W	Vert.	N50E	N40W	Vert.	Peak Horiz.	Vert.
Full Randomness								
v_o = 800								
Maximum Acceleration	1.20	0.64	0.23	0.23	0.32	0.15	3.8	1.5
Maximum Velocity	77	25	15	19	13	8.4	4.1	1.8
Maximum Displacement	20	8.7	2.1	5.9	7.1	1.6	2.8	1.3
Removing Micro Incoherence								
v_o = 800								
Maximum Acceleration	2.46	1.59	0.25	0.36	0.55	0.14	4.5	1.8
Maximum Velocity	82	41	15	21	16	8.3	3.9	1.8
Maximum Displacement	20	9.2	2.1	5.9	7.2	1.6	2.8	1.3
Removing Initiation Time Randomness								
v_o = 800								
Maximum Acceleration	1.87	1.57	0.32	0.32	0.32	0.10	5.8	3.2
Maximum Velocity	114	68	15	23	16	9.5	5.0	1.6
Maximum Displacement	35	13	3.1	6.6	8.8	2.3	4.0	1.3
Removing Rupture Direction Randomness								
v_o = 800								
Maximum Acceleration	1.47	0.83	0.27	0.30	0.29	0.11	4.9	2.5
Maximum Velocity	80	32	14	22	12	8.1	3.6	1.7
Maximum Displacement	20	9.1	2.1	5.8	7.2	1.7	2.8	1.2
Removing Fault Orientation Randomness								
v_o = 800								
Maximum Acceleration	1.33	0.64	0.15	0.23	0.25	0.12	5.3	1.3
Maximum Velocity	85	31	6.8	15	13	8.4	5.7	0.8
Maximum Displacement	24	11	1.4	7.8	9.5	1.8	2.5	0.8
Removing Receiver Orientation Randomness								
v_o = 800								
Maximum Acceleration	1.37	0.36	0.23	0.20	0.38	0.15	3.6	1.5
Maximum Velocity	92	24	15	15	19	8.4	4.8	1.8
Maximum Displacement	22	8.0	2.1	6.8	9.6	1.6	2.3	1.3
No Randomness								
v_o = 1,000								
Maximum Acceleration	6.57	1.38	0.27	0.30	0.35	0.23	18.8	1.2
Maximum Velocity	201	47	12	26	23	13	7.7	0.9
Maximum Displacement	55	16	2.6	11	14	3.33	3.9	0.8

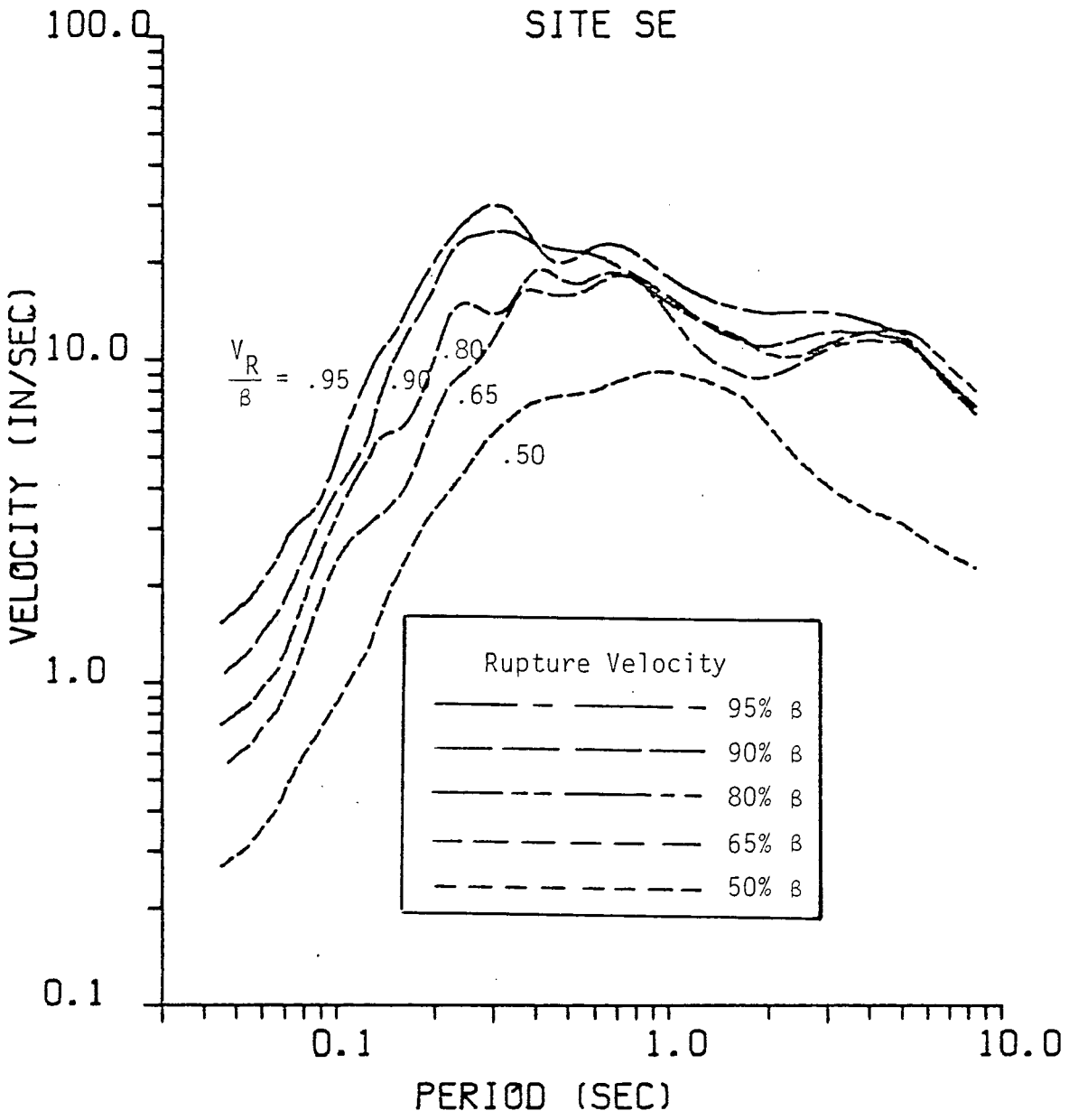

Figure 6-21. Effect of rupture velocity on site specific response for southeast component.

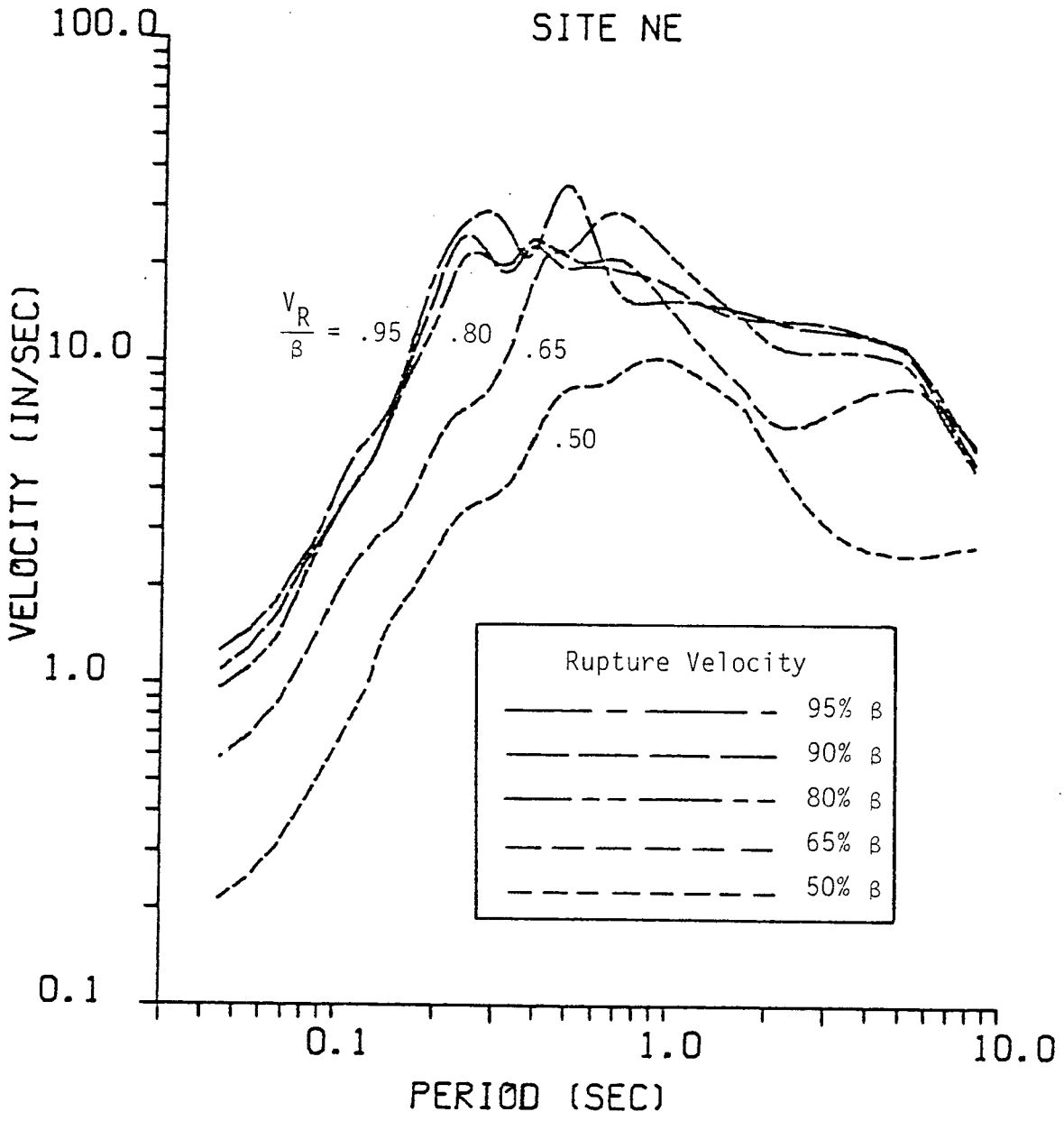

Figure 6-22. Effect of rupture velocity on site specific response for northeast component.

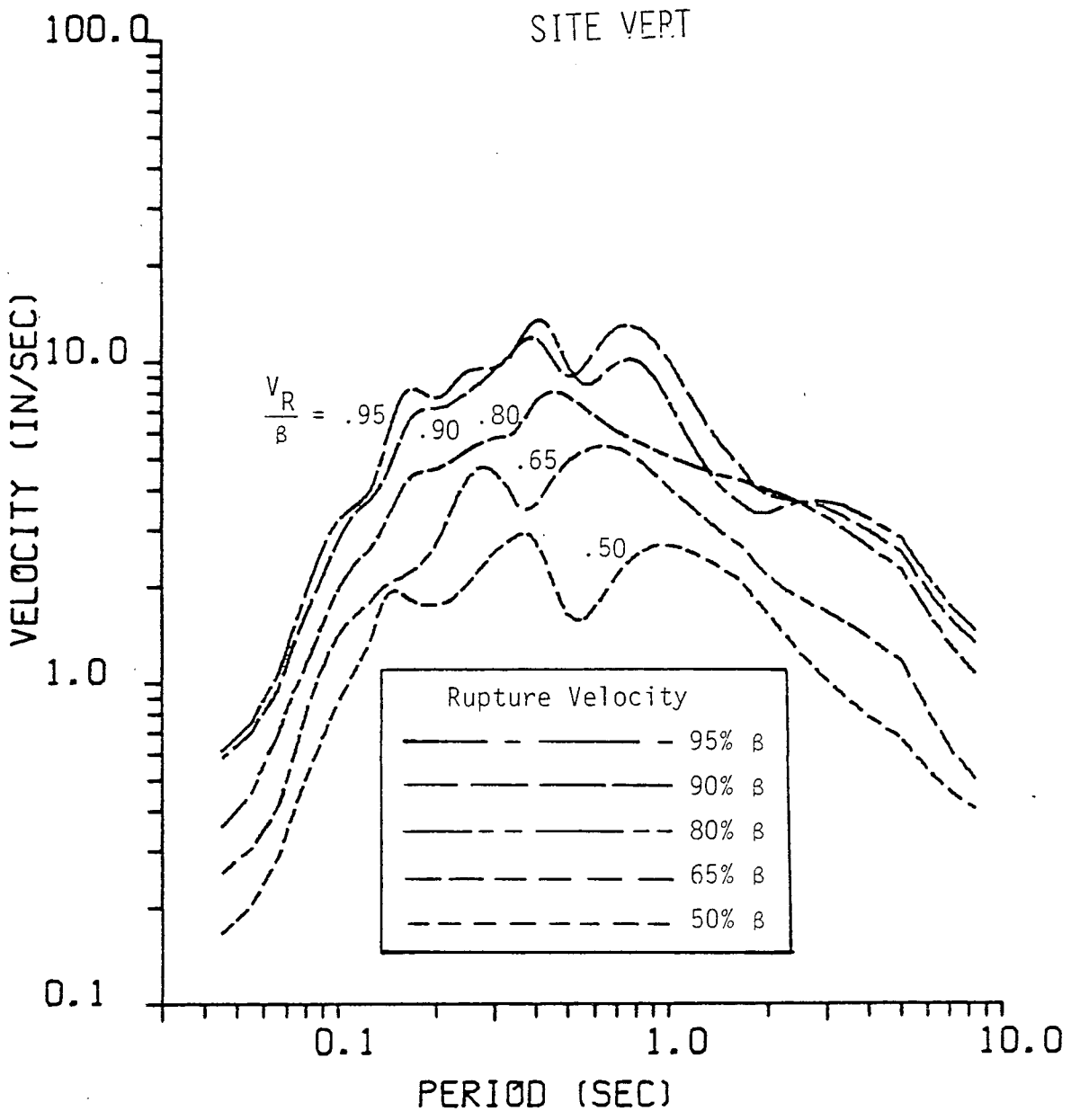

Figure 6-23- Effect of rupture velocity on site specific response for vertical component.

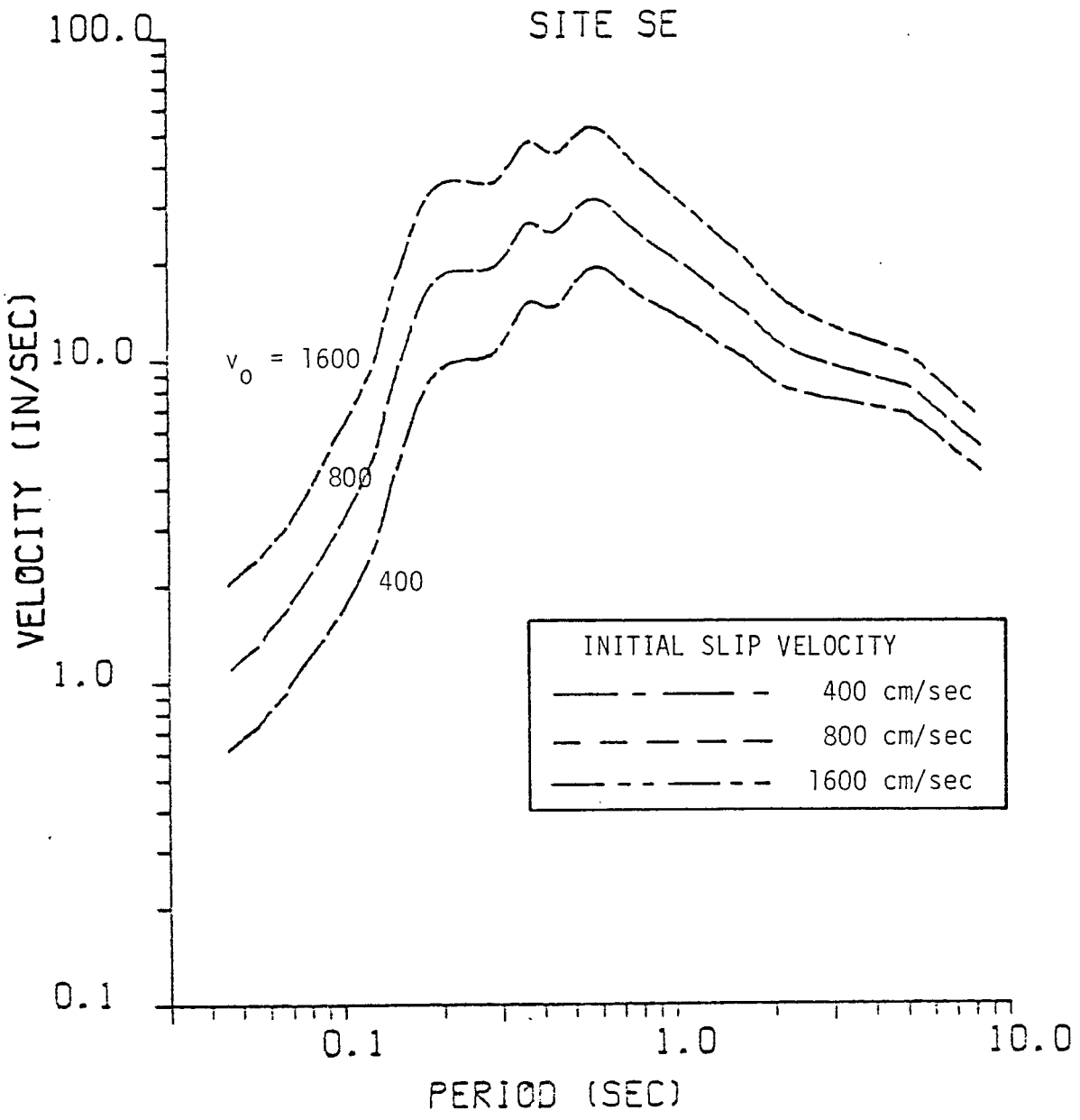

Figure 6-24. Effect of initial slip velocity on site specific response for southeast component.

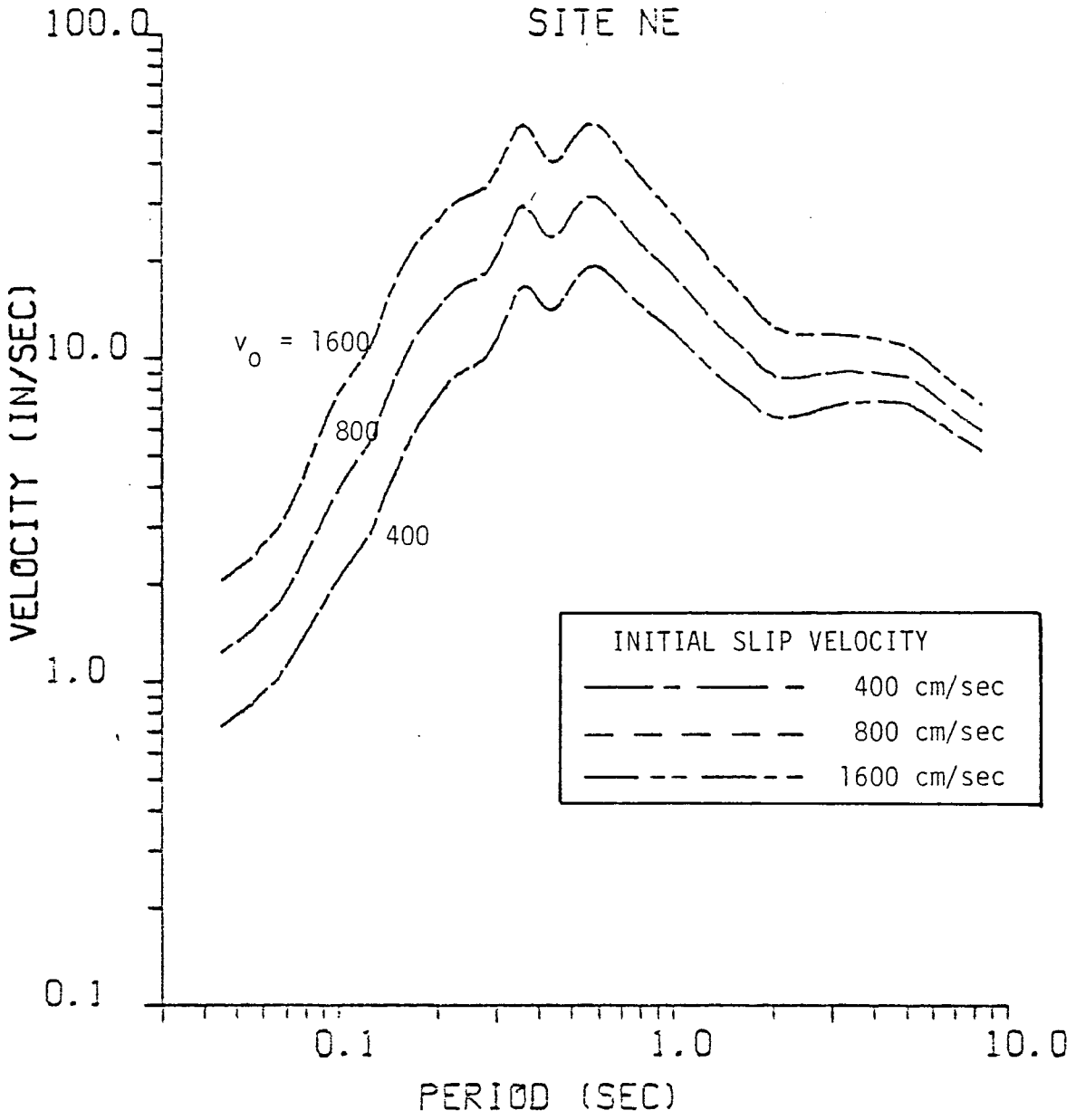

Figure 6-25. Effect of initial slip velocity on site specific response for northeast component.

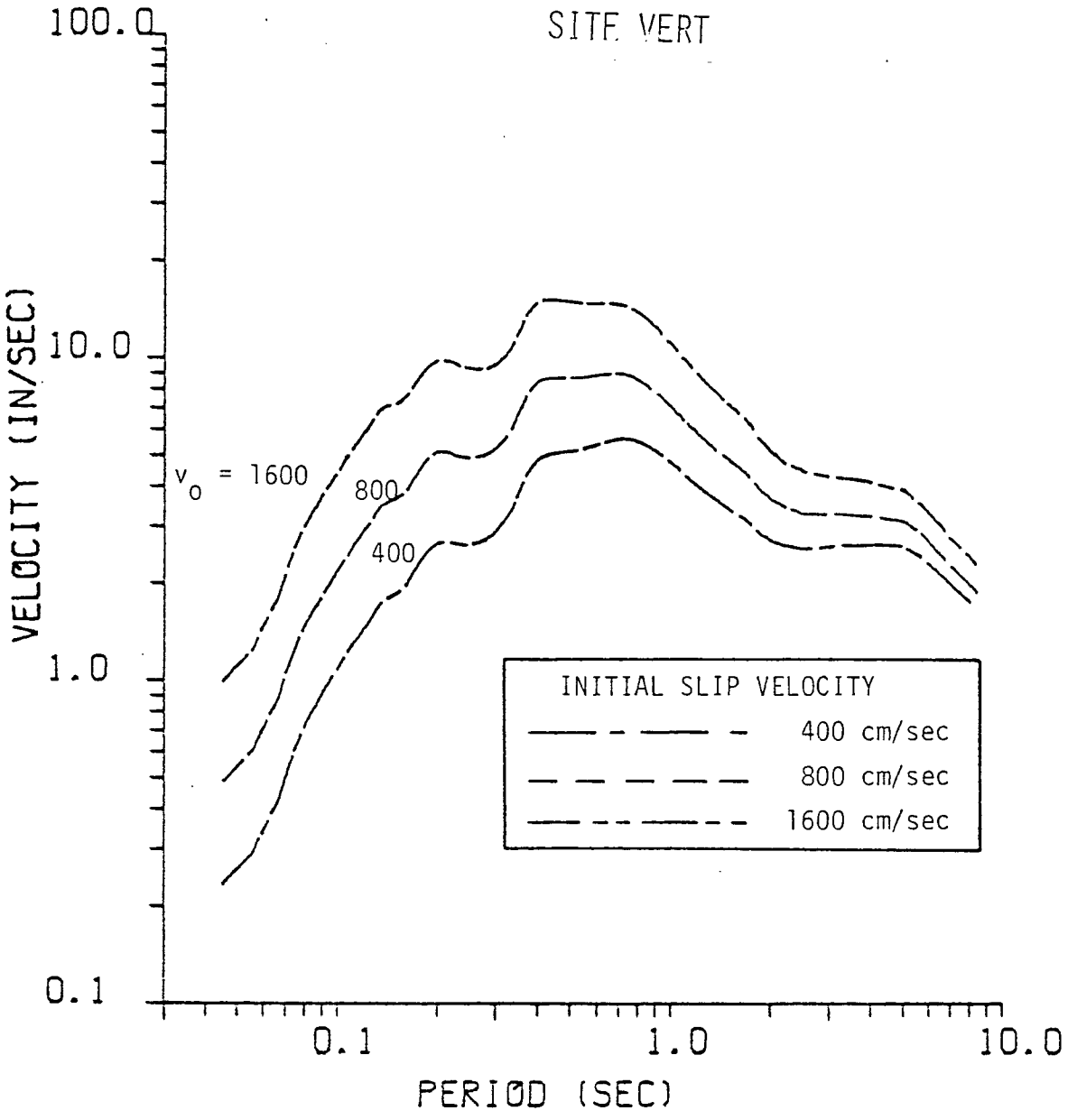

Figure 6-26. Effect of initial slip velocity on site specific response for vertical component.

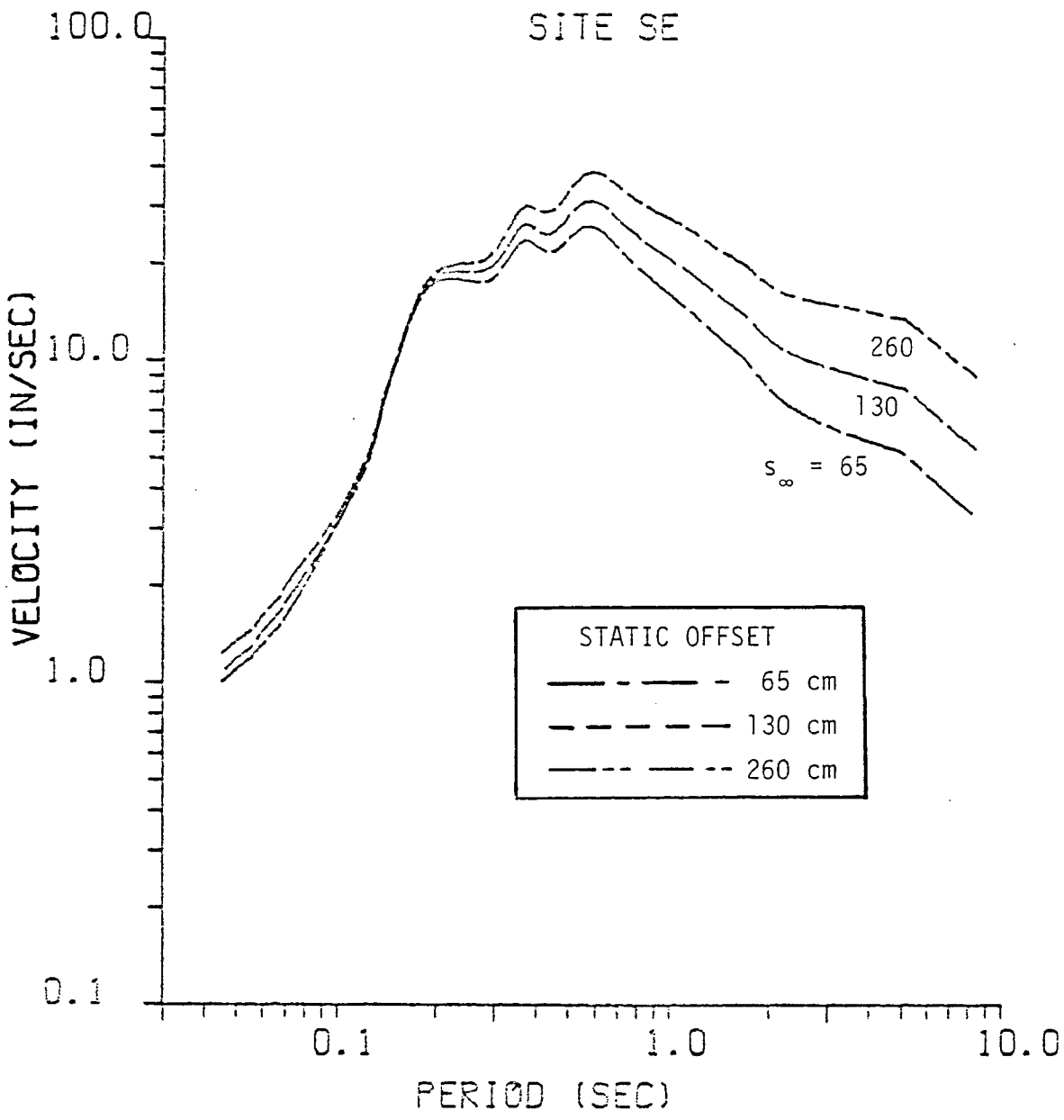

Figure 6-27. Effect of static offset on site specific response for southeast component.

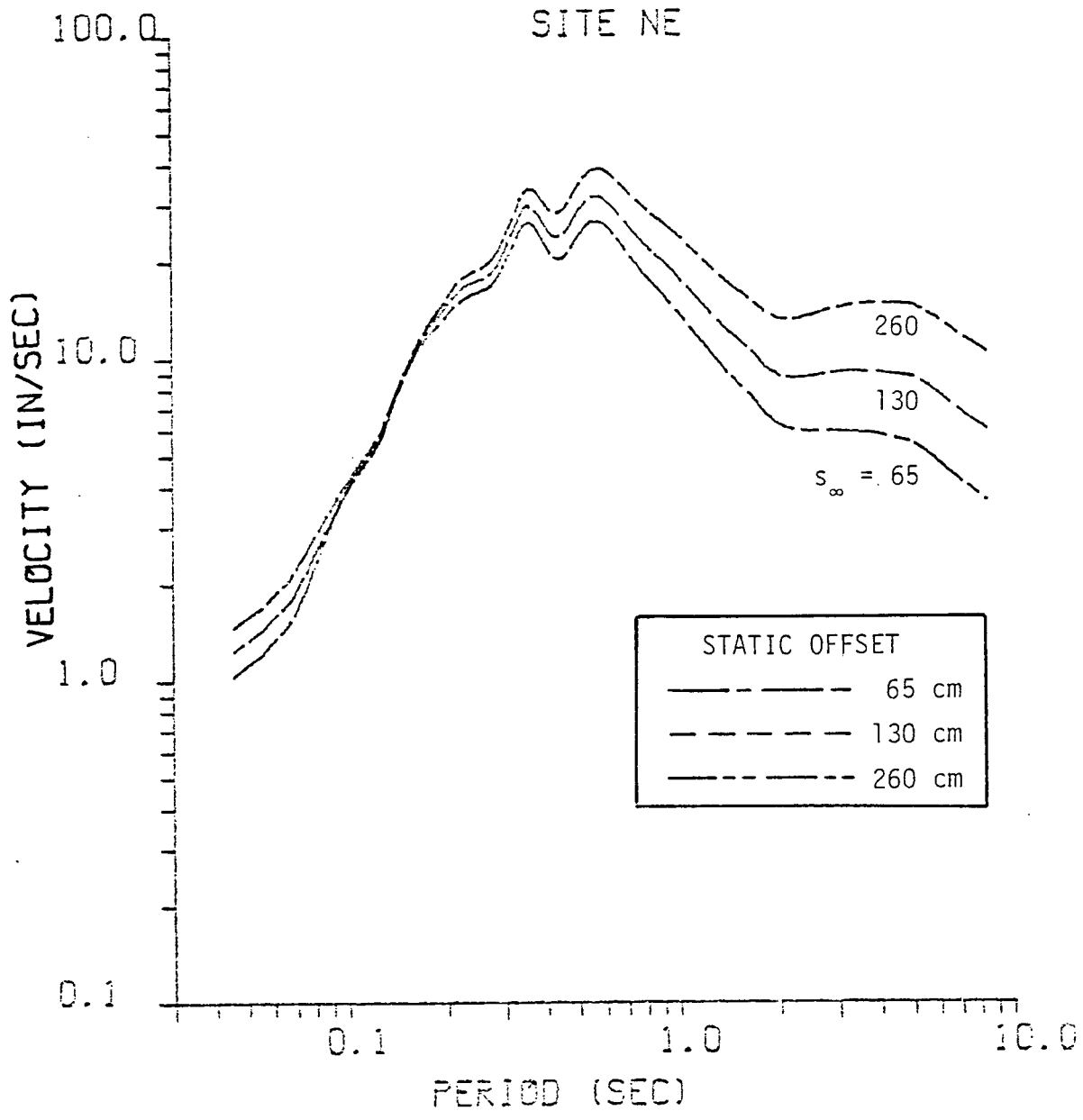

Figure 6-28. Effect of static offset on site specific response for northeast component.

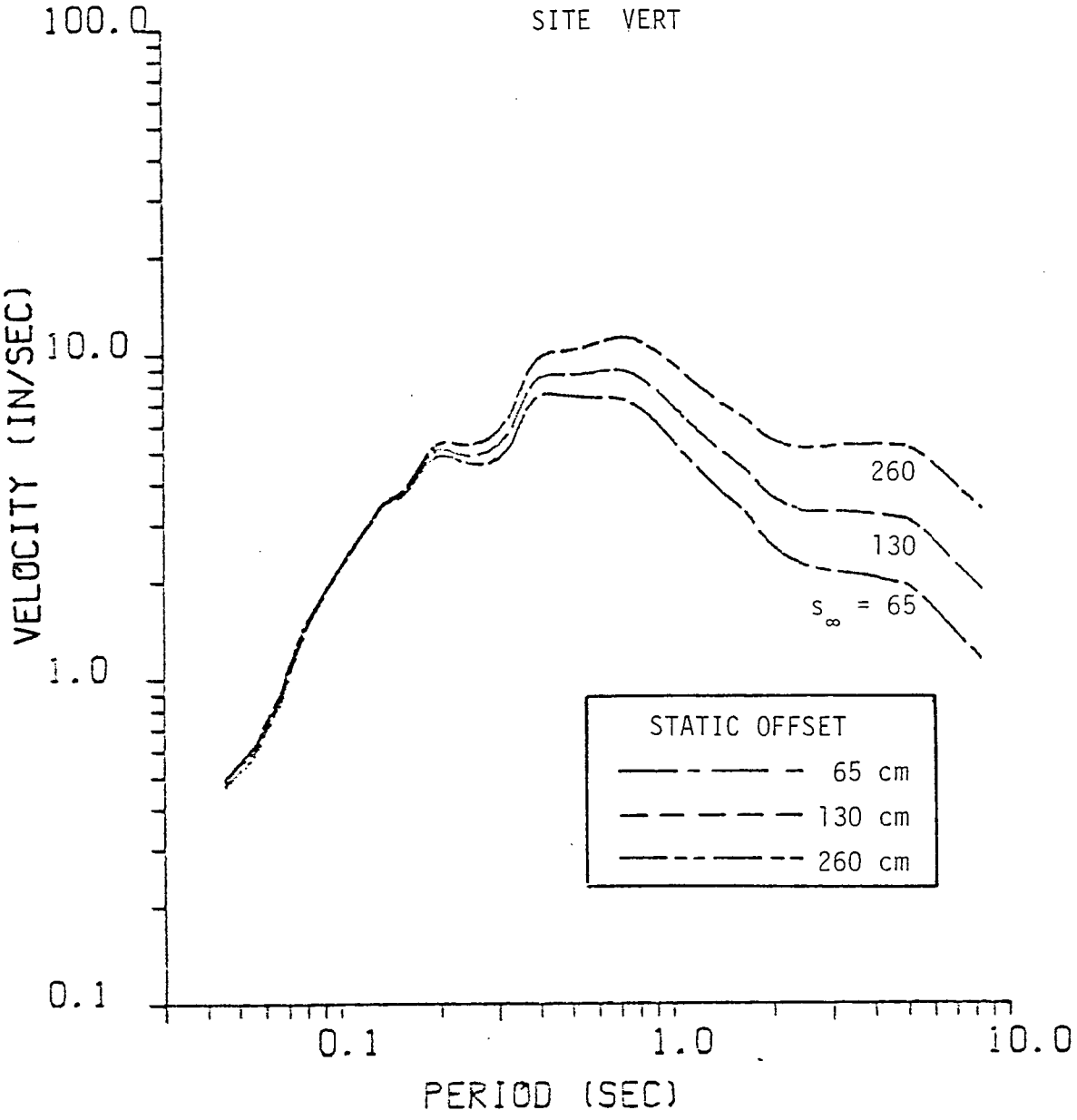

Figure 6-29. Effect of static offset on site specific response for vertical component.

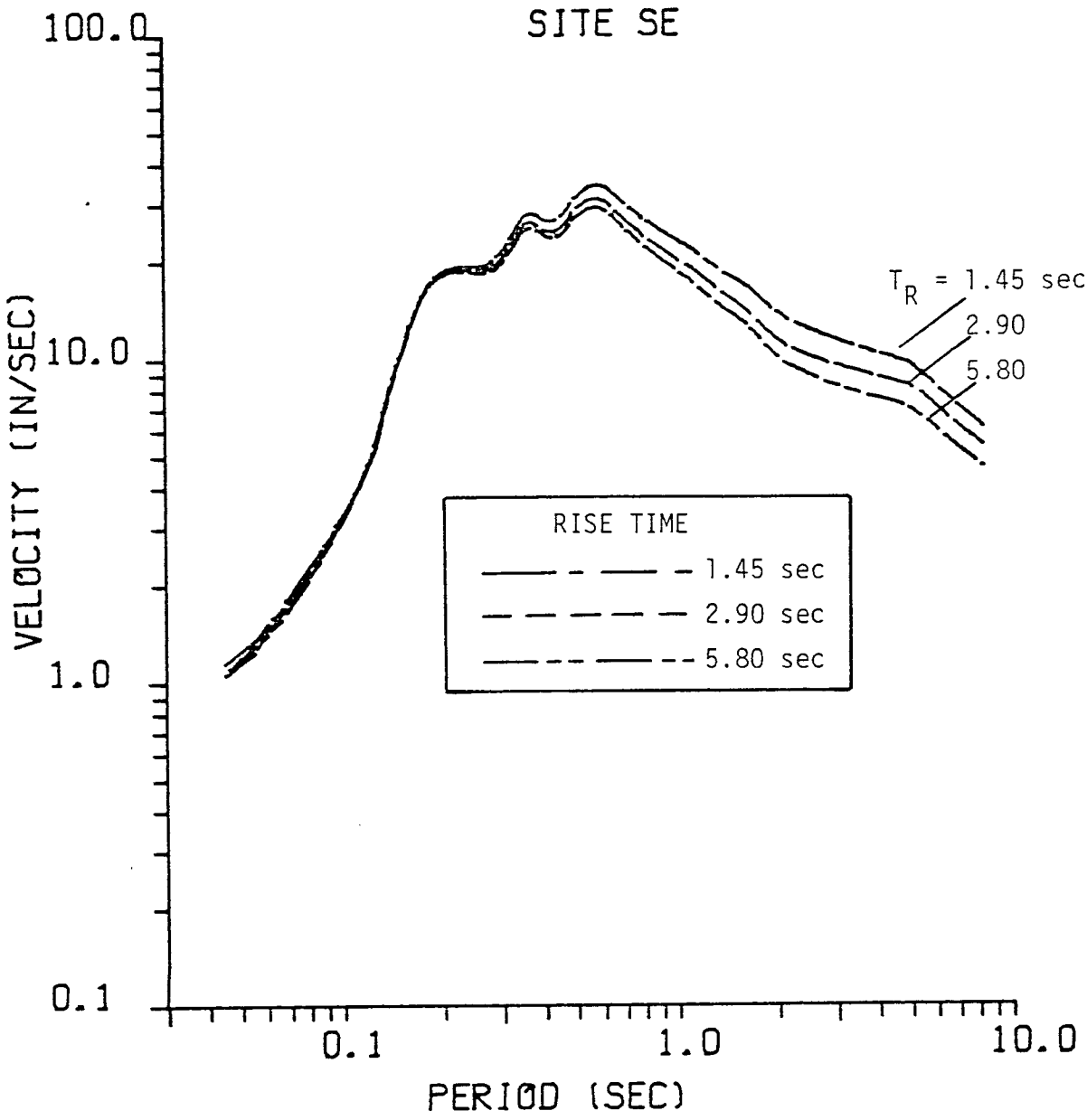

Figure 6-30. Effect of rise time on site specific response for southeast component.

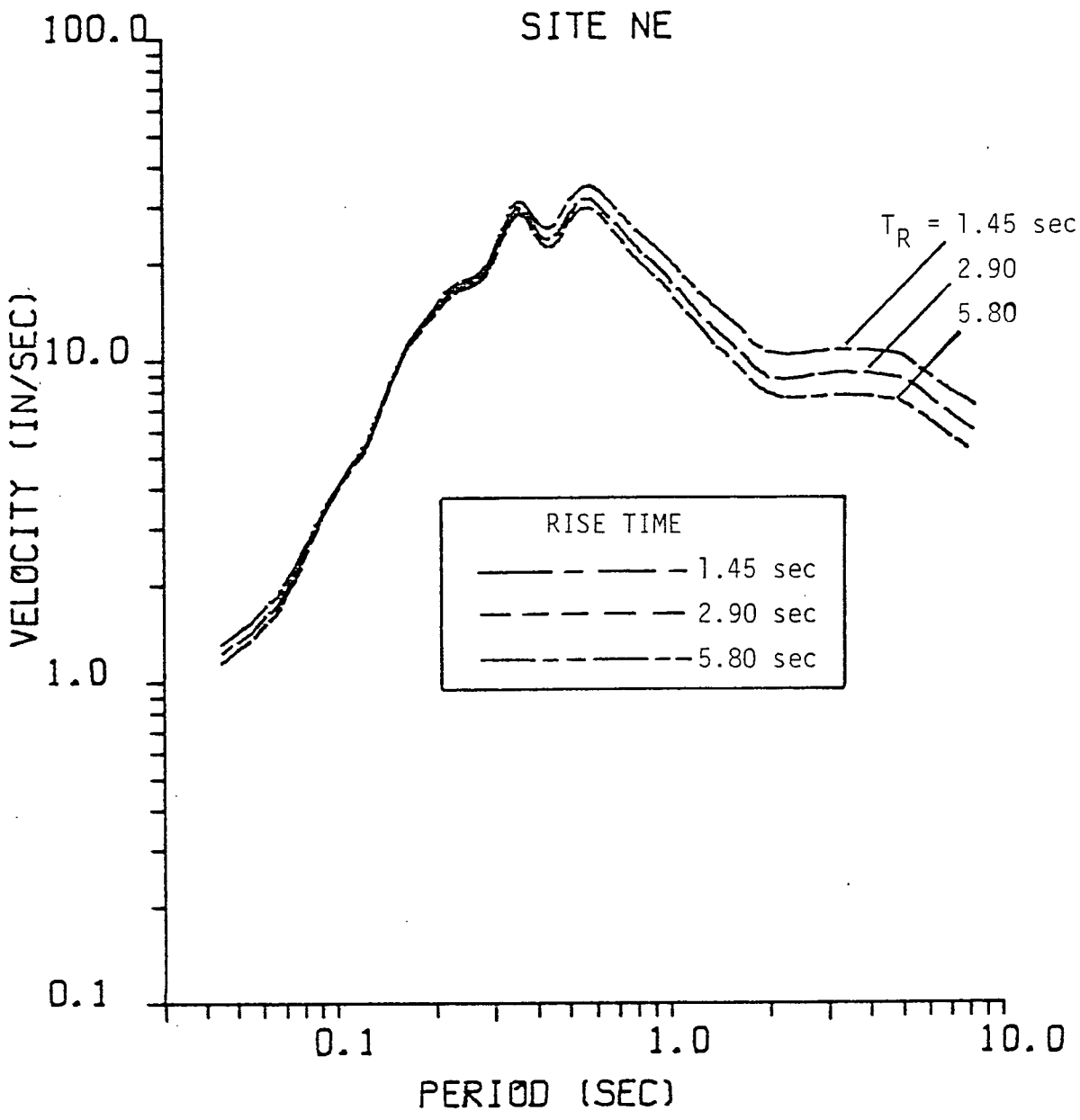

Figure 6-31. Effect of rise time on site specific response for northeast component.

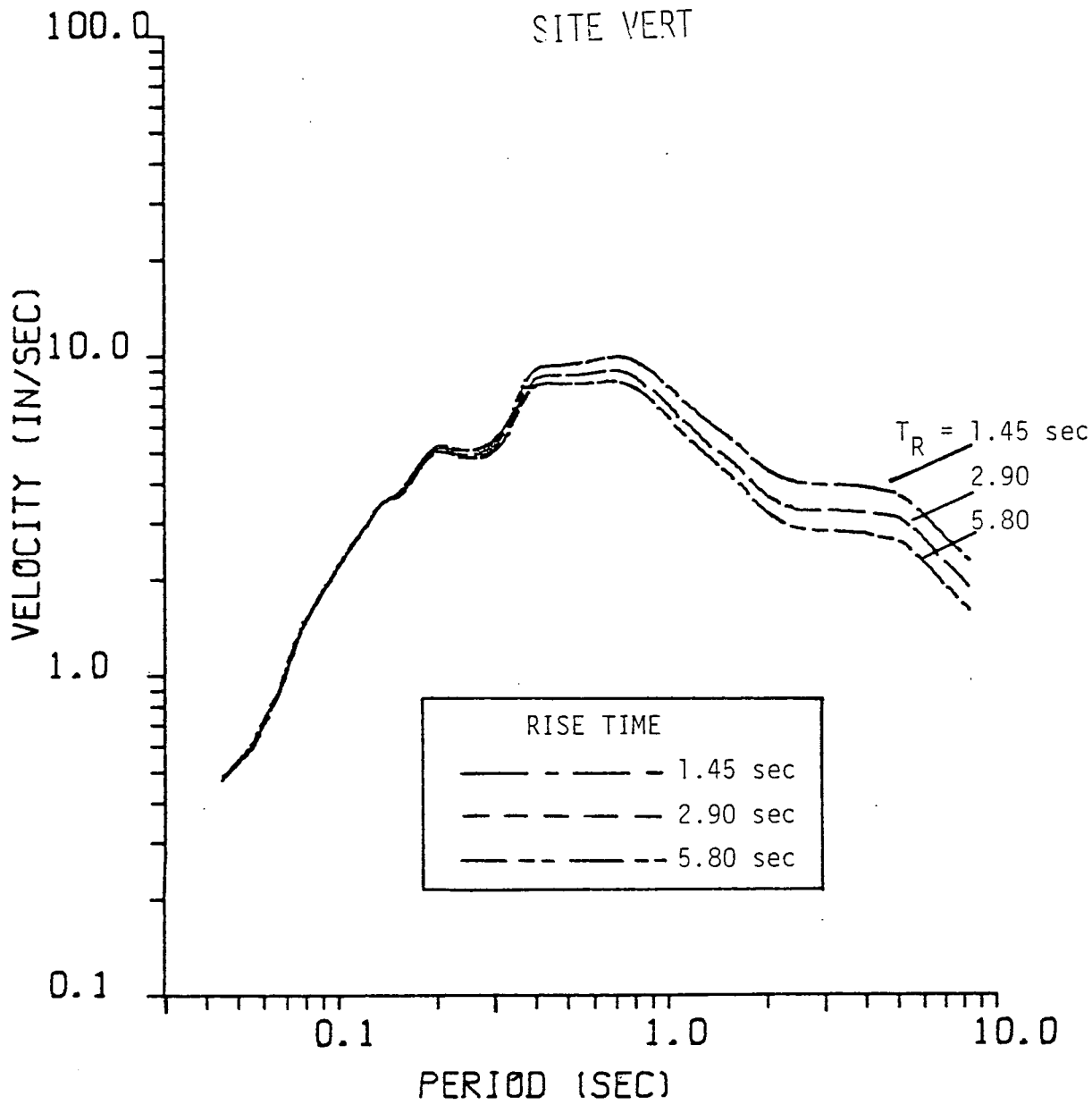

Figure 6-32. Effect of rise time on site specific response for vertical component.

The influence that static offset (which is related to the static stress drop) has on response spectra is illustrated in Figures 6-27 through 6-29. An increase in the static offset leads to a proportional increase in the low-frequency response. DELTA's Earthquake Model assumes a static offset corresponding to the value observed in the field and deduced from distant seismic observations for the verification earthquakes, and a conservative value for static stress drop (100 bars) is used for the hypothetical offshore earthquake.

The sensitivity to the slip duration at a point (rise time) is shown in Figures 6-30 through 6-32. Similar to the static offset, the effects are basically low frequency in nature, except that now, a decrease in rise time leads to the increase in low-frequency response. In DELTA's Earthquake Model, the slip duration corresponds to the time for a shear wave to traverse the width of the fault.

An expedient way to convey the effects of incoherence is to study the behavior of the maximum accelerations, velocities, and displacements when removing one type of randomness at a time from the model. The results of such a study are displayed in Table 6-2 and represent a summary of the trade-off between Stations 2 and 8 at Parkfield. Also appearing in Table 6-2 are the maxima using the full randomness model as well as the no-randomness model. The three components of the computed maxima are shown in columns 2 and 3 for stations 2 and 8, respectively; the ratios of the peak horizontal and vertical components for Station 2 divided by the corresponding values for Station 8 appear in column 4.

The ratios in column 4 most clearly depict how the randomness breaks up the focusing effects. Using the maxima ratios from the full randomness model as a point of reference, it is found that removing either the micro incoherence, or the initiation time randomness, or the rupture direction randomness, or the fault orientation randomness leads to more pronounced focusing (larger ratios). Comparing the full randomness model with the model removing receiver orientation randomness, it can be seen how the receiver orientation randomness tends to

equalize the horizontal components. Finally, comparing the full randomness model with the model having no randomness serves to review the drawbacks associated with the totally coherent model. The parameters defining the incoherence in DELTA's Earthquake Model are discussed in Section 4.2.

6.3 EARTH PARAMETERS

The sensitivity of computed ground motions to inadvertent biases or uncertainties in earth parameters is investigated in this section. The sensitivity could be examined by varying the earth structure and holding the geometric and rupture properties of the earthquake model constant, as in the May 1978 report. Alternatively, studies can be performed to determine how changes in layer properties directly influence the Green's functions, as presented in the sequel.

The Green's functions are computed at several representative frequencies with variations in the following three sets of layer parameters: material attenuation factors (Q); layer thickness; and shear and compressional wave velocities. The earth parameters of reference for the three resulting sensitivity studies correspond to the layered geologic structure at the San Onofre site, as defined in Table 6-1. The measure of sensitivity to the particular earth parameter to be varied is defined presently.

The sensitivity measure is derived in terms of the function G(p), which represents the spectral amplitude of the Green's function at a particular frequency and source-receiver geometry for earth parameter set p. Thus, to study the sensitivity to the material attenuation in the third layer, p will denote Q in the third layer. The sensitivity, S, of G(p) with respect to p is defined as the logarithmic derivative, i.e.,

$$S(G,p) = \frac{\partial \ln G}{\partial \ln p} = \frac{p}{G} \frac{\partial G}{\partial p}$$

$$\simeq \frac{1}{2\,\delta p} \frac{p}{G(p)} \left[G(p + \delta p) - G(p - \delta p)\right]$$

in which $G(p \pm \delta p)$ is obtained by simply performing calculations with small variations, δp, above and below the reference earth parameter p.

In the ensuing sensitivity studies, the function G(p) corresponds to either the vertical, radial, or azimuthal component of the displacement field at the free surface resulting from a buried vertical strike-slip point dislocation. The receivers are located at epicentral distances of 1, 10, 30 and 70 km at an azimuth of 22.5 degrees from the strike to eliminate bias due to radiation pattern. Source depths of .484, 2.4, 6.9 and 15.0 km are considered and the results are presented at frequencies of 1, 2, 5, 10 and 20 Hz. Due to the roughness of the amplitude spectra, the functions G are computed at a particular frequency by taking the arithmetic average of the spectral amplitudes at discrete frequencies in a narrow band above and below the frequency of interest.

In studying the sensitivity to material attenuation, the parameter set p corresponds to the material attenuation factors from each layer. The variations, δp, are assumed to be 10 percent of the attenuation factors for shear and compressional waves ($0.1\ Q_\beta$ and $0.1\ Q_\alpha$) in each layer. The sensitivity results are displayed in Table 6-3 for the azimuthal displacement component. The values of the sensitivity measure appear in the 4×4 subtables for a given frequency. In each subtable, the four rows represent the four source depths, while the four columns represent the four epicentral distances.

It is possible to estimate the sensitivity to the material attenuation by considering plane wave propagation. Assuming a complex shear wave velocity, β^*_j, of the form

$$\frac{1}{\beta^*_j} = \frac{1}{\beta_j} - \frac{i}{2\beta_j Q_{\beta_j}}$$

where j refers to the layer number, then a plane SH-wave in layer j can be written as

TABLE 6-3

SENSITIVITY OF AZIMUTHAL DISPLACEMENT
DUE TO Q CHANGES IN ALL LAYERS

Depth (km) \ Epicentral Distance (km)	CALCULATED 1.0	10.	30.	70.	RAY THEORY 1.0	10.	30.	70.
				FREQUENCY = 1.0				
.484	0.16	1.1	2.1	1.4	0.14	0.82	2.3	5.4
2.4	0.15	0.36	1.3	1.9	0.13	0.22	0.40	0.78
6.9	0.20	0.21	0.44	0.68	0.16	0.20	0.33	0.58
15.0	0.25	0.26	0.33	0.45	0.21	0.23	0.33	0.55
				FREQUENCY = 2.0				
.484	0.28	2.8	1.2	1.4	0.27	1.6	4.6	11.
2.4	0.27	0.27	1.2	2.7	0.26	0.43	0.80	1.5
6.9	0.32	0.46	0.82	1.5	0.32	0.40	0.65	1.2
15.0	0.41	0.51	0.70	0.98	0.41	0.45	0.65	1.1
				FREQUENCY = 5.0				
.484	0.71	0.92	3.1	3.4	0.68	4.1	12.	27.
2.4	0.62	0.95	2.2	3.5	0.66	1.1	2.0	3.9
6.9	0.67	1.0	1.6	3.2	0.80	1.0	1.6	2.9
15.0	0.89	1.1	1.6	2.6	1.0	1.1	1.6	2.7
				FREQUENCY = 10.0				
.484	1.4	2.6	6.5	11.	1.4	8.1	23.	53.
2.4	1.3	2.0	4.4	5.0	1.3	2.1	4.0	7.7
6.9	1.5	2.0	3.5	3.1	1.6	2.0	3.3	5.8
15.0	2.1	2.2	3.3	2.4	2.1	2.3	3.3	5.4
				FREQUENCY = 20.0				
.484	2.7	5.3	-0.90	3.6	2.7	16.	46.	107.
2.4	2.6	4.4	2.7	1.9	2.6	4.3	8.0	15.
6.9	3.0	4.1	6.1	6.5	3.2	4.0	6.5	12.
15.0	3.1	4.5	6.9	4.8	4.1	4.5	6.5	11.

$$G_{SH}(Q_j) \sim \exp\left[i\omega(t - R_j/\beta_j^*)\right] = \exp\left[\frac{-\omega R_j}{2\beta_j Q_{\beta_j}}\right]\exp\left[i\omega(t-R_j/\beta_j)\right].$$

The variable R_j represents the distance travelled by a shear wave in the j^{th} layer. Using geometric ray tracing (i.e., Snell's law for the direct paths) between source and receiver, the "theoretical" sensitivity of G_{SH} with respect to Q is expressed in terms of the sum

$$S(G_{SH}, Q_{\tilde{\beta}}) \sim \sum_j \frac{\omega R_j}{2\beta_j Q_{\beta_j}}$$

in which j extends over the layers traced by the SH wave.

This "theoretical" estimate of the sensitivity to material attenuation serves as a basis for comparison with the calculated sensitivity values given in Table 6-3. At small epicentral distances, the sensitivity of the calculated azimuthal displacement is closely predicted by the theoretical results, especially for the deeper sources. As the epicentral range or the frequency is increased, there is a general trend toward increased sensitivity. However, the increase is far less pronounced than predicted by the theoretical estimates. For instance, the theoretical sensitivities at an epicentral distance of 70 km for the shallowest source highly overestimate the corresponding calculated sensitivities. This is due to complexities in the propagation paths through the dispersive surface layers and to the transmission and reflection losses unaccounted for in the "theoretical" sensitivity values.

In the next study, the sensitivity to changes in layer thickness is examined. The definition of the logarithmic derivative in the sensitivity measure is altered to accommodate one-sided variations. Thus, the effect of considering a refined geologic structure relative to the reference geology is analyzed separately from the corresponding effects associated with considering a cruder geologic structure

relative to the reference geology. Table 6-4 presents the layer parameters used to define both the refined and gross layer structures (Table 6-1 presents the reference layer structure).

The sensitivity values are displayed in Tables 6-5 and 6-6 in the same format as the previous study on material attenuation, except that now, the two sets of results in each table represent the vertical and radial displacement components. The sensitivity to refining the geologic structure shows no trends as a function of frequency or source-receiver geometry in Table 6-5. Similarly, no trends are apparent in Table 6-6 when considering a cruder approximation to the reference geology.

In Table 6-7, the sensitivity of the vertical and radial displacement components to a 10 percent shift in the values of all the shear and compressional wave velocities is examined (Poisson's ratios are held constant in all layers). As in the sensitivity to layer thickness, no trends are apparent in the results.

TABLE 6-4

VISCOELASTIC PARAMETERS FOR THE GEOLOGIC STRUCTURES USED TO ANALYZE THE SENSITIVITY TO LAYER THICKNESS AT SAN ONOFRE

Layer Thickness (km)	β s-wave Velocity (km/sec)	α p-wave Velocity (km/sec)	ρ Density (g/cc)	Q_s Shear Quality Factor	Q_p Compressional Quality Factor
Layer Properties for the Refined Structure:					
0.1000E-01	0.615000	1.864800	2.160000	16.34	112.7
0.1000E-01	0.625080	1.895400	2.160000	16.67	115.0
0.2200E-01	0.635000	1.934800	2.160000	17.01	118.4
0.2200E-01	0.645080	1.965500	2.160000	17.34	120.8
0.1600E-01	0.655000	2.014600	2.160000	17.68	125.4
0.1600E-01	0.665080	2.045600	2.160000	18.02	127.8
0.5650E-01	0.775000	2.089600	2.100000	21.81	118.9
0.5650E-01	0.805590	2.172000	2.100000	22.90	124.8
0.5500E-01	0.900000	2.206500	2.100000	26.30	118.6
0.5500E-01	0.962070	2.358600	2.100000	28.58	128.9
0.1650	1.100000	2.420000	2.100000	33.80	122.7
0.1650	1.226920	2.540000	2.100000	38.74	124.5
0.1350	1.350000	2.700000	2.240000	43.66	131.0
0.1350	1.432440	2.801900	2.240000	47.01	134.9
0.1350	1.455000	2.830000	2.240000	47.94	136.0
0.1350	1.485310	2.870300	2.240000	49.19	137.8
0.5000E-01	1.640000	3.070000	2.470000	55.68	146.3
0.5000E-01	1.680490	3.130000	2.470000	57.40	149.3
0.5000E-01	1.700000	3.170000	2.470000	58.23	151.9
0.5000E-01	1.720120	3.230600	2.470000	59.10	156.3
1.060	2.700000	4.400000	2.600000	103.8	206.8
1.060	3.226830	5.280000	2.600000	129.7	260.5
3.485	3.350000	5.599999	2.760000	136.0	285.0
3.485	3.642210	5.803599	2.760000	150.9	287.4
0.1000E 21	3.730000	6.099999	2.760000	155.5	311.9
Layer Properties for the Crude Structure:					
0.9600E-01	0.642200	1.960500	2.160000	17.25	120.6
0.5530	1.013200	2.359600	2.100000	30.50	124.1
0.7400	1.490000	2.885800	2.355000	49.39	138.9
0.1000E 21	3.463100	5.658000	2.707000	141.7	283.7

TABLE 6-5

SENSITIVITY OF VERTICAL AND RADIAL DISPLACEMENT
DUE TO A REFINED LAYER STRUCTURE

Depth (km) \ Epicentral Distance (km)	VERTICAL 1.0	10.	30.	70.	RADIAL 1.0	10.	30.	70.
				FREQUENCY = 1.0				
.484	0.11	-0.39	-1.2	8.34E-02	0.26	-0.64	-2.2	1.1
2.4	-0.83	-0.39	-0.58	1.32E-02	-0.30	-2.0	-1.9	0.77
6.9	0.52	-1.2	0.75	-1.2	-0.16	0.87	2.2	-0.46
15.0	1.7	0.95	0.79	0.54	-0.17	2.56E-02	0.36	1.4
				FREQUENCY = 2.0				
.484	-2.51E-02	4.80E-02	1.1	1.1	0.68	2.0	1.4	-1.1
2.4	-0.51	-1.9	-3.0	3.0	-1.68E-02	-0.89	1.9	3.3
6.9	-0.71	-1.1	0.57	0.58	8.35E-02	-0.34	-1.8	-1.7
15.0	-3.5	0.21	-3.2	-4.52E-02	0.24	8.34E-02	-0.52	-2.7
				FREQUENCY = 5.0				
.484	-0.27	-0.11	-3.4	0.24	0.42	0.27	-1.8	1.1
2.4	-2.4	-1.4	-0.84	0.11	0.22	-2.1	2.8	2.4
6.9	0.27	0.42	2.3	2.7	0.21	1.4	2.7	3.4
15.0	-0.72	-0.22	1.7	1.5	0.22	0.12	2.2	0.49
				FREQUENCY = 10.0				
.484	1.6	0.61	1.3	0.32	-0.45	8.45E-03	3.5	2.4
2.4	0.12	4.84E-02	-0.30	-0.97	0.27	3.6	0.85	-1.3
6.9	-1.8	-1.7	0.97	-1.9	0.10	-1.1	2.7	-0.75
15.0	-0.83	0.40	0.37	0.59	-2.24E-02	0.24	0.72	2.4
				FREQUENCY = 20.0				
.484	0.75	-0.95	1.0	-0.90	-1.3	0.24	2.0	-3.7
2.4	3.5	-0.54	-2.6	2.4	0.14	-0.17	-3.8	3.1
6.9	-1.7	1.8	1.2	0.73	0.11	1.1	1.4	1.4
15.0	-0.67	0.79	0.16	-0.14	-1.0	-0.44	0.89	-0.31

TABLE 6-6

SENSITIVITY OF VERTICAL AND RADIAL DISPLACEMENT
DUE TO A GROSS LAYER STRUCTURE

Depth (km) \ Epicentral Distance (km)	VERTICAL 1.0	10.	30.	70.	RADIAL 1.0	10.	30.	70.
				FREQUENCY = 1.0				
.484	-0.95	1.2	1.6	-3.4	6.32E-02	-2.3	-3.3	-1.7
2.4	-3.4	0.22	-0.96	-2.9	-4.79E-02	0.75	-0.44	-2.5
6.9	0.86	-0.23	-1.5	-2.3	-0.37	1.2	0.99	-1.9
15.0	2.4	-0.22	0.47	-3.5	-0.74	-0.19	2.8	1.9
				FREQUENCY = 2.0				
.484	0.75	-2.2	-1.3	-3.8	0.30	-2.7	2.8	-3.0
2.4	4.46E-03	-0.30	-3.2	-4.2	-0.43	-0.54	-1.4	-1.9
6.9	-0.22	-0.70	0.97	-3.8	-0.92	6.87E-02	0.51	-3.4
15.0	0.93	1.1	-4.4	-1.1	-0.94	-0.50	-0.73	0.90
				FREQUENCY = 5.0				
.484	1.5	-1.8	-1.9	-1.2	1.4	-1.2	-0.64	-0.44
2.4	2.1	-3.1	-4.2	-4.5	-0.11	-2.5	-3.2	-2.5
6.9	-0.27	-1.7	0.66	-0.74	-9.88E-02	0.39	2.4	1.2
15.0	0.48	-0.20	0.77	0.70	-0.14	-0.15	-2.4	1.4
				FREQUENCY = 10.0				
.484	2.1	-0.77	-0.21	-4.1	-0.30	-0.49	1.1	-2.8
2.4	-0.50	-1.5	-2.6	-1.9	-0.16	3.3	-2.0	-2.3
6.9	-0.54	-3.2	-0.71	-3.0	-0.68	-2.0	1.3	-1.7
15.0	-1.8	0.36	-1.9	0.69	-1.1	-0.72	-1.2	3.0
				FREQUENCY = 20.0				
.484	-1.9	-2.2	-2.4	-2.9	-0.62	-2.2	-0.11	-3.4
2.4	4.1	-1.3	-2.3	-2.3	0.76	-1.1	-2.3	7.33E-02
6.9	0.67	0.43	1.1	-0.54	-0.07	1.1	2.1	-2.4
15.0	-0.71	-0.28	-0.91	-0.61	1.3	0.27	-0.19	-1.3

TABLE 6-7

SENSITIVITY OF VERTICAL AND RADIAL DISPLACEMENT
DUE TO A SHIFT IN THE VALUE OF VELOCITY
FOR ALL LAYERS

Depth (km) \ Epicentral Distance (km)	VERTICAL 1.0	10.	30.	70.	RADIAL 1.0	10.	30.	70.
				FREQUENCY = 1.0				
.484	0.33	2.9	9.1	0.58	-0.24	-1.5	0.42	5.3
2.4	-2.5	0.13	1.4	0.60	-1.1	-0.65	4.0	2.5
6.9	-9.1	-4.0	-1.9	1.7	-1.4	4.2	-2.0	1.0
15.0	-4.0	8.1	3.5	1.2	-2.0	-2.0	2.8	6.6
				FREQUENCY = 2.0				
.484	-0.34	3.4	-0.40	-0.70	0.91	5.6	1.4	9.0
2.4	1.2	-1.8	0.30	-6.6	-0.46	4.7	6.2	4.0
6.9	-1.2	0.44	9.5	2.3	-0.21	-2.1	3.4	0.38
15.0	-10.	2.4	-0.43	-1.1	5.14E-02	-0.65	1.2	4.7
				FREQUENCY = 5.0				
.484	1.7	1.4	4.2	1.9	4.7	1.6	-2.6	3.9
2.4	6.6	-0.99	2.2	1.3	-0.28	-0.82	-4.7	3.2
6.9	-3.73E-02	1.4	4.7	6.2	-0.38	-2.0	7.9	12.
15.0	-1.7	0.25	-3.6	0.44	-1.88E-02	6.80E-02	1.8	2.0
				FREQUENCY = 10.0				
.484	7.9	0.90	-3.6	-1.8	3.9	1.3	4.4	13.
2.4	0.17	1.8	1.5	1.7	-8.21E-02	-2.2	-3.8	-1.0
6.9	-4.3	0.64	3.8	-1.2	0.61	3.3	7.4	0.79
15.0	-0.24	-2.2	0.13	2.2	0.92	2.2	7.1	9.5
				FREQUENCY = 20.0				
.484	-0.58	-5.0	0.62	10.	-2.8	-5.1	11.	7.6
2.4	-14.	-6.3	-4.2	0.93	4.2	-1.7	0.94	30.
6.9	-2.9	-7.3	-0.68	24.	2.1	-4.3	-3.9	10.
15.0	0.97	-2.2	-5.28E-02	2.1	4.0	10.	-5.2	-0.58

7.0 REFERENCES

1. Apsel, R. J., 1979. Dynamic Green's Functions for Layered Media and Applications to Boundary-Value Problems, Ph.D. Thesis, University of California at San Diego, La Jolla, California.

2. Archuleta, R. J. and G. A. Frazier, 1978. Three-Dimensional Numerical Simulations of Dynamic Faulting in a Half-space, Bull. Seism. Soc. Am., 68, 573-598.

3. Del Mar Technical Associates, 1978. Simulation of Earthquake Ground Motions for San Onofre Nuclear Generating Stations -- Unit 1, May 1978, Final Report.

4. Eaton, J. P., and M. E. O'Neill and J. N. Murdock, 1970. "Aftershocks of the 1966 Parkfield Sequence," Bull. Seism. Soc. Am., 57, 1245-1257.

5. Heaton, T. H. and D. V. Helmberger, 1978. Predictability of Strong Ground Motion in the Imperial Valley: Modeling the M4.9, November 4, 1976 Brawley Earthquake, Bull. Seism. Soc. Am., 68, 31-48.

6. Hurty, W. C., and M. F. Rubinstein, Dynamics of Structures, Prentice-Hall, 1964.

7. Kostrov, B. V., 1964. Self-similar Problems of Propagating Shear Cracks, J. Appl. Math. Mech., 28, 1077-1087.

8. Trifunac, M. D. and J. N. Brune, 1970. Complexity of Energy Release During the Imperial Valley, California Earthquake of 1940, Bull. Seism. Soc. Am., 62, 1283-1302.